

**Development of an Alternative
Ventricular Catheter and an
In Vitro Model of its Obstruction**

Supraja Suresh, M.Eng

Biomedical Engineering

University of Strathclyde

This thesis is submitted in fulfilment of the requirements for the degree
of Doctor of Philosophy (PhD) in Biomedical Engineering

2014

Copyright Statement

This thesis is the result of the author's original research. It has been composed by the author and has not been previously submitted for examination which has led to the award of a degree.

The copyright of this thesis belongs to the author under the terms of United Kingdom Copyright Acts as qualified by University of Strathclyde Regulation 3.50. Due acknowledgment must always be made of the use of any material contained in, or derived from, this thesis.

Signed:

Date:

Acknowledgements

Firstly, I would like to thank my supervisor Dr Richard Black for his abundant support, wisdom and guidance during the course of the research on which this thesis is based. Thank you for making all the challenges made out of my PhD a learning experience.

I would like to extend my thanks to Mr Paul Chumas (MBBS), Consultant Paediatric Neurosurgeon at Leeds General Infirmary for generously donating the Codman Hakim shunt device for the purpose of this work.

I would like to express my gratitude to Dr Trevor Bushell for providing me access to use his lab for Astrocyte isolation and staining protocol. Thanks to Mr Graham Robertson for his invaluable help around the lab for the work with Astrocytes.

I am grateful to Dr Heba Lakany for her advice with the statistical analysis of data. Finally, I would like also to acknowledge late Dr J.D.S. Gaylor for his expertise and advice for the development of modules to test hydraulic permeability.

Thanks to Mr Stephen Murray for his advice and knowledge in assisting me to build the constituents for shunt testing system. Thanks to Mrs Katie Henderson for her extensive practical knowledge, experience, kindness and tireless efforts in helping me to develop my cell culture experimental model and protocols. Thanks to Mr Brian Cartlidge for his technical support, knowledge and patience in training me to use the microscopes. Thanks to Mr. Dimitrios Trikkaliotis and Miss Geetika Dubey for their involvement in my cell culture work. I would like to thank all the staff of Biomedical Engineering department for being kind and welcoming.

Heartily thanks to my parents Dr Suresh Babu and Dr Thilaka Suresh for their endless inspiration and love. My most special thanks to my dearest husband Mr Praveen for his boundless patience and encouragement in helping me obtain this achievement. This work would not have been possible without my family's constant support to keep me motivated and overcome all the challenges.

*I dedicate this thesis to my late Aunt Kala Kannan, my lovable sister Sindhuja
Suresh and brother Raj Suresh*

Abstract

Intracranial pressure and volume varies considerably between hydrocephalic patients, and with age, health and haemodynamic status; if left untreated intracranial pressure rises and the ventricular system expands to accommodate the excess cerebrospinal fluid (CSF), with significant morbidity and mortality. Although considerable improvements in design have been made since their introduction all CSF shunts in use today have a high incidence of failure with shunt obstruction being the most serious. Conventional proximal shunt catheters are made from poly (di-methyl) siloxane (PDMS), the walls of which are perforated with holes for the CSF to pass through. The limited range of catheters, in terms of material selection and flow distribution, is responsible in large part for their poor performance.

The aim of the study is to design and fabricate an alternative design of proximal catheter with permeable walls, and to evaluate its performance in the presence of glial cells, which are responsible for blockage. Electrospun Poly-ether Urethane (EPU) samples were fabricated from solvent, by means of an electrospinning technique, to yield microfibrinous polymer conduits. The hydrodynamic properties of EPU and conventional shunt were studied using a purpose-built shunt testing system.

The viability and growth of cells on candidate catheter materials such as PDMS and polyurethane in the form of cast films, microfibrinous mats and porous sponges were studied in presence of proteins present in CSF after 48h and 96h in culture. The number of viable cells was significantly less on EPU samples compared to the other substrates, which suggests that the fibrous form of the material from which the catheter is made has a bearing on the cell growth. A cell culture model of shunt obstruction was developed in which the cells were subjected to flow during culture *in vitro*, and the degree of obstruction quantified in terms of hydraulic permeability post static and perfusion culture. The results indicate that a catheter made of EPU would be able to maintain CSF flow even with the presence of cells for the time period chosen for this study. These findings have implications for the design and deployment of micro porous shunt catheter systems for the treatment of hydrocephalus.

Table of Contents

Copyright Statement	i
Acknowledgements.....	ii
Abstract	iv
List of Figures.....	ix
List of Tables.....	xiv
List of Abbreviations	xv
List of publications	xvii
Chapter 1: Introduction	1
Chapter 2: Background and Literature review	5
2.1 Introduction.....	5
2.2 Cerebrospinal Fluid	5
2.2.1 CSF Production, Circulation and Absorption.....	7
2.3 Hydrocephalus condition and treatment	13
2.3.1 Types of Hydrocephalus.....	16
2.3.2 Hydrocephalus Treatments	20
2.3.3 Hydrocephalus/CSF Shunt System	22
2.3.4 Types, Designs and Mechanism of Valve and Shunt Accessories	24
2.4 <i>In vitro</i> and Numerical modelling to understand and evaluate shunt behaviour after implantation	34
2.4.1 <i>In vitro</i> Models of shunt system	36
2.4.2 Numerical Models of the shunt system	52
2.5 Shunt failure and its consequences.....	54
2.6 Recent developments and advancements of CSF shunt systems	59
2.7 Review of current ventricular catheter progresses	64
2.8 Assessment of alternative ventricular catheter materials and fabrication techniques	70

2.8.1 Polyurethane as an alternative catheter material.....	73
2.8.2 Fabrication techniques of porous polyurethane	75
2.9 Aims and Objectives of the Study	78
Chapter 3: Fabrication and Evaluation of an Alternative Ventricular Catheter	79
3.1 Introduction.....	79
3.2 Materials and Methods	80
3.2.1 Design, fabrication and characterisation of alternative catheter.....	80
3.2.2 Experimental rig to test hydraulic properties of shunt series	83
3.2.3 Shunt Component testing	86
3.2.4 Hydraulic permeability determination	87
3.2.5 Statistical Analysis.....	90
3.3 Results.....	91
3.3.1 Characterisation of EPU catheter.....	91
3.3.2 Pressure flow relationship of conventional CSF shunt system.....	94
3.3.3 Hydraulic resistance of conventional shunt components	95
3.3.4 Pressure flow relationship of EPU catheter	96
3.3.5 Hydraulic Permeability of EPU catheter	97
3.4 Discussion	103
3.5 Conclusion	106
Chapter 4: Comparison of CSF shunt catheter materials <i>in vitro</i>	107
4.1 Introduction.....	107
4.2 Materials and Methods	108
4.2.1 Reagent Preparation	108
4.2.2 Primary Astrocytes isolation and culture	109
4.2.3 Immortalised 3T3 cell culture.....	112
4.2.4 Shunt catheter materials fabrication and preparation for cell culture	113

4.2.5 Protein adsorption	117
4.2.6 Cell viability measurement	118
4.2.7 Microscopy imaging of cell type on different substrates	119
4.3 Results.....	120
4.3.1 Astrocytes Immunofluorescence Image	120
4.3.2 Standard curve for 3T3 cells and Astrocytes	121
4.3.3 Growth curve for 3T3 cells and Astrocytes	122
4.3.4 Control Experiment	124
4.3.5 Evaluation of 3T3 and Astrocytes cell viability	126
4.3.6 Effect of protein coating on substrates	131
4.3.7 Form of material influences cell adhesion.....	136
4.3. 8 Fluorescence microscopy control images.....	139
4.3. 9 Fluorescence microscopy images of catheter material.....	140
4.4 Discussion	143
4.5 Conclusion	147
Chapter 5: <i>In vitro</i> model of an alternative CSF shunt catheter obstruction	148
5.1 Introduction.....	148
5.2 Materials and Methods	149
5.2.1 EPU Preparation and Cell Culture	149
5.2.2 <i>In vitro</i> Shunt Obstruction Model.....	150
5.2.3 Cell viability measurement	153
5.2.4 Hydraulic Permeability measurement	154
5.3 Results.....	155
5.3.1 Control Experiments for perfusion study	155
5.3.2 Effect of sample permeability on cell adhesion and growth	157

5.3.3 Hydraulic permeability after obstruction	159
5.4 Discussion	161
5.5 Conclusion	164
Chapter 6: Discussion.....	165
Chapter 7: Conclusions and Future Work	174
7.1 Overall Conclusions	174
7.2 Future Work	176
References	178
Appendix A	191
Appendix B.....	194
Appendix C.....	197
Appendix D	201

List of Figures

Figure 2.1: Circulation of CSF flow in human CNS. (Oreskovic and Klarica 2010)..	8
Figure 2.2: Frontal plane illustration of CSF absorption sites (Oreskovic and Klarica, 2010)	9
Figure 2.3: Cerebral blood flow and CSF flow in form of circuit diagram (Rekate 2008)	12
Figure 2.4: Normal and Hydrocephalus child's ventricle of the brain (http://www.cyh.com/HealthTopics)	13
Figure 2.5: Six months old child with a severe hydrocephalus condition (Faghieh Jouibari <i>et al.</i> 2011)	15
Figure 2.6: Non-communicating versus Communicating Hydrocephalus. (Pena <i>et al.</i> 2002)	17
Figure 2.7: Codman Hakim Hydrocephalus shunt series and an implanted shunt diagram in a child. (http://nhfonline.org/treatment.php).....	23
Figure 2.8: Design of different valve types available. (Drake <i>et al.</i> , 2000).....	25
Figure 2.9: A photographic and scanning electron microscope image of Codman [®] Hakim [®] Precision fixed pressure valve and programmable valve	27
Figure 2.10: Schematic representation of Strata Valve.(Czosnyka Z. H. <i>et al.</i> 2005)	28
Figure 2.11: Miethke ProGAV [®] shunt mechanism diagrams. (Allin <i>et al.</i> , 2006)...	30
Figure 2.12: Pictorial representation of Sophysa Polaris Valve. (Allin <i>et al.</i> , 2008)	31
Figure 2.13: Miethke Dual Switch Valve construction. (Kiefer <i>et al.</i> , 2002; Meier and Mutze 2004).....	32
Figure 2.14: Miethke Dual Switch Shunt Assistant mechanism illustration. (Kiefer <i>et al.</i> , 2002).....	33
Figure 2.15: Experimental test rig. (Whitehouse <i>et al.</i> , 1994).....	37
Figure 2.16: Hydrocephalus shunt testing apparatus. (Paes 1996).....	39
Figure 2.17: Schematic diagram representing shunt testing rig (Allin <i>et al.</i> 2008, Czosnyka M. <i>et al.</i> 1997, Czosnyka Z. <i>et al.</i> 2002, Czosnyka Z. H. <i>et al.</i> 2005)	40
Figure 2.18: Outline of shunt test rig (Schuhmann <i>et al.</i> , 2000).....	43

Figure 2.19: Schematic representation of valve, reservoir and inlet/outlet used in the set-up. (Francel <i>et al.</i> , 2001).....	45
Figure 2.20: Experimental set up. (Arnell <i>et al.</i> 2009, Eklund <i>et al.</i> 2004b, Lundkvist <i>et al.</i> 2003).....	47
Figure 2.21: A: Laboratory test rig to study the shunt behaviour along with pumping action (Bromby <i>et al.</i> 2007).	49
Figure 2.22: Graphic representation of shunt testing system. (Cheatle <i>et al.</i> 2012)..	51
Figure 2.23: Photographic images of explanted proximal catheters (Lin, <i>et al.</i> , 2003)	57
Figure 2.24: Outline of the implantable transducer (Bork <i>et al.</i> , 2010).....	60
Figure 2.25: Diagrammatic representation of Miethke’s mechatronic valve system (Momani <i>et al.</i> 2011)	61
Figure 2.26: Intelligent way of controlling mechatronic valve (Momani <i>et al.</i> , 2011)	62
Figure 2.27: Photographic image of iPhone assisted ventricular catheter placement (Thomale <i>et al.</i> 2013).....	63
Figure 2.28: A 3-dimmmensional structure of the proximal catheter fitted with the magnetic microactuator. (Lee <i>et al.</i> 2011).	66
Figure 2.29: Outline of Hydrocephalus shunt catheter bioreactor system (HSCB). (Harris <i>et al.</i> 2010).....	68
Figure 2.30: Ideal properties of proximal catheter	71
Figure 3.1: Photographic representation of electrostatic spinning rig. (Andrews <i>et al.</i> 2008)	81
Figure 3.2: Illustration of in-house built physical model.....	85
Figure 3.3: Photograph of an EPU module for hydraulic permeability determination..	89
Figure 3.4: Scanning electron microscpy images for a range of EPU catheter.....	92
Figure 3.5: Comparison of pressure vs. flow relationship for the shunt components	94
Figure 3.6: EPU hydrodynamics for all the samples	97
Figure 3.7: Average EPU hydrodynamics for low, medium and high.....	101

Figure 3.8: Hydraulic permeability of EPU groups (low, medium and high).....	101
Figure 3.9: The correlation between hydraulic permeability and I _{fs} (a) and, F _{dia} (b).....	102
Figure 4.1: Cross-sectional view of sample secured in a 96 well plate.....	114
Figure 4.2: Cross-sectional view of sample secured in a petri dish.....	115
Figure 4.3: Immunofluorescence image of Astrocytes culture after isolation.....	120
Figure 4.4: Standard curve of 3T3 and astrocytes after 8 hours in culture.....	121
Figure 4.5: Growth Curve of 3T3 and Astrocytes for lower seeding densities.....	123
Figure 4.6: Growth Curve of 3T3 and Astrocytes for higher seeding densities.....	123
Figure 4.7: The mean reduction in AB expressed in percentage terms after 48h (a) and 96h (b) for 3T3 cells grown on non-treated PDMS, Z1A1, Z3A1, EPU, SF, Positive Control (TCP P1) and Negative Control (H).	125
Figure 4.8: The mean reduction in AB expressed in percentage terms after 48 hours for 3T3 cells grown on non-treated substrates (PDMS, Z1A1, Z3A1, EPU, SF, P1 and P2) on non-plasma treated plates (a) and TCP (b).....	127
Figure 4.9: The mean reduction in AB expressed in percentage terms after 48 hours for astrocytes cells grown on non-treated substrates (PDMS, Z1A1, Z3A1, EPU, SF, P1 and P2) on non-plasma treated plates (a) and TCP (b).	128
Figure 4.10: The mean reduction in AB expressed in percentage terms after 96 hours for 3T3 cells grown on non-treated substrates (PDMS, Z1A1, Z3A1, EPU, SF, P1 and P2) on non-plasma treated plates (a) and TCP (b).	129
Figure 4.11: The mean reduction in AB expressed in percentage terms after 96 hours for astrocytes cells grown on non-treated substrates (PDMS, Z1A1, Z3A1, EPU, SF, P1 and P2) on non-plasma treated plates (a) and TCP (b).	130
Figure 4.12: The mean reduction in AB expressed in percentage terms after 48 hours for 3T3 cells on PDMS, Z1A1, Z3A1, EPU, SF, Negative Control (Non-treated Plate P1) and Positive Control (Treated Plate P1) with BSA (a), non-treated (b) and Fn-BSA (c).....	132
Figure 4.13: The mean reduction in AB expressed in percentage terms after 48 hours for astrocytes cells on PDMS, Z1A1, Z3A1, EPU, SF, Negative Control (Non-	

treated Plate P1) and Positive Control (Treated Plate P1) with BSA (a), non-treated (b) and Fn-BSA (c).	133
Figure 4.14: The mean reduction in AB expressed in percentage terms after 96 hours for 3T3 cells on PDMS, Z1A1, Z3A1, EPU, SF, Negative Control (Non-treated Plate P1) and Positive Control (Treated Plate P1) with BSA (a), non-treated (b) and Fn-BSA (c).....	134
Figure 4.15: The mean reduction in AB expressed in percentage terms after 96 hours for astrocytes on PDMS, Z1A1, Z3A1, EPU, SF, Negative Control (Non-treated Plate P1) and Positive Control (Treated Plate P1) with BSA (a), non-treated (b) and Fn-BSA (c).	135
Figure 4.16: The relative cell number on Z1A1, Z3A1, EPU and SF in comparison to PDMS in percentage terms after 48 hours for 3T3 cells (a) and astrocytes (b) before and after treatment.	137
Figure 4.17: The relative cell number on Z1A1, Z3A1, EPU and SF in comparison to PDMS in percentage terms after 96 hours for 3T3 cells (a) and astrocytes (b) before and after treatment.	138
Figure 4.18: Fluorescence microscope images of 3T3 cells taken after 48 hours in culture on glass coverslips. Image on left shows viable fibroblasts (left) and fibroblast following exposure to ethanol by way of control (right).....	139
Figure 4.19: Fluorescence microscope images of 3T3 cells taken after 96 hours in culture on Fn-BSA treated and non-treated samples.....	141
Figure 4.20: Fluorescence microscope images of Astrocytes taken after 96 hours in culture on Fn-BSA treated and non-treated samples.....	142
Figure 5.1: Schematic diagram of the shunt obstruction model.	152
Figure 5.2: Mean percentage reduction of AB for astrocytes and 3T3 grown on EPU catheters post seeding and perfusion.....	155
Figure 5.3: Hydraulic Permeability compared with no cells and perfusion for astrocytes and 3T3 grown EPU catheters.....	156
Figure 5.4: Mean percentage reduction of AB compared with post seeding and perfusion/static for non-treated and Fn-BSA treated EPU catheters.	158

Figure 5.5: Hydraulic permeability compared with before seeding and post perfusion/static for non-treated and Fn-BSA treated EPU catheters.....	160
Figure A.1: Dimensional analysis of proximal and distal catheter.....	192
Figure B.1: Elemental analysis of proximal and distal catheter.....	194
Figure B.2: Scanning electron microscopy image of proximal catheter.....	195
Figure B.3: Scanning electron microscopy image of distal.....	196
Figure C.1: Conventional proximal catheter flow dynamics.....	198
Figure C.2: Distal catheter flow dynamic.....	199
Figure C.3: Fixed pressure and programmable valve flow dynamics.....	200
Figure D.1: Fluorescence microscope images without the presence of cells on EPU and glass slide.....	201

List of Tables

Table 2.1: Composition of CSF and blood serum (Maurer 2010).....	6
Table 2.2: Causes of early and late shunt failure (Browd et al., 2006b).....	55
Table 2.3: Comparison of methods to prepare porous PU	76
Table 3.1: The Ifs (a) and fibre diameter (b) of EPU inner and outer surface	93
Table 3.2: Resistance of the shunt components.....	95
Table 3.3: Resistance to flow for flow in direction of inside to outside and outside to inside for four EPU catheter.....	96
Table 3.4: EPU samples hydraulic permeability and resistance.....	99
Table A.1: Dimensional analysis of hydrocephalus catheter.....	193

List of Abbreviations

AB	alamarBlue®
ABP	Arterial Blood Pressure
AP	Atmospheric Pressure
BSA	Bovine Serum Albumin
CH	Communicating Hydrocephalus
CNS	Central Nervous System
CSF	Cerebrospinal Fluid
CT	Computerised Tomography
DAPI	4', 6-diamidino-2-phenylindole
DMAc	Dimethylacetamide
DMEM	Dulbecco's modified Eagle's medium
DMSO	Dimethyl Sulfoxide
DNA	Deoxyribonucleic Acid
ECM	Extracellular Matrix
EPU	Electrospun Polyurethane
F.dia	Fibre Diameter
Fn	Fibronectin
FBS	Foetal Bovine Serum
GFAP	Glial Fibrillary Acidic Protein
H	Silicone Hydrogel
HSCB	Hydrocephalus Shunt Catheter Bioreactor
ICP	Intracranial Pressure
ID	Inner Diameter
Ifs	Inter-Fibre Separation

MEMS	Micro-Electro-Mechanical Systems
MRI	Magnetic Resonance Imaging
NAC	N-acetyl L-cysteine
NCH	Non-communicating Hydrocephalus
NPH	Normal Pressure Hydrocephalus
OD	Outer Diameter
PBS	Phosphate Buffered Saline
PEG	Poly (Ethylene) Glycol
PDMS	Poly (Dimethyl) Siloxane
PTFE	Polytetrafluoroethylene
PU	Polyurethane
RAP	Restricted Arterial Pulsation
TCP	Tissue Culture Plastic
SAS	Subarachnoid Space
SEM	Scanning Electron Microscopy
SF	Silicone Foam
UV	Ultra Violet
VC	Venous Congestion

List of publications

Journal Publication

Suresh S, Black RA (2014), Electrospun polyurethane as an alternative ventricular catheter and *in vitro* model of shunt obstruction. *J Biomater Appl* (Accepted on 20th Aug 2014)

Conference Proceedings

Suresh S, Black RA (2013), Comparison of cell growth on CSF shunts catheter materials during static and dynamic perfusion culture. *UK Bioengineering Conference, Glasgow*

Suresh S, Black RA (2013), *In vitro* model of shunt catheter obstruction. *Int J Artif Organs*, 36 (8): 547-548

Suresh S, Black RA (2013), Comparison of CSF shunt catheter materials *in vitro*. *12th Annual Conference of the UK Society for Biomaterials, Birmingham*

Suresh S, Black RA (2013), Comparison of CSF shunt catheter materials *in vitro*. *Glasgow Neuroscience Day, Glasgow* (Won Best Poster Award)

Suresh S, Chumas P, Black RA (2012), Modelling intracranial pressure and flow of cerebrospinal fluid in hydrocephalus shunt. *World Congress Medical Physics and Biomedical Engineering, Beijing (China)*

CHAPTER 1

INTRODUCTION

Hydrocephalus is a neurological condition characterised by the accumulation of cerebrospinal fluid (CSF) in the ventricles or cavities of the brain, brought about by an imbalance in formation and absorption of CSF. The excess CSF causes the intracranial pressure (ICP) to rise, and progressive enlargement of the ventricles, giving rise to brain damage which may lead to death if untreated. For the paediatric neurosurgeon hydrocephalus remains to be the most commonly faced clinical problem (McAllister 2011).

The prevalence in infants is reported to be almost 1 in 1000 babies, both live and stillborn (Faghih Jouibari *et al.*, 2011). The enlarged ventricles from computerised tomography (CT) scans and abnormal head circumference are the common diagnostic indicators in children (Naradzay *et al.*, 1999). In the elderly (population), normal pressure hydrocephalus is more prevalent, the symptoms of which include urinary incontinence, gait disturbance, dementia and confusion (Czosnyka Marek *et al.*, 2004; Eide *et al.*, 2010). In neonates, intracranial haemorrhage occurs due to lack of formation of brain ventricles or acquired due to other central nervous disorders; whereas in later stage of life, it is caused by meningitis, tumour or traumatic head injury (Bork *et al.*, 2010; Zhang *et al.*, 2006).

Hydrocephalus is an incurable condition at present (Williams *et al.*, 2007). The most common treatment option available is implantation of CSF shunt device, to divert the excess CSF to another part of the body, where it is absorbed. The three main components to the hydrocephalus shunt series are, i) a proximal collecting catheter, which is inserted into the ventricle of the brain allowing excess CSF to flow through the shunt, ii) a valve to control the flow/pressure through the shunt, and iii) a distal catheter that passes excess CSF to either the peritoneum or right atrium. Although the mortality rate has decreased since their introduction in the 1950s, the incidence

of shunt failure remains unacceptably high, which may be attributed in large part to the lack of substantial development in the advancement of the device (Drake *et al.*, 2000; Tuli *et al.*, 2000).

Shunts fail for many reasons, but the failure that causes the greatest impact is obstruction of the shunt catheters; proximal occlusion being the most common (Browd *et al.*, 2006b). In fact, 20 to 30 % of shunt failure in the first year of surgery is caused by obstruction (Bork *et al.*, 2010). The main sources of obstruction are the glial cells, which invade the perforations (fenestrations) in the walls of the ventricular catheter, preventing the entry of the CSF (Thomale *et al.*, 2010). The obstruction in all cases necessitates replacement of the catheter, which, in turn, may lead to further complications and discomfort for the patients (Achyuta *et al.*, 2010).

Since shunt devices were introduced, several improvements in shunt design have been made, including alternative drainage locations, ventricular catheter placements, new valve designs, catheter assembly design, anti-siphon device, on-off devices, gravity-actuated changes in opening pressure and externally adjustable valve (Stein and Guo 2008). Nevertheless, to date, there is no one valve that is proven to be superior (Drake *et al.*, 2000). Arguably one of the most contemporary and cutting-edge areas of research being explored involves creating a smart shunt in which the valve is capable of being controlled remotely. A shunt that can regulate CSF more effectively, and is less susceptible to malfunction, would have obvious benefits to the patient (Bork *et al.*, 2010; Momani *et al.*, 2011). Although such advances would represent a milestone in hydrocephalus shunt device development, a blocked catheter will inevitably lead to revision surgery (Lutz *et al.*, 2013).

Having conducted a comprehensive review of the literature it would appear that relatively few researchers have engaged in research on the development of an alternative catheter system for hydrocephalus shunt systems. There is a lack of design criteria for the proximal catheter available at present (Harris and McAllister 2011; Lin *et al.*, 2003; Thomale *et al.*, 2010). More than 80% of the perforations present in the proximal catheter are not in use, and may become easily blocked (Lin *et al.*, 2003). Conventional catheters are made of poly(dimethyl)siloxane (PDMS),

with few, if any, exceptions, although there are studies which involve surface modification of PDMS to reduce the cell attachment (Achyuta *et al.*, 2010; Harris *et al.*, 2011a; b).

The aim of the research detailed in this thesis is to develop an alternative ventricular catheter, which can overcome the drawbacks of conventional catheter forms.

The layout of the thesis is detailed below:

Chapter 1: begins with the brief introduction of the research field. This chapter highlights the importance and precedence of current research in the field, as well as identifying gaps in knowledge and establishing the rationale for the research on which this thesis is based.

Chapter 2: details the fundamentals of the ventricular system of the human brain, the complications leading to hydrocephalus, the conditions and nature of the disease, available treatment options. It explores the cutting-edge medical device systems in use today, their performance, and types of failure conditions of the system and their causes. It describes also the various modelling approaches, both physical and numerical, that have been applied to study the pressure/flow relationships in shunt devices. Recent improvements in shunt technology and performance are presented and discussed. The chapter concludes with the importance of the proximal catheter, developments and material choices, and the possible polymer processing techniques available for the fabrication of an alternative form of catheter.

Chapter 3: presents the materials and methods employed to characterise the material properties and quantify the hydraulic performances of existing hydrocephalus shunt components and systems. The experimental methods to quantify the hydrodynamic properties of the proposed alternative ventricular catheter forms, in particular, along with the results obtained are discussed. The suitability of the new catheter is determined by direct comparison with a conventional catheter in terms of pressures and flows.

Chapter 4: focuses on the interaction of cells with a number of candidate catheter materials. The isolation and culture of primary astrocytes and 3T3 are outlined. Both the cell types were exposed to cast film and macro/micro porous substrates (PDMS and polyurethane) in the presence of two key proteins present in CSF (albumin and fibronectin). Cell viability on each substrate was quantified using commercially available assays, and expressed both qualitatively and quantitatively, with reference to appropriate control surfaces. The statistical significances of the data are reported.

Chapter 5: describes the series of experiments designed to quantify cell growth and viability of cells cultured on the alternative form of catheter under static and perfusion culture, and in the presence of fibronectin. The presence of cells and their effect on the hydraulic permeability of the catheter material are reported. The hydraulic permeability was taken as the measure of the degree of CSF obstruction.

Chapter 6: evaluates the contribution of this work with reference to the original research objectives. The significance of the results and limitation of the study are discussed.

Chapter 7: summarises the work on which this thesis is based. The chapter concludes the author's perspective and recommendation for taking the research forward.

CHAPTER 2

BACKGROUND AND LITERATURE

REVIEW

2.1 Introduction

This chapter presents the relevant background information about hydrocephalus and summarises past and more recent developments in hydrocephalus shunt systems. The critical review of the drawbacks of current shunt catheter systems, innovations made so far in the field and investigation of possible solutions to enhance the quality of life of the hydrocephalus patient. The aims and objectives for the research will be drawn out from this chapter.

2.2 Cerebrospinal Fluid

The brain is one of the most important organs of the body, and is secured inside the skull for its protection. The rigidity of the skull gives rise to interesting haemodynamic characteristics of the cerebral circulation, which is unique. The highly pulsatile nature of blood flow through the cerebral arteries, and outflow via veins, can potentially damage the microcirculation within the brain (Madsen *et al.*, 2006). This risk of damage is mitigated by cerebrospinal fluid (CSF), which is found in four cavities, or ventricles, inside the brain, and bathes the entire brain and central nervous system (CNS) (Linninger *et al.*, 2007). The intracranial dynamics are complex, but it is controlled through a series of synchronised feedback processes (autoregulation) involving the brain, cerebral blood flow, CSF and intracranial pressure (ICP) to ensure the smooth flow of blood to the brain (Cohen *et al.*, 2009; Panerai 2003) which is explained in detail in the following section.

In air, the human brain weighs about 1400 g, whereas it has an effective weight of about 50 g when submerged in CSF; a relative density of 1.04 (Ross and Eynon 2005). The role of CSF is to protect the brain by acting as a reservoir to

accommodate intracranial volume expansions (Eklund *et al.*, 2007). CSF forms the major part of the extracellular fluid of the CNS (Oreskovic and Klarica 2010). The brain and the entire spinal cord are contained in CSF, which, in adults, occupy a volume of approximately 1650 ml (Eklund *et al.*, 2007).

CSF is a colourless liquid composed of saline solution containing ~0.3% plasma proteins at concentrations in the range 15 to 40 mg/dL (Linninger *et al.*, 2007), of which albumin and fibronectin are the most abundant (Brydon *et al.*, 1998). The detailed composition of CSF and serum is outlined in Table 2.1. CSF bathes the brain and the entire spinal cord to keep the brain tissue hydrated, to act as a shock absorber and to reduce the brain weight inside the skull by ~97 % (Eklund *et al.*, 2007; Stivaros and Jackson 2007). The absence of a lymphatic system in the brain is replaced by CSF in terms of the transport of nutrients, waste and neurotransmitters (Segal 1993). CSF clears the metabolites formed in the brain such as CO₂ and lactate (Eklund *et al.*, 2007).

Component/ Parameter	CSF	Serum
Water (%)	99	93
Protein (mg/dL)	35	7000
Glucose (mg/dL)	60	90
Osmolarity (mosm/l)	295	295
Na ⁺ (mmol/l)	138	138
K ⁺ (mmol/l)	2.8	4.5
Ca ²⁺ (mmol/l)	2.1	4.8
Mg ²⁺ (mmol/l)	0.3	1.7
Cl ⁻ (mmol/l)	119	102
pH	7.33	7.41

Table 2.1: Composition of CSF and blood serum (Maurer 2010)

2.2.1 CSF Production, Circulation and Absorption

CSF is produced and circulated by the choroid plexus and ependymal cells present in the lateral, third and fourth ventricular walls (Bork *et al.*, 2010; Eklund *et al.*, 2007; Maurer 2010). CSF occupies the space between the subarachnoid and pial layers of the meninges (Reiber 2003), as shown in Figure 2.1. The choroidal cells are joined together on the CSF by occluding band of tight junctions, the site of the blood-CSF barrier (Segal 1993).

The electrolyte such as Na^+ , K^+ and Cl^- are key ions which is responsible for CSF secretion (Maurer 2010). From Table 2.1 it is evident that Na and Cl ions present within CSF and serum are relatively the same. However, non-electrolytes such as glucose and proteins present in CSF are lower in concentrations when compared to serum. The choroid plexus takes up Na^+ from the blood side and the rate of entry of this ion into the CSF reflects the rate of CSF secretion. Segal (1993) states that production of CSF depends upon 1) active transport of Na ion to generate a gradient for this ion across the chorodial walls and 2) exchange of Cl ions on the blood side of cells leading to a raised intracellular concentration of Cl^- anion in the cell. The ionic movement generates osmotic gradient drawing water from the cells and tight junctions.

An average secretion rate of CSF is 0.35 ml/min (500 ml/day) means that at any one point of time there is about ~150 ml of CSF in the brain, which is replenished 3 to 4 times a day (Czosnyka Marek *et al.*, 2004; Smillie *et al.*, 2005; Stivaros and Jackson 2007). The pressure within the ventricular system, known as ICP, ranges from 20 to 25 mmHg on average (Czosnyka M. and Pickard 2004; Momani *et al.*, 2011; Ross and Eynon 2005). The pressure gradient that exists between the arterio-venous system acts as the driving force for the production and flow of CSF in most cases.

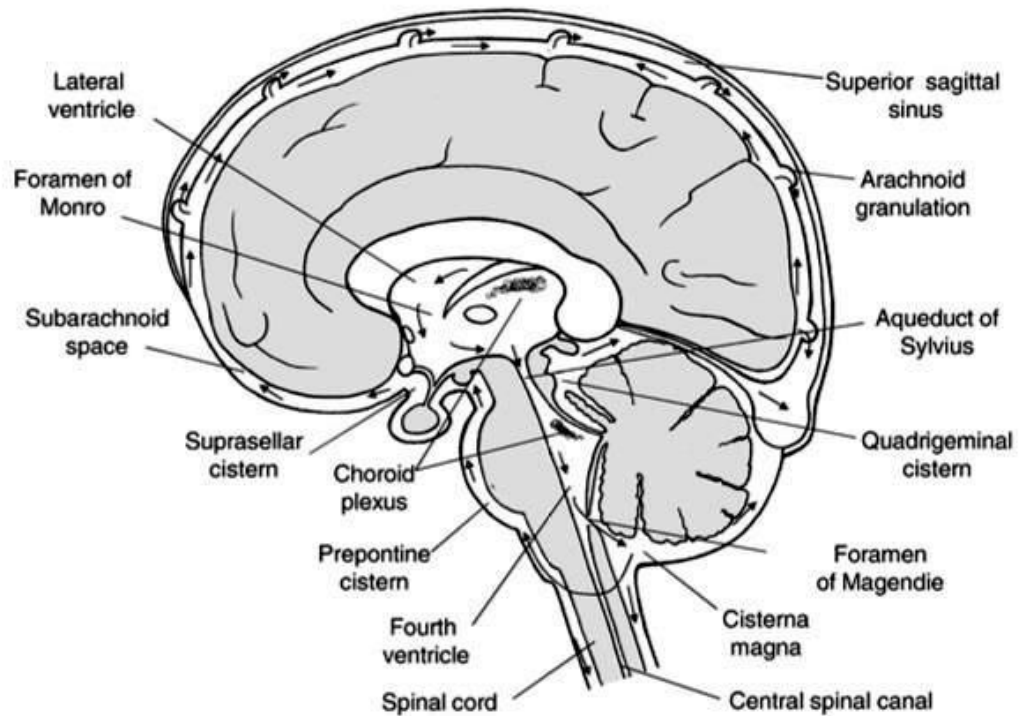


Figure 2.1: Circulation of CSF flow in the human CNS. Grey area represents the CSF and the arrows indicate the direction of CSF circulation and the sites of CSF absorption (Oreskovic and Klarica 2010). CSF is mainly generated in the lateral and third ventricles, from where it flows along the Aqueduct of Sylvius to reach the fourth ventricle. From the fourth ventricle, CSF travels out of the midline Foramen of Magendie into the Subarachnoid Space, which contains a network of cisterns (Eklund et al., 2007). The majority of CSF absorption occurs around the tentorium, which lies upwards to the Superior Sagittal Sinus (Czosnyka Marek et al., 2004; Stivaros and Jackson 2007).

CSF drainage into the venous compartment takes place in the arachnoid granulation, which penetrates the walls of the sagittal sinus (Fig. 2.2) (Eklund *et al.*, 2007).

Venous drainage is directly proportional to the pressure gradient that exists between the CSF side of granulation and the sagittal sinus. The outflow resistance of CSF flow is the inverse of the coefficient of proportionality, which in normal subjects varies from 6 to 10 mmHg ml⁻¹ min⁻¹ (Czosnyka Marek *et al.*, 2004; Stivaros and Jackson 2007).

Reverse transport of CSF through the arachnoid granules is not possible: CSF absorption will not take place if the subarachnoid ICP is less than the sagittal sinus pressure. It follows that the ICP is affected by the production and absorption of the CSF. This concept of CSF production and absorption is called the bulk flow theory. There are limitations to this concept, since it does not include the absorption via the capillaries of CNS; nor does it explain the maintenance of constant pressure within the cranium (Stivaros and Jackson 2007).

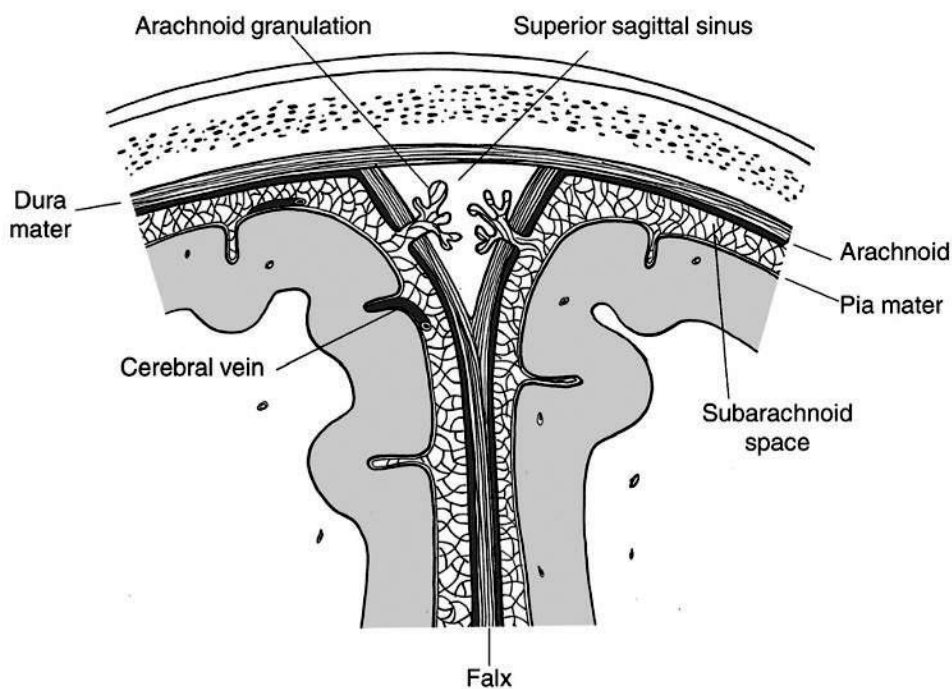


Figure 2.2: Frontal plane illustration of CSF absorption sites including arachnoid granulation and superior sagittal sinus (Oreskovic and Klarica, 2010)

Intracranial dynamics is complex in nature because of the unique structural and geometric properties of the human brain and surrounding tissues. It consists of fluid compartments including ventricles, blood and subarachnoid space and porous parenchymal tissue (Linninger *et al.*, 2007). Since the skull has a fixed volume, the laws of continuity dictate that any increase in volume or pressure in one compartment must be accommodated by another. This explains why CSF pressure variations are directly affected by arterial blood pressure; hence the pressure-volume relationship of CSF and the vascular system of the CNS should be considered together (Friden and Ekstedt 1982). This theory is referred to in the literature as the Monro-Kellie hypothesis, which states: “if the skull is intact, then the sum of the volume of the brain, CSF and intracranial blood is constant”. As the intracranial blood volume increases the CSF volume has to decrease or vice versa to accommodate change in volume (Ross and Eynon, 2005).

The normal systolic expansion of the basal cerebral arteries, or increase in intracranial blood volume, generates a pressure wave within the subarachnoid space. This leads to an outflow of CSF through the foramen magnum, which can accommodate an increase in intra-cerebral blood volume of up to ~50%. There is also an increase in ICP, which is compensated by flow of CSF from the subarachnoid space through the arachnoid villi into the venous sinuses. Under normal circumstances, the production of CSF is balanced by constant absorption. On the other hand, relaxation of the artery during diastole, or decreased intracranial blood volume, causes CSF to flow into the cranium from the foramen magnum. This mechanism affords a means whereby stored CSF is returned into the cranium compartments, to compensate for any decrease in ICP and/or intracranial blood volume. This completes the cycle of CSF flow into and out of the cranium through foramen magnum, in order to keep the volume in the brain constant (Magram 1995; Stivaros and Jackson 2007).

The pressure within the cranium (ICP) is also liable to vary drastically due to pressure generated in the arteries and veins in the brain. During the systolic pulse wave in the subarachnoid space, the cortical surface of veins is compressed. This

means the systolic pressure is transmitted to the major dural venous sinuses by systolic expansion of arachnoid granulation (Magram, 1995). Variance in pressure is accepted only up to a limited range: when it exceeds 25 mmHg, it is considered to be abnormal. This problem is addressed by the placement of arteries, which are in direct contact with veins: the Windkessel effect, where capillary flow is maintained at a constant level by the elastic properties of the artery walls, which absorb the energy created during systole and release it during diastole (Stivarous and Jackson, 2007).

The Monro-Kellie and Windkessel effects exemplify just two of the mechanisms that help to sustain a constant flow in the cerebral capillary bed and to accommodate the pressure changes that take place throughout the cardiac cycle whilst maintaining ICP within the normal physiological range (Stivarous and Jackson, 2007). While our understanding of the theory behind CSF circulation has improved in recent years (Fig. 2.3), cerebral haemodynamics and autoregulation is still a vibrant topic for debate (Angarita-Jaimes *et al.*, 2014; Panerai 2013).

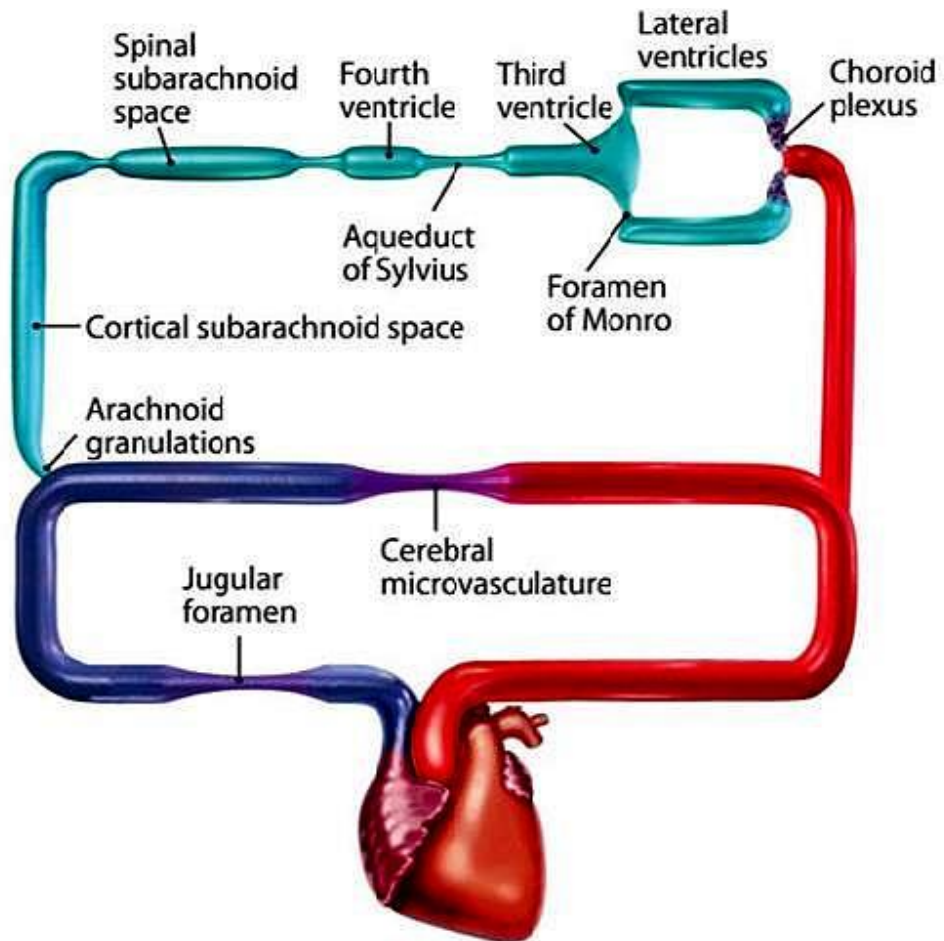


Figure 2.3: Cerebral blood flow (dark blue and red colour) and CSF flow (light blue) in form of circuit diagram. CSF is produced at choroid plexus. Arteries (red) are connected to veins through cerebral microvasculature (capillaries). CSF flows from arachnoid granulations to venous sinus during systole. CSF flows into the cranium from foramen of monro during diastole. (Rekate 2008)

2.3 Hydrocephalus condition and treatment

There are many neurological disorders that alter the brain ventricular dynamic system, of which hydrocephalus is one. Hydrocephalus, known colloquially as “water on brain”, is a neurological condition caused by the abnormal accumulation of CSF in the ventricles, cavities or capillaries of the brain (Fig. 2.4) (Bayston 1994; Schley *et al.*, 2004). Eklund and co-workers (2007) describe the various manifestations of hydrocephalus as being caused by disturbance in CSF, which leads to enlarged ventricles. Von Koch *et al.* (2003) state that hydrocephalus occurs when there is an incompatibility between CSF absorption and production, while Bork *et al.* (2010) describe hydrocephalus as one of the most common congenital disorders of the central nervous system. Tuli *et al.* (2000) mentions hydrocephalus as the most endemic condition seen in paediatrics. Hydrocephalus is usually diagnosed within the first six months of life, in some cases later detection or inception occurs (Bayston, 1994).

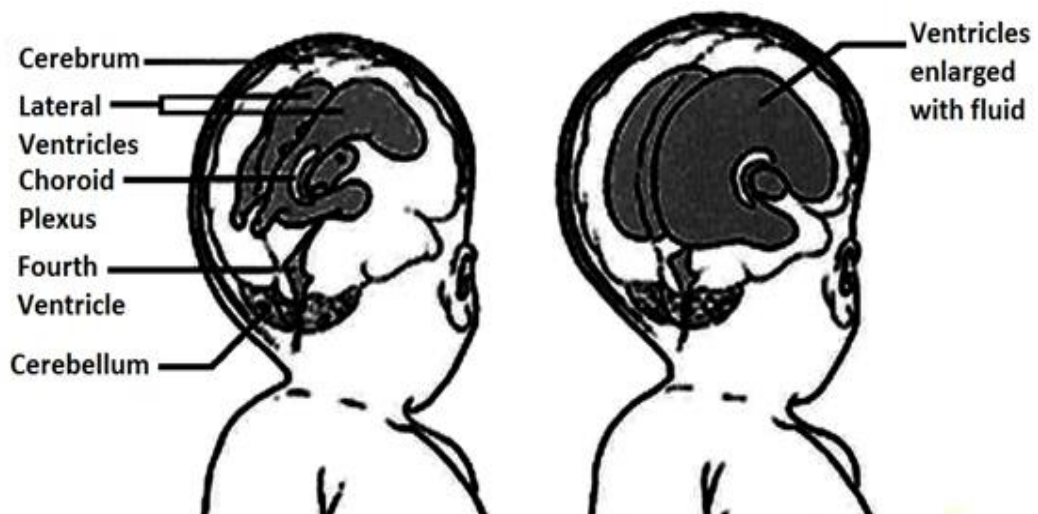


Figure 2.4: Normal (left) and Hydrocephalus child's (right) ventricle of the brain. Enlargement in ventricles due to the accumulation of CSF is clearly seen in the diseased brain (<http://www.cyh.com/HealthTopics>)

In the hydrocephalic patient, normal CSF drainage and absorption are affected because of an increase in resistance to CSF circulation. According to Magram, (1995) while there is a sharp increase in ICP during systole, there is not a corresponding increase in intracranial blood volume because the CSF is not adequately drained. During diastole, there is a drop in intracranial blood volume and subsequent reduction in ICP. Over time, however, the continual production of CSF and compromised drainage/absorption results in the accumulation of CSF in the intracranial compartment.

Schley *et al.* (2004) explains that the excess CSF causes rise in ICP inside the skull and progressive enlargement of the head leading to brain damage and may lead to death if untreated. In children and adults, the excess ICP is compensated by raised arterial blood pressure (ABP) so as to maintain the cerebral perfusion pressure; hence, the brain will have a constant supply of oxygen and glucose. In neonates and infants, on the other hand, the skull bones are not completely formed, with the result that the skull expands in volume to accommodate the accumulation of CSF and rise in ICP, which is painful and, ultimately, life-threatening (Fig. 2.5). An abnormal head circumference remains an important diagnostic indicator for the condition in children.



Figure 2.5: Six months old child with a severe hydrocephalus condition with a head circumference of 94 cm which is almost twice the normal circumference (Faghieh Jouibari et al. 2011)

There are many medical reasons for the development of hydrocephalus, but dilation of ventricles is one of the most common outcomes (Faghieh Jouibari *et al.*, 2011). Bayston (1994) argues that aqueduct and other pathways of the CSF circulation may be obstructed due to the presence of a blood clot, inflammation within the CNS, and oedema secondary to infection and/or intracranial injury. The most common anatomically-related development disorders of the CNS associated with hydrocephalus are spina bifida and chiari malformations. In neonates, periventricular haemorrhage and neural tube defects are often contributing factors. Hydrocephalus may also occur later in life following haemorrhage, stroke or other cerebrovascular accident in later life, meningitis, CNS tumours and benign ventricular cysts (Bayston, 1994; Bork *et al.*, 2010).

2.3.1 Types of Hydrocephalus

Human hydrocephalus is classified into two categories: congenital and acquired (Zhang *et al.*, 2006). Congenital hydrocephalus is the most common category. It occurs on its own (non-syndromic) or as a complication secondary to other syndromes (syndromic) (Zhang *et al.*, 2006). To date, there is no clear understanding of this condition, and progression of the disease is dynamic. One of the main causes of congenital hydrocephalus is intraventricular haemorrhage. Other predisposing factors include premature birth, where there is lack of brain ventricular development, and disturbed cellular function (McAllister 2011).

In 1960, another form of this disease was identified, namely acquired or adult onset hydrocephalus. Here, there is no increase in ICP but there is an abnormality in CSF reabsorption and ventricular enlargement (Stein and Guo 2009; Zhang *et al.*, 2006). Because there is no elevation in ICP, this condition is referred to as Normal Pressure Hydrocephalus (NPH). NPH is a chronic form of hydrocephalus that mostly affects adults older than 60 years of age (Bork *et al.*, 2010). The causes of acquired hydrocephalus are unclear, but it is thought to be due to the gradual deterioration of the normal compensatory mechanisms or the result of disturbances in CSF absorption due to ageing (Zhang *et al.*, 2006). The clinical symptoms of NPH are dementia, gait disturbance and urinary incontinence (Bork *et al.*, 2010; Eide *et al.*, 2010; Eklund *et al.*, 2007).

There are three sub-types of hydrocephalus: communicating (CH), non-communicating/obstructive (NCH), and NPH (Momani *et al.*, 2008). McAllister (2011) states that partial or complete hindrance in the cerebral ventricles, specifically in the cerebral aqueduct, causes obstructive hydrocephalus, whereas a blockage anywhere in the subarachnoid space leads to CH. The site of blockage in CH is not very easy to visualise, even with use of high resolution image technology, and there is free movement of CSF within the ventricles and subarachnoid space. The cause of ventricular enlargement in NCH, on the other hand, is much clearer according to Pena and co-workers. By using the biomechanics tools to study the condition, these authors attributed the cause of ventricular dilation in CH to a reduction in reversal of

interstitial flow into the parenchyma, and shrinkage in tissue elasticity. In NCH, obstruction in the aqueduct of Sylvius gives rise to a pressure gradient between the lateral ventricles and subarachnoid space. The excess CSF follows the gradient into the parenchyma, to be absorbed at the sagittal sinus (shown in black to the left of Figure 2.6). In CH, on the other hand, since the site of obstruction is located in the sagittal sinus rather than the aqueduct of Sylvius, the prevailing pressure gradient allows excess CSF to be absorbed by the parenchyma (shown in black on the right of Figure 2.6).

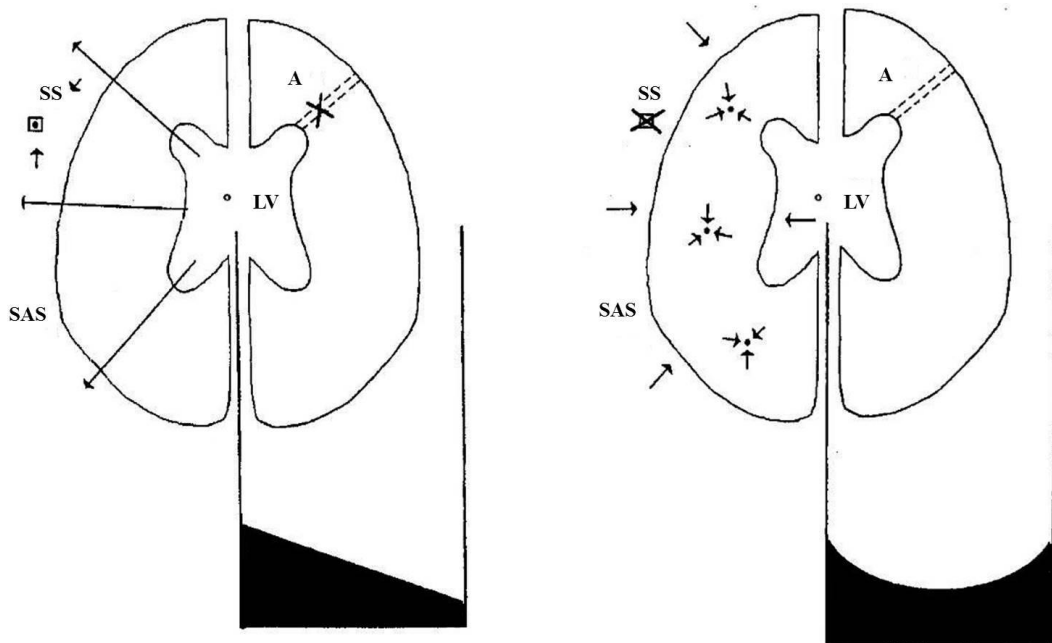


Figure 2.6: Non-communicating (left) versus Communicating (right) Hydrocephalus.

Arrow - interstitial CSF flow, open dot - CSF source, close dot - CSF drainage, square - sagittal sinus, cross - obstruction, dotted lines - Aqueduct of Sylvius, LV - lateral ventricles, SAS - subarachnoid space and black portion - CSF flow due to pressure gradient (Pena et al., 2002)

Communicating hydrocephalus develops when there is a restriction in arterial pulsation. Greitz *et al.* (1994) refer to the condition as restricted arterial pulsation hydrocephalus (RAP hydrocephalus) and “increased capillary pulsation hydrocephalus” (Greitz *et al.* 2004). Here, a decrease in arterial expansion during systole leads to a corresponding decrease in compliance in the arterial wall or subarachnoid space, which is reflected on the flow of CSF through the foramen magnum (Chumas *et al.*, 2001; Greitz *et al.*, 1997). The decrease in compliance of the artery walls has been ascribed to various factors, including ectasia, arteritis, spasm, diabetic microangiopathy or small vessel disease (of Binzwanger type caused by damage to white brain matter). The reasons for reduction in compliance taking place in subarachnoid includes arachnoiditis secondary to subarachnoid haemorrhage or meningitis (Greitz *et al.*, 1997).

Non-communicating/obstructive hydrocephalus, on the other hand, is referred to by Greitz *et al.* (1994) as venous congestion (VC hydrocephalus), which occurs when there is restriction of CSF flow within the ventricular system. An imbalance between the CSF production and absorption may also contribute to a decrease in CSF outflow. The enlarged ventricles compress the cortical veins, which may lead to increase in cerebral blood volume and ICP. From a haemodynamic point of view, VC hydrocephalus is associated with venous obstruction and raised venous pressure (Chumas *et al.*, 2001; Greitz *et al.*, 1997).

NPH is a sub type of communicating hydrocephalus (Stivarous and Jackson, 2007). Here, as the name suggests, there is no increase in the ICP, but the absorption of CSF is compromised owing to enlargement of the ventricles, which may be the result of many factors, including ageing of ventricular system, damage caused by dementia and expansion/swelling of blood vessels in the brain. According to Eide *et al.*, (2010) the static and pulsatile ABP in NPH patient’s remains normal, which means the elevated ICP in these patients, are most likely due to decreased intracranial compliance.

Almost 1 in 1000 live and stillbirths worldwide are affected by hydrocephalus (Faghieh Jouibari *et al.*, 2011). According to The National Institutes of Health, in the United States almost 1 in 500 children are diagnosed with hydrocephalus every year (Lee *et al.*, 2011). The incidence of hydrocephalus in new-borns is reported to be between 0.3 to 2.5 per 1000 live births (von Koch *et al.*, 2003) and 1 in 500 – 2000 in new-borns (Bork *et al.*, 2010). Chumas *et al.* (2001) summarised current patient outcomes, reporting that 50% of the children suffering from hydrocephalus die before 3 years of age; only 20 to 23% reach adulthood, and of those only 38% will have normal intelligence. Most of the patients living with hydrocephalus will have some kind of neurological deficits (60% motor and 25% visual).

2.3.2 Hydrocephalus Treatments

There is no cure at the moment for hydrocephalus but several treatment options are available. Diuretics such as frusemide and acetazolamide, for example, are known to reduce CSF production, whereas intraventricular fibrinolytic treatment may be administered in the case of post haemorrhagic hydrocephalus (Chumas, *et al.*, 2001).

The most common treatment is the implantable ventriculo-atrial shunt (Borgbjerg *et al.*, 1995; Drake *et al.*, 2000; Kurtom and Magram 2007). Invented by Nulsen and Spitz over 60 years ago, the cerebrospinal shunt is a flexible catheter tube that drains the CSF from the intracranial cavity of the brain to an internal delivery site such as intra-abdominal cavity or right atrium of the heart in some cases, under the control of a passive mechanical valve system (Eklund *et al.*, 2007; Momani *et al.*, 2008). By draining excess CSF from the brain, it helps to restore and maintain intracranial pressure within certain limits. A variety of materials has been used for shunt treatment including silver, gold, glass, rubber tubes and threads of linen, but none of these were durable. The breakthrough came in 1950 when catheters made from poly(dimethyl)siloxane (PDMS) became available. This polymer, which could be loaded with Barium Sulphide (to be visible on X-Ray, Magnetic Resonance Imaging (MRI) and CT scan), was considered to be the most suitable material for this application (Bayston, 1994).

According to Eklund *et al.* (2004) hydrocephalus shunt implantation is one of the most common neurosurgical procedures, there being about 70,000 shunts implanted annually in developed countries in 1991. By 2010, Bork *et al.* reported that more than 100,000 shunt valves were being implanted each year worldwide. The corresponding figures for the UK, according to Chumas *et al.*, are about 3500 to 4000 procedures being carried out per year. In 2011, Lee *et al.* estimated that in the USA alone, some 400,000 shunt operations take place annually, costing the government about \$1 billion. The cost of each device ranges from £350 to £1100, and there are about dozen type available (2013 figures). The valve contributes to the majority of the costing.

In 1990, a neurosurgical procedure called endoscopic third ventriculostomy was introduced as an alternative to CSF shunt implantation (Romero *et al.*, 2013). The process involves creating an opening using an endoscope, which is inserted inside the ventricular system through a burr hole, in order to connect the third ventricle to the subarachnoid space (Chabrierie and Black 2002). This provides a new pathway for CSF to flow, bypassing the blocked aqueduct of Sylvius and outlet of foramina of the fourth ventricle, thereby restoring CSF reabsorption (Rekate 2008). The treatment is mostly suggested for patients suffering from non-communicating hydrocephalus with a single site of obstruction, and in a very few cases of communicating hydrocephalus. The success rate depends on many factors: the patient's age, anatomy, the existence of any additional disorders, and the origins of hydrocephalus (Romero *et al.*, 2013). Clinical evidence indicates that there is no great benefits of third ventriculostomy surgery over the implantation of shunt device for paediatric patients in terms of quality of life (Kulkarni *et al.*, 2010). For these reasons, the only treatment available for all types and cases of hydrocephalus remains the implantation of shunt device.

2.3.3 Hydrocephalus/CSF Shunt System

A typical CSF shunt series consists of three major components, as shown in Figure 2.7. The flow of CSF through the shunt is driven by the differential pressure between the ICP and peritoneal/arterial pressure (Aschoff *et al.*, 1995).

- **In flow/Proximal/Ventricular catheter**, which helps to drain the CSF from the ventricles/lumbar subarachnoid space by means of a tube positioned to transmit CSF to a valve. The proximal catheters feature a number of perforations, through which the CSF flows from the ventricular space into the shunt system.
- **Valve and Shunt Accessories** regulate the differential pressure and controls the flow of the CSF through the shunt tubing. There is a whole range of available valves, having different mechanism and properties, which are described in the following sections. Shunt accessories are used in some cases to prevent siphonage, and to facilitate the operation of the valve.
- **Outflow/Distal catheter**, which directs CSF from the valve to the peritoneum (ventriculoperitoneal shunt) or the right atrium of the heart (ventriculatrial shunt) where the excess CSF will be digested. A typical distal catheter is about 90 to 100 cm long. In infants, the catheter is coiled as it is inserted, which allows it to unwind as the child grows.

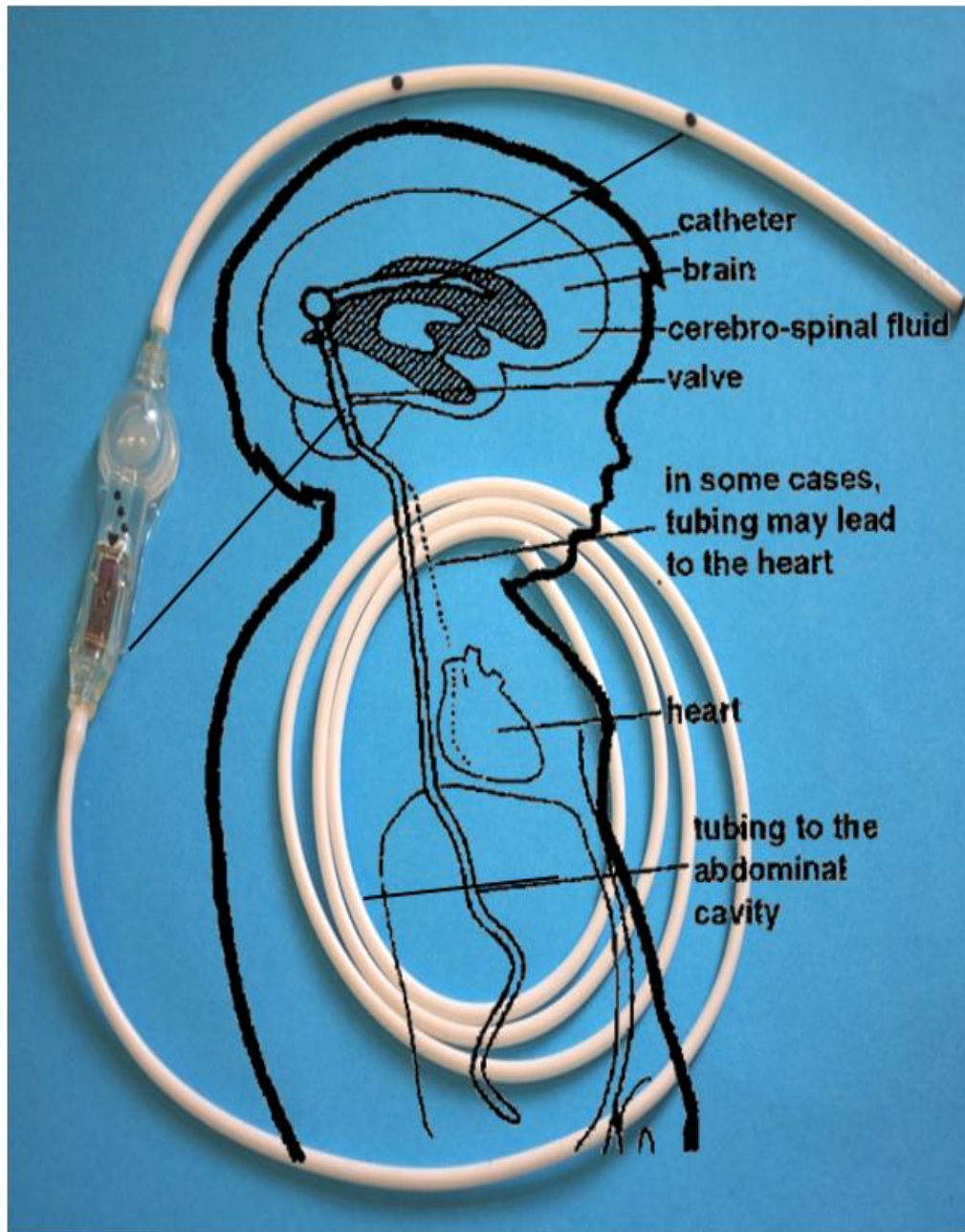


Figure 2.7: Codman Hakim Hydrocephalus shunt series and an implanted shunt diagram in a child. Perforated portion of the proximal catheter is positioned inside the ventricle (choroid plexus). Valve connected to the proximal catheter is implanted behind the ear or in some cases to the surface of the skull. Distal catheter connected to the valve is extended to the peritoneal cavity or in some cases to the atrium of the heart (<http://nhfonline.org/treatment.php>)

2.3.4 Types, Designs and Mechanism of Valve and Shunt Accessories

Valve and shunt accessories have been considered to be one of the vital components of the shunt system. Although the design has remained virtually unchanged since its introduction in 1950 by Nulsen and Spitz, there have been numerous incremental improvements and innovations in design since then (Drake *et al.*, 2000). The design of the different types of valves, including the very first valve is illustrated schematically in Figure 2.8. Most of the valves in use currently are designed to be controlled by the intracerebral variations of hydrostatic pressure (Sotelo 2012).

Most current valve designs are passive, their operation being determined by the differential pressure. Thus, circumstances may arise during normal activities that may lead to overdrainage (Lundkvist *et al.*, 2003). According to Kurtom and Magram (2007) the siphoning of the CSF through the shunt takes place when the outlet of the distal catheter is below the level of CSF present in the CNS, hence the change in posture of the patient has a direct impact on the operation of the shunt. The anti-siphon device was first introduced in 1971 by Portnoy and Schulte (Francel *et al.*, 2001). The need to incorporate a means of siphon regulation or prevention was recognised in the early '80s, and since that time a number of devices have become available that serve this purpose (Eklund *et al.*, 2004b; Francel *et al.*, 2001). There follows a brief overview of the shunt accessories available to counteract siphon effects.

Programmable/Adjustable valves were introduced 20 years ago, allowing surgeons for the first time to alter the opening pressure setting precisely without the patient having to undergo surgery for a replacement (Allin *et al.*, 2006; McGirt *et al.*, 2007). These devices enable the control the CSF flow non-invasively by means of a hand-held magnetic coupling device, which can adjust the opening pressure of the valve to a desired setting (Turner and Hall 2006). However, the exposure of any programmable valve to an unknown magnetic field can cause involuntary effects on the opening pressure of the valve (Lefranc *et al.*, 2010).

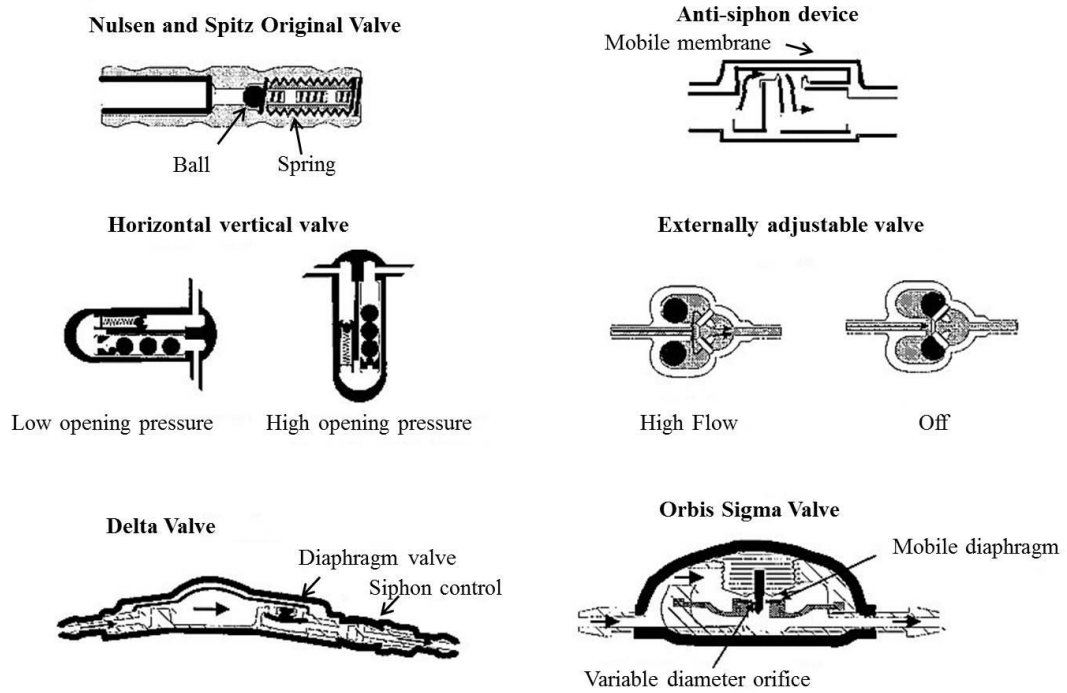


Figure 2.8: Design of different valve types available including the very first Nulsen and Spitz original ball valve on the top left corner, anti-siphon regulating valves, posture adjustment valve, magnetic adjustment to regulate pressure and flow restricting valves (Drake et al., 2000)

Codman[®] Hakim[®] (Codman, Johnson & Johnson, Raynham, Mass) produces a range of fixed-pressure valves with opening pressures of 10, 40, 70, 100 and 140 mm H₂O, and a magnetic programmable shunt valve, the opening pressure of which may be set to between 30 and 200 mm H₂O by means of an 18 step adjustment system depending on the patient's needs (Kurosaki *et al.*, 2002; Miwa *et al.*, 2001). The fixed pressure valve setting is identified with the dots present on the valve (Fig. 2.9 a, c). The programmable valve settings are achieved by rotation of a magnetic cam actuator (Fig. 2.9 e, f) which adjusts the deflection of the leaf spring element acting on the sapphire ball valve in the flow path (Fig. 2.9 b, d).

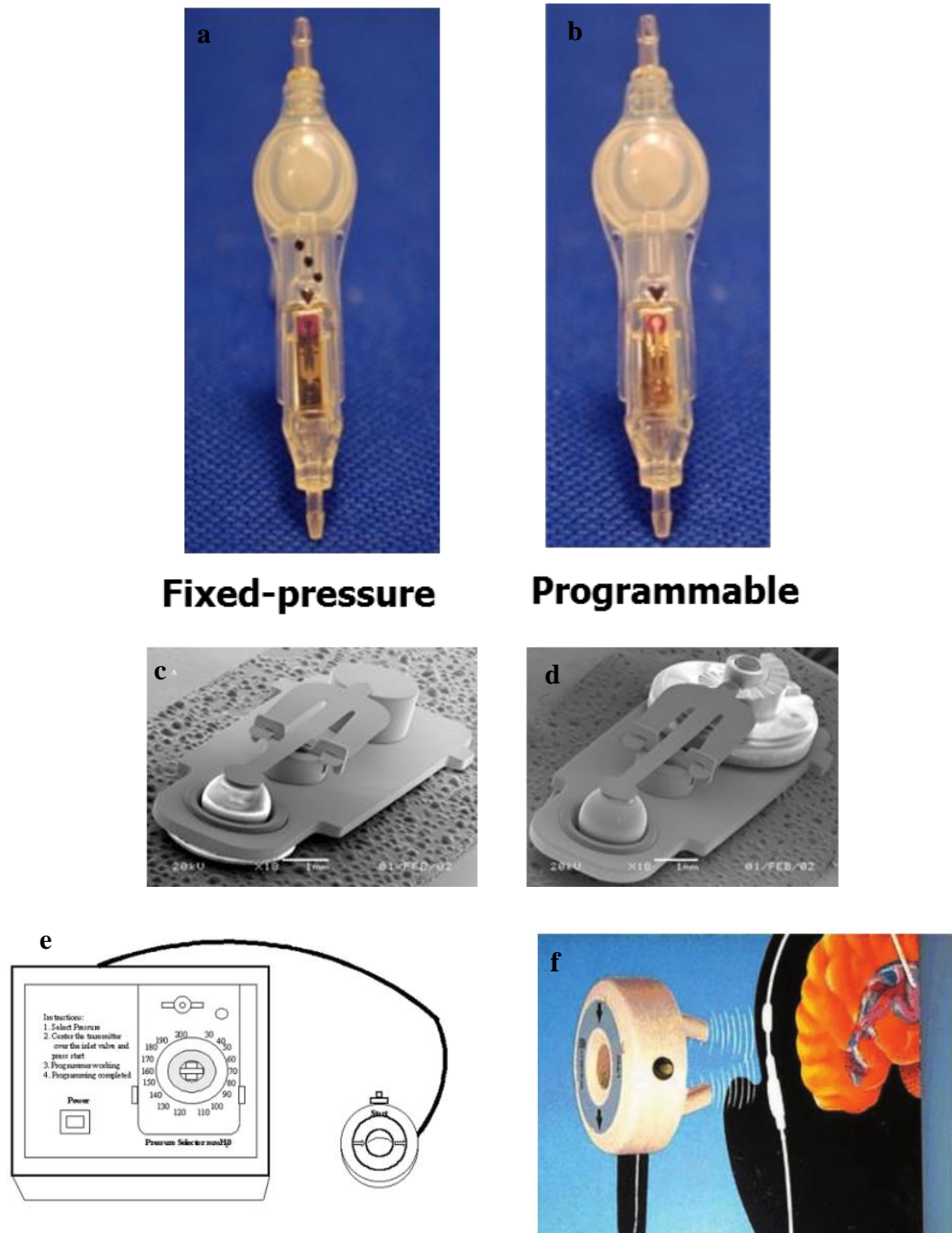


Figure 2.9: A photographic and scanning electron microscope image of Codman[®] Hakim[®] Precision fixed pressure valve (3 dots indicates opening pressure of 70 mm H₂O) (a and c) and programmable valve (b and d). Magnet present inside the rotor is adjusted using the external magnetic field produced by the programmer (e and f) (Chabrierie and Black 2002).

Strata valve (Medtronic, PS Medical, USA) is a magnetically adjustable differential pressure valve, which also works by the principle of ball on spring (Fig. 2.10). When compared to Codman Hakim Precision, in addition to having the ability to change the valve's opening pressure after implantation; it includes a feature to prevent siphonage. The overdrainage due to change in posture is prevented by combining Strata valve to the Delta chamber (Siphon Control Device). The component acts as a single pressure differential valve at normal conditions. However, when there is negative pressure occurrence (due to upright position) suction on the distal silicone diaphragm blocks the outlet port (Chabrerie and Black 2002).

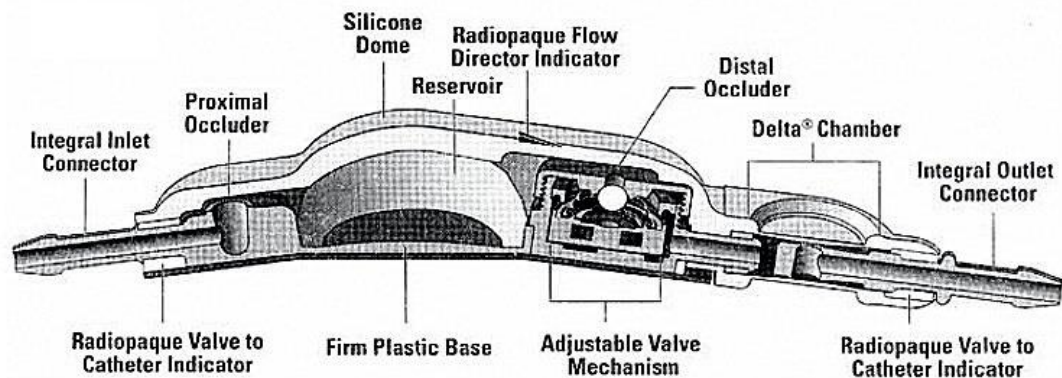


Figure 2.10: Schematic representation of Strata Valve. Adjustable valve mechanism can be magnetically adjusted in five steps. (Chabrerie and Black 2002; Czosnyka Z. H. et al., 2005)

ProGAV[®] (Miethke GMBH & Co GH Potsdam, Germany) is a programmable valve with integrated anti-siphon device and brake system that prevents accidental setting changes due to the presence of an external magnetic field (up to 3 Tesla). The valve is made of an adjustable unit and non-adjustable gravitational unit, both enclosed in a titanium shell (Fig. 2.11). A ball-in-cone valve system forms the adjustable part of the device. Like the aforementioned devices, the opening pressure is adjusted by changing the tension in a spring, which grips the ball in place, by turning the rotor with aid of an external magnetic tool. After setting the opening pressure, the ‘brake’ is applied to hold the rotor in place and avoid undesired re-adjustments. The brake can only be released by applying a force of 800 to 1600 g; again, a magnetic tool is supplied for this purpose. When the patient moves from a prone to an upright position, there is a corresponding increase in the opening pressure, which is achieved by the ‘shunt assistant’ feature, whereby a second ball bearing moves under the action of gravity to block the path of CSF flow. When the patient is in a horizontal position, the ball does not block the flow path, and the opening pressure returns to the level set by the non-return valve (Allin *et al.*, 2006).

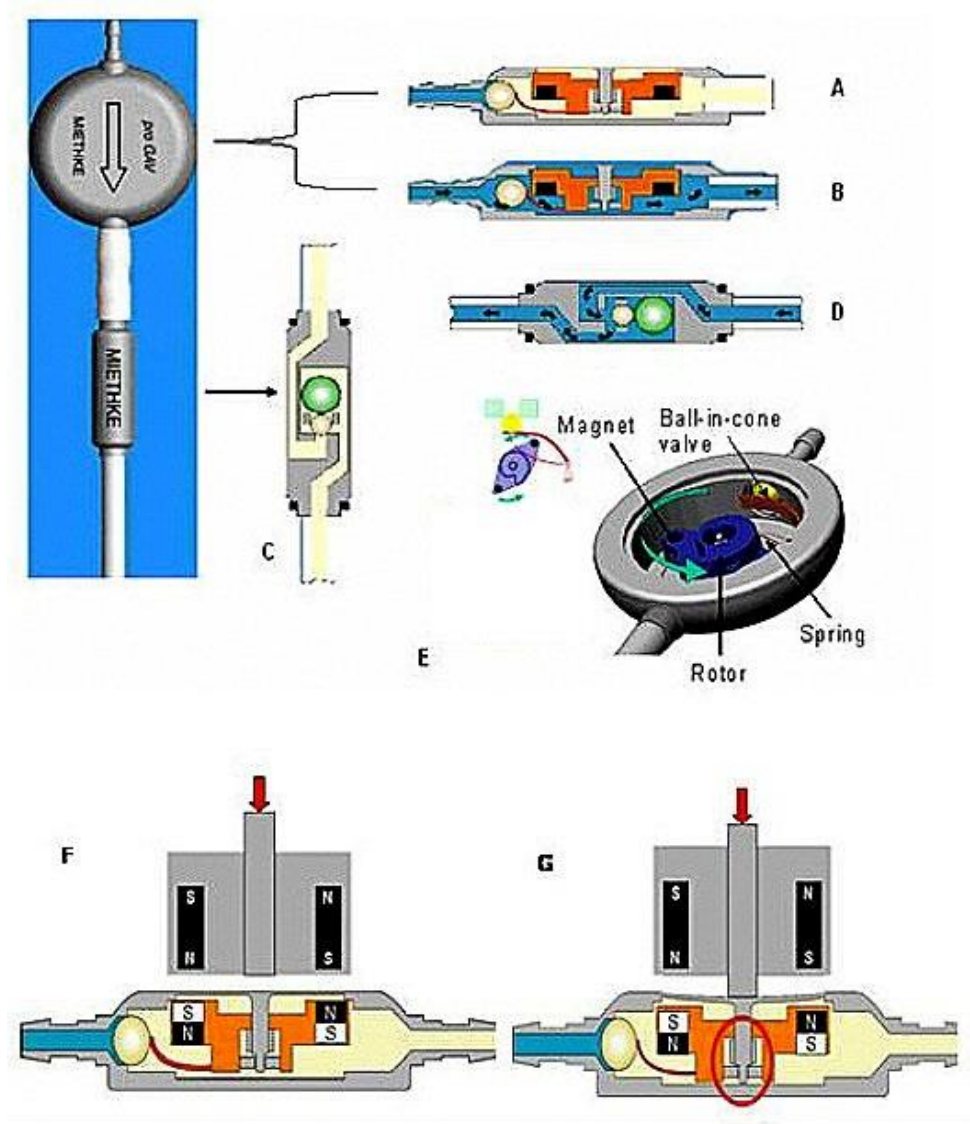


Figure 2.11: Miethke ProGAV® shunt mechanism diagrams. A: Adjustable component in 'closed state'. Ball in cone is blocked which results in no drainage. B: Adjustable unit in 'open state'. Differential pressure overcomes the spring pressure initiating the ball to move out of the cone resulting in drainage. C: Gravitational unit in vertical position. Discharge is initiated when differential pressure is higher than the combined opening pressure of both units. D: Gravitational unit in horizontal position. Opening pressure is determined by the adjustable unit alone. E: Internal mechanism of the adjustable unit. F: Representation of the magnetic tool used for adjustment. G: Indicating that brake has to be released so as to turn the valve. (Allin et al., 2006)

The Polaris programmable valve (Sophysa Ltd, Orsay, France) is another type of adjustable/differential pressure valve, which includes components to prevent accidental re-adjustment of the opening pressure on exposure to a magnetic field strength of up to 3 Tesla (Allin *et al.*, 2008). Here, a ruby ball seated in a cone, and balanced by a flat semi-circular spring, forms the valve component (Fig. 2.12). When there is an increase in inlet pressure, the ruby ball rises out of the cone and CSF flows into the distal catheter via the valve housing. The valve setting is non-invasively adjusted by an external programming magnetic device, which adjusts the tension of the flat spring by means of a rotor. The valve is housed within the rotor, which contains two permanent magnets. The role of these magnets is to prevent re-programming due to external magnetic forces. In the resting position, the magnets are attracted to each other and the adjustment lugs slide into position, thereby restraining the rotor. The external magnetic device must generate a unique magnetic field in order to move the rotor. The pressure setting is changed by rotating the position of the rotor, which, in turn, shifts one end of the spring between consecutive indexing notches. This action can be achieved only when the magnetic device unblocks the rotor.

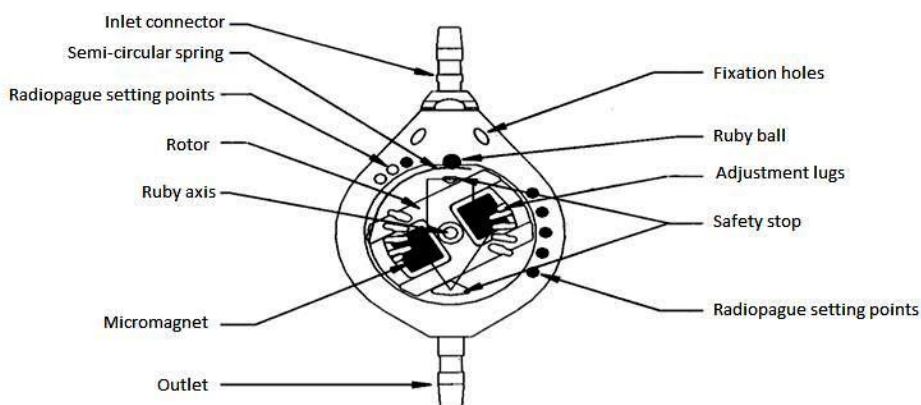
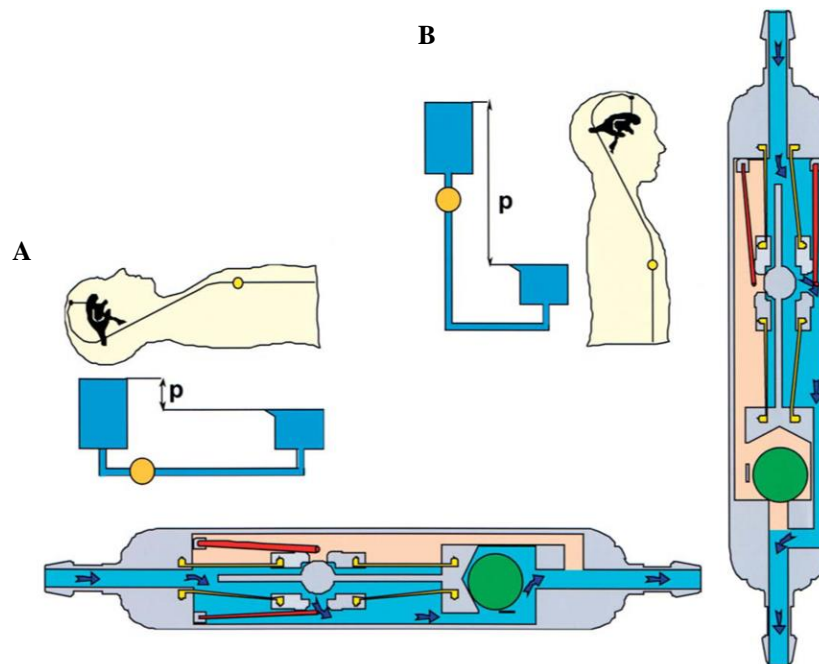


Figure 2.12: Pictorial representation of Sophysa Polaris Valve with labelled components (Allin et al., 2008)

The Miethke Dual Switch Valve[®] (Germany) is constructed by placing two valves with low and high opening pressure in the one chamber, each of which functions independently of the other (Meier and Mutze 2004). The low pressure valve is activated when the patient is in prone position and high when in the upright position. The valve is available in nine different configurations, comprising low pressure (10, 13, and 16 mm H₂O) and high pressure (30, 40, and 50 mm H₂O) valves (Czosnyka *et al.*, 2005). The switching mechanism is achieved with the help of Tantalum ball, which acts as a diverter: the prone position valve is activated when the patient's body position is in angle between flat lying to 60° and for body position from 60° to 90° upright position valves takes control. The duration of the activation depends on the body position and the flow of CSF (Kiefer *et al.*, 2002) (Fig. 2.13). The manufacturer claims that the design maintains a physiological ICP within the patients at all times and prevents overdrainage.



*Figure 2.13: Miethke Dual Switch Valve construction. P represents pressure, the functional part of the valve is indicated as blue in colour, whereas non-functional part in cream colour. A: Patient at horizontal position so low resistance valve is activated. B: Patient at vertical position so high resistance valve is in function (Kiefer *et al.*, 2002; Meier and Mutze 2004)*

Miethke Shunt Assistant[®] (Germany) participates in compensating for the raise in pressure during posture change. The hydrostatic pressure changes that arise from a change in position regulate the position of a metal ball within a cone-shaped housing. When the patient is in the upright position, the metal ball is seated within the cone, and CSF passes only if the intra-ventricular pressure is higher than the sum of all the individual resistance elements of the shunt system. Conversely, when the patient is prone, the metal ball is displaced out of the cone, and the resistance to CSF flow decreases. At all other intermediate positions, the metal ball acts as a simple resistance element to the shunt system (Kiefer *et al.*, 2002) (Fig. 2.14).

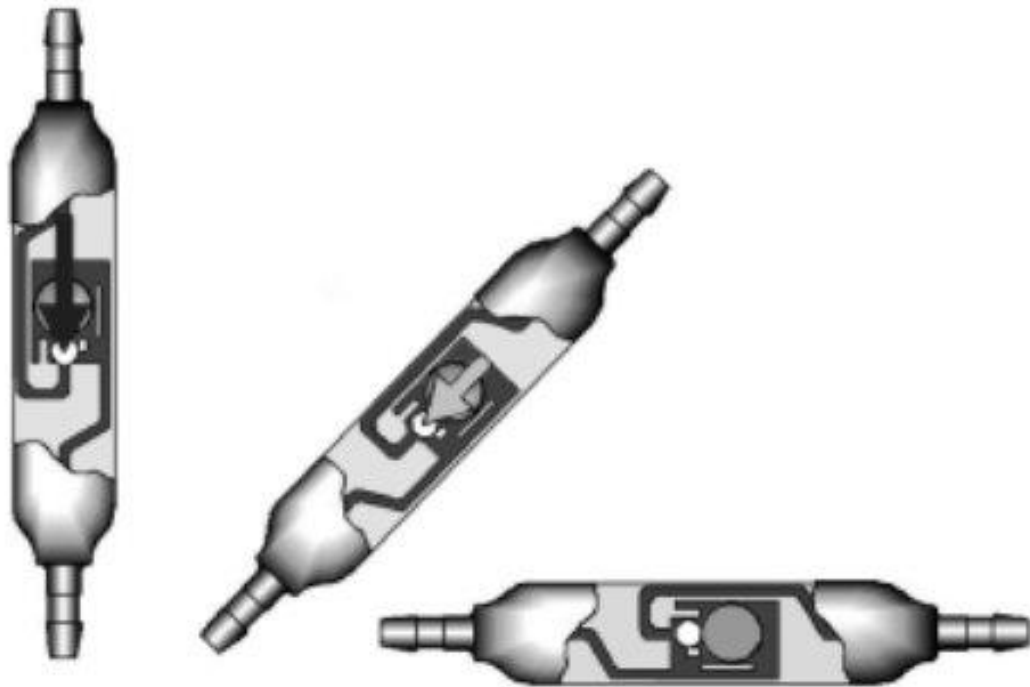


*Figure 2.14: Miethke Dual Switch Shunt Assistant mechanism illustration. Combined with the traditional differential pressure valve modifies the valve into gravitational shunt (Kiefer *et al.*, 2002)*

2.4 *In vitro* and Numerical modelling to understand and evaluate shunt behaviour after implantation

Allin *et al.*, (2006) state that the purpose of the CSF shunt is to drain the excess fluid into another part of the body. In an ideal world, the shunt should restore the CSF circulation to within the normal physiological range. In other words, the rate of drainage should be directly proportional to the positive difference in pressure between the ventricle and the sagittal sinus, and fall to zero when the pressure gradient is reversed. In reality, however, this does not happen because the driving pressure gradient in the case of a shunt is determined by the difference in pressure between the ventricles and the peritoneal cavity or right atrium (Czosnyka *et al.*, 2004).

Research suggests that only 30 to 50% of CSF production needs to be drained in order to maintain ICP within the desired range (Momani *et al.*, 2011); in other words, a significant proportion of CSF will drain of its own accord naturally. Unfortunately, existing shunts are too primitive to match the level of dependency required, instead encourage the patients to be completely dependent on shunting.

The performance of a shunt catheter system depends on many factors, including the intra-ventricular pressure, the diameter and length of catheter, the size and number of perforations in the wall of the proximal catheter, the resistance present in the shunt system itself, and the outflow pressure at the CSF drainage site (Cheatle *et al.*, 2012). Ideally, the resistance of the shunt should be close to the CSF outflow resistance (6 to 10 mmHg/ml/min), and the relationship between CSF pressure and flow should be within the physiological range. Moreover, changes in posture should not affect the shunt mechanism, opening and closing pressure should be adjustable, and there should be no reverse flow through the shunt (Allin *et al.*, 2006). The extent to which these criteria are met in practice can only be determined *in vivo*, using appropriate models.

Quality control issues with some of the early commercially available shunts systems led researcher develop their own bench-top models in an effort to understand the

CSF shunt hydrodynamics (Trost 1995), and numerous *in vivo*, *in vitro* and numerical models have been developed since to test entire shunt and their components independently. Clearly, the conditions present *in vivo* are far more complex. Nevertheless, these models have helped researchers to study and validate the hydrodynamic performance of commercially available shunt components with reference to the manufacturer's guidelines (Francel *et al.*, 2001).

British standards for sterile, single use hydrocephalus shunts and components were first established in 1986 (BS 6788-1:1986). Since then there were three subsequent British standard derived from ISO standards with updates related to the valve technology also have been developed, the latest being 2009 (BS EN ISO 7197:2009). These standards provide the researchers with the guidelines to test the hydrocephalus system in laboratory conditions and essential parameters (pressure and flow) to measure.

2.4.1 *In vitro* Models of shunt system

One of the first, and well-known, groups of researchers to have made major contributions towards the development of *in-vitro* models for use in hydrocephalus research is the Cambridge shunt evaluation laboratory (Cambridge, UK), which was established in 1993 (Allin *et al.*, 2006; Czosnyka Z. *et al.*, 2002). In addition, there are a number of models based on the Cambridge shunt model, as well as a number of models that have been developed independently by researchers who have adopted different approaches (Schuhmann *et al.*, 2000). The following section will describe the principles of operation of the most common laboratory models that have been used to test and validate shunt behaviour.

The system developed by the Cambridge group is based on a test rig designed to study the shunt performance in the long term, details of which were first published in 1994 (Fig. 2.15). The system has been used in a number of studies of shunt behaviour under static and dynamic modes, under both pressure and flow control, and in low and high resistance flow circuits. In the static mode of operation, the valve is permanently open whereas in dynamic mode there is a fluctuation in opening and closing of valve. This system is capable of measuring valve opening and closing pressures, shunt resistance for high (static mode) and low (dynamic mode) flow, and in longer term studies of these parameters. In addition to these parameters, temperature, external pressure and siphon pressure can also be controlled.

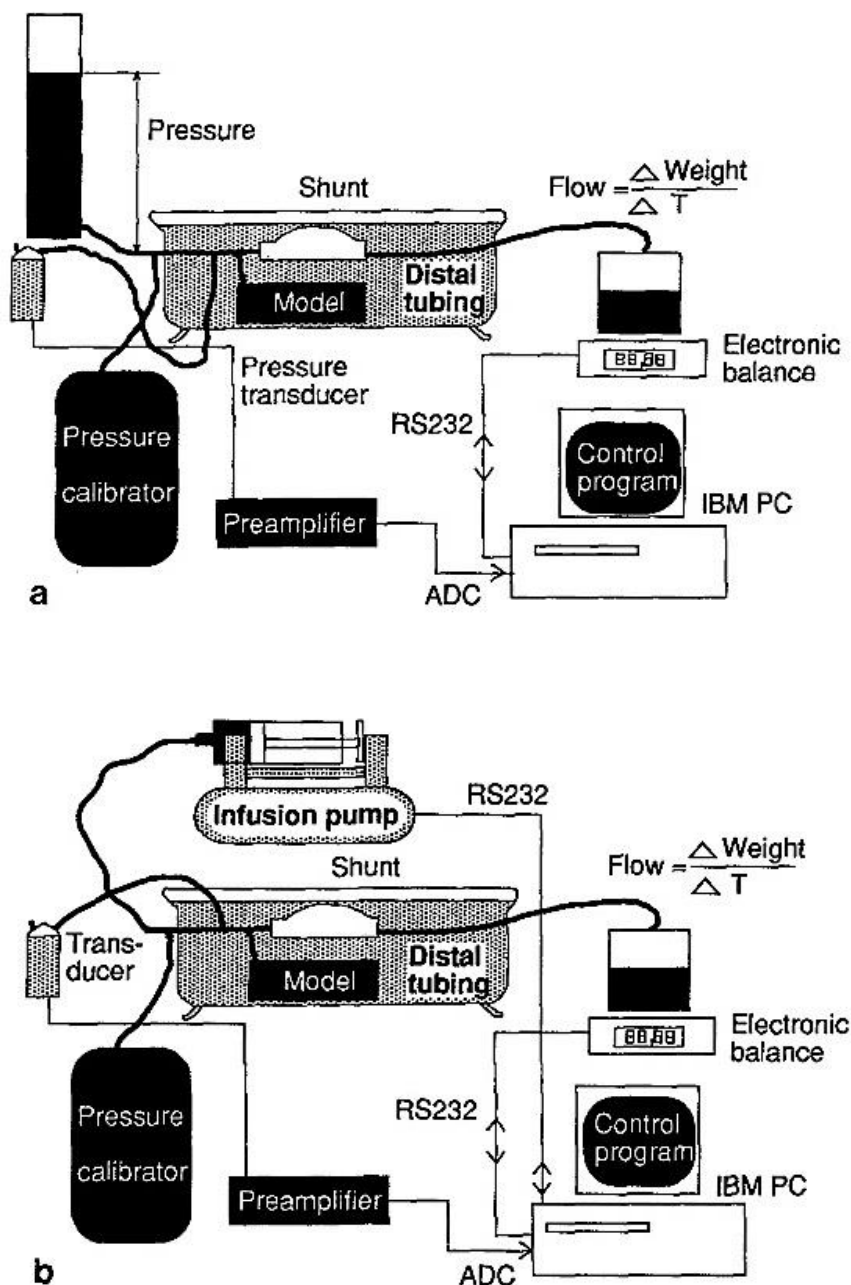


Figure 2.15: Experimental test rig a: pressure-flow studies and b: flow-pressure studies. The test rig consists of fluid reservoir, pressure transducer, water bath, electronic balance and a microcomputer. The system operates under either a constant head of pressure (pressure control), or constant flow control, the latter being generated by an infusion pump. In either case of control the test rig is fully computer controlled, and the data from a number of transducers is recorded simultaneously. (Whitehouse et al., 1994)

Paes (1996) designed and built the *in-vitro* model illustrated schematically in Figure 2.16. The main objective of this work was to study an adjustable flow-regulating device for shunting of CSF, and the function of this valve when the patient rises from the supine to erect position. There was no significant difference in the two different input flow rates modelled (10 and 20 ml/hr). The author of this work did not disclose any information about how the flow rate was measured, what CSF analogue was used, nor the temperature under which the experiment was carried out. Even though the system had all the basic materials required to test shunt performance, it lacked capabilities in data monitoring and control, accuracy in positioning of the distal catheter to mimic change in position, and precision in pressure measurement. Although relatively unsophisticated, this model was one of the first reported systems for testing a shunt system *in vitro*. Further advances in the designs of experimental models are presented in the following paragraphs.

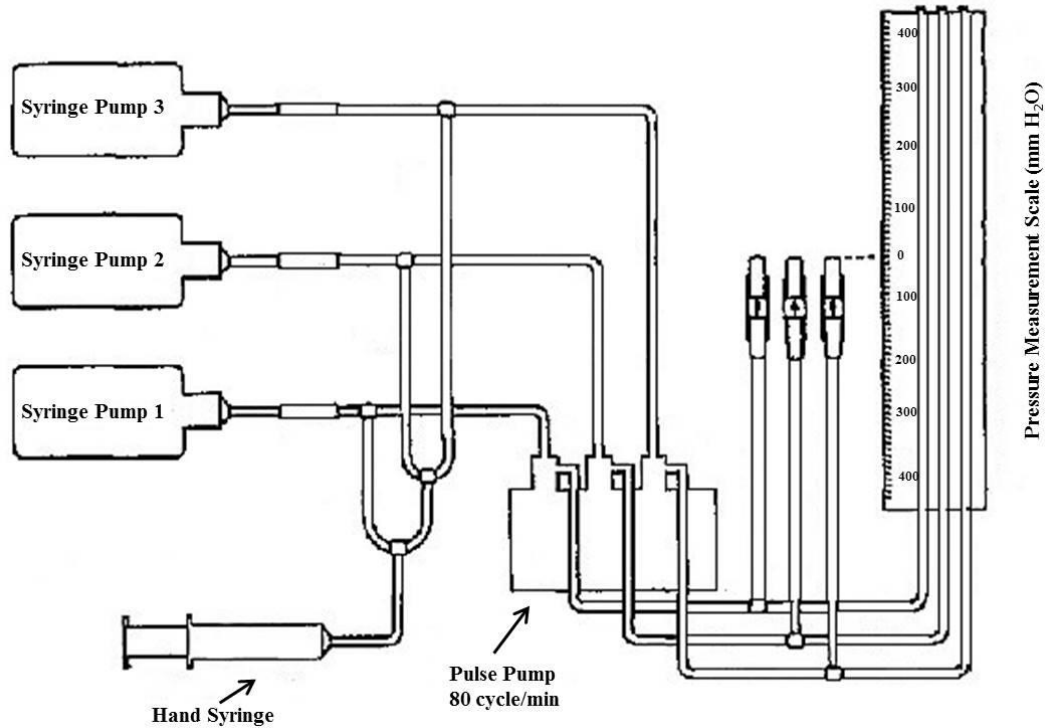


Figure 2.16: Hydrocephalus shunt testing apparatus. CSF production is mimicked using a syringe pump that injects CSF at a constant or variable rate into the circuit. Pulsation achieved by pulsatile pump, while the manometer recorded the pressure on the proximal side of the valve. The pressure change associated with a change in posture was stimulated by adjusting the position of the distal catheter relative to the proximal catheter: by lowering the distal catheter position it was possible to simulate the patient rising from a supine to upright stance (Paes 1996)

A few years later, in 1997, the Cambridge group published details of a much more advanced experimental rig, which is outlined in Figure 2.17. This test rig was used subsequently in a number of studies conducted by the same group to evaluate different shunt valves under more realistic operating conditions, which included a means to simulate shunt drainage. The rig they developed consisted of the following key elements: a pulse pressure generator, pressure transducer and infusion pump, which was capable of measuring pressure and flow through the shunt over a minimum period of 28 days. This system was controlled by a personal computer, with software designed in-house (Czosnyka M. *et al.*, 1997; Czosnyka Z. *et al.*, 2002; Eymann *et al.*, 2012).

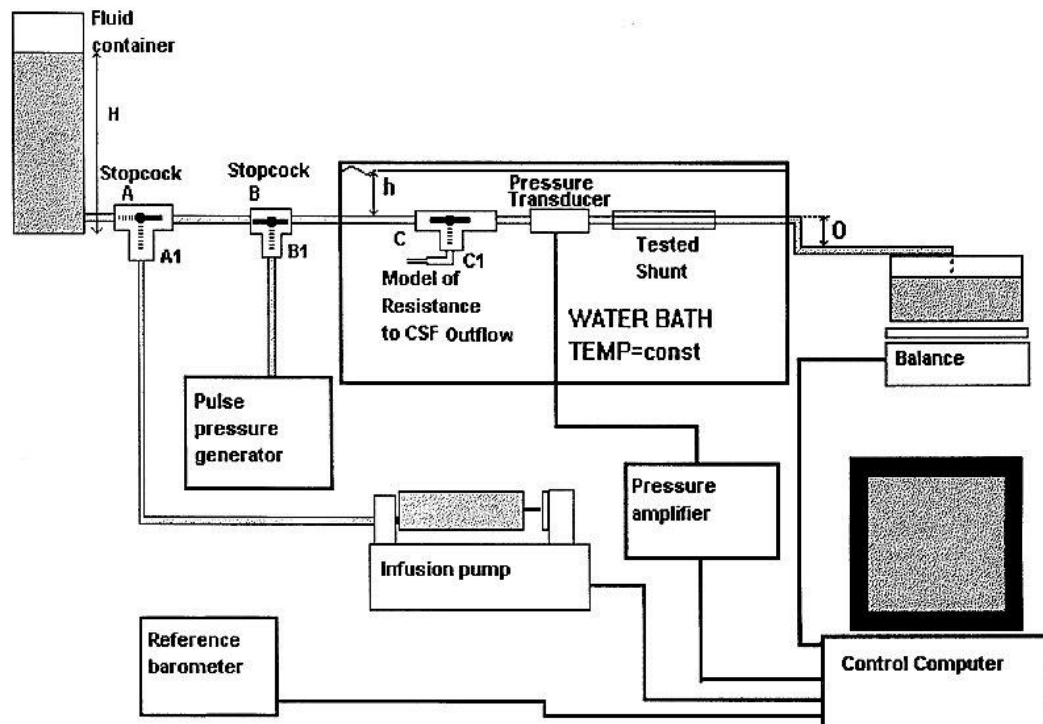


Figure 2.17: Schematic diagram representing shunt testing rig (Allin *et al.*, 2008; Czosnyka M. *et al.*, 1997; Czosnyka Z. *et al.*, 2002; Czosnyka Z. H. *et al.*, 2005)

The shunts to be tested were primed with deionised/deaerated water before being mounted in the test rig. For the experimental purpose in their study, pressure-flow curves were recorded over a period of 16 days. The performance of each shunt was studied over a wide range of operating conditions. For instance, by changing the position of the outlet and depth at which the valve is submerged in the water tank researchers were able to demonstrate the extent to which the shunt under test was susceptible to CSF over/under drainage caused by postural changes and external pressure (Allin *et al.*, 2008; Czosnyka M. *et al.*, 1997; Czosnyka Z. *et al.*, 2002; Czosnyka Z. H. *et al.*, 2005).

The effect of change in ambient temperature was also assessed, as was the influence of a pulsatile inlet pressure simulating the ICP pulse wave. Susceptibility to reflux is tested according to ISO standard. Since a long distal catheter may affect drainage, particularly in valves with a low hydrodynamic resistance, the pressure-flow performance was studied with and without a distal catheter. The valve's durability was tested by comparing the pressure-flow performance at the beginning and end of the protocol. Testing typically takes around 40 days, and involves daily testing as recommended by the international standard (Czosnyka Z. *et al.*, 2002).

In work carried out by Allin *et al.* (2008), the above test rig was used to test shunt systems under two sets of contrasting conditions: 1) flow through the shunt was controlled and differential pressure was measured and 2) differential pressure was controlled and flow was measured. The derived parameters included the closing pressure (differential pressure required for the valve to shut), opening pressure (minimum pressure required for the valve to open), hydrodynamic resistance (change in pressure/change in flow) and operating pressure (pressure measurement at 0.3 ml/min flowrate).

There are many factors that can affect the functions of a shunt system after implantation, and which often leads to shunt failure. The shunt testing system is designed to be capable of exploring those conditions in an effort to understand the mechanism(s) of shunt failure in depth, and hopefully to improve the design of the shunt. Some of the techniques used by those researchers to address the problems

include the introduction of microspheres, which are injected into the valve chamber to simulate the presence of larger particles in CSF, for example, erythrocytes or tissue debris (10 – 25 μm in size) to assess their possible influence on drainage (Czosnyka *et al.*, 2002). Previous studies carried by the same group have demonstrated that shunts are not sensitive to increased protein content, even at very high concentration. Therefore, the microspheres were not intended to mimic a change in viscosity of the CSF analogue, but to mimic the physical effect of those particles on the opening and closing mechanism of the valve. Other studies carried out by the group include those in which the responses to shock waves of up to 200 mm Hg (simulating the maximal CSF pressure increase provoked during coughing), reverse pressure of the same magnitude, and behaviour in the presence of static magnetic fields comparable in magnitude to those generated during MRI scan, for example (Czosnyka *et al.*, 2002)

The Cambridge set up comprises all the essential components of a shunt testing system. However, some components – the pulse pressure generator and software designed for data acquisition, for example – are not disclosed in any detail in their published works. Moreover, the test rig was not intended to study a particular patient group or individual patient's condition, nor is it clear whether or not it is possible with the existing system.

In an effort to address those questions, Schuhmann *et al.* (2000) developed a test rig with human-like compliance so as to mimic actual *in vivo* ICP waveforms. The other constituents of the set-up includes fluid reservoir, computer controlled peristaltic pump, a pear-shaped fluid container known as human compliance simulator (HCS), standard ascending pipe (SAP), water bath at 37⁰ C in which the valve to be tested is placed, and an electronic high-precision balance to collect the fluid from the distal catheter (Fig. 2.18). The CSF analogue in this case was de-aerated distilled water. Pressure in the system is controlled by the HCS and SAP, whereas the flow of CSF is generated by the peristaltic pump, which determines the waveform. The results of the pressure-flow relationship showed no significant difference when traditional linear compliance measurements compared with human-like-compliance. Using this set-up the authors have developed a method of reproducing ICP patterns.

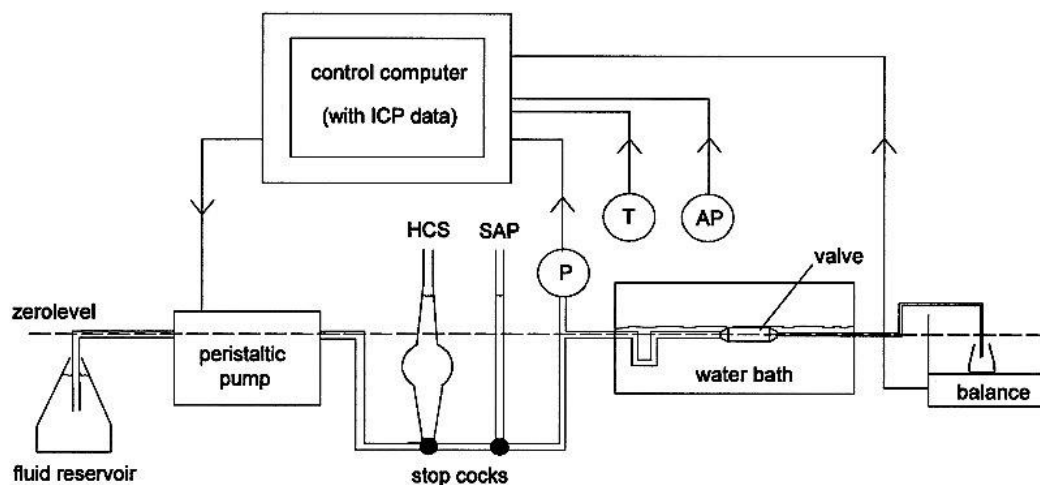


Figure 2.18: Outline of shunt test rig (*T*- ambient temperature, *P*-pressure on valve, *AP*- atmospheric pressure, *HCS* - human compliance simulator and *SAP*-standard ascending pipe) (Schuhmann *et al.*, 2000)

The test set up designed by Francel *et al.*, (2001) is illustrated in Figure 2.19. These authors used their system to explore the pressure-flow relationships for a number of flow-control valves as a function of the orientation/position of the valve housing.

Two types of commercial product: the Phoenix biomedical diamond valve and Orbis Sigma valve were tested in this rig, with and without an overdrainage resistance element being present. The pressure-flow relationships for both the valves were also calculated using this set up. A constant outflow rate was achieved by the valves as the valve position incremented with respect to the proximal catheter tip.

Unfortunately, there is no record of how the data was controlled and collected for this study. Also, no information on the temperature control during the experiments was disclosed.

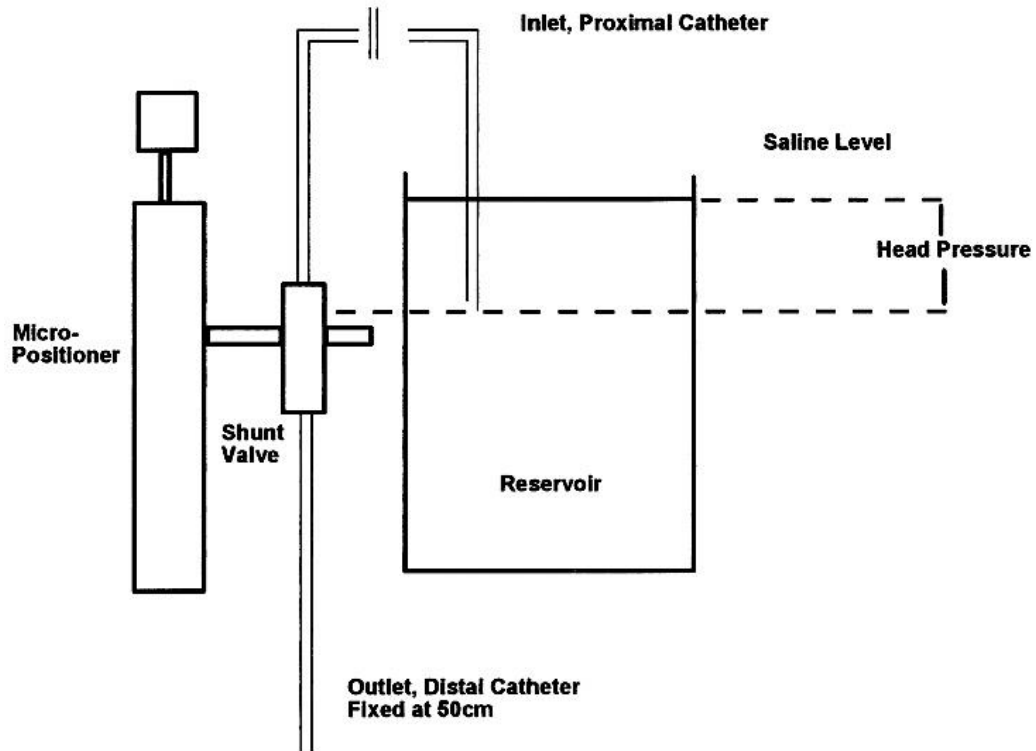


Figure 2.19: Schematic representation of valve, reservoir and inlet/outlet used in the set-up. The valve was fitted to a micrometre positioner; the desired head pressure was set at the starting position of the valve, which is horizontal to the tip of the proximal catheter. The flow rate of the valve was recorded as the valve position incremented. The outflow rate was held constant under a constant head of pressure of between 5 and 30 cm H₂O. The artificial intracranial pressure head was represented by using an infinite reservoir of sterile saline water. The proximal catheter was positioned relative to the constant head so as to maintain a desired pressure gradient across the valve. (Francel et al., 2001)

Lundkvist *et al.* (2003) designed an *in-vitro* model with which to compare the differential pressure valve, with (Strata[®] valve) and without (Delta[®] valve) an anti-siphon device being present. The vital component of the experimental set-up is shown in Figure 2.20. The group studied the opening/closing pressures, and the resistance of the shunt, with and without anti-siphon device. The authors claimed that the test rig was very stable, and capable of producing results to a high degree of accuracy. All the shunt systems tested were brand new; hence the performance of the valves in the above report will likely differ with prolonged testing, or in systems that had previously been implanted.

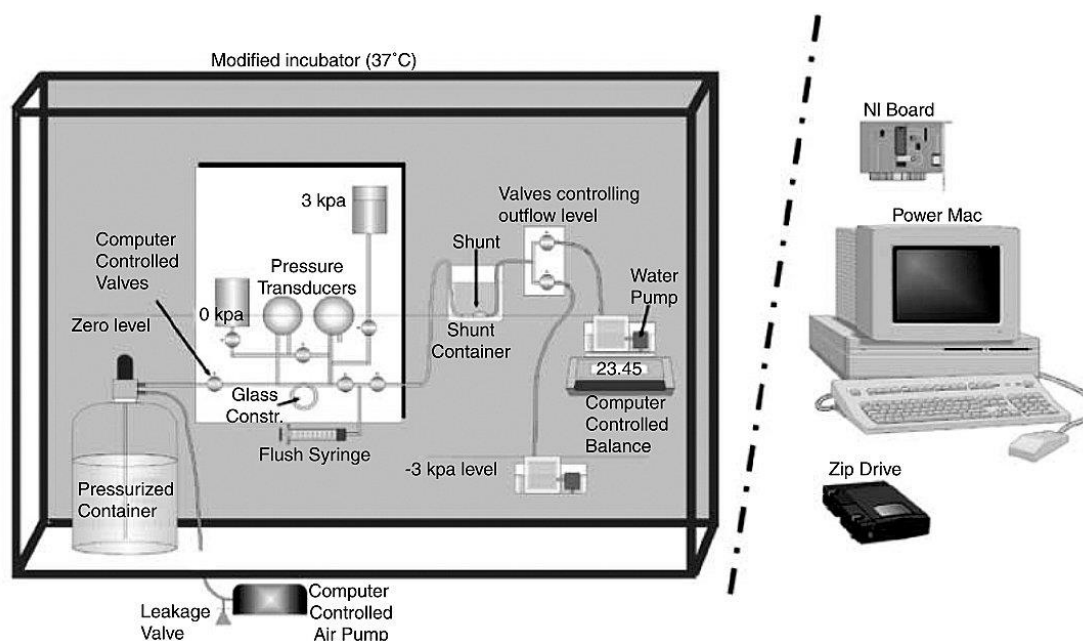


Figure 2.20: Experimental set up comprises of a microcomputer to collect data and regulate fluid pressure, a pressurised fluid reservoir, pressure transducers and computer-controlled balance. The flow was measured from the pressure drop across the glass vessel construction with known resistance. The shunt was submerged in water to a depth of 65 mm. The computer balance was placed at zero pressure level or at 30 cm below the zero level during testing, with anti-siphon device. The experiment set-up was maintained at 37 °C. Software for the control and data acquisition took the form of a LabVIEW program, which regulated the pressure to a triangular waveform. (Arnell et al., 2009; Eklund et al., 2004b; Lundkvist et al., 2003)

Only a few reports in the literature have studied shunt performance in response to manual pumping. Bromby *et al.* (2007) have since reported on the construction of a physical model that is capable of measuring the effect of pumping the pre-chamber of hydrocephalus shunt on intracranial hypotension. The pre-chamber of the valve is a small reservoir to contain CSF before it enters the valve mechanism. In some cases, patients and their families have been encouraged to pump the shunt periodically to prevent occlusion of the valve, or to relieve pressure. However, too much pumping may cause overdrainage.

The testing model is shown in Figure 2.21, which consists of a wide-necked feeding bottle filled with de-aerated and de-ionised water to represent CSF. The system includes a compliance factor, which was achieved by punching a 2 cm diameter hole in the cap. The downstream resistance was governed by the lumbar puncture outflow needle. A constant volume flow of 0.3 ml/min is infused into the system to mimic the CSF production rate. The shunt to be tested was placed inside a 10 cm long low resistance tubing representing proximal catheter; the same tubing, about 80 cm in length, represented the distal catheter. A pulse pressure waveform was used to stimulate ICP pulse pressure.

Using this set-up, the authors evaluated the performance of eleven types of shunt system, including differential pressure valves and valves with an anti-siphon device fitted. The shunts used in this set-up were either new or had been used for other experimental purposes. These shunts were tested to determine how repetitive pumping affects CSF pressure. There are several limitations to this model. For example, the increased volume of CSF (270 ml), low compliance, and the assumptions required to obtain a pressure-volume curve that reaches an asymptote. However, the authors are very confident and determined that pumping the pre-chamber of the shunt for any shunt type is more likely to decrease the proximal CSF pressure, and thereby increasing the chances for overdrainage.

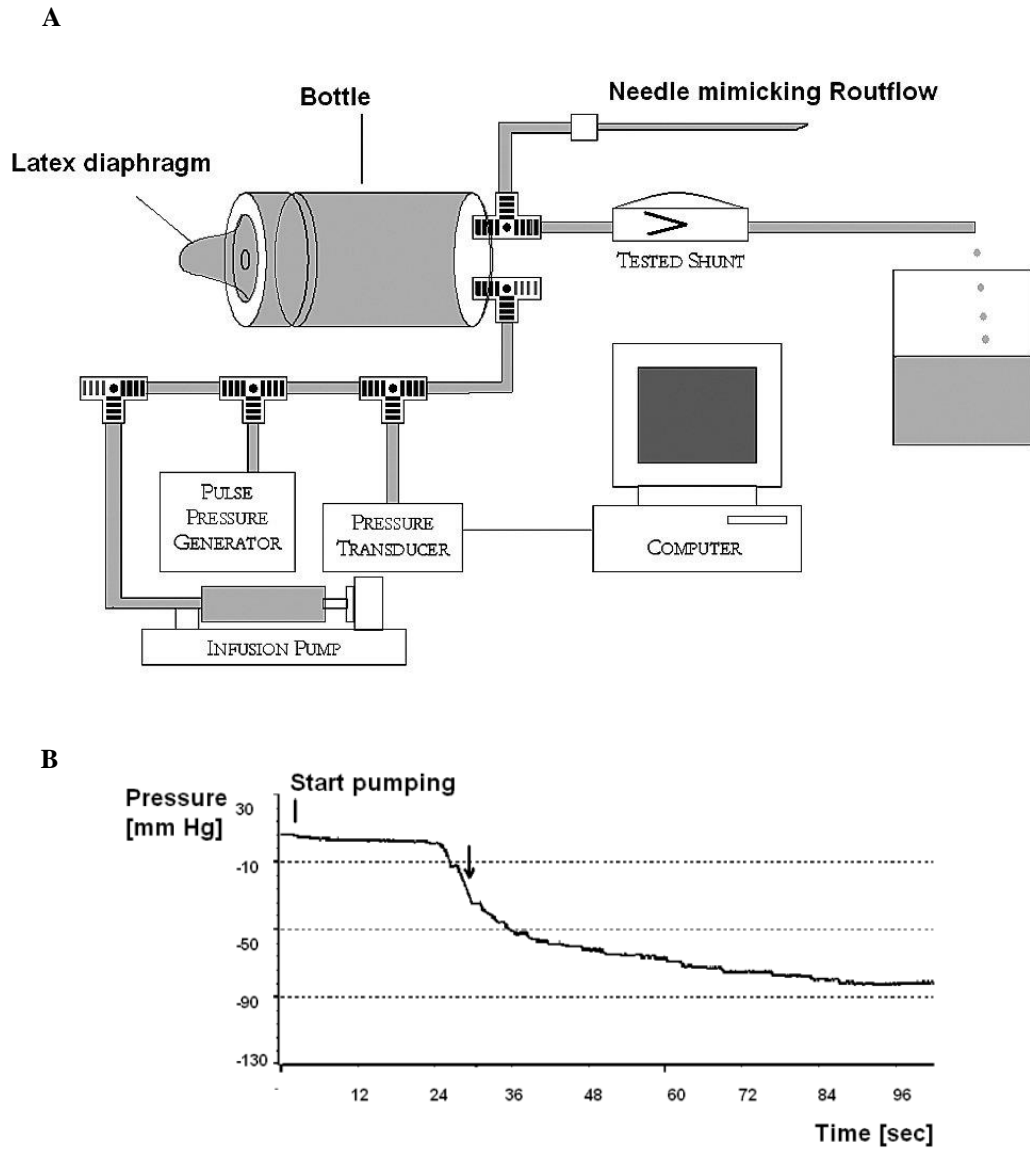


Figure 2.21: A: Laboratory test rig to study the shunt behaviour along with pumping action. B: Negative pressure in the model represents ICP which leads to asymptote. Asymptote can be acquired at a constant pumping of the reservoir at the rate of 1 per second. Number of pumps required to reach the asymptote was recorded. Arrow represents the area where the pressure changes are highest per pump. (Bromby et al., 2007)

In fact, it is the distal catheter that contributes the most resistance in the shunt system, owing to its length. Therefore, a significant change in the resistance over a due course of time after implantation may have a significant impact on shunt performance. Cheatle *et al.* (2012) studied the hydrodynamic properties of a range of length and diameter of explanted and new distal catheter, using the experimental set-up illustrated in Figure 2.22. In addition, they also examined the contribution made by the connectors used in a given shunt system to its resistance. The authors concluded that while the resistance of the catheter is directly proportional to the length and indirectly related to the diameter of the catheter as expected, the resistance of the distal catheter depended also on the number of connectors.

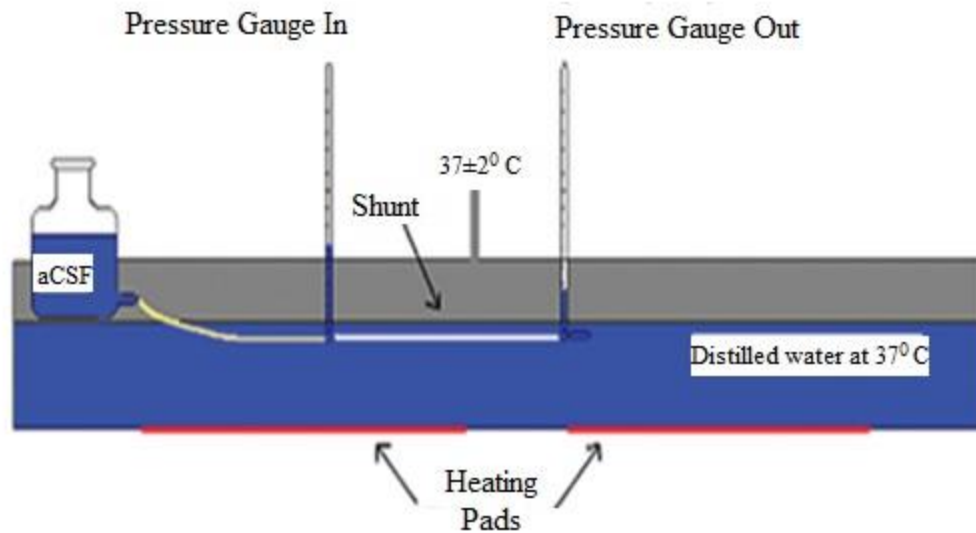


Figure 2.22: Graphic representation of shunt testing system. Artificial CSF (aCSF) having a salt content that matched closely the constitution of CSF was used. Pressure in the set-up was measured using manometers placed at either end of the shunt system. A flask containing 350ml of aCSF was connected to the proximal end of the catheter, and constant flow of 15 ml/hr is achieved using a pump. The distal catheter and connectors to be tested were placed between the proximal and distal manometers. The height of water in the columns of the proximal and distal manometers gave an indication of the pressure drop, whereas the volume change represented the flow of CSF, which was recorded after one hour. (Cheatle et al., 2012)

2.4.2 Numerical Models of the shunt system

Mathematical models have the potential to give insights into cerebral autoregulation, the nature of CSF flow through the various compartments in the normal and diseased brain, and through simulation in patient-specific studies give guidance to surgeons on the implantation of the catheter. They may also allow researchers to model the behaviour of hydrocephalus shunt systems, and to predict those conditions most likely to give rise to failure of the shunt.

Linninger *et al.* (2007), for example, combined MRI and computer-aided numerical modelling techniques to re-construct patient-specific model of the CSF filled spaces, and predict the CSF flow and pressure fields. Their study involved comparison of acute Cine phase contrast MRI of normal subjects and hydrocephalus patients using a numerical model which was obtained from first principles of fluid-solid mechanics of human intracranial dynamics (Linninger *et al.*, 2007). The researchers found that the results generated from their computer modelling complemented the MRI measurements in terms of the predicted CSF flow.

Subsequent work carried out by these authors led to the development of a dynamic model of communicating hydrocephalus (Linninger *et al.*, 2009a; Linninger *et al.*, 2009b). The model of intracranial dynamics included all the critical components, namely the vascular system, CSF and parenchyma. The results of the study comprises the dynamic flow of CSF affected by cardiac cycle and offered a mechanistic explanation of communicating hydrocephalus (Linninger *et al.*, 2009b). Using a more advanced version of their numerical model, these authors presented a more complete explanation of the role of reduced CSF reabsorption rate in hydrocephalus conditions (Linninger *et al.*, 2009a).

At around the same time, Clatz *et al.* (2007) were developing a dynamic model of CSF flow and ICP regulation in order to study communicating hydrocephalus. Their model combined clinical data with a 3-D representation of the brain parenchyma, including the extracellular space within the brain and venous systems. The simulation was based on a case study of a patient with a shunt, which was inserted

along with a pressure probe to record ventricular pressure. A finite element model was constructed using the computed tomography of the specific patient along with experimental measurement and simulated data (Clatz *et al.*, 2007).

The information obtained from the direct physiological measurements, and using that data to refine those models in order to understand CSF dynamics in hydrocephalus patients, can yield vital information for the surgeon (Czosnyka Marek *et al.*, 2004). Examples of clinical parameters recorded from hydrocephalus patients include ICP and cerebral blood flow. Czosnyka *et al.* (2004) reviewed the fundamentals of CSF dynamic and function of implanted hydrocephalus shunt systems. It is widely accepted that pressure independent CSF outflow resistance, pressure dependent compliance, and constant formation rate of CSF is to model CSF dynamics (Eklund *et al.*, 2007).

In practice, this involves infusing artificial CSF and observing the corresponding change in ICP, combined with the mathematical expression obtained from the model to characterise between different types of hydrocephalus, prediction towards shunting and possible assessment of shunt function *in vivo* (Eklund *et al.*, 2007). With the available clinical data, a mathematical model of shunt drainage system was developed in order to study the blockage and other malfunctions occurring in the shunt system (Schley *et al.*, 2004). Armed with such knowledge, surgeons are able to locate the optimal position for shunt implantation, and adjust the shunt valves accordingly. The properties of the ventricular wall in shunted patients were modelled by applying linear viscoelastic theory, and assuming the brain behaves as a porous elastic substance containing incompressible fluid (Sivaloganathan *et al.*, 2005).

2.5 Shunt failure and its consequences

Although the introduction of shunt devices for the treatment of hydrocephalus has led to a marked decline in neurological complications and death, shunt failure remains a major problem (Stein and Guo 2008; Tuli *et al.*, 2000). Brydon *et al.*, (1998) point out that shunt revisions are very common; on average, 16% of procedures require revision within one month of surgery. Moreover, in some 40 – 50% of cases, shunt failures occur within just a couple of years after surgery (Cheatle *et al.*, 2012). The results of a longer-term clinical study of shunt performance showed that 81% of devices fail within 12 years (Whitehouse *et al.*, 1994).

The most common failure in any implanted device is infection, which is due to many factors (Paes, 1995). The overall incidence of infection is about 5 to 10%, and usually occurs soon after surgery (Browd *et al.*, 2006a, Chumas *et al.*, 2001, Bayston, 1994). Infection needs to be treated immediately since mortality rates for untreated cases can be as high as 30 to 40%, which is higher than those attributed to a malfunctioning shunt (Naradzay *et al.*, 1999).

Unfortunately, no records exist to show the decrease in failure rate since the inception of the device (Stein and Guo 2008). Shunt retrieval is uncommon: hydrocephalus patients are more likely to retain a shunt device for their entire lifetime, even if the device should fail. Evidence of more than one episode of failure is common. In fact, the ratio of first shunt insertion to subsequent surgical revision is 1 to 1.25 (Tuli *et al.*, 2000). The types of failures attributed to this device are categorised according to the time period of occurrence (Table 2.2).

Early Shunt Failure (within 2 years of surgery)	Late Shunt failure (after 2 to 10 years of surgery)
Disconnections	Obstruction/Blockage of shunt components
Misplacement	Tubing fractures and Overdrainage
Migration	Abdominal complication

Table 2.2: Causes of early and late shunt failure (Browd et al., 2006b)

Examples of disconnections likely to occur during surgery include poor knot placement, improper insertion of the catheter, or inadequate positioning of the tip. A disconnected shunt is identified by the presence of CSF around the shunt at the site of disconnection and/or increased intracranial pressure. Scans of the shunt series will reveal an opening between components of the shunt system, either at the intraventricular catheter-valve connection or at the valve-distal tubing connection. Such disconnections can be repaired by reoperation (Browd *et al.*, 2006b).

Malposition/misplacing of the ventricular (proximal) catheter into brain parenchyma, the choroid plexus, or temporal horn leads to early shunt failure. The reasons for misplacement include incorrect assessment of anatomic landmarks, causing improper orientation upon insertion, and improperly inserting a catheter tangential to the targeted cavity. Equally, the use of an inappropriate catheter can lead to misplacement. Migration occurs when a properly placed catheter moves from its initial position to a position where CSF is no longer drained, or the drainage is highly challenged (Browd *et al.*, 2006b).

Obstruction/Blockage of the shunt components is one of the most common failures compared to other failures. Bork *et al.* (2010) reported that shunt blockage occurs in 20 to 30% cases within the first year after surgery. Obstruction is responsible for a portion of 70% of patients with shunt failure (Thomale *et al.*, 2010). Catheter

occlusion is responsible for up to 50% of all shunt failures with a 12 year follow up (Eymann *et al.*, 2012). Obstruction, which may occur at any time after the insertion, results in reduced CSF flow through the shunt and a concomitant rise in ICP. Tuli *et al.* (2000) reported that as the proportion of shunt failure episodes increases the incidents caused by obstruction has subsequently increased. Out of all the shunt components, obstruction of the valve itself is relatively rare; blockage happens most often in the ventricular catheter (Kurosaki *et al.*, 2002). The perforated part of the proximal catheter is the most favourable location for the obstruction to occur (Fig. 2.23): occlusion of one or more of those openings (fenestrations) may lead to failure of the entire shunt, unlike the distal catheter, which rarely becomes blocked (Lin *et al.*, 2003). The matter responsible for causing the obstruction may originate from the choroid plexus, debris and blood present in the ventricular system, brain tissue invading the catheter, and tumour growth near the region of insertion (Browd *et al.*, 2006b; Chabrierie and Black 2002). In rare cases, the peritoneal catheter may become blocked owing to adhesions, scarring, or twisting of the distal portion of the catheter.

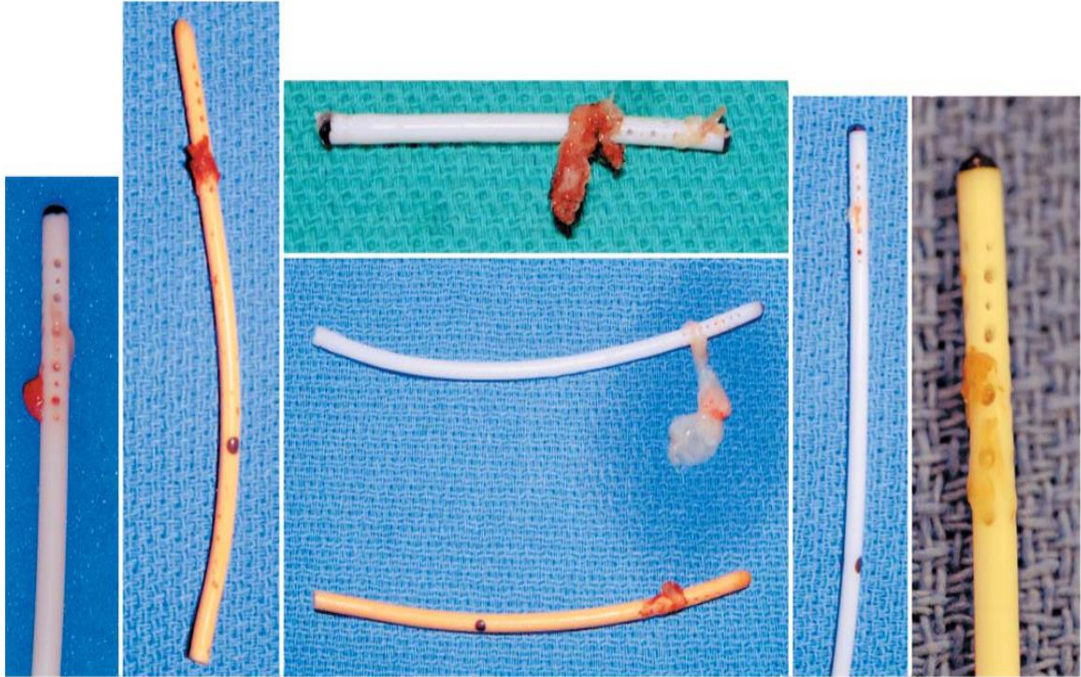


Figure 2.23: Photographic images of explanted ventricular catheters showing examples of blockage of the perforations present within the catheter wall (Lin, et al., 2003)

When obstruction occurs, unlike other mechanical failures, the shunt series fails to show any evidence of disconnection or fracture. Obstruction can be resolved only by surgical revision (Achyuta *et al.*, 2010). This may range from partial revision of the intraventricular catheter, valve, or distal tubing, to replacement of the entire system. Relocation of the shunt to a completely new position may be required, depending upon the location and circumstances involved in the obstruction (Browd *et al.*, 2006b).

Shunt failure as a result of fracture of the distal tubing is considered as a biomechanical failure. Failures of this type are mainly due to biomechanical stress, as the subject grows (Browd *et al.*, 2006a), or as a consequence of deterioration of the implanted components over time. Examination of explanted tubing components reveals that the accumulation of proteinaceous material around the periphery plays a major role; degradation may also occur in the tubing due to scar formation in the tissues that surround the tubing (Browd *et al.*, 2006a).

Overdrainage occurs when too much CSF is drained, as happens during changes in posture. Initiated by siphoning, it follows a momentary increase in pressure gradient across the ventriculo-peritoneal shunt system, which presents a relatively low hydrodynamic resistance when the valve opens (Bromby *et al.*, 2007; Eklund *et al.*, 2004a; Francel *et al.*, 2001; Kurtom and Magram 2007). Studies report an incidence of between 5 to 55%. It is more often in infants who had their shunt implanted before 6 months of age (Naradzay *et al.*, 1999). Likewise, in NPH patients, overdrainage is a common problem. Overdrainage also leads to subdural collection, which is very common (Faghieh Jouibari *et al.*, 2011). Overdrainage may lead to shunt occlusion in some cases (Paes, 1995).

The most common abdominal complications include ascites and pseudocyst. Ascities is more commonly associated in contemporary illnesses like cirrhosis, congestive heart failure, nephrosis, or disseminated carcinomatosis. Pseudocyst is the formation of loculated intra-abdominal fluid occurring in the site of peritoneal catheter insertion. In both cases, the digestion of CSF is eventually reduced causing complications in the shunt mechanism (Browd *et al.*, 2006a).

2.6 Recent developments and advancements of CSF shunt systems

In recent years, the most notable advances in shunt design include the use of alternative drainage locations, for example, ventricular catheter placements; new valve designs; catheter assembly design; anti-siphon devices; on-off devices; gravity-actuated and externally-adjustable valves (Stein and Guo, 2008).

Nevertheless, the overall impact on shunt patient outcomes has been relatively limited. CSF dynamics are unique to each patient, which makes it challenging to design a device that can readily adapt according to the needs of the patient (Kurtom and Magram, 2007).

To date, clinical evidence that one shunt outperforms another is lacking (Kurtom and Magram 2007; Lundkvist *et al.*, 2003). Both Drake *et al.* (2000) and Chumas *et al.* (2001) reported that the outcomes associated with three types of valve (sigma, standard and delta) were no different in terms of failure after 2 years. It follows that any slight improvement in valve design is unlikely to contribute for a major improvement to the shunt design. Indeed, based on the evidence available suggest that, instead of improving outcomes, almost all new shunt designs create more problems than solutions (de Jong *et al.*, 2000; Drake *et al.*, 2000). The areas that have been suggested for development by the authors include the introduction of shunt designs that can overcome the problem of overdrainage and regulate shunt flow according to postural changes. Equally, more research should focus on new biomaterials to avoid obstruction in catheter (Williams *et al.*, 2007).

Kurtom and Magram (2007) discussed the concept of controlling the shunt mechanism using computer technology, which is expected to become available in near future. The aim is to harness recent advances in sensor and micro-electro-mechanical systems (MEMS) technology to detect ICP, or changes in body positioning using sensors, and to transfer this information wirelessly to a remote computer. A control signal from the computer would then be used to bring about the changes required to regulate the flow of CSF through the catheter, or any of the shunt accessories. One of the variables that have been proposed to control the system

is ICP: as ventricular compliance decreases, the amplitude of ICP signals increases; which, in turn, triggers the valve to open. Such sensors may be used also to detect a partial proximal obstruction.

Bork *et al.* (2010) designed and developed a novel implantable flow sensing transducer to monitor and control the flow of CSF. A schematic of the system is illustrated in Figure 2.24. The transducer transfers real-time flowmetry data directly to clinicians via passive telemetry. The purpose of the sensor is to enhance the performance of the shunt valve by monitoring its function, and to collect information about the flow of CSF under physiological conditions. The external control of the valve prevents the user from suffering the most common problem of CSF shunt systems, namely over/under drainage of CSF. An *in-vitro* model is used to study the overall performance and accuracy of flow measurements of the flow sensor with and without CSF proteins present on the surface.

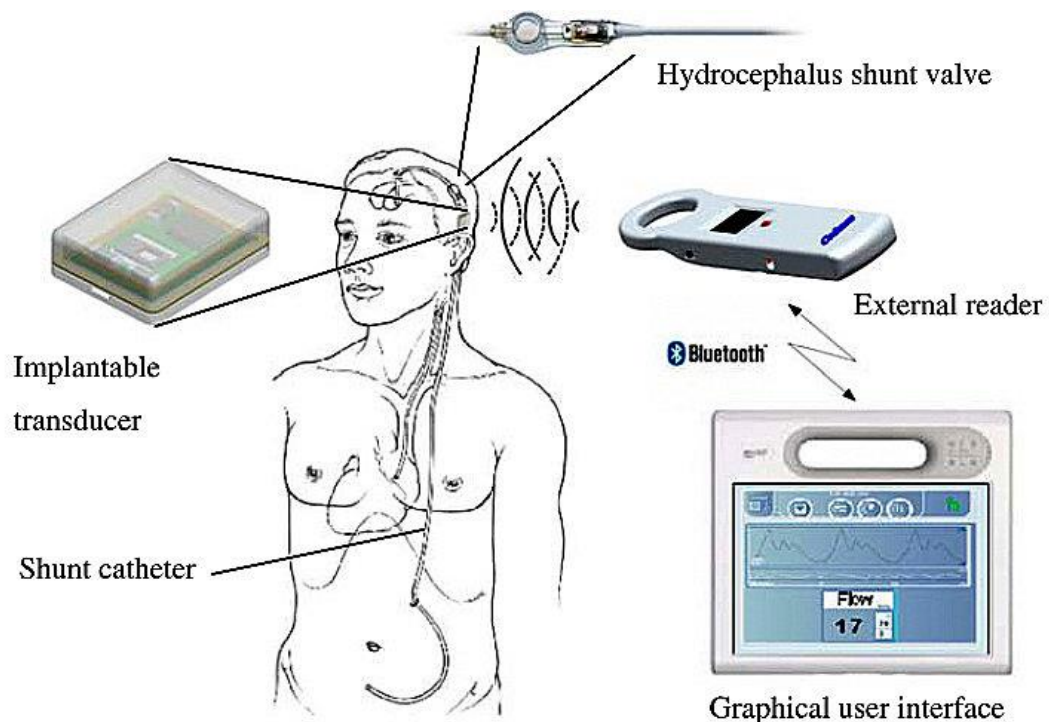


Figure 2.24: Outline of the implantable transducer (Bork *et al.*, 2010)

Recently, Momani *et al.* (2011) proposed a mechatronic valve for this application, in contrast to a passive mechanical valve, which attempts to maintain ICP within the physiological range by opening and closing according to differential pressure across the valve. Considering the limitations imposed by current valves, these researchers explore the feasibility of a mechatronic valve, which is electronically controlled via software so that shunt responds to the dynamic needs of the patient; such a system will also allow controlled reduction of patient's shunt dependency.

The pictorial representation of the above mentioned mechatronic ball valve is shown in Figure 2.25. The so-called Miethke system comprises a diverter valve, which is controlled by a battery-powered solenoid actuating system. Energy is not required to maintain the open and close position of the valve because the electrical actuating system is not active at these points. When closed, the spherical body is seated over the valve aperture. The ball is displaced horizontally under the action of the solenoid to a position adjacent to the valve aperture. The valve status can be detected by a detector.

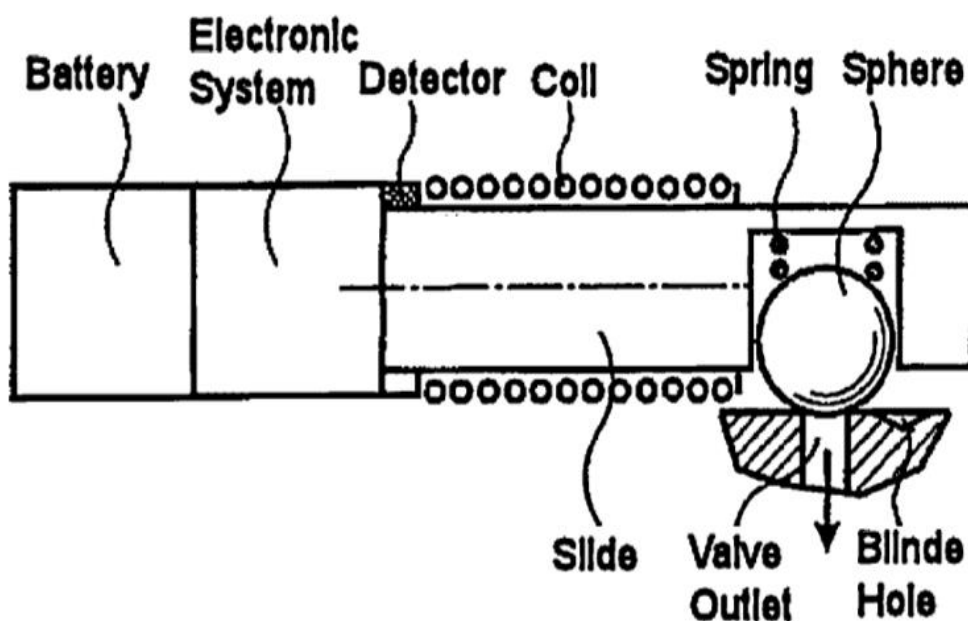


Figure 2.25: Diagrammatic representation of Miethke's mechatronic valve system
(Momani *et al.*, 2011)

The autonomous control and actuation of the mechatronic valve allows it to respond dynamically according to the measured ICP. Moreover, the continuous recording of ICP signals along with patient's feedback permits the clinician to update and manually adapt the program (Fig. 2.26). The researchers go on to explore the performance of various shunting approaches through multidimensional numerical 'figure of merit' (FoM). The parameters they chose to study include: normality, maintainability, over/under drainage, open durations, ICP fall, effective opening period and shunt dependency. The resulting FoM may be used as selection criteria in an intelligent shunting system to assess any prospective management and modification issues, according to a patient's specific needs.

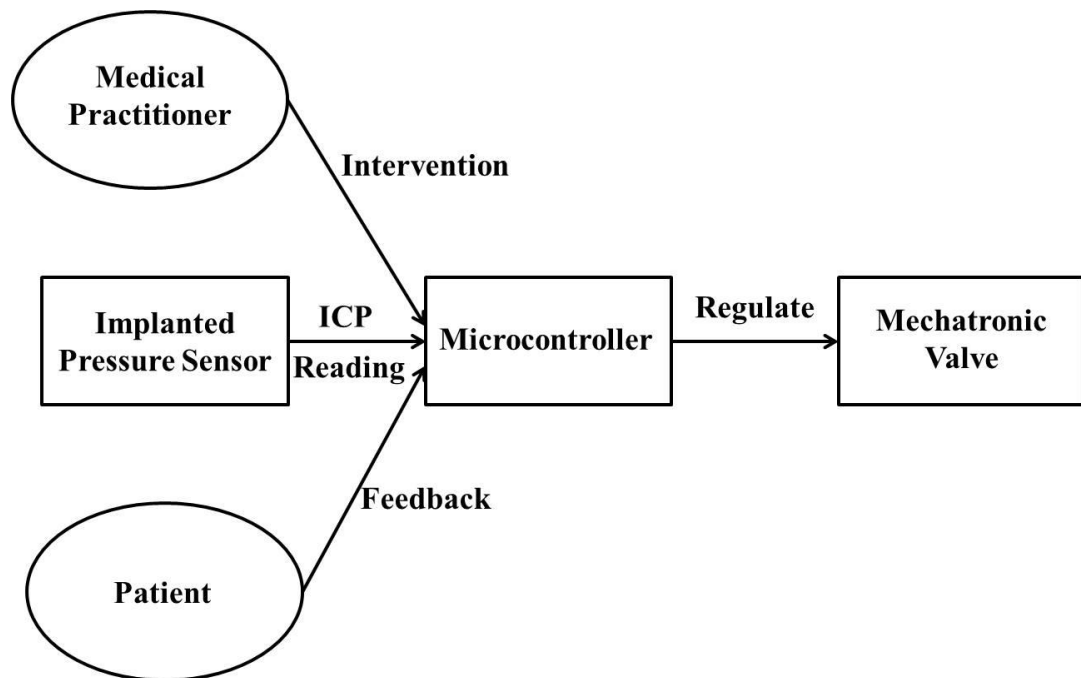


Figure 2.26: Intelligent way of controlling mechatronic valve (Momani et al., 2011)

Ventricular catheters are misplaced in as many as 10 to 40% of surgical procedures (Thomale *et al.*, 2013). Although techniques like endoscopy, ultrasound and neuro-navigation tools provide assistance for placement of the catheters, these procedures are time consuming, and are technically very demanding. Thomale *et al.* (2013) developed smart-phone assisted guidance tool to aid the insertion of a proximal catheter. A photograph showing the procedure is shown in Figure 2.27. Using 3D-MRI data cross referenced with CT images to quantify the relevant parameters, the coordinates were then fed into the guiding tool in order to compute the precise trajectory for catheter placement within the ventricles via a frontal precoronal incision. A clinical trial involving 35 patients was carried out, and preliminary results suggest that it is a safe and reliable ventricular catheter guiding system.



Figure 2.27: Photographic image of iPhone assisted ventricular catheter placement (Thomale et al., 2013)

2.7 Review of current ventricular catheter progresses

The hydrodynamic characteristics of a given shunt system are highly complex and dependent on many variables: for example, the function of proximal and distal catheter, valve behaviour, valve and siphon control communication, and any external pressure applied on the valve by the subcutaneous tissues (Francel *et al.*, 2001). Despite numerous advances in the last 60 years, the ideal shunt system has yet to become a reality (Sotelo 2012). Taking a holistic view, while some of the above approaches may prevent a valve from malfunctioning and improve the performance of the device, it must not be forgotten that obstruction in the proximal catheter will lead to a complete failure of the shunt, and replacement of the catheter is inevitable.

A typical proximal catheter is made of poly(dimethyl)siloxane (PDMS), and has thirty two, 500 μ m-diameter holes, approximately 500 μ m apart, aligned in four rows along its length (Appendix A). There appears to be no logical explanation for the size and number of holes, the shape of each hole, or the spacing between them (Harris and McAllister 2011). One manufacturer has commented that the design was chosen to place them as close to the tip as possible, but no further information about the length of the inlet and other design criteria is available (Kaufman and Park 1999). Although 1 or 2 holes may be sufficient to allow adequate amount of CSF to flow through the shunt (Ginsberga *et al.*, 2000), alternative designs are available, which include the addition of flanges and slots. However there is no evidence to prove that these changes in any way enhance the efficiency of the catheter, or are clinically effective (Lin *et al.*, 2003).

Lin *et al.* (2003) studied the proximal catheter design using computational fluid dynamics, a 2D water table model of a shunt catheter, and 3D automated testing apparatus. The results from the computational and experimental studies indicate that more than 80% of the CSF flows through the two most proximal set of holes. Thus, majority of the holes in the proximal catheter appear to be redundant. The authors of this study suggest that the CSF flow can be uniformly distributed by increasing the resistance to flow proximally, by increasing the area of the proximal end and decreasing the area of the distal perforated end of the catheter. Another suggestion is

to vary the diameter of the holes along the length of the catheter so as to allow CSF to enter the catheter more uniformly along its length.

Thomale *et al.* (2010,) hypothesised that decreasing the number of holes present in the catheter might decrease the risk of obstruction. Using flow visualisation techniques, they compared the flow characteristics of a catheter with six perforated holes with one having sixteen holes under steady pressure gradients ranging from 2 to 14 cm H₂O. Clinical studies were also carried out involving hydrocephalic patients (n = 55) with follow up study to evaluate the catheter revisions. The authors concluded that in the case of the 16-hole catheter, only the proximal perforations had any functional role, while all the perforations in the 6-hole catheter, on the other hand, contributed to the flow of CSF. There was no significant difference between the 16-hole and 6-hole catheters in terms of flow velocity, however. The results from the clinical study demonstrated an overall success rate of 77.4% for the mean follow up period of 15±9 months.

Proximal catheters explanted due to occlusion were also examined in their study to determine the type of cells responsible for obstructing the catheter. It was noted that extra-ventricular tissue contributed to blockage to the same extent as the intra-ventricular tissue. This study calls into question the necessity for the presence of excess hole in the conventional catheter: in ventricular occlusion, the perforations present outside the ventricle (i.e., not exposed inside the ventricles), increases the risk of shunt failure. The proposed new design has fewer holes present closer to the tip. Moreover, reducing the perforated length of the catheter allows correct intraventricular positioning. This research group outline the importance of precise placement of the perforated holes in the ventricular region and reduction in number of holes to minimise the blockage.

Lee *et al.* (2011) presented a novel MEMS concept to address the problem of cell accumulation in the perforations of a proximal catheter. Here, micro scale magnetic actuators are placed inside the holes of the proximal catheter (Fig. 2.28). The purpose of the microactuators is to generate large, out-of-plane movement with sufficient force to disrupt or prevent the cell accumulation: cell aggregates and debris

are physically removed from the catheter pores by the rotation of the magnetic microactuators in the presence of strong magnetic field. The authors undertook a feasibility study to compare different torsional designs and micro-fabrication techniques. They reported that their design of magnetic microactuators was able to remove 37.4% of the adherent cells on the surface of the actuator itself. One limitation of this study lies in the choice of cell type (vascular smooth muscle cell line), which are representative of the cells present in the ventricle.

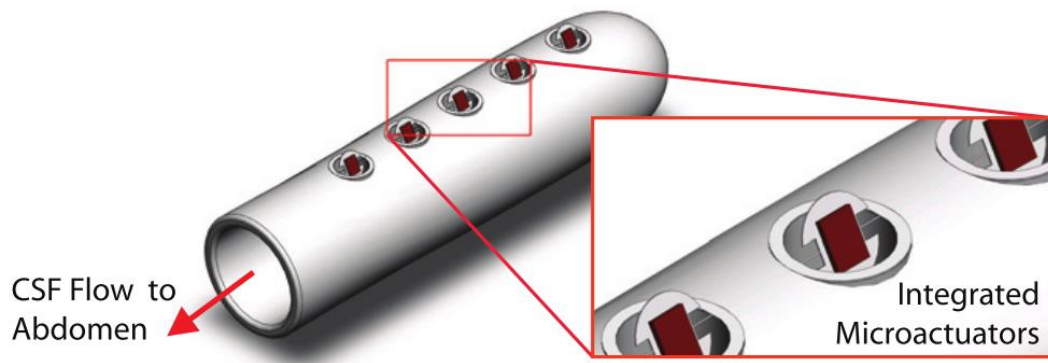


Figure 2.28: A 3-dimensional structure of the ventricular catheter fitted with the magnetic microactuator. The image on the right shows the microactuator in the actuated form (Lee et al., 2011).

Achyuta *et al.* (2010) identified that the attachment of cells to the surface of PDMS is the root cause of obstruction of the catheter. Hence, to address this problem they modified the PDMS surface chemistry by covalently conjugating trypsin – a chelating enzyme commonly used in cell culture to induce detachment of cells from a substrate. Human astrocytes were grown on the surface of the modified PDMS to study the cell adhesion in a static environment. The results from this study demonstrated that trypsin was able to maintain its proteolytic activity, and performed in a dose dependent manner. The modified PDMS exhibited significantly less cell adhesion compared to the un-modified polymer, even in the presence of fibronectin and albumin, two of the most abundant proteins present in the CSF. A limitation of this study is that these findings may not be replicated in the presence of flow.

Harris *et al.* (2010) have also devoted a considerable effort to develop an alternative catheter material that does not promote cell growth. They developed an *in-vitro* model to study the cell adhesion in hydrocephalus catheter under physiological conditions and compared them with static environment. They are one of the first groups to study the cell adhesion to a surface-modified proximal catheter material under a physiological flow conditions: the Hydrocephalus Shunt Catheter Bioreactor (HSCB) is designed to study astrocytes/macrophages cell adhesion under *in vitro* conditions of CSF pressure, flow rate and pulsation rate (Fig. 2.29). They reported significant differences in cell adhesion as a function of flow rate (0.25 and 0.3 ml/min), elevated pressure conditions and pulsation rates.

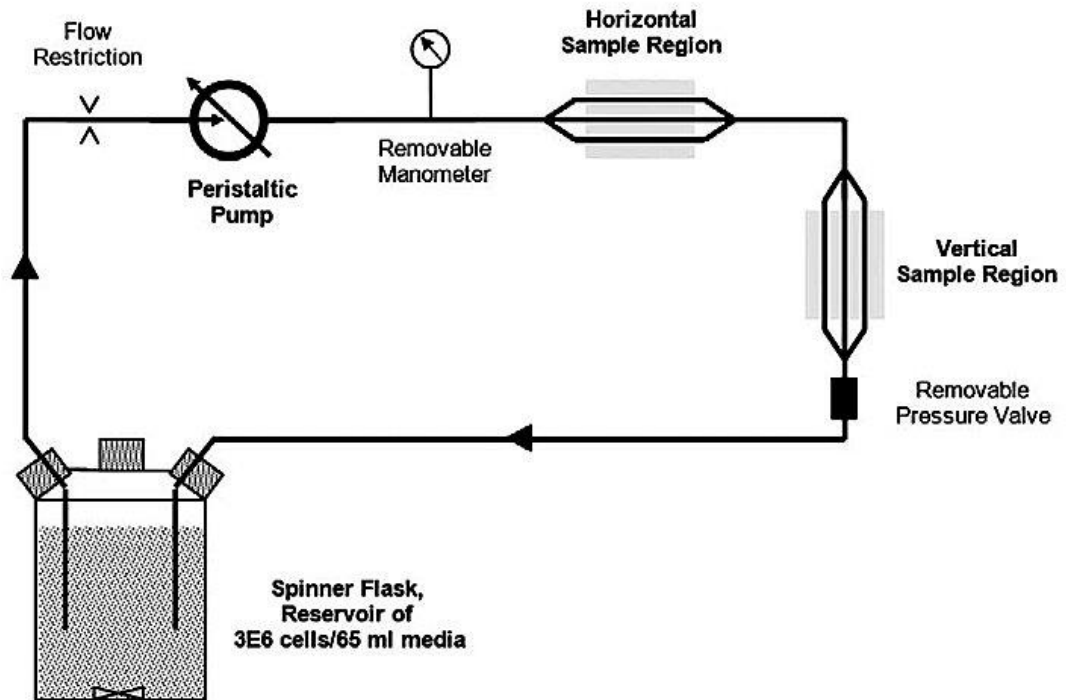


Figure 2.29: Outline of Hydrocephalus shunt catheter bioreactor system (HSCB). The behaviour of cell adhesion on a conventional PDMS catheter under static and dynamic conditions for up to 20 hours was studied using this system. Group of three channels were used to pump the cell suspension from the spinner flask into the catheter which is placed either vertical or horizontal to pulsatile flow. Flow restriction is achieved by varying the diameter of the tube so as to alter flow and pulsation rate. (Harris et al., 2010)

Harris and McAllister (2011) extended the above study to consider the effect of hole size on cell adhesion to a proximal catheter. They hypothesised that a reduction in shear stress brought about by maintaining the same surface area and increasing the perforated diameter would reduce astrocyte/macrophage adhesion. A fabrication technique to punch precise holes was developed in-house. PDMS samples with perforations ranging from 282 to 975 μm in diameter were considered. Using a fluorescence assay to quantify cell adhesion they found that cell adhesion was greatest on catheters with the smaller holes. The magnitude of shear stress increased as the perforated size decreased, with the 975 μm diameter holes giving rise to the lowest shear stress among the tested sample. A limitation of this study is the degree of sample of roughness, which may have an effect on cell adhesion on the samples.

Harris *et al.* published two further studies using the HSCB system (Harris *et al.*, 2011a; b) in which these authors explored the role of surface modification and protein adsorption on PDMS in terms of cell adhesion. In one experiment, they rendered the surface of PDMS hydrophilic by plasma oxidation, which introduces hydroxyl groups and remove methyl groups at the surface. Another approach involved modifying the surface with hydrophilic materials like polyethylene glycol (PEG) and N-acetyl L-cysteine (NAC). In order to study the protein adsorption effect on cell adhesion on the materials, before introducing the cells in the HSCB the cells were exposed to either lower (0.5% FBS with an albumin additive) or higher (standard 10% FBS) protein concentration for 24 hours to mimic the protein present in the CSF. Under fluidic conditions, cell adhesion increased according to the concentration of protein present on the samples; these effects were not significant, however. The authors concluded that patients with higher concentration of proteins in their CSF are at a greater risk of shunt obstruction (Harris *et al.*, 2011b).

Plasma-oxidised PDMS, on the other hand, was less conducive to cell adhesion in comparison to the untreated PDMS. Moreover, both PEG and NAC coated PDMS, coupled with plasma-oxidisation exhibited a greater and significant reduction in cell adhesions compared to the untreated PDMS (Harris *et al.*, 2011a).

2.8 Assessment of alternative ventricular catheter materials and fabrication techniques

The life span of a CSF shunt depends on the performance and durability of its components. It is clear from our search of the literature that the proximal catheter is one of the most vital components of the shunt-catheter system. Eymann *et al.* (2012) claim that 70% of all the hardware related issues affecting shunt patients is due to catheter malfunction. The explanation for this observation may lie in the consequences and inconvenience of carrying out shunt revision surgery, and the inflammatory responses of ventricular tissue to damage, which may give rise to subsequent shunt obstruction (Tuli *et al.*, 2000). The proximal catheter is considered to be the weakest link of the shunt device, yet efforts to improve its performance of this device are lacking (Harris and McAllister, 2011). Clearly, further research and development into new materials and designs is needed.

The ideal proximal catheter should have longer life span, and be made of biocompatible materials that do not encourage cell attachment and protein adsorption. It should promote the uniform distribution of CSF through the catheter (Fig. 2.30). The proximal catheters available at present do not satisfy most of the qualities identified.

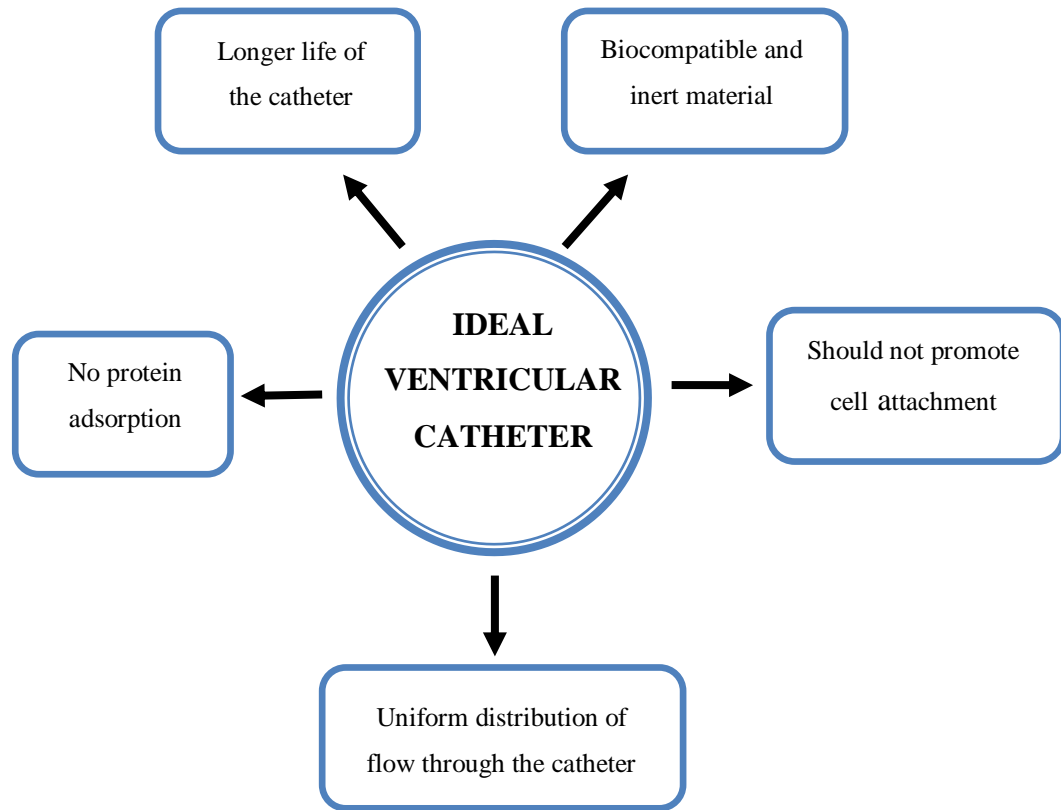


Figure 2.30: Ideal properties of ventricular catheter

The operating life span of a shunt is shortened significantly because of the failure of the proximal catheter, subjecting patients to the inconvenience of having to undergo repeated surgical procedures. Poor design criteria and a propensity for the proximal catheter to occlude have led historically to very poor outcomes.

The ideal catheter material might be thought of as being inert or bio-tolerated, whereas at present they are described as being 'bioactive' (Eymann *et al.*, 2012). Arguably, the designs and choice of material currently used to produce the proximal catheters have not considered the importance of minimising protein absorption and cell growth. Protein adsorption on its own will not affect the mechanism of the

shunt, but the presence of protein is likely to encourage cell growth on these materials, which, in turn, may block the holes through which CSF passes. Hence, future designs and catheter materials should aim to minimise protein adsorption and cell adhesion.

Moreover, the problem of catheter obstruction may be exacerbated by present designs of catheter, which do not promote uniform flow of CSF. This is due to the position of the catheter within the intraventricular space, which favours CSF flow only through the most proximal holes of the catheter (Lin *et al.*, 2003). There is no scientific explanation for the design of the conventional proximal catheter, the most likely reason being to ensure adequate CSF flow from the ventricles of the brain (Harris and McAllister 2011). Then again, Thomale *et al* (2010) pointed out in their study that there is a flaw in the design of the catheters available at the moment, which is that the CSF flows only through the most proximal perforated holes.

Unlike most other catheters used in medical applications, the hydrocephalus shunt may be implanted in patients for many years. Surprisingly, there is little to distinguish the CSF catheters used at present from other types of catheter, and efforts to design a catheter that is less prone to obstruction from cell growth, and which therefore has a longer working life in the patient are long overdue. From the preceding assessment of the current literature on this topic, the proximal catheter has been identified as the weak link in the design of current shunt catheter systems. There follows some specific proposals for research that builds on what has been achieved thus far, with a view to improving the success rate of shunt catheters in the longer term.

2.8.1 Polyurethane as an alternative catheter material

To our knowledge, there is no record of any other kind of biomaterial besides PDMS having been implemented for this application. From the wide range of biomaterials available for use in medical applications, many alternative materials are very successful and still in use today. Synthetic polymeric materials like polyethylene, polyvinyl chloride, fluoropolymers, hydrogels and silicones have found application in the field of biomaterials. Polyurethane elastomer has had a long history in this sector owing to its remarkable physical-mechanical properties and versatile blood and tissue compatibility (Khorasani and Shorgashti 2006; McMilln 2006; Zdrahala and Zdrahala 1999). Likewise, Stokes *et al.* (1995) argues that the application of polyurethane elastomer in the medical field has improved patients' quality of life remarkably, and that the full potential of this polymer is yet to be realised.

Polyurethane (PU) is a polymer comprising repeated - [NH-COO-] – linkages, which make up the molecular chain. PU is considered to be one of the most multi-purpose materials in the field of medical devices. PU can be synthesised to have a wide range of molecular weights and different chemical structures, yielding a wide range of material properties appropriate for a variety of medical applications (Reed *et al.*, 1994). Since 1966, PU has been used widely in the field of medical devices because of its good bio/blood compatibility, which is attributed to its structure and property diversity (Boretos 1980). PU has certain properties that make it very attractive for use in clinical practice: its durability; fatigue resistance in tension, compression or shear; elasticity; compliance; elastomeric behaviour; good electrical insulation; biostability; and tendency to promote healing (McMilln 2006; Stokes *et al.*, 1995; Zdrahala and Zdrahala 1999).

There are numerous examples of medical applications where PU has found application including: blood bags, vascular catheters, left ventricular assist devices, total artificial heart, pacemaker wire insulation, flexible-leaflet heart valves, vascular/arterial grafts, transcutaneous access sets, ventricular assist bladders, arteria-venous shunts, drug delivery system, cardiac patches, mammary prostheses, dental materials and many more long-term implants (Boretos 1980; Reed *et al.*,

1994; Stokes *et al.*, 1995; Zdrahala and Zdrahala 1999). More recently, PU has been effectively implemented as a peripheral catheter (Rivera *et al.*, 2005).

The form of PU used in medical devices is usually block/segmented copolymers, which is made by combining a hard segment (isocyanate) and soft segment (glycol). A variety of polyurethanes with diverse physical properties can be created by varying the ratio of hard and soft segments (Stokes *et al.*, 1995). There are three major varieties of PU: thermoplastic, thermosetting and cross-linked (Reed *et al.*, 1994). At present there are a number of types of polyurethane commercially available for medical applications: Zytar[®], Tecoflex HR[®], Pellethane Series 2363, Texin[®] Medical Polyurethane, Bioelectric Polyurethane and Avcothane[®] copolymer. PU lends itself to surface modification (Józwiak *et al.*, 2008), as appropriate to the purpose of the application. Some of the modifications include balancing the hydrophilic/hydrophobic nature, attachment of bioactive molecules, for example heparin like compounds for anti-coagulant, tissue growth inhibitor, or anti-microbial agents. These modifications enhance the implants success rate in reference with wound healing and host response. Hence, for this application, PU is a plausible candidate. As demonstrated by Harris *et al.*, by manipulating the surface of the catheter to render it to more hydrophilic, the likelihood of protein adsorption and cell attachment is reduced.

The medical grade polyurethane elastomers used in this study are commonly used to fabricate, amongst other things, balloon catheters for use in angioplasty procedures. Their elastic properties are not dissimilar to those of PDMS.

2.8.2 Fabrication techniques of porous polyurethane

There are numerous techniques that are used to produce polyurethane to suit this application. The most common and widely used method of processing involves dissolving polyurethane in a suitable solvent. Casting and dipping techniques are used to produce a cast film which is used in the application of heart valves/diaphragms, ventricular assist bladder and blood bags. Vascular grafts and patches are produced using electrospinning method. Finally, phase separation processes yield a porous membrane structure appropriate for use in filtration and wound healing applications.

The limitations in the design of conventional shunt catheters identified in the previous section concerns the form the material takes (polymer extrusion) and the presence of perforated holes for CSF transport. For the purpose of this study, we employed a method of fabrication that can yield a polymer catheter having permeable wall, the pores of which provides an alternate path for CSF transport. There are many methods available to produce porous PU, such as electrospinning, solvent casting/salt leaching, phase inversion, laser excimer ablation, and thermally induced phase separation (Guan *et al.*, 2005; Khorasani and Shorgashti 2006). Table 2.3 shows the advantages and disadvantages of each method, by way of justification for the method that was chosen for the present study.

Method	Brief description	Pros	Cons	Reference
Electrospinning	Fibre scaffold are produced under an electric field	Accurate fibre dimensions Natural extracellular matrix	Fail to produce large pore size	(Demir et al., 2002; Doshi and Reneker 1995; Grasl et al., 2010; Martins et al., 2008)
Solvent casting/Salt Leaching	Porous scaffold is produced by mixing polymer with salt particulate according to pore size	Various porous scaffold can be produced	Poor control of interconnectivity of pores	(Carlberg et al., 2009; Guan et al., 2005; Sharifpoor et al., 2010; Sin et al., 2010)
Phase Inversion	Mixing homogeneous mixture of polymer with non-solvent and solvent to result in phase separation	Good interconnectivity	Less control over accuracy in pore size	(Khorasani and Shorgashti 2006; Tsui and Gogolewski 2009)
Laser Excimer	High energy ultraviolet (UV) is used to break the chemical bond to form hole	Accurate pore size	Poor connectivity	(Doi and Matsuda 1997; Doi et al., 1996; Khan and Newaz 2010)
Thermally Induced Phase Separation	Polymer solution is moulded by controlling the temperature	Good control over pore size and structure	Mismatch in compliance	(Guan et al., 2005; Liu and Kodama 1992)

Table 2.3: Comparison of methods to prepare porous PU

From the information presented in Table 2.3, it is clear that the electrospinning method allows greater control of fibre diameter and density (Guan *et al.*, 2005). The technique is versatile, in that it can yield polymer fibres having diameters over a wide range, from a few tens of nanometres to micrometres in diameter, and between 0.05 – 5 micrometres in length (Demir *et al.*, 2002).

Doshi and Reneker (1995) presented the physical principles behind the electrospinning technique, which involves the application of an electric field to a polymer solution held by surface tension at the end of needle. Mutual charge repulsion generates a force that acts in direct opposition to the surface tension. By increasing the intensity of the electric field, the polymer adopts a conical shape – known as Taylor Cone, which forms due to the elongation of the hemispherical surface of the solution at the tip of the needle. When the electric field reaches a critical value, at which the repulsive electric force exceeds the surface tension force, a charged jet of polymer solution is ejected from the tip of the Taylor Cone. The electric field can be manipulated to control the path taken by the polymer jet. The polymer jet elongates into a fine fibre, which partially solidifies as the solvent evaporates, and is randomly deposited onto the surface a negatively-charged collecting screen or target. Depending on the exact processing parameters the process yields non-woven fibrous mats possessing a wide range of fibre diameters, orientation, porosity and thickness.

The fibre dimension can be altered by varying the following parameters: the viscosity properties, conductivity and surface tension of the polymer solution; processing variables include polymer flow rate, electrostatic potential at the tip, and the distance between the tip and the collection screen. The process depends also on environmental factors, which include ambient temperature, humidity and air velocity in the electrospinning chamber.

2.9 Aims and Objectives of the Study

Ventricular catheter performance in terms of hydraulic and biocompatibility, is affected by the choice of the material and form it is made. Therefore, aim of this research, was to evaluate an alternative ventricular catheter that can overcome some of the aforementioned problems, namely proximal catheter obstruction. To address this problem, the following specific objectives have been identified:

1. Materials characterisation. To explore electrostatically spun polyurethane (EPU) as an alternative to PDMS for the proximal catheter.
2. Hydraulic performance. The candidate EPU catheter material will be evaluated in terms of its hydraulic performance in comparison to the components of a commercially available shunt catheter series. To this end, a computer-controlled shunt testing system will be built to monitor CSF and ICP under steady flow conditions of the conventional hydrocephalus shunt system. By examining the impedance characteristics of each system and their ability to regulate the flow of CSF, we aim to specify a new catheter system that can accommodate variations in the pressure without rapid changes in the ventricular volume.
3. Biocompatibility assessment. The biocompatibility of a number of polymers in the form of cast films, microporous polymer foams and mats will be examined. In addition to viability assays (Live-Dead[®], almarBlue[®]) and epifluorescence microscopy for the assessment of cell viability and growth on each material, a cell culture model of shunt obstruction will be developed in order to study quantitatively the effect that the presence that cells will have on hydraulic permeability of the fibrous materials in the presence and absence of key CSF proteins.

CHAPTER 3

FABRICATION AND EVALUATION OF AN ALTERNATIVE VENTRICULAR CATHETER

3.1 Introduction

This chapter presents the methods used to fabricate the alternative form of hydrocephalus shunt catheter, and the apparatus that was used to evaluate its hydrodynamic properties. The physical and hydraulic properties of the components of an existing shunt series were studied for comparison. Numerous centres have reported on the development and use of *in vitro* shunt models for the purpose of evaluating hydrodynamic performance of commercially available systems (Section 2.4.1). The operational characteristics of a given shunt device are typically determined by a combination of pressure (ICP) and flow (CSF) control. The most common modelling approach is to control the pressure and measure the flow, or vice versa. The components of a typical test circuit will include pressure and flow transducers, a flow source and fluid reservoirs. Studying the hydraulic properties of each component individually, and in combination, provides an overall picture of the importance and the effect of each component.

The method of fabrication for the alternative catheter was described in Section 2.8. Here, the hydraulic properties of the new catheter will be examined *in vitro* using a purpose built shunt-testing system. The results from this study will help to establish the feasibility of the new catheter design to serve its purpose in the application of hydrocephalus shunts.

3.2 Materials and Methods

3.2.1 Design, fabrication and characterisation of alternative catheter

The EPU catheter samples used in this study were prepared at the University of Liverpool by Mr Richard Heyes under the direct supervision of the author's supervisor (personal communication, Dr RA Black).

The apparatus and methods used to fabricate the electrospun polyurethane (EPU) catheter material are described in detail elsewhere Andrews et al. (2008). Briefly, the electrostatic spinning apparatus consisted of mandrel, grid, traverse with spray nozzles, syringe pump, high-voltage power supplies and heater. The set up was housed inside a Class II laminar flow hood as shown in Figure 3.1. The process was carried out at 25 ± 2 °C and humidity of 30-35%. The polyurethane used was Tecoflex™ SG-80A (Thermedics Polymer Products, USA) which was purchased from a commercial source.

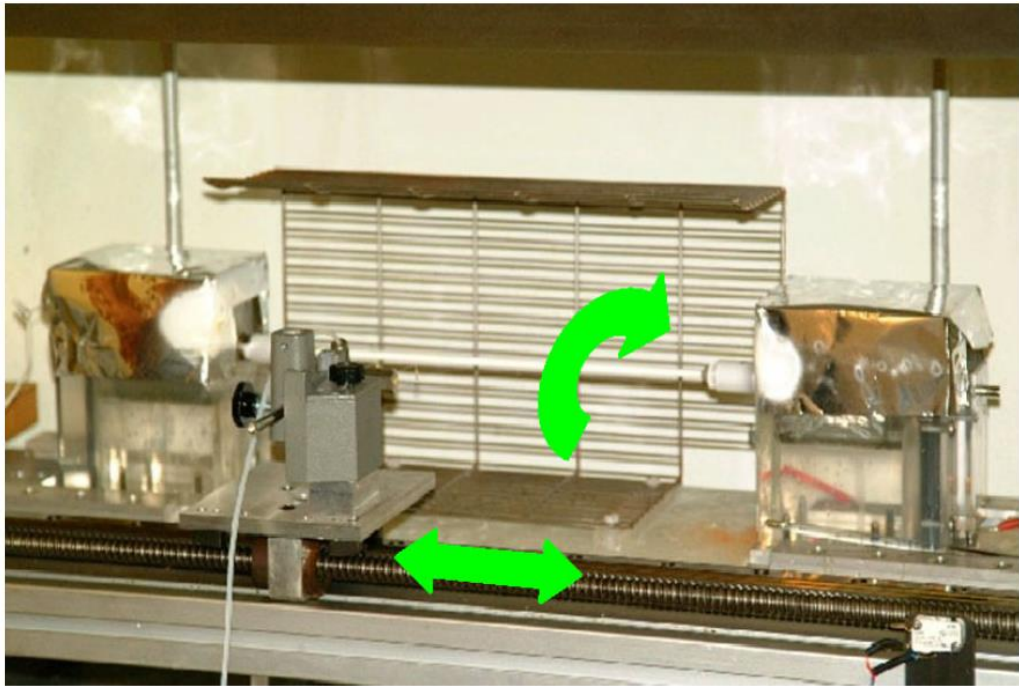


Figure 3.1: Photograph showing the electrostatic spinning rig used to produce the microfibrinous specimens used in this study. The mandrel in the centre is covered with polymer fibre, and on either side the bearing housings and drive mechanism. The direction of rotation is indicated by the arrow. The sliding carriage shown here on the left side of the image carries the spray nozzle, and translates back and forth in the direction indicated by the arrow (Andrews et al., 2008)

The polymer dispersion comprised 10% w/v polymer in an organic solvent – n,n-dimethylacetamide (DMAc). The polymer was dispensed via a delivery manifold comprising two or three stainless-steel 24-gauge needles, at a flow rate of between 1-10 ml/h. The polymer solution was drawn towards an aluminium-covered target or stainless-steel mandrel by the electrostatic field created by two voltage-regulated DC power supplies (alpha III series, Brandenburg, UK) each generating voltages in the range –10 and –20 kV relative to the needles.

The distance between the mandrel and delivery manifold was in the range 10 – 15cm. The polymeric fibres that formed under the action of the electrostatic field were deposited onto a 3-mm diameter mandrel rotating at a nominal speed of 1000±50 rpm. The manifold traversed the length of the mandrel repeatedly until 150±20 µm wall thickness was achieved, after which the catheter was air dried and then soaked in distilled water to remove further solvent residues and traces of NaCl. For final stage of drying, the samples were dried under vacuum at 25 °C for 24 to 48 hours to remove further traces of any chemical present.

The morphology of the EPU material was determined by Scanning Electron Microscopy (SEM) (Hitachi TM 1000 SEM) to characterise the EPU material. A small portion of the catheter was cut and affixed to a stub ready for imaging. Micrographs of both the inner and outer surfaces of the electrospun material were acquired and analysed to determine the inter-fibre separation, fibre diameter and alignment of the fibres.

3.2.2 Experimental rig to test hydraulic properties of shunt series

There are some assumptions that need to be considered before building the experimental apparatus to test the shunt system. The amount of CSF flowing through the shunt should be equivalent to the total amount of CSF produced. The production and absorption of CSF for a hydrocephalus patient is 0.35 ml/min, the total volume of CSF at any time is 150 ml, and resistance to flow in normal circulation is 6 to 10 mmHg ml⁻¹ min⁻¹ (Schley and Billingham, 2002). In order to model the hydrocephalus condition, it is assumed that the CSF production is normal but the absorption is absent or compromised, leading to rise in pressure. Hence the excess CSF shunt will drain through the device under the action of the elevated pressure gradient. Steady and laminar flow of CSF through the shunt devices is assumed. It is also a common assumption when modelling the flow of CSF that pressure and flow are directly proportional, that resistance to flow is pressure independent, and compliance is pressure dependent (Eklund *et al.*, 2007).

The flow through a cylindrical vessel is defined by the Hagen-Poiseuille Law:

$$Q = \frac{\Delta P \pi r^4}{8 \eta L} \quad \text{Eqn. 3.1}$$

where,

Q = Volumetric flowrate (m³/s)

ΔP = Differential pressure (Pa)

η = Viscosity (Pa s)

r = Radius (m)

L = Length (m)

From Equation 3.1, it is clear that the resistance to flow is influenced by the viscosity of the fluid and length of the tube. Under normal conditions, the viscosity and density of CSF is equivalent to that of water (Czosnyka M. *et al.*, 1997). Hence, CSF

is assumed to be a Newtonian fluid that is not affected by any proteins or cells it may contain (Schley *et al.*, 2004). Hence in the experiments that follow, de-aerated/distilled water was used to mimic CSF. The valves were tested with and without the distal catheter present, because length of the catheter has an influence on the flow.

The experimental set up was based on the system developed in UK Shunt Evaluation Laboratory in Cambridge (Czosnyka Z. *et al.*, 2002). The outline of the design is illustrated in Figure 3.2. Reservoir 1 is filled with 200ml of water to mimic the excess accumulation of CSF within the ventricle of the brain. The fluid is replenished continually with the help of syringe pump (Cole Parmer, Vernon Hills, USA) so that the volume of the liquid remains constant even when the liquid is withdrawn at a constant rate (0.35 ml/min). This constant replenishment of liquid into the system represents the production of CSF. The difference in pressure between reservoir 1 and 2 is achieved by raising it to the required height on the cross-head of a tensile test apparatus (Z005 Zwick Roell, Ulm, and Germany), which can travel up to 1 m in height, and this give a wide range of pressure to study. The pressure within the shunt components was measured by means of 2 catheter pressure transducers (Millar Mikro -Tip[®]). The mass flow rate was determined by placing reservoir 2 on a 1000g load cell (Bose Electroforce, MI, USA). The software provided by the manufacturer (WinTest 4.1, Bose Electroforce) recorded the pressure and mass flow in mmHg and Newtons, respectively, and the data were saved to disk. The experiment was carried out at room temperature.

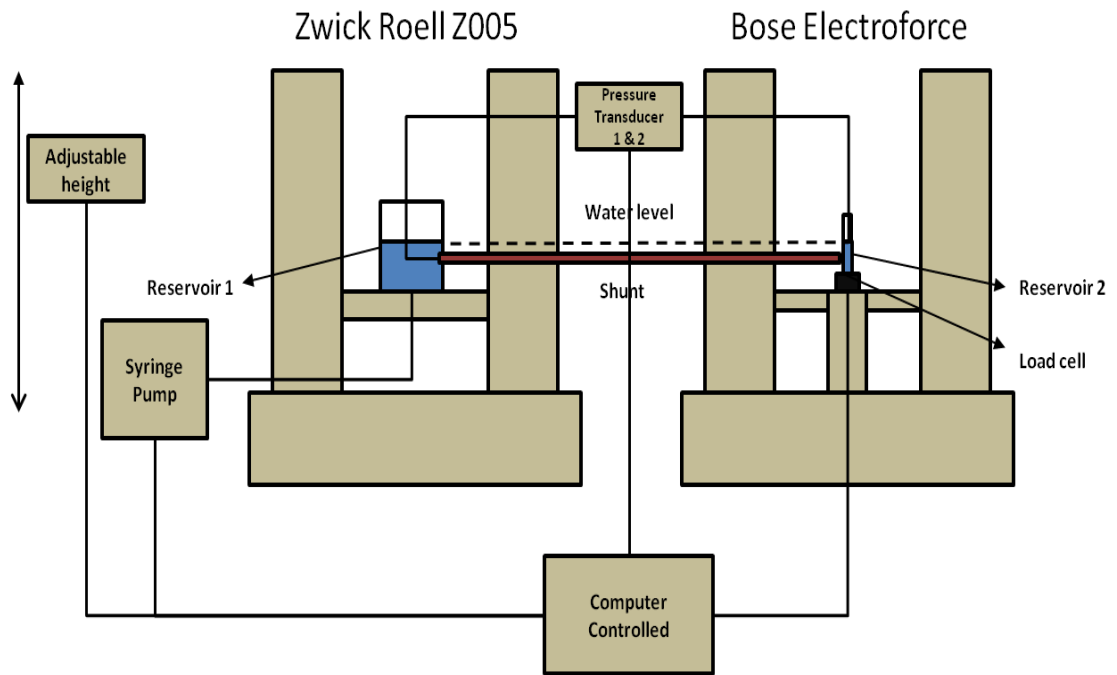


Figure 3.2: Illustration of hydrodynamic test apparatus. A constant head of pressure was maintained at the desired pressure by adjusting the height of reservoir 1 (Zwick Roell 2005), while the Electroforce software records the pressures within the shunt system and the mass of fluid displaced. The syringe pump was programmed to deliver a constant flow of 0.35 ml/min.

3.2.3 Shunt Component testing

The *in vitro* model was used to determine the pressure-flow relationships for the hydrocephalus shunt series as a whole, or each individual component in isolation. To test shunt as a whole, the proximal catheter was connected to the reservoir 1 via a port, mimicking the insertion of this catheter into the skull of the patient. The fluid from the reservoir 1 drained via the proximal catheter to the valve, which was connected to the end of the proximal catheter and affixed to the outside wall of the reservoir. Once the opening pressure was achieved, the valve opened and the fluid passed through the distal catheter to the second reservoir, where the mass flow was recorded. The first pressure transducer was inserted into the reservoir 1 to record inlet pressure while a second recorded the pressure at the outlet of the distal catheter located within reservoir 2. The pressure flow relationships for the individual shunt components were determined in a similar way. Three sets of pressure and flow data were recorded over a prescribed range of pressures over a period of 5 minutes.

3.2.4 Hydraulic permeability determination

Flow through a porous material is governed by D'Arcy's Law as stated below,

$$Q = \frac{k A \Delta P}{\mu L} \quad \text{Eqn. 3.2}$$

Where,

Q = Volumetric flowrate (m^3/s)

k = Hydraulic permeability (m^2)

ΔP = Differential pressure (Pa)

A = Area (m^2)

L = Length (m)

μ = Viscosity (Pa s)

Hydraulic permeability (as distinct from conductivity, which depends on the combined effects of the fluid properties and those of the porous medium through which it flows) is a measure of the intrinsic properties of the medium, and may be related to the porosity and micro-structure of the medium. The S.I. unit for hydraulic permeability is [m^2].

The flow across the porous materials is assumed to be laminar flow with low Reynolds number. The relationship states that in a porous material volumetric flowrate is a function of the flow area, fluid pressure, viscosity, elevation and proportionality constant. The above equation is developed for materials which are assumed to be porous along the cross-sectional area (Batu, 2005) (Smillie *et al.*, 2005)(Smillie *et al.*, 2005)(Smillie *et al.*, 2005). Hence, the hydraulic permeability is defined by ratio of volumetric flowrate and differential pressure multiplied by length over area. However, since the EPU catheter has porous walls with hollow tube structure. The hydraulic permeability is defined by ratio of volumetric flowrate and product of differential pressure and area.

In order to facilitate the measurement of hydraulic permeability of the EPU catheter material, each catheter was assembled into a module fashioned out of an acrylic tube. A pictorial representation of one such module is shown in Figure 3.3. A short length of catheter tubing (8cm) was placed inside an acrylic tube, and sealed at either end by injecting polyurethane resin, one end at a time. The potting resin is made by mixing aromatic polyisocyanate (Texaflex XP 5394 A, Cerano, Italy) and polyether polyol (Texaflex XP 5395 B) to a ratio of 50:50. After injection, the module was centrifuged at 1000rpm for 1hour at room temperature, and placed in a 37° C in oven overnight to cure. The process was repeated for the other end. After the resin had completely cured, a thin section was cut from each end to expose the catheter. Each end was capped and sealed with silicone adhesive. After the silicone adhesive had cured completely, the module was checked for any leakage or damage before use.

The hydraulic permeability of each module was determined according to both pressure and flow controlled methods described in Section 3.2.3, with de-aerated/distilled water being used to mimic CSF. An annotated photograph of a module is shown in Figure 3.3, showing the inlet and outlet ports, and locations of the pressure transducers. In order to determine the hydraulic permeability of the catheter by flowrate, a syringe pump (Cole Parmer, Vernon Hills, USA) injected fluid at a set flowrate directly into the module inlet port, and the differential pressure across the walls of the catheter were recorded. The hydraulic permeability of each catheter was also determined under a constant head of pressure over a set range of pressures, and the corresponding mass /volumetric flow calculated according the mass of fluid passing through the module. The EPU samples were categorised into low, medium and high hydraulic permeability groups after measurements.

Hydraulic permeability was determined under both a positive and negative pressure gradient (i.e., by adjusting the pressure gradient so that the flow passed through the walls of the catheter from inside to outside and from outside to inside of the EPU catheter). However, at higher pressures, the tube collapsed when the direction of flow was reversed. The choice of flow direction for the analysis of shunt-obstruction was made largely for practical reasons: it is easier to seed cells uniformly onto the

inner surface of a cylindrical tube by means of rotation and allowing the cells to settle under the action of gravity. Therefore, for practical purposes only inside-outside flow measurements were considered for further studies.

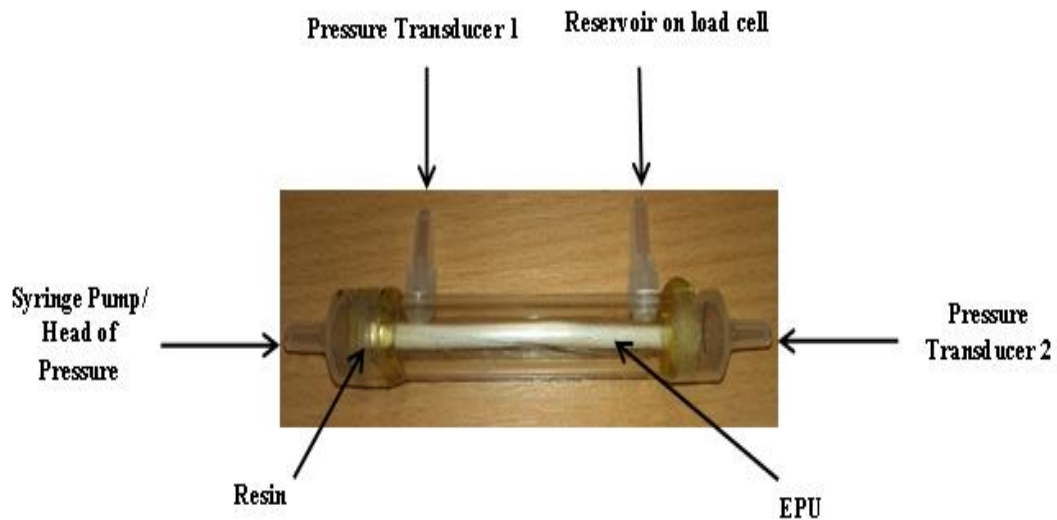


Figure 3.3: Photograph of an EPU module for hydraulic permeability determination. The inlet port has connections connected to the syringe pump/head of pressure. A catheter pressure transducer is inserted via the opposite port to record the pressure within the lumen of the EPU catheter. Fluid displaced from the module exits via the port that is connected to the reservoir with load cell. Pressure transducer 2 measures the pressure inside the catheter and pressure transducer 1 measures pressure within the module.

3.2.5 Statistical Analysis

The data presented throughout this work is represented as mean \pm standard error. All the experiments present throughout this thesis were triplicated unless stated otherwise. Student's t-test or one-way analysis of variance (ANOVA) with post-hoc Dunnet's or Tukey's was used to determine the statistical significance where appropriate. The level of significance was considered to be $p < 0.05$, unless stated otherwise.

3.3 Results

3.3.1 Characterisation of EPU catheter

The morphology of the EPU catheter material was determined by SEM; both the inner and outer surfaces were analysed and the resulting images are displayed in Figure 3.4. The plaques visible on the inner surface of EPU (Fig. 3.4 C) are where some of the polymer has flowed onto the surface of the mandrel during the electrospinning process. The outer surface, by contrast, is comprised entirely of discrete fibres (Fig. 3.4 A, B). The thickness of each EPU catheter (not shown), being a function of the processing time, was relatively consistent ($150 \pm 20 \mu\text{m}$).

Inner and outer surface of EPU catheter topography was characterised in terms of inter-fibre separation (Ifs) and fibre diameter (F.dia). Dimensions were obtained with an aid of ImageJ software tool. Ifs (pore size) of the sample are defined as the distance between adjacent fibres at the widest separation. F.dia is defined as the distance across a single fibre edge to edge. Measurements were documented from fibres on the uppermost layer which was determined using the SEM (only the top fibrous layer was focused). All the measurements were repeated a dozen times. Table 3.1 shows Ifs and F.dia measurements of six different EPU catheters of which three different scan areas of each EPU catheters were examined; corresponding means and standard error are illustrated.

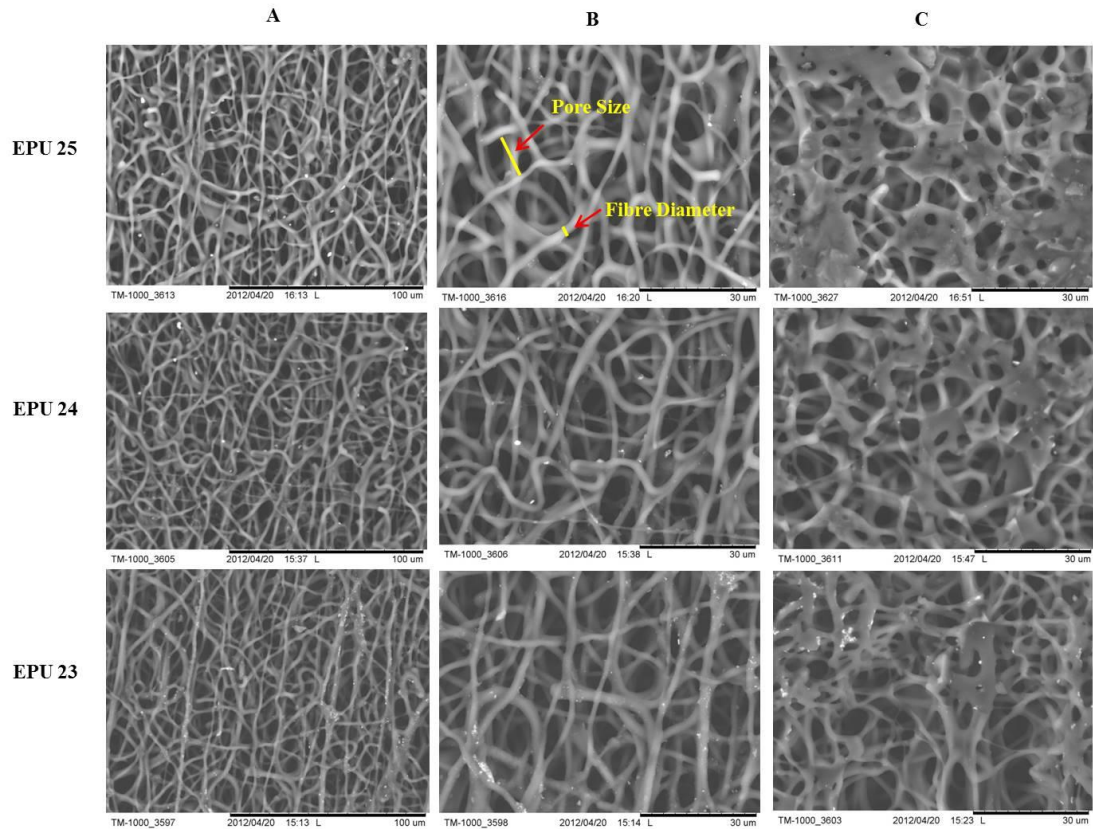


Figure 3.4: SEM micrographs illustrating the range of morphologies of the EPU catheters used in this study. A represents the outer surface of the material with a scale bar of 100μm, B represents outer surface of the material with a scale bar of 30μm; and C represents the inter surface with a scale bar of 30 μm. The arrows shown in B (EPU 25) denotes where a typical measurement was made.

a

Sample	Ifs of inner surface \pm SD (μm)	Ifs of outer surface \pm SD (μm)	Un-paired Student Ttest (p value)
EPU 19	6.82 \pm 1.74	6.67 \pm 1.2	0.68
EPU25	9.15 \pm 2.78	8.27 \pm 2.15	0.18
EPU 24	13.5 \pm 1.96	14.3 \pm 1.8	0.07
EPU 26	12.01 \pm 1.67	13.88 \pm 1.89	0.09
EPU 20	17.07 \pm 3.51	18.73 \pm 3.44	0.09
EPU 23	16.17 \pm 2.02	19.79 \pm 2.71	0.05

b

Sample	Fibre diameter of inner surface \pm SD (μm)	Fibre diameter of outer surface \pm SD (μm)	Un-paired Student Ttest (p value)
EPU 19	2.17 \pm 0.39	2.32 \pm 0.39	0.11
EPU25	1.92 \pm 0.44	1.92 \pm 0.34	0.96
EPU 24	1.72 \pm 0.22	1.6 \pm 0.24	0.05
EPU 26	1.67 \pm 0.38	1.75 \pm 0.37	0.44
EPU 20	1.55 \pm 0.29	1.49 \pm 0.22	0.40
EPU 23	1.22 \pm 0.24	1.37 \pm 0.26	0.08

Table 3.1: The Ifs (a) and fibre diameter (b) of EPU inner and outer surface with SD is shown along with the Student Ttest p value. Number of repeats is 36.

3.3.2 Pressure flow relationship of conventional CSF shunt system

The pressure-flow relationships for two shunt series, and the individual components, were measured to determine their hydrodynamic behaviour. The series included a proximal catheter, one fixed and one programmable opening-pressure valve, and a distal catheter. The pressure-flow relationships for all the combinations of the shunt components are shown in Figure 3.5. The inclusion of distal catheter has a significant effect on the pressure-flow relationship of the valve. There is no significant difference between the respective combinations of fixed pressure valve and programmable pressure valve. Detailed results for the individual shunt components are presented in Appendix C.

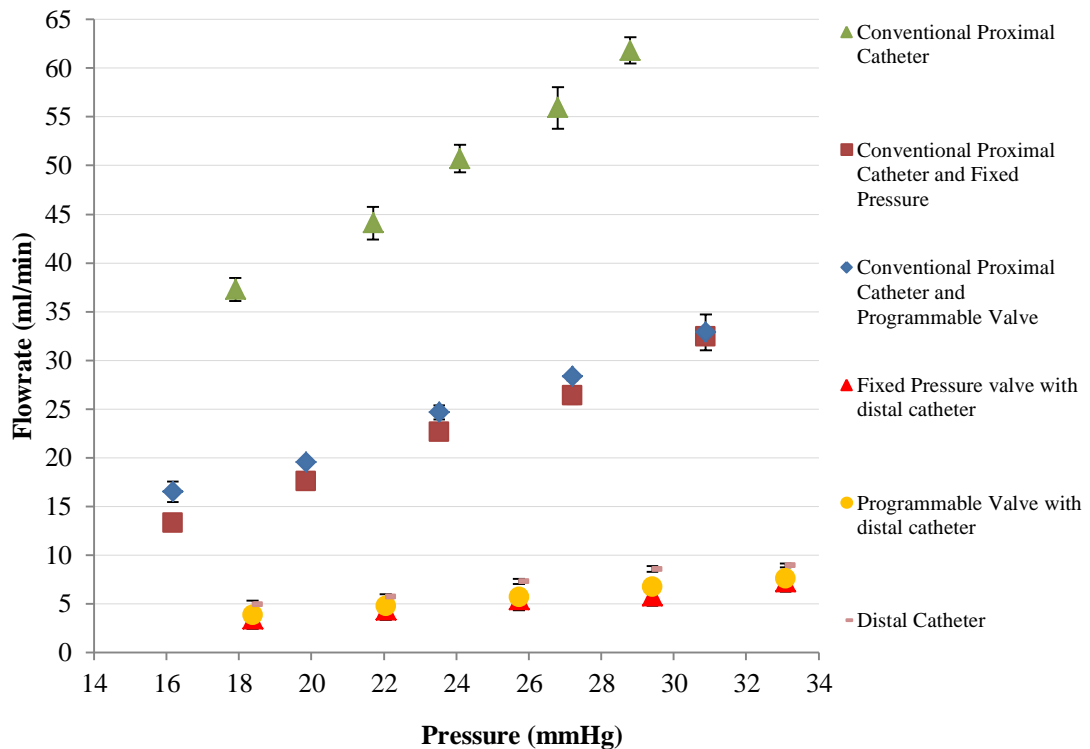


Figure 3.5: Comparison of pressure vs. flow relationship for the shunt components.

Data points represents the mean \pm standard error ($n = 3$)

3.3.3 Hydraulic resistance of conventional shunt components

The hydraulic resistance of the each shunt component and in series is calculated to be an average of pressure over flow, which is summarised in Table 3.2. Of all the individual components, the proximal catheter presents the least resistance to flow whereas the distal catheter has the highest; hence the resistance of the shunt series where the distal catheter is present is higher than without. The contribution of the proximal catheter to the resistance of the shunt series as a whole is almost negligible.

Shunt Components	Resistance (mm Hg/ml/min)
Proximal catheter	0.468
Fixed pressure valve	2.484
Programmable valve	3.351
Distal catheter	3.649
Proximal catheter and fixed pressure valve	0.7681
Proximal catheter and programmable valve	0.7814
Shunt series (Fixed pressure valve)	4.989
Shunt series (Programmable valve)	4.575

Table 3.2: Resistance of the shunt component

3.3.4 Pressure flow relationship of EPU catheter

The hydrodynamic characteristics of the EPU catheters in terms of resistance (n=4) were measured using the experimental set-up as described in Section 3.2.4. The rate of flow and its direction was controlled, and its corresponding pressures were measured to determine whether there was any difference in resistance due to change in direction of flow. The resistance for all the samples and under both conditions are shown in Table 3.3. The average of three resistances measurements for each sample is shown. The resistance to flow for EPU 45 and 54 is not affected by the change in flow direction. However, EPU 46 and 47 shows a significant difference due to change in flow; this might be due to the collapse of the sample at elevated pressures.

Sample	Resistance to flow (inside to outside) ± SD (mmHg/ml/min)	Resistance to flow (outside to inside) ± SD (mmHg/ml/min)	Un-paired Student Ttest (p value)
EPU 45	4.25 ± 0.88	3.52 ± 0.68	0.06
EPU 46	6.85 ± 1.46	3.52 ± 0.37	0.02
EPU 47	5.910 ± 1.68	4.170 ± 1.28	0.03
EPU 54	4.16 ± 0.98	3.52 ± 0.81	0.05

Table 3.3: Resistance to flow for flow in direction of inside to outside and outside to inside for four EPU catheters

3.3.5 Hydraulic Permeability of EPU catheter

The pressure-flow relationships of 15 EPU catheters were measured to determine their hydrodynamic behaviour. The pressure-flow relationships for all the samples are shown in Figure 3.6. The flow direction for this experiment was inside to outside of the EPU. The average of three pressure-flow measurements for each sample at each flow rate is shown.

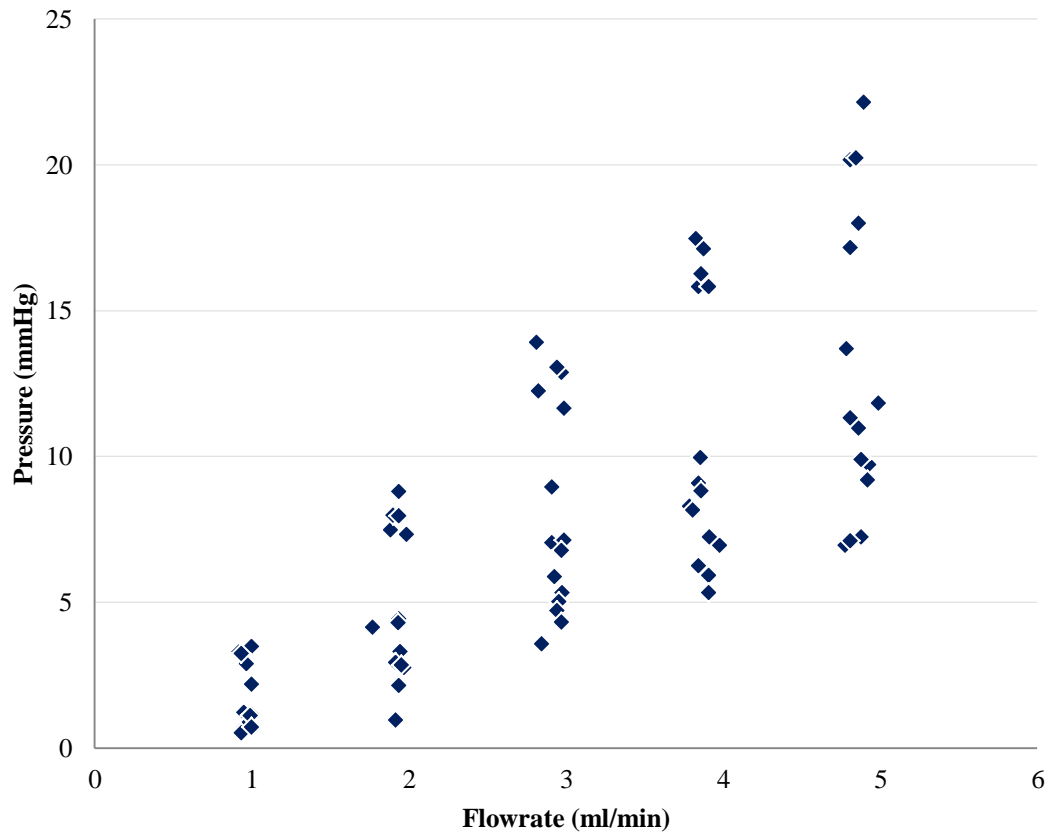


Figure 3.6: EPU hydrodynamics for 15 samples

The hydraulic permeability of the EPU catheter is governed by the flowrate, surface area of the catheter and the differential pressure, as detailed below in Equation 3.3.

$$\text{Hydraulic Permeability} = \text{Flowrate} / \text{Surface Area} \times \text{Pressure} \quad \text{Eqn. 3.3}$$

Where,

$$\text{Surface Area} = 2\pi RL$$

R – Radius of the tube

L – Length of the tube

The hydraulic permeability of the samples was calculated using Equation 3.3 for each pressure and flow value according to the surface area for all the samples. All the catheters were 3mm in diameter and the exposed length varied between 8 and 9 cm.

The average hydraulic permeability allowed the samples to be categorised according to their permeability: samples with values in the range 0.02 to 0.04 ml/min cm² mm Hg were categorised as having low permeability; those in the range 0.05 to 0.07 ml/min cm² mm Hg were considered to have medium permeability; and values in the range 0.08 to 1 ml/min cm² mm Hg were classed as high permeability samples (Table 3.4). The resistance of these samples are represented by the gradient of the pressure versus flow curve (Fig. 3.8).

Category according to permeability	Hydraulic permeability (ml/min cm ² mmHg)	Resistance (mm Hg/ml/min)
Low	0.0311	4.2342
	0.0305	5.0665
	0.0374	4.6293
	0.0316	4.849
	0.0322	4.5238
Medium	0.0635	3.2668
	0.0586	2.5384
	0.0604	2.1465
	0.0534	2.516
	0.0666	2.0015
High	0.0822	2.448
	0.134	1.7631
	0.0893	2.6862
	0.0831	1.5184
	0.0926	1.6719

Table 3.4: Hydraulic permeability and resistance of the EPU samples. Samples are categorised according to the hydraulic permeability (low, medium and high)

The hydrodynamic of 15 EPU catheters were grouped according to their permeability and re-plotted in Figure 3.7, which shows an average of all the catheters (n =5) for each group. There is a significant difference within the groups ($p < 0.01$) as shown in Figure 3.8.

There is a direct correlation between hydraulic permeability and fibre morphology (Fig. 3.9). Specifically, there is a direct (positive) correlation between hydraulic permeability and inter-fibre separation (Fig. 3.9 a; $R^2 = 0.95$). The correlation between fibre diameter and catheter permeability is weak ($R^2 = 0.79$) but the permeability appears to decrease as the fibre diameter increases (Fig. 3.9b).

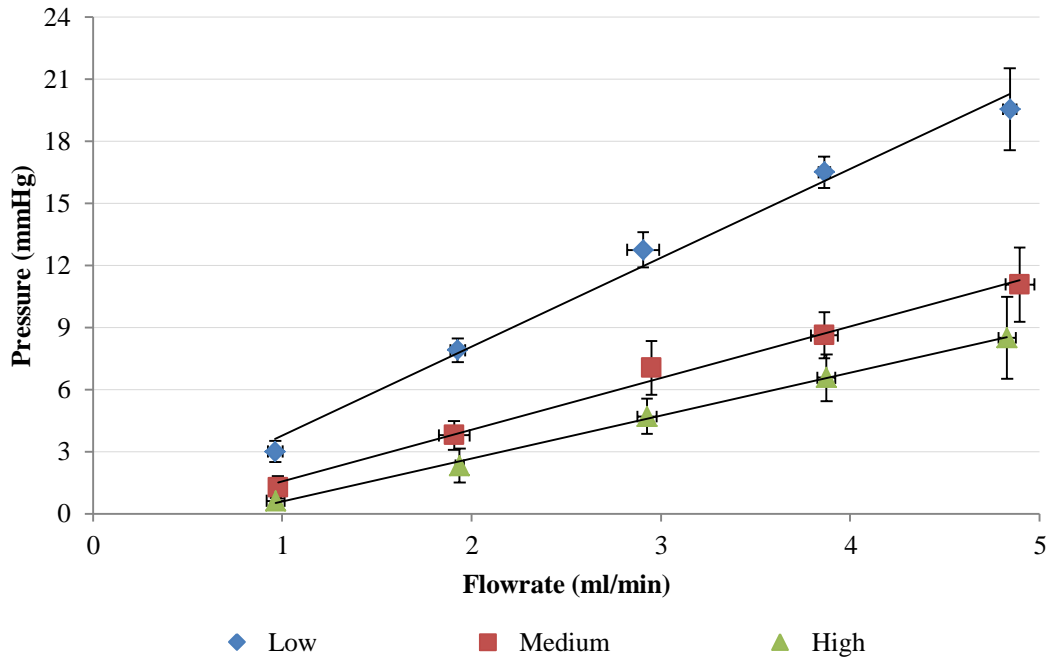


Figure 3.7: Average EPU hydrodynamics for low, medium and high.

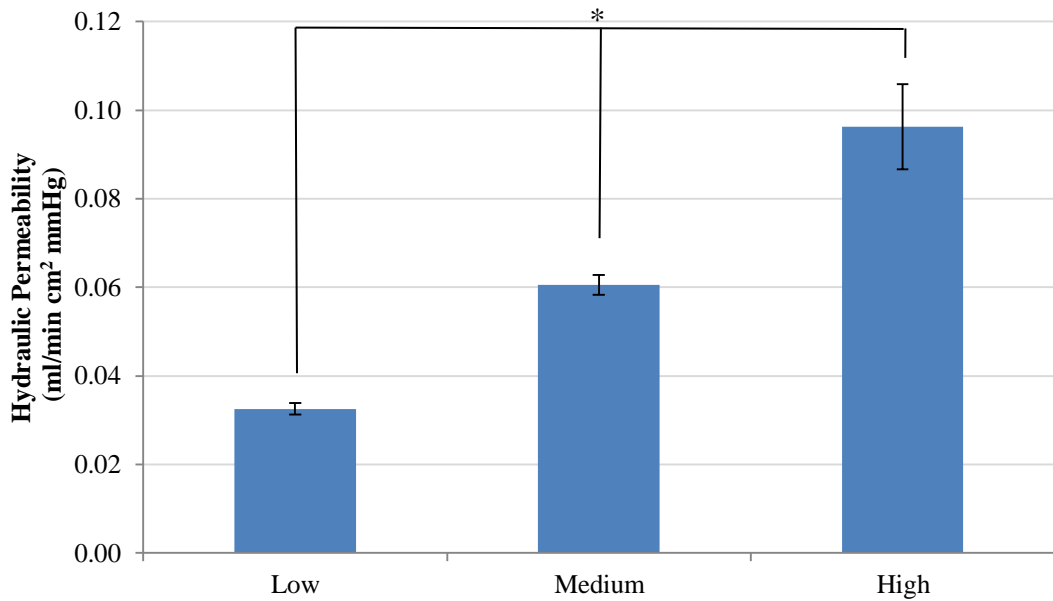


Figure 3.8: Hydraulic permeability of EPU groups (low, medium and high). Data points represent mean \pm standard error and $n = 5$. * denotes significant difference ($p < 0.01$) in hydraulic permeability between the groups determined by one way ANOVA with a Tukey's post hoc analysis.

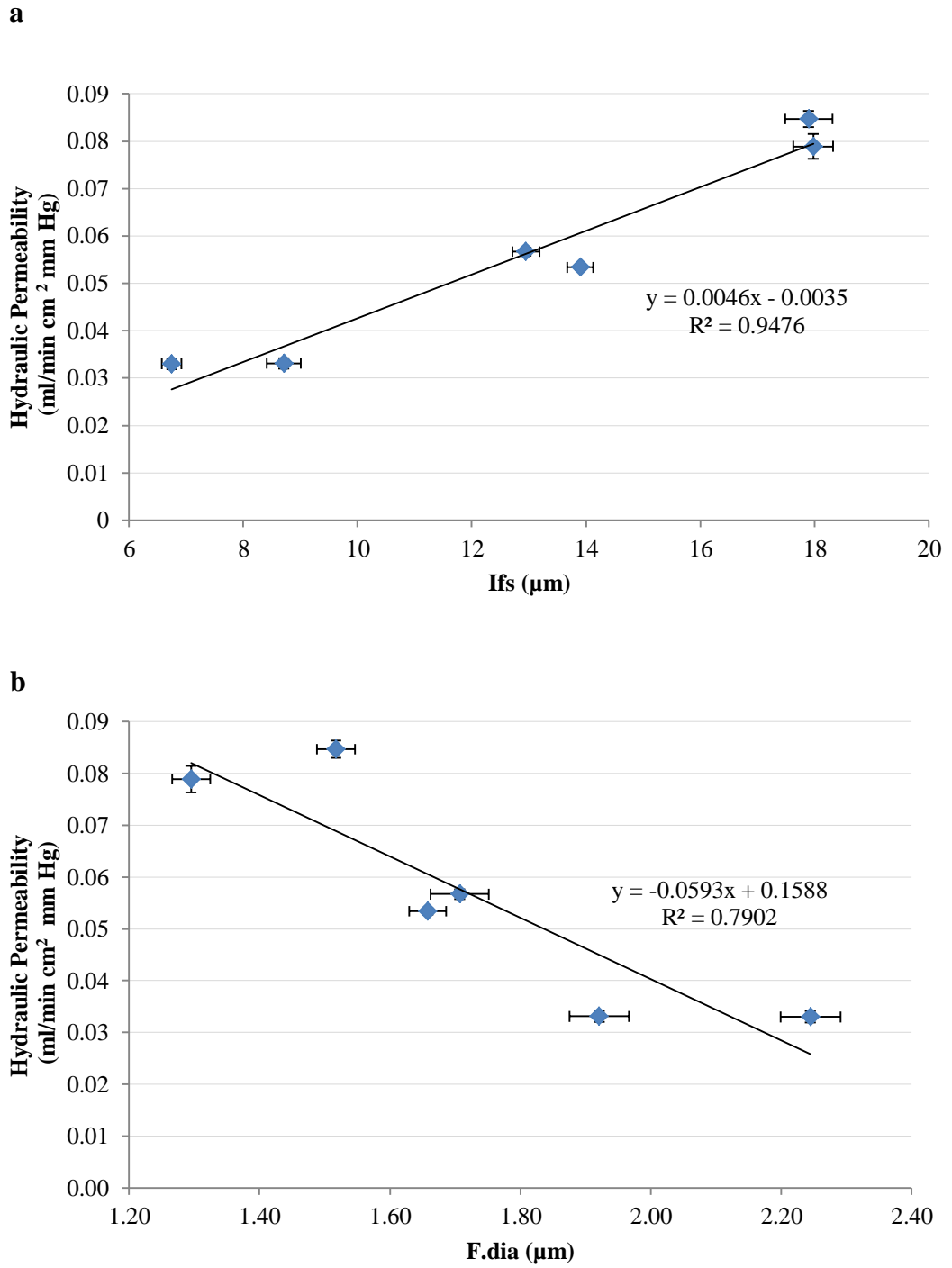


Figure 3.9: The correlation between hydraulic permeability and *Ifs* (a) and, *F.dia* (b) for six EPU samples. Data points represent the mean \pm standard error.

3.4 Discussion

The aim of this study is to explore the hydrodynamic performance of a new proximal catheter having microporous walls. A typical proximal catheter must comply with the space restrictions of the ventricular system of the patient. In general, it should be no more than 3mm in diameter and 2 cm in length. The flow of CSF through a catheter is, according to Poiseuille's Law, a function of the internal diameter of the tube and its length. Hence in the design careful consideration has been given to increasing the surface area of the catheter material without resulting in high resistance. Due to the restrictions in the diameter and length of the catheter, increasing the surface area to flow is not simple. Hence, consideration was given to modifying the surface property of the material. The chosen catheter material, polyurethane, was processed by an electrospinning technique into microfibrinous tubes that were permeable along their entire length (Section 2.8.2). The technology behind electrospinning is versatile, and allows the user to process materials into a wide range of porous forms having the desired fibre dimensions and pore size distribution (Doshi and Reneker 1995). The hydraulic permeability of a porous material is governed by D'Arcy's Law.

In vitro testing of commercially available shunts is essential to understand the hydrodynamic properties since this information is not readily disclosed by the manufacturer (Czosnyka Z. *et al.*, 2002). The hydraulic resistances of the fixed-pressure and programmable valves examined in this study were 4.989 mmHg/ml/min and 4.575 mmHg/ml/min, respectively. These values increase by around 36% in the case of the programmable valve and 100% in the case of the fixed pressure valve when the distal catheter is present. These results are consistent with the findings by other groups, who report that the resistance to flow of CSF is highly dependent on distal catheter (Czosnyka M. *et al.*, 1997; Czosnyka Z. *et al.*, 2002). The resistance of an ideal shunt device should be close to the physiological resistance to flow of CSF, which is between 6 to 10 mm Hg/ml/min (Czosnyka Z. *et al.*, 2002). Hence, it is clear from these results that the conventional shunt system is not able to meet this criterion.

From the hydrodynamic properties of the shunt components it is clear that the proximal catheter offers minimal resistance to flow when compared to the shunt as a whole. The multiple holes present in the catheter act like resistances in parallel, each one offers pathway to flow, which explains the decrease in overall resistance (Ginsberga *et al.*, 2000). In most of the experimental models described in Section 2.4.1, it was unclear whether or not the hydrodynamic properties of the proximal catheter were taken into account. However, it is clear from the present study that contribution made by the proximal catheter to the resistance of the shunt overall shunt is extremely low, which is in keeping with work conducted by Ginsberga and co-workers.

In this study, the physical properties of the EPU were examined qualitatively in terms of I_{fs} and F_{dia} using SEM and quantitatively in terms of hydraulic permeability using in-built testing rig; the latter it is a useful quantity to measure in order to demonstrate the feasibility of the EPU catheter for this application. It is clear from the results presented in the chapter that the hydraulic apparatus is sensitive to detect even a slightest change in porosity within the samples, enabling the samples to be grouped according to their permeability (low, medium, high). A positive correlation between the hydraulic permeability and I_{fs} was found; whereas no solid conclusion can be drawn from the correlation graph representing the permeability and F_{dia} of the EPU catheters.

The resistance to flow of the conventional proximal catheter is relatively lower when compared to EPU for all groups. The results of the EPU samples tested by both pressure and flow controlled systems showed were no significant difference in terms of hydraulic permeability. Hence, the measurement in each case can be said to be pressure independent. The variables which have the greatest impact on the resistance are the dimensions of the catheter. For a cylindrical catheter, resistance is directly proportional to its length and inversely proportional to the fourth power of diameter (Hagen-Poiseuille – eqn 3.1). The length and outer diameter of a typical proximal catheter is 15 and ~0.3 cm, respectively, whereas for the EPU tested ranges from 8 to 9 and ~0.3 cm respectively. Although the resistance values of the latter samples

exceed that of the proximal shunts used clinically, the fabrication process parameters could be altered to yield catheters having a greater void fraction, by decreasing the F_{dia} and/or increasing the I_{fs} .

As with any laboratory-based model, the methods described in this chapter have their limitations. All the experiment work detailed above was carried out in the short term with the shunt components and EPU catheters maintained at room temperature. The test fluid was water, and the influence of CSF proteins on the viscosity and surface properties of the materials under test were neglected. While in future studies these limitations can be easily addressed, these results give a preliminary indication of the feasibility of employing an EPU catheter, which could form the basis of an alternative form of proximal catheter.

EPU catheters pore sizes were achieved by qualitative images using SEM. However, such data may also be obtained by nitrogen porosimetry, which provides a more precise quantification of pore size and surface area. Also, further characterisation such as surface wettability by measuring the contact angle should be considered for future work. Since cell attachment is likely to be affected by the wettability of the material surface.

The ideal hydrocephalus catheter should be relatively inert and invoke a minimal host response over its working life, but in practise this is far from true (Eymann *et al.*, 2012). Hence, the next phase of any study to investigate the feasibility of the alternative proximal catheter should consider how these materials perform in the presence of those cells that are responsible for the obstruction in the proximal catheter, namely astrocytes. Equally, the extent to which the surface properties and distribution of flow through the catheter influences cell growth should be considered. In order to answer these questions careful consideration must be given to the control groups and experimental parameters to study the prospects of EPU as a successful alternate catheter.

3.5 Conclusion

A reliable and robust *in vitro* test rig was built in-house to quantify the hydrodynamic performance of an alternative form of shunt catheter with a conventional hydrocephalus shunt series. The hydraulic resistances presented by the individual shunt components, as well as that for the shunt system as a whole, were compared. The element that made the greatest contribution to the resistance of the shunt series was the distal catheter, followed by the valve (fixed pressure and programmable). The contribution of proximal catheter was negligible.

The apparatus was used to characterise a range of alternative proximal catheter materials in the form of EPU, which were grouped according to their hydraulic permeability. The measurement of resistance of the conventional and alternative proximal catheter shows that distributed porosity may offer a means to regulate the flow of CSF. The results obtained from these studies will provide a baseline for comparison in the subsequent programme of testing of this material in the presence of cells under static and perfusion culture.

CHAPTER 4

COMPARISON OF CSF SHUNT CATHETER MATERIALS *IN VITRO*

4.1 Introduction

All shunt catheters at present are made of PDMS because of its good tensile strength, tear resistance, hydrophobicity and inertness (Bayston 1994). The hydrophobic nature of this material gives rise to unwanted protein adsorption and cell adhesion, which is undesirable for the application of hydrocephalus (Harris *et al.*, 2011b). Astrocytes are one of the major cell types present in the ventricles of the brain. These cells migrate onto the surface of the proximal catheter where they grow to form a thin sheet or film, which then slowly spreads and eventually blocks the perforations in the walls of the catheter (Harris *et al.*, 2010).

Although the proteins present in the CSF are known to enhance cell attachment and proliferation, there are very few attempts recorded so far to manipulate the surface properties of shunt catheter to restrict (inflammatory) cell binding. There is no catheter available at the moment which is surface treated to overcome catheter occlusion or discourage protein adsorption on material surface.

The hypothesis of this study is that cell attachment and growth can be inhibited by changing the nature and porosity of the substrate. In order to test this hypothesis, the viability and growth of cells on PDMS (control) and polyurethane materials in different forms (cast film, macro porous sponge and micro porous mats) were studied. For the purpose of this study, primary astrocytes isolated from rat cortices, and immortalised fibroblasts, were chosen. The viability and growth of these cell types on each substrate was determined using commercially available viability assays.

4.2 Materials and Methods

4.2.1 Reagent Preparation

The following reagents are used for both astrocytes and 3T3 cell culture study.

Glial growth medium

Prepared by using Dulbecco's modified Eagle's medium (DMEM) supplemented with 10% FBS (PAA Laboratories, UK), 1% penicillin/streptomycin (Sigma-Aldrich, UK), 1% non-essential amino acids (PAA Laboratories, UK).

Versene (0.02 % w/v)

Prepared by dissolving 12g of NaCl, 0.3g of KCl, 1.73g of anhydrous Na₂HPO₄, 0.3g of KH₂PO₄, 0.3g of EDTA and 4.5 ml of 0.5% solution of Phenol Red in 1.5 litres of distilled water. The solution was then aliquoted into 20 ml universal bottles and stored at room temperature for use.

Tris Buffered Saline

Prepared by dissolving 4g of NaCl, 0.05g of Na₂HPO₄, 0.5g of glucose, 1.5g of Tris, 0.19g of KCl and 1.5 ml of 0.5% solution of Phenol Red in 500 ml of distilled water. The pH was set to 7.7 at room temperature with approximately 0.94 ml of concentrated HCl. Sterile trypsin solution was then added to give a final concentration of 0.25% (w/v), 50 ml of 2.5% stock. Later the solution was aliquoted into 20 ml universal bottles and stored at -20°C. For experimental purpose 0.05 % of trypsin was prepared from the stock solution.

4.2.2 Primary Astrocytes isolation and culture

The isolation and culture of astrocytes from the rat brain cortex was followed by the methods described by Kim and Magrane (2011). The dissection procedure required small scissors, fine forceps, blunt spatula, scalpel, blades and petri dishes (60 mm and 35 mm). Glass tissue grinder pestle, 70 and 100 μ m cell strainers (Scientific lab supplies, Ltd), glial growth medium, versene and 0.05% trypsin were also required for isolation and culturing the astrocytes.

Astrocyte cultures were collected from Sprague Dawley rat pups (1-2 days old) after sacrificing them via cervical dislocation, a Schedule I procedure carried out in accordance to UK Home Office guidelines. The dissection protocol to remove the cortices was done by my colleague and EngD candidate Mr Graham Robertson (SIPBS). After the movement of the pup had stopped, decapitation with scissors was followed by placing the head in a 60 mm petri dish. After pinning the head downwards with forceps, small scissors were used to cut between the scalp and the skull. The skin was cut from the base of the skull through the mid eye area which leaves the skin to flap by holding back. The skull was cut carefully along the midline of the brain without damaging the brain tissue. Using the forceps the raised skullcap was removed from the surface allowing removal of the brain from the olfactory bulbs along with the cerebellum using a spatula.

The cortices were then separated from the brain by the following step-by-step procedure (Kim and Magrane 2011). With the help of the scalpel, the cerebrum was removed and cerebral hemispheres were detached from each other by cutting along the midline. The ventral side of the brain was placed upwards and by placing the spatula in medial position of the ventral cortex and mid-brain to cut the mid brain off parting the cortex. At this stage the posterior portion of the cortex includes hippocampus, which needs to be isolated from the frontal cortex. This is achieved by placing the spatula into the lateral aspect of the frontal cortex and cutting through the cortex from rostral to caudal. Now the hippocampus was removed from the cortex. This was achieved by placing the spatula in the lateral ventricle beneath the

hippocampus (resembles seahorse) which is easily identified from its structure. A fine cut was made to separate the cortex from the hippocampus and finally spatula was used to scoop them out of the cortex and discarded. Forceps were used to clear the meninges which were present on the surface of the cortex. The cleaned cortices were placed into a 35 mm petri dish and cut into small pieces with a scalpel.

The minced cortices were then sieved through a 100 μ m cell strainer using a sterile glass tissue grinder pestle; 8 μ l of glial growth medium was added drop wise on the cell strainer and the cell suspension was collected in a 50 ml centrifuge tube. The cell suspension was then passed for final sieve through 70 μ m cell strainer, which was collected again in a fresh 50 ml centrifuge tube. After a 5min centrifugation at 800 rpm, the supernatant was discarded and pellet was re-suspended in 5 ml DMEM medium. The cell suspension was seeded at 3×10^5 cells/cm² in a 75 cm² tissue culture flask and grown at 37 °C at 5% CO₂. After 24 hours of culture, the medium was removed to discard the cell debris and fresh medium was added. The medium was changed every three days until the cells are confluent (usually 7 to 9 days after seeding).

After the cells reach confluence the medium was changed and left in incubator for 2 hours, before isolation. In order to isolate the astrocytes from this mixed culture, which includes oligodendrocytes and microglial cells, the flask was shaken on a rocker platform (Gyro-rocker, Stuart S170) at 60 rpm for 12 hours at 37 °C and 5% CO₂. The medium was removed and fresh growth medium was added and shaken with hand to remove any more undesired cells attached and washed with medium twice. Thereafter, versene (0.02 % w/v) a chelating agent, was added twice to wash the cell monolayer and remove any traces of serum from medium. The cells were detached from the flask by incubating at 37 °C for 5 minutes with 2ml of trypsin (0.05% w/v) enough to cover the cell layer and 10 ml of growth medium was added to inhibit the action of trypsin and pipetted up and down to break up any cell clumps using a 10 ml pipette before harvesting the cells. The cells were then centrifuged at 800 rpm for 5 minutes and pellet was then re- suspended in 5 ml of culture medium and cell count was performed. The cell line was maintained by passaging with 3 x

10^4 cells/ml in culture medium, using the same procedure described above. For the experimental purpose multiple cortices were isolated and a maximum of 3 passages were used.

The astrocytes were confirmed by using biomarkers to stain the cultured cell line. The isolated astrocytes were seeded in a 35 mm petri dish with seeding density of 3×10^4 cells/cm² and left until confluent (3 days). To prepare the samples for staining, they need to be fixed with paraformaldehyde. The astrocyte sample was washed with phosphate buffered saline (PBS) three times and ice-cold 4% paraformaldehyde was added, left for 10 minutes and then washed again with PBS for three times. Then, ice-cold 100% methanol was added and left for a further 10 minute period and again washed with PBS for three times. The cells were permeabilised with 0.01% Triton-X (PBS) for 10 minutes. A blocking solution (5% FBS v/v and 1% Bovine Serum Albumin w/v in HBS/PBS) for blocking non-specific binding sites was added to the samples and incubated the cells for 1 hour.

Mouse anti-gial fibrillary acidic protein (GFAP) was used as the primary antibody, made to a dilution of 1:5000 in blocking solution applied directly to the sample and incubated overnight (16-20 hours) at 4°C in a wet box. The cultures were then washed three times with PBS to remove any unbound primary antibody. Alexa fluor 488 conjugated donkey anti-mouse fluorescent was used as the secondary antibody made to a dilution of 1:200 in blocking solution and incubated for 1 hour at room temperature in the dark. Then the unbound antibody was removed by washing the cells with PBS. The cells were then counter stained using 4', 6-diamidino-2-phenylindole (DAPI), which stains the Deoxyribonucleic acid (DNA) of the cell. A stock solution of 5mg/ml was diluted to 300 nM in PBS and added to the samples to cover the surface and left for 2 minutes. The surplus stain was removed from the sample by washing with PBS three times and 1 ml of PBS was added before viewing under microscope. Fluorescence images were achieved using the Apotome function of an Axio Imager Z1 microscope (Zeiss, Hertfordshire, UK).

4.2.3 Immortalised 3T3 cell culture

Immortalised mouse fibroblast (3T3) cells were established from NIH Swiss mouse embryo. The cell line was cultured in DMEM growth medium and it was prepared as described above. 3T3 cells were cultured as monolayers in 25 cm² tissue culture flasks in 5% CO₂ at 37°C. The medium from the culture flask was removed and 5 ml of versene (0.02 % w/v) was added to wash the cells monolayer. After removing the solution of versene from the flask, 1 ml of 0.05 % trypsin in versene (w/v) was added. The flask was left undisturbed for 2-3 minutes allowing the cells to detach themselves from the surface. Later 5 ml of DMEM was added to inhibit the action of trypsin and pipetted up and down to break up any cell clumps using a 10 ml pipette. The volume of the solution was measured using a pipette and the cells were reseeded at the split ratio 1:10 to maintain the cell line. The flasks were then kept in the incubator set at 37⁰ C and 5 % CO₂ for 3 days.

4.2.4 Shunt catheter materials fabrication and preparation for cell culture

The candidate materials were medical grade PDMS (Dow Corning MDX4210), PDMS foam microcarriers (ImmobaSil[®], Ashby Scientific Ltd, UK) and medical grade polyurethanes Z1A1 and Z3A1 (*b₉*[™], Biomer Technology Ltd, UK) supplied under the terms of a Materials Transfer Agreement with the University of Strathclyde and Tecoflex[™] (SG-80A, Thermedics Polymer Products, USA). In the studies that followed, Nelficon silicone hydrogel (Bausch and Lomb, Ltd.) was used as negative control. Both treated and non-treated polystyrene 96-well plates were used, into which the test samples were secured at the base of the well before seeding. The base of the wells served as a further control in these experiments.

Silastic[®] MDX4210 medical grade elastomer base and curing agent were prepared by mixing at a ratio of 10:1 respectively. Approximately 20 μ l of the combined PDMS solution was injected into each well and allowed to cure at 50 ⁰ C for 12 hours. Immobasil[®] Silicone Foam (SF) is a macro porous sponge made of PDMS, available as a 10 mm diameter disc with a thickness of 3 mm. SF was punched to fit the base of the well, which is 6 mm in diameter.

Z1A1 and Z3A1 are different grade of polyurethanes. Thin films of Z1A1 and Z3A1 were cast from solution (15% w/w polymer in dimethylformamide/DMAc). Before casting, the polymer solution was placed on a roller mixer for 48 hours at room temperature and atmospheric pressure to ensure thorough mixing. The polymer solution was poured into a flat bottomed glass petri dishes and the solvent evaporated under vacuum at 65 ⁰ C for 48 hours. Thereafter, the cast films were removed from the petri dishes and soaked in deionised water for 24 hours before use to ensure complete removal of all remaining solvent. The surface in contact with the air was used so as to minimise substrate variation due to the properties of petri dish surface. The samples were punched out of the dry sheets to the desired size and secured to the base of the well plate.

EPU was produced using an electrospinning process as explained in Section 3.2. The EPU was available in tubular form. Each tube was cut along its axis and laid flat

before samples were punched out to the appropriate diameter (6mm). The samples were secured in the bottom of a well plate with the aid of a medical grade polytetrafluoroethylene (PTFE) sleeve having an outer diameter (OD) of 6 mm and inner diameter (ID) of 4mm. The sleeve was placed inside the well and glued into position using PDMS adhesive taking care to ensure that the adhesive did not come into contact with the sample material (Fig 4.1).

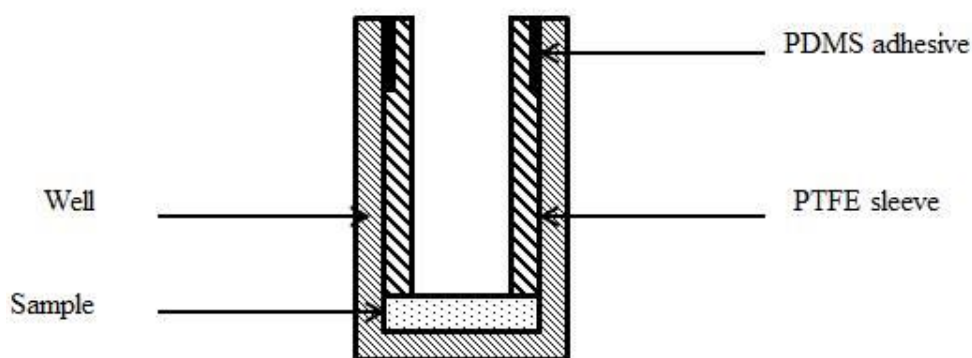


Figure 4.1: Cross-sectional view of sample secured in a 96 well plate.

For consistency, the above procedure was followed to secure all samples in the base of each well. As a control group, treated and non-treated culture plates were also used with (P1) and without (P2) PTFE tubing for validation. After each plate had been prepared it was incubated at 40 °C overnight before use. The first and last columns and rows of a 96 well plate were not used during material preparation since evaporation of medium was found to be higher in these wells. Each sample type occupies 6 wells of the plate column wise. Each 96-well plate contained all the candidate materials so as to eliminate the possibility of systematic error, and to ensure uniform seeding of cells across all the materials and treatments studied.

Owing to the difficulty in viewing samples in 96-well plates, samples having the same dimensions as used for the plate (6 mm diameter) were secured to the base of a 35-mm petri dish instead. The methods used to prepare each catheter material for

microscopy was otherwise the same as stated above. The samples were placed in the centre of the petri dish and secured by placing the PTFE tube with the same length (10 mm) as the 96 well plate and PDMS adhesive was used to glue the tube to the surface of the petri dish without contacting the sample (Fig 4.2). The prepared samples were left in the oven at 40⁰ C overnight. When viewing the samples under the microscope, the PTFE tube was carefully removed to gain access. During the cell culture on these petri dishes, to avoid evaporation of medium due to low surface area of the sample, 2ml of growth medium was added to petri dish isolating the sample.

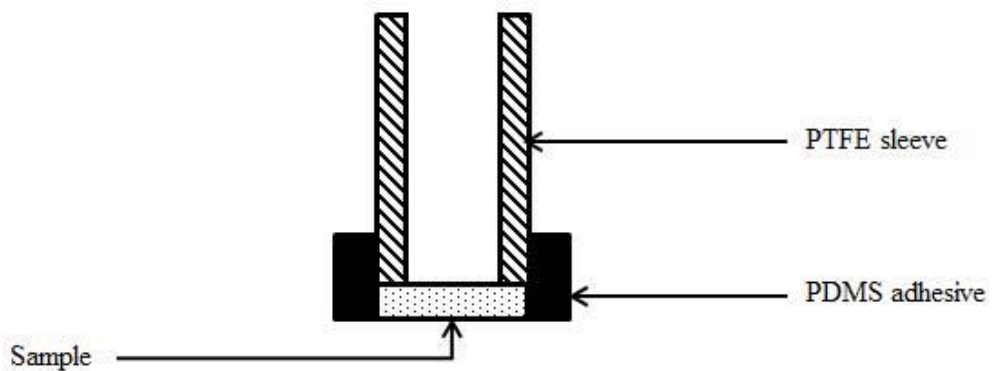


Figure 4.2: Cross-sectional view of sample secured in a petri dish.

All the materials used in this study were secured flat in the base of each well. It was assumed that the curvature of the EPU catheter material did not influence the cell attachment. The plates and petri dishes should be sterilised before coming in contact with cells. The available options for sterilisation without damaging the samples were considered. Autoclave was eliminated because during the process the temperature goes up to 121 °C, which is close to the melting point of the polyurethanes employed in this study. Using 70 % ethanol as an alternative was also rejected because the fibre of EPU samples is known to swell on exposure to alcohol with possible detrimental effects on the structure if not the material. Hence, the prepared samples were UV sterilised for 15 minutes before protein adsorption and cell seeding. Thereafter, 3T3 cells or primary astrocytes were cultured under static conditions at a seeding density of 1.2×10^4 cells/cm² on samples of each material. All the experiments were carried out in triplicate, the total number of samples being 18.

4.2.5 Protein adsorption

Bovine plasma fibronectin (Fn) (2g/ml) (Invitrogen, Paisley, UK) was diluted in PBS to a final concentration of 4µg/ml to make Fn solution. 20 µl of this solution was added to cover the surface of the material and left in incubator for 1 hour at 37 °C. The unbound Fn was removed by washing twice with PBS. The treated surface was then blocked by adding 20 µl of 1% w/v bovine serum albumin (BSA) (Sigma-Aldrich, UK) for 1 hour at 37 °C. After the time period the unbound BSA was removed by washing twice with PBS. The surface was not left to dry out at any point during the surface treatment process.

4.2.6 Cell viability measurement

Cell viability was determined quantitatively using alamarBlue[®] (AB, ABDserotec). AB is an indicator dye, integrates an oxidation-reduction (REDOX) indicator that both fluoresces and change colour in reaction to the chemical reduction of growth medium resulting from cell growth. The principle behind the assay is that growing cells induce chemical reduction of the dye. Hence, continued growth of cells maintain a reduced environment and turns the dye to pink colour; whereas inhibition of cell growth maintains oxidised environment retaining the blue colour of the dye.

AB was added to the samples at 10% volume of the growth medium and left for 24 hours for the dye to reduce before taking a measurement. The time points chosen to measure were 48 and 96 hours in culture. The absorbance was measured at 540 (lower wavelength – A_{OLW}) and 620 (higher wavelength – A_{OHW}) nm using a 96 well plate reader (Multiskan Ascent). The absorbances of growth medium with and without (blank) AB addition for the same volume as the samples were measured at both the wavelengths. The calculation of converting the absorbance value into percentage of reduction of the dye which determines the cell viability is given below:

$$A_{OLW} = \text{Absorbance of AB in medium} - \text{Absorbance of medium}$$

$$A_{OHW} = \text{Absorbance of AB in medium} - \text{Absorbance of medium}$$

$$\text{Correction Error (R}_0\text{)} = A_{OLW} / A_{OHW}$$

$$\text{Percentage reduction of AB} = [A_{LW} - (A_{HW} \times R_0)] \times 100$$

Where,

$$A_{LW} = \text{Sample absorbance at the lower wavelength minus the blank}$$

$$A_{HW} = \text{Sample absorbance at the higher wavelength minus the blank}$$

4.2.7 Microscopy imaging of cell type on different substrates

A commercially available viability assay (LIVE/DEAD[®], Molecular Probes, Invitrogen) was used to stain the cells before viewing under a fluorescence microscope (Carl Zeiss, Hertfordshire, UK). The kit contained two stock solutions

- 1) Component A: 40 µl of 4 mM Calcein AM in anhydrous Dimethyl Sulfoxide (DMSO), a green fluorescence dye to identify live cells; and
- 2) Component B: 200 µl of 2 mM Ethidium homodimer – 1 in DMSO/H₂O 1:4 v/v, red fluorescence dye to identify dead cells.

The working solution of the stain contained 2 µM Calcein AM and 4 µM Ethidium homodimer – 1. It was prepared by adding 4 µl of component B and 1 µl of component A to 2 ml of sterile PBS. To ensure thorough mixing of the components the solution was agitated in a vortex before use. The final concentration of the DMSO was <0.01 which is not harmful to most of the cell types. Calcein AM in aqueous solution is liable to hydrolysis; hence the working solution was not used after 24 hours for staining.

As a control groups the cells were cultured in coverslip using a same protocol as described above. In order to measure the Ethidium homodimer – 1 activity, the samples were treated with 70% ethanol for 5 minutes. The samples were then compared with and without exposure to ethanol.

The samples were washed with PBS before adding 20 µl of combined LIVE/DEAD[®] assay to cover the surface of the cell for staining. The samples were then incubated at 37 °C for 30 minutes. Then, the stains were decanted and washed with PBS twice and 1 ml of PBS was added to the petri dish containing the sample. The Apotome function of an Axio Imager Z1 microscope (Zeiss, Hertfordshire, UK) was used to achieve fluorescence images and confocal laser scanning microscope was used to acquire optical image of the cells.

4.3 Results

4.3.1 Astrocytes Immunofluorescence Image

The astrocyte cultures that had been processed according to the immunofluorescence protocol described in Section 4.2.2 to stain for the GFAP marker for astrocytes, while DAPI was used to counterstain the nuclear DNA. A representative image showing astrocytes stained with both the dyes is shown in Figure 4.3.

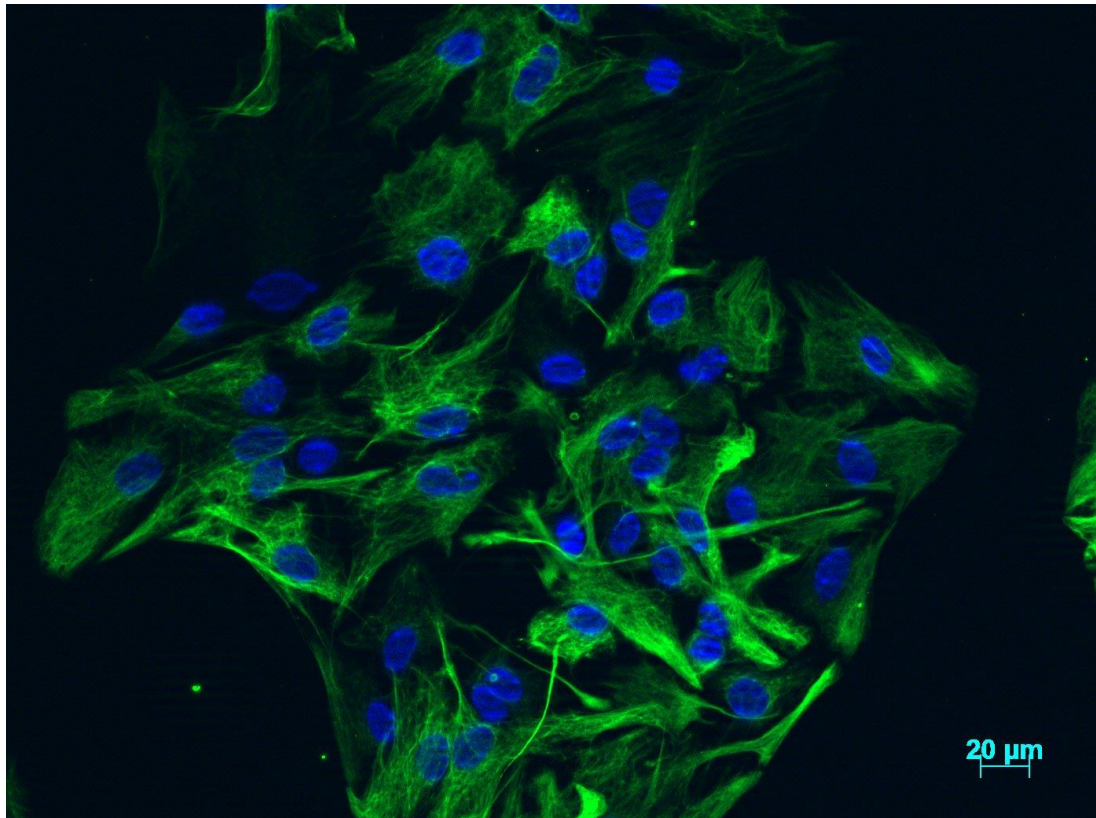


Figure 4.3: Immunofluorescence image of Astrocytes culture after isolation. GFAP stained in green. Nuclear DNA stained in blue. Scale bar is 20 μm .

4.3.2 Standard curve for 3T3 cells and Astrocytes

3T3 cells and astrocytes were cultured at different seeding densities in a treated 96-well plate and the percentage reduction of AB was quantified in a plate reader. AB was added after seeding the plate and AB absorbance value was measured after 8 hours in culture. The absorbance value was then converted into percentage of reduction as mentioned in Section 4.2.6. The standard curve for 3T3 and astrocytes is shown in Figure 4.4. The curve is plotted with cell number (seeding density) against corresponding percentage of reduction. The graph shows a linear relationship between cell number and percentage of reduction. This result confirms that AB is reduced by viable cells, and is directly proportional to the number of cells. There is no significant difference between the percentage reductions of AB for either cell type at the 8 hour time point.

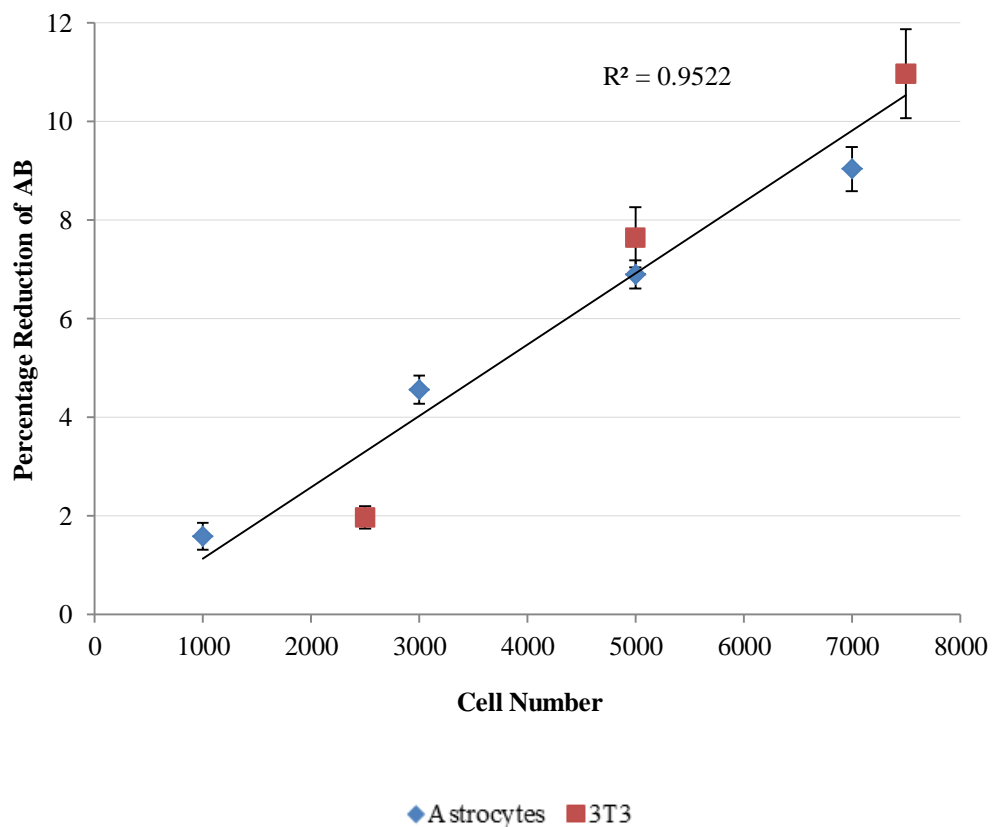


Figure 4.4: Standard curves for 3T3 and astrocytes after 8 hours in culture. Data points represent mean \pm standard error, $n = 18$.

4.3.3 Growth curve for 3T3 cells and Astrocytes

Figure 4.5 and Figure 4.6 show the growth curves for both cell types at lower seeding densities and higher seeding densities respectively. The following seeding densities, 1×10^3 , $(2.5 \text{ or } 3) \times 10^3$, 5×10^3 and $(7 \text{ or } 7.5) \times 10^3$ cells/well were chosen to culture on 96 well treated culture plates to understand the cell growth over time. There was no significant difference in reduction of AB for 3T3 cells and astrocytes for all the seeding densities. The purpose of this study was to establish an appropriate seeding density to use for further studies. From Figure 4.5 it can be seen that in lower seeding densities both cell types remained in log phase during the first 48 hours of the study. At higher seeding densities, however, astrocytes appear to remain in log phase whereas the 3T3 cells enter the stationary phase after 48 hours in culture (Fig. 4.6). Hence, lower seeding density was suitable for extended time period of the experiments. On the basis of these results, a seeding density of 1.5×10^3 cells/well was used for all subsequent experiments.

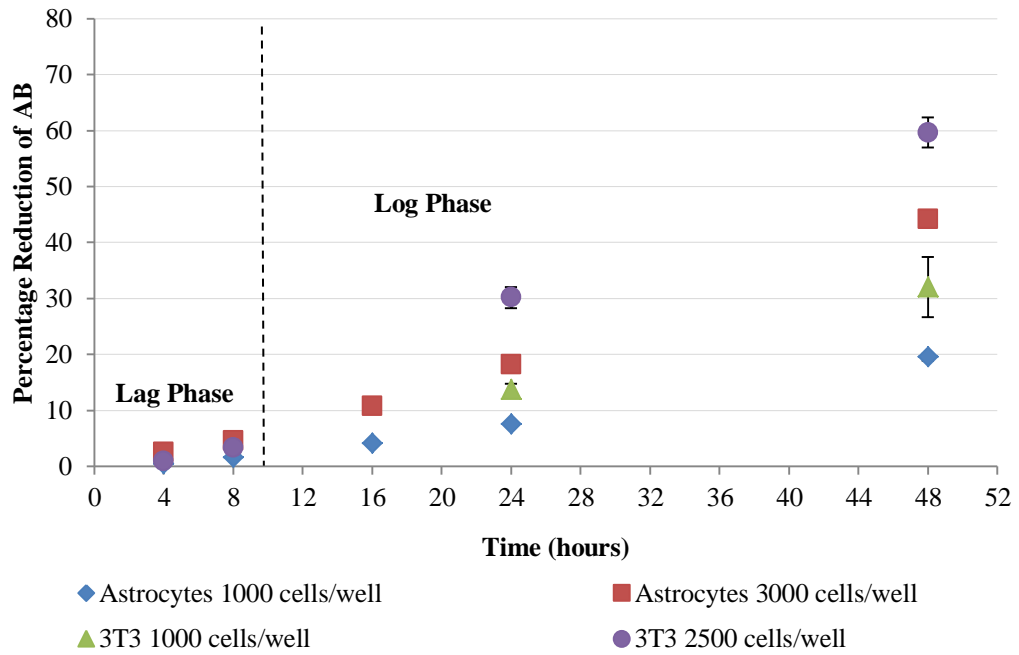


Figure 4.5: Growth Curve of 3T3 and Astrocytes for lower seeding densities. Data points are represented as mean \pm standard error, $n = 18$.

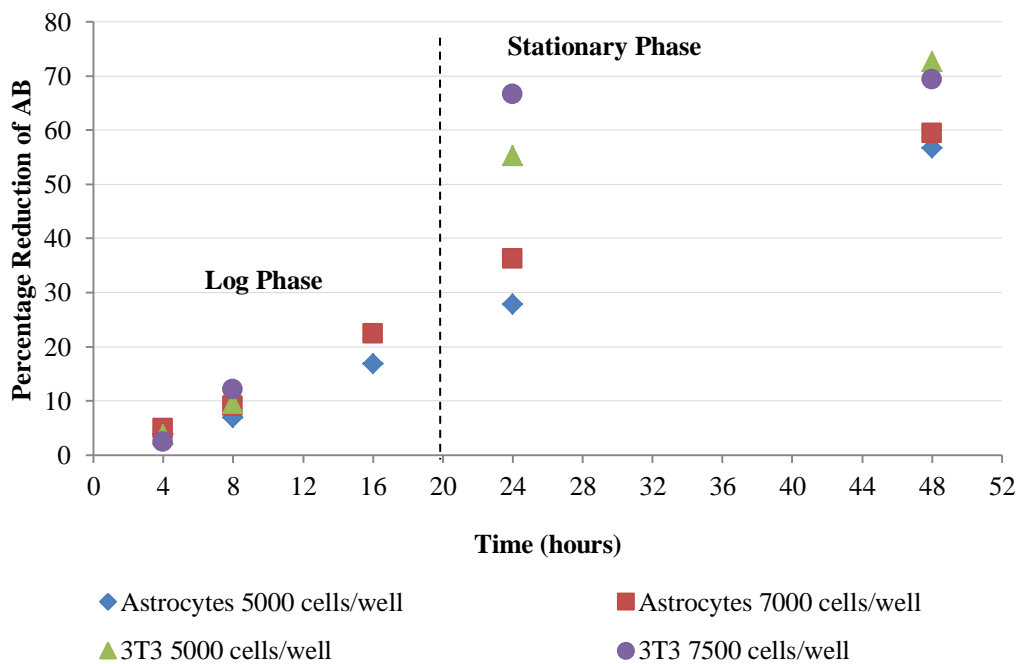


Figure 4.6: Growth Curve of 3T3 and Astrocytes for higher seeding densities (cells/well). Data points represents mean \pm standard error, $n = 18$.

4.3.4 Control Experiment

The treated 96-well plates were used to prepare the substrates as described in Section 4.2.4. The numbers of viable 3T3 cells present on non-treated PDMS, Z1A1, Z3A1, EPU, SF, P1 (wells with PTFE tube) and H was assessed by means of the AB assay. The silicone hydrogel (H) was used as negative control on the assumption that this material would be less conducive to cell growth. The plasma treated plates (also known as tissue culture plastic (TCP)) were used as positive control (P1) because they are plasma treated specifically to promote cell attachment and proliferation.

The numbers of 3T3 cells after 48 and 96 hours in culture is shown in Figures 4.7 (a) and (b), respectively. As expected, the greatest reduction in AB is exhibited by the positive control in all cases, whereas the negative control does not show an appreciable reduction (corresponding to an increase in cell numbers) even after 96h in culture. In contrast, all other substrates show a marked reduction in AB relative to the controls. When compared to the negative control, PDMS and positive control shows a statistically significant ($p < 0.05$) increase in the reduction of AB at after 48 hours. However, after 96 hours all materials except EPU shows higher ($p < 0.05$) cell viability than negative control.

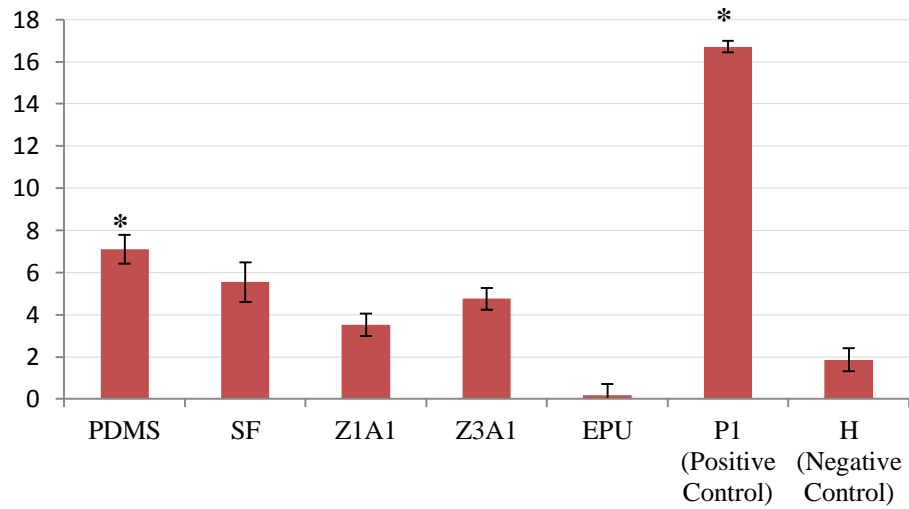
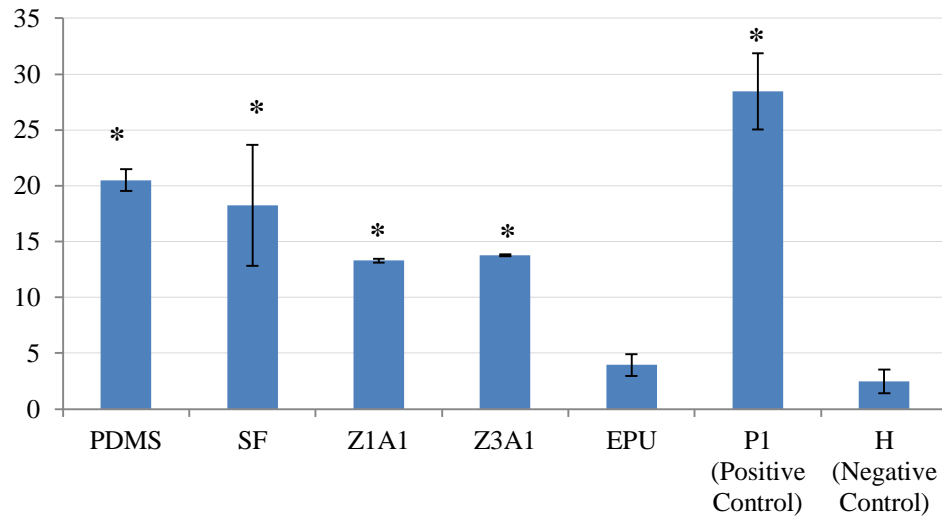
a**b**

Figure 4.7: The mean reduction in AB expressed in percentage terms after 48h (a) and 96h (b) for 3T3 cells grown on non-treated PDMS, Z1A1, Z3A1, EPU, SF, Positive Control (TCP P1) and Negative Control (H). Data points represent mean \pm standard error and $n = 18$. * denotes significant difference ($p < 0.05$) in cell viability compared to negative control (relevant time point) determined by one way ANOVA with a Dunnett's post hoc.

4.3.5 Evaluation of 3T3 and Astrocytes cell viability

There follows a comparison of TCP and non-treated 96-well plates used to prepare the substrates. Again, the AB assay was used to compare the numbers of 3T3 and astrocytes on each non-treated surface: PDMS, Z1A1, Z3A1, EPU, SF, P1 (wells with PTFE tube) and P2 (wells without PTFE tube). The control for this experiment is P2 in treated and non-treated plate. Figure 4.8 (a) and (b) and Figure 4.9 (a) and (b) show the percentage reduction of AB for 3T3 cells and astrocytes respectively for non-plasma treated materials after 48 hours in culture. Figure 4.10 (a) and (b) and Figure 4.11 (a) and (b) show the percentage reduction of AB for 3T3 and astrocytes respectively for non-treated materials after 96 hours in culture.

The growth of each cell type does not appear to be affected by the form of each substrate. There is a significant increase ($p < 0.05$) in cell numbers (expressed as a percentage of reduction of AB) for all the samples and cell types over time, except for P1 and P2, which recorded no significant difference when using non-treated plates for both cell types.

The positive control (P2) of TCP and non-plasma treated plate exhibits shows the highest percentage reduction ($p < 0.05$) compared to all other substrates at 48 hours for both cell types. However, after 96 hours in culture, the PDMS and SF are comparable to P2 (non-plasma treated) for both cell types whereas the cast film polyurethanes (Z1A1 and Z3A1) are significantly less than P2 (non-plasma treated) only for 3T3 cells. On the other hand, cell growth on the EPU samples remain significantly less ($p < 0.05$) than on P2 (non-plasma treated) substrates for both cell types. Cells grown on the P2 (TCP) exhibit the greatest reduction ($p < 0.05$) in percentage terms compared to all other substrates at 96 hours for both cell types.

The percentage reduction of AB on all substrates was the same regardless of their presence on TCP or non-plasma treated plates and irrespective of cell type. Cells grown on P1 and P2 show a significant difference ($p < 0.05$) at 48 hours for treated and non-treated plate for both cell types. TCP P1 and P2, on the other hand, show a significant difference ($p < 0.05$) only for astrocytes after 96 hours.

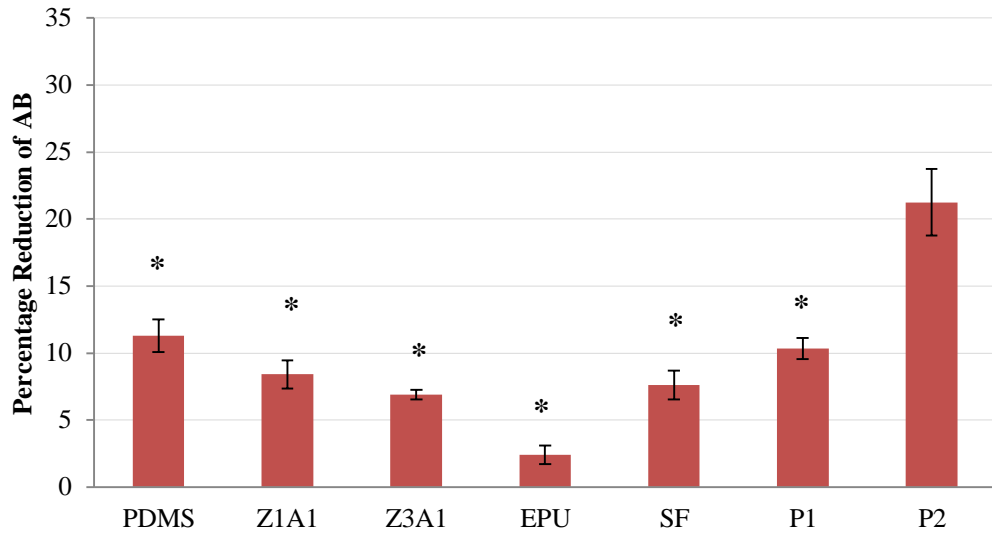
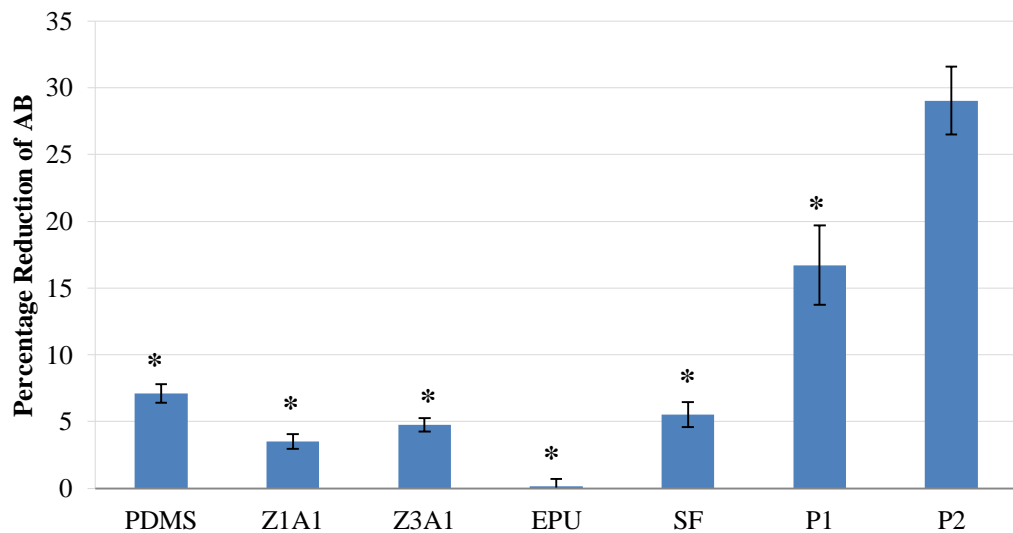
a**b**

Figure 4.8: The mean reduction in AB expressed in percentage terms after 48 hours for 3T3 cells grown on non-treated substrates (PDMS, Z1A1, Z3A1, EPU, SF, P1 and P2) on non-plasma treated plates (a) and TCP (b). Data points represent mean \pm standard error and $n = 18$. * denotes significant difference ($p < 0.05$) in cell viability compared to positive control P2 (relevant time point) determined by one way ANOVA with a Dunnett's post hoc.

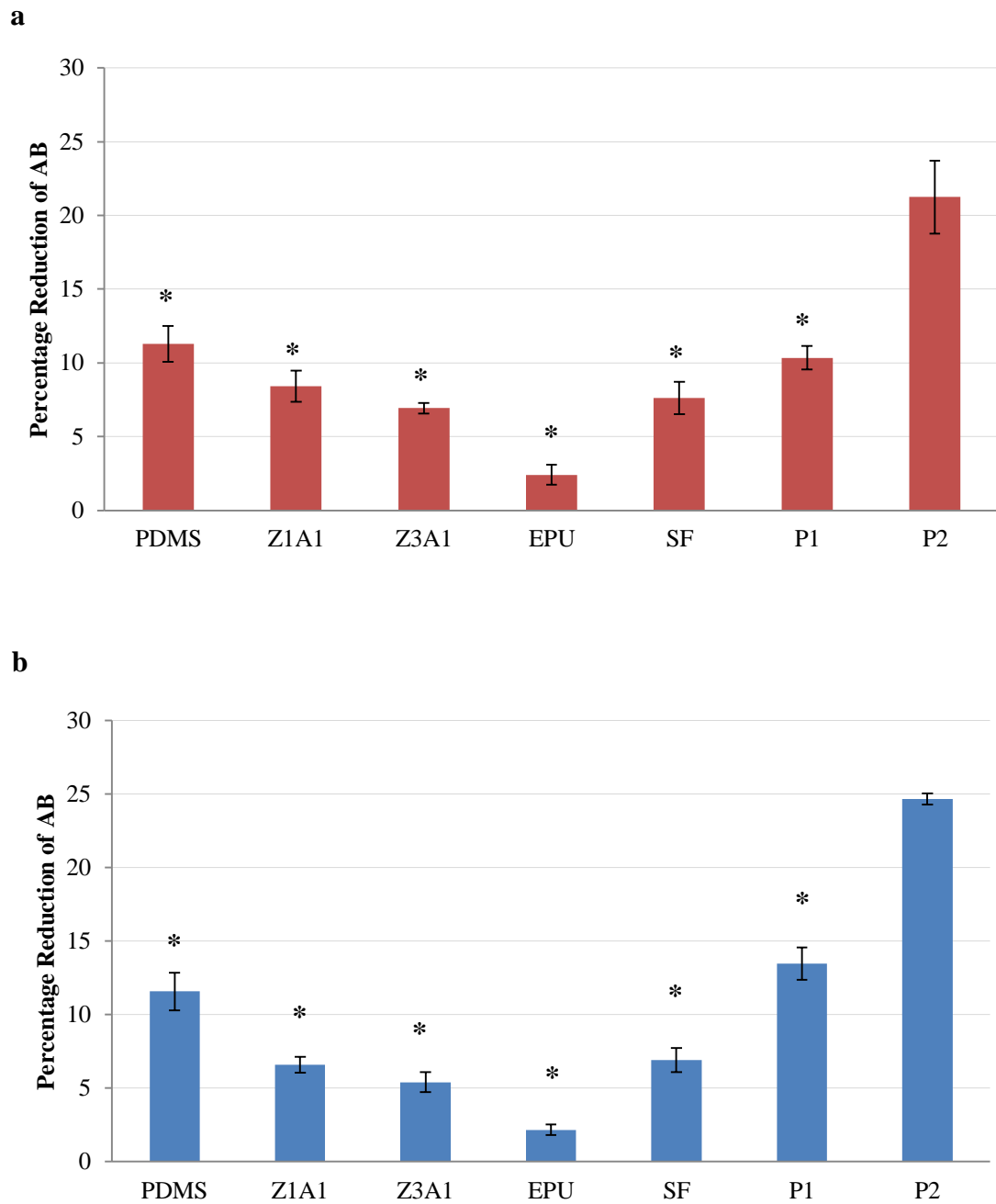


Figure 4.9: The mean reduction in AB expressed in percentage terms after 48 hours for astrocytes cells grown on non-treated substrates (PDMS, Z1A1, Z3A1, EPU, SF, P1 and P2) on non-plasma treated plates (a) and TCP (b). Data points represent mean \pm standard error and $n = 18$. * denotes significant difference ($p < 0.05$) in cell viability compared to positive control P2 (relevant time point) determined by one way ANOVA with a Dunnett's post hoc

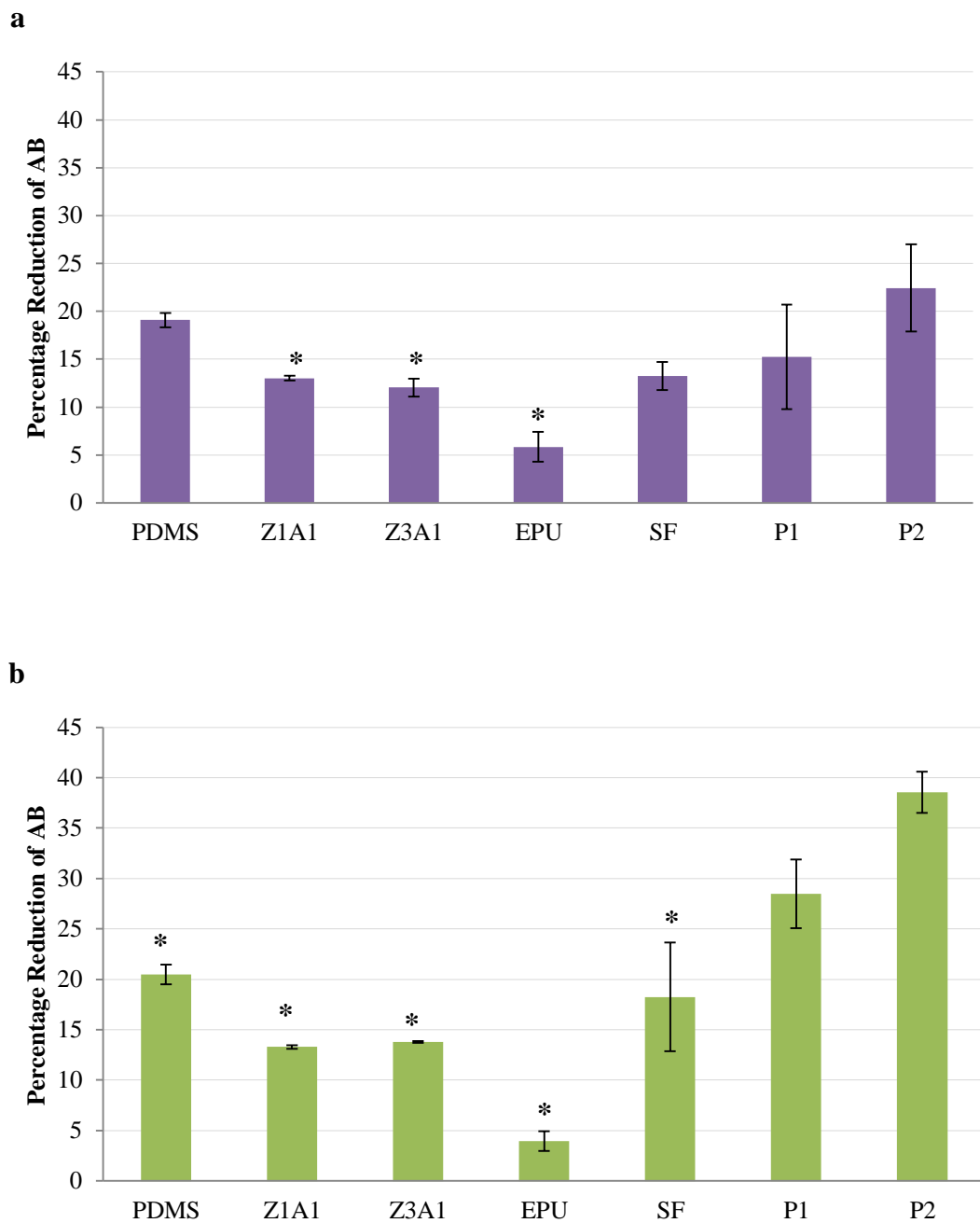
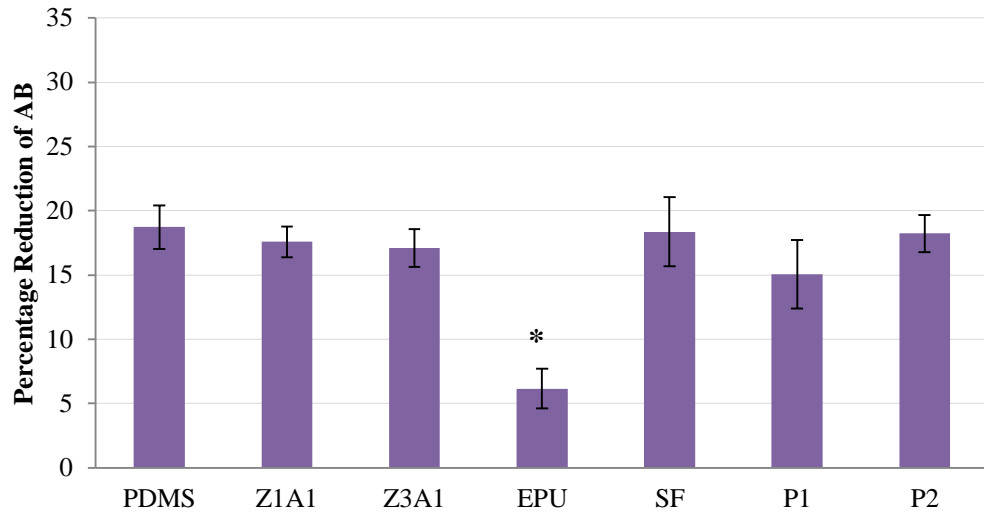


Figure 4.10: The mean reduction in AB expressed in percentage terms after 96 hours for 3T3 cells grown on non-treated substrates (PDMS, Z1A1, Z3A1, EPU, SF, P1 and P2) on non-plasma treated plates (a) and TCP (b). Data points represent mean \pm standard error and $n = 18$. * denotes significant difference ($p < 0.05$) in cell viability compared to positive control P2 (relevant time point) determined by one way ANOVA with a Dunnett's post hoc.

a



b

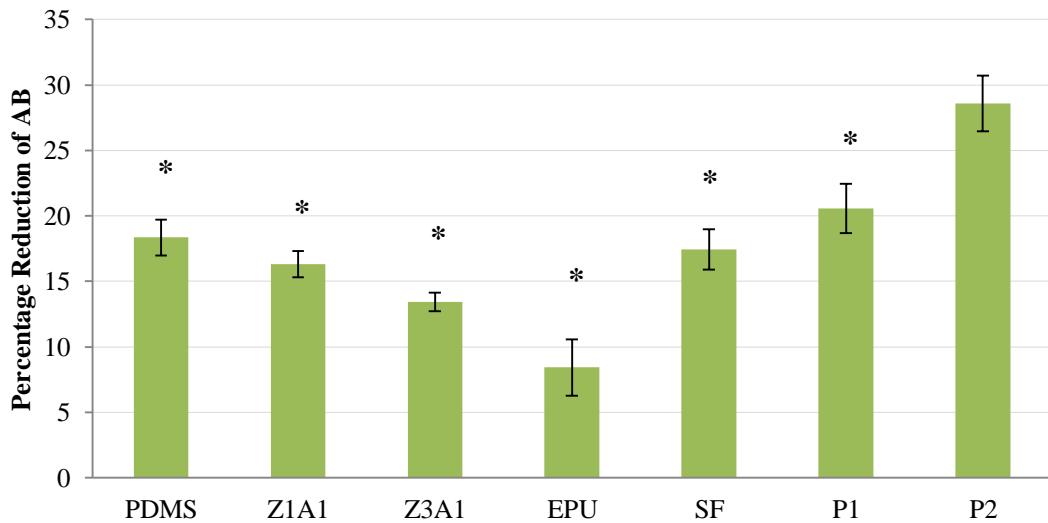


Figure 4.11: The mean reduction in AB expressed in percentage terms after 96 hours for astrocytes cells grown on non-treated substrates (PDMS, Z1A1, Z3A1, EPU, SF, P1 and P2) on non-plasma treated plates (a) and TCP (b). Data points represent mean \pm standard error and $n = 18$. * denotes significant difference ($p < 0.05$) in cell viability compared to positive control P2 (relevant time point) determined by one way ANOVA with a Dunnett's post hoc.

4.3.6 Effect of protein coating on substrates

All the substrates (PDMS, Z1A1, Z3A1, EPU and SF) were prepared in TCP and non-plasma treated well plates as before (Section 4.3.5). The samples were then further treated with proteins (either BSA or fibronectin adsorbed and blocked with albumin (Fn-BSA)) and seeded with either 3T3 or astrocytes according to the above protocols. The controls are: non-treated plate P1 (negative control) and plasma-treated plate P1 (positive control). Figures 4.12 and 4.13 present the percentage reduction of AB corresponding to cell viability for treated and non-treated samples for 3T3 and astrocytes, respectively, after 48 hours in culture. Figures 4.14 and 4.15 show the percentage reduction of AB for treated and non-treated samples for 3T3 and astrocytes respectively after 96 hours in culture.

The treated and non-treated samples were compared with the respective negative controls. After 48 and 96 hours in culture, only the non-treated positive control substrates show significantly higher percentage reduction of AB for 3T3 cells. In the case of astrocytes, on the other hand, only the BSA-treated wells of the positive control show significantly higher reduction. Cell numbers on the PDMS sample were the same after 48 and 96 hours in culture, when compared to the negative control. In contrast, the numbers of 3T3 cells on the macroporous form of PDMS were less at 48h for all treatments, whereas the numbers of astrocytes on non-treated samples. However, the longer the period in culture, the numbers of cells are significantly greater ($p < 0.05$) in the case of astrocytes growing on the Fn-BSA treated surfaces.

Turning our attention now to the cast polyurethane films, the numbers of cells on both treated and non-treated surfaces are lower for 3T3 cells ($p < 0.05$) but for astrocytes only Z3A1 with Fn-BSA treated, for initial time point. After a longer period in culture there is no difference for Z1A1 for all treatments but Z3A1 shows less cell growth for BSA treated (3T3 cells) and Fn-BSA treated (both cell types). The microporous form of polyurethane, on the other hand, does not appear to support the growth of either cell type, even after the longer period in culture in the presence and absence of proteins ($p < 0.05$).

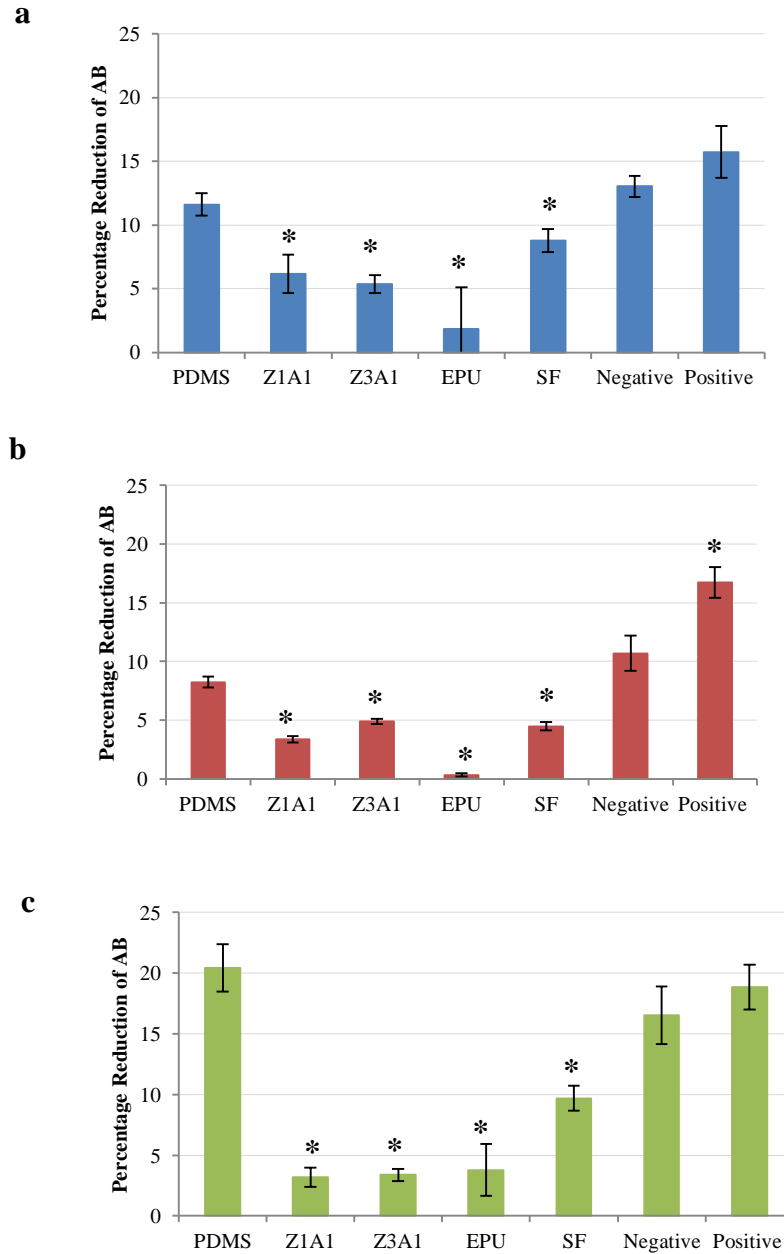


Figure 4.12: The mean reduction in AB expressed in percentage terms after 48 hours for 3T3 cells on PDMS, Z1A1, Z3A1, EPU, SF, Negative Control (Non-treated Plate P1) and Positive Control (Treated Plate P1) with BSA (a), non-treated (b) and Fn-BSA (c). Data points represent mean \pm standard error and $n = 18$. * denotes significant difference ($p < 0.05$) in cell viability compared to negative control for the corresponding treatment condition determined by one way ANOVA with a Dunnett's *post hoc*.

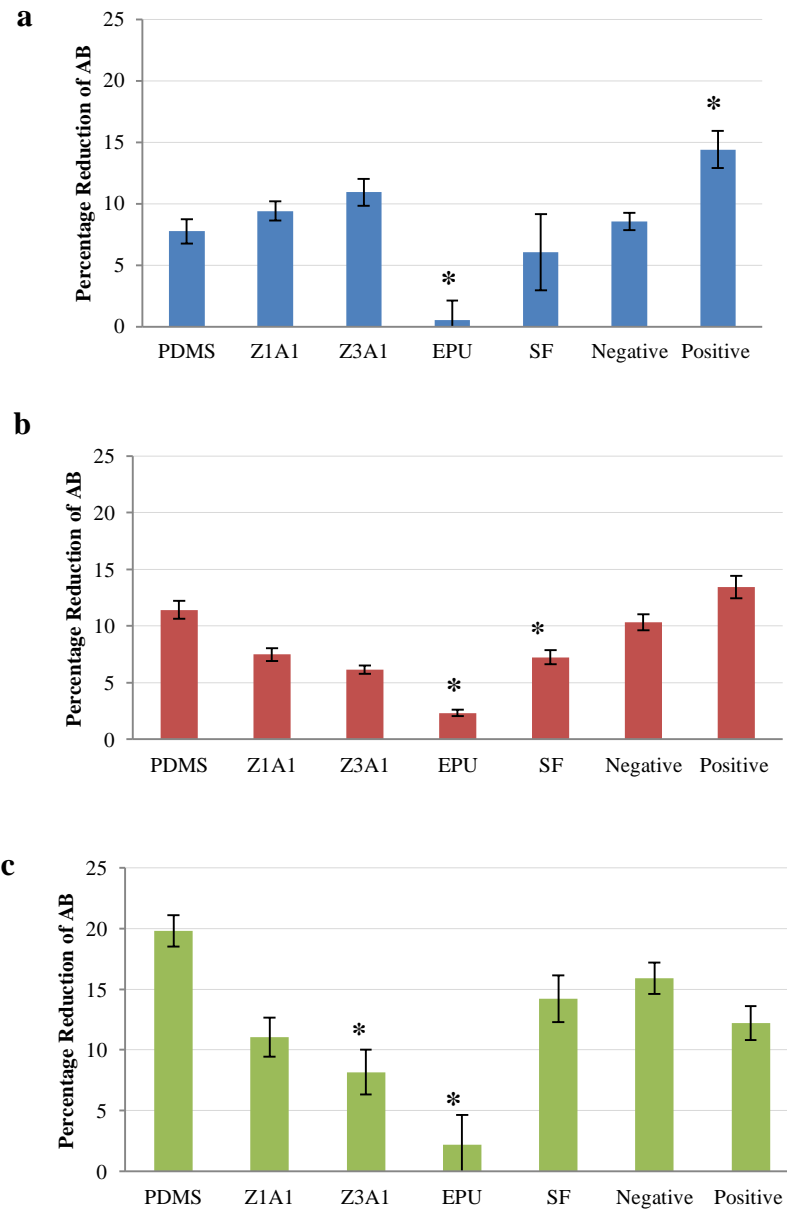


Figure 4.13: The mean reduction in AB expressed in percentage terms after 48 hours for astrocytes cells on PDMS, Z1A1, Z3A1, EPU, SF, Negative Control (Non-treated Plate P1) and Positive Control (Treated Plate P1) with BSA (a), non-treated (b) and Fn-BSA (c). Data points represent mean \pm standard error and $n = 18$. * denotes significant difference ($p < 0.05$) in cell viability compared to negative control for the corresponding treatment condition determined by one way ANOVA with a Dunnett's post hoc.

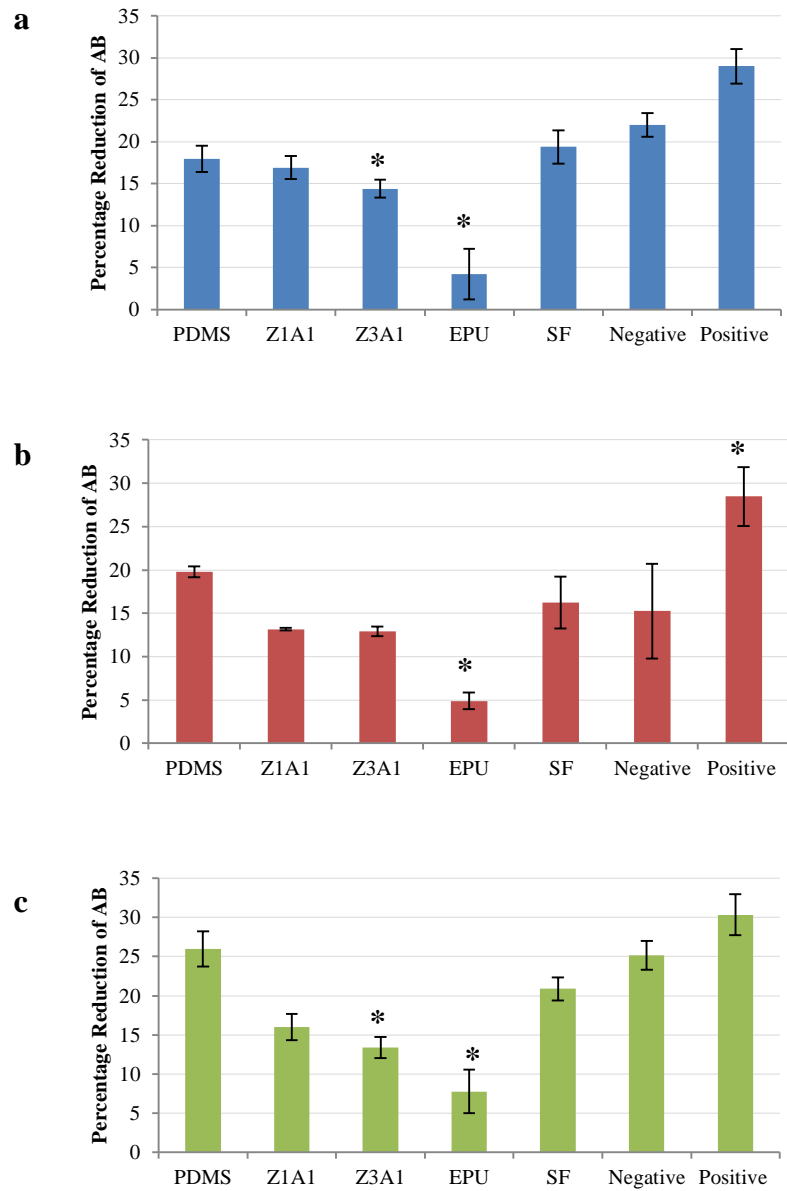


Figure 4.14: The mean reduction in AB expressed in percentage terms after 96 hours for 3T3 cells on PDMS, Z1A1, Z3A1, EPU, SF, Negative Control (Non-treated Plate P1) and Positive Control (Treated Plate P1) with BSA (a), non-treated (b) and Fn-BSA (c). Data points represent mean \pm standard error and $n = 18$. * denotes significant difference ($p < 0.05$) in cell viability compared to negative control for the corresponding treatment condition determined by one way ANOVA with a Dunnett's *post hoc*.

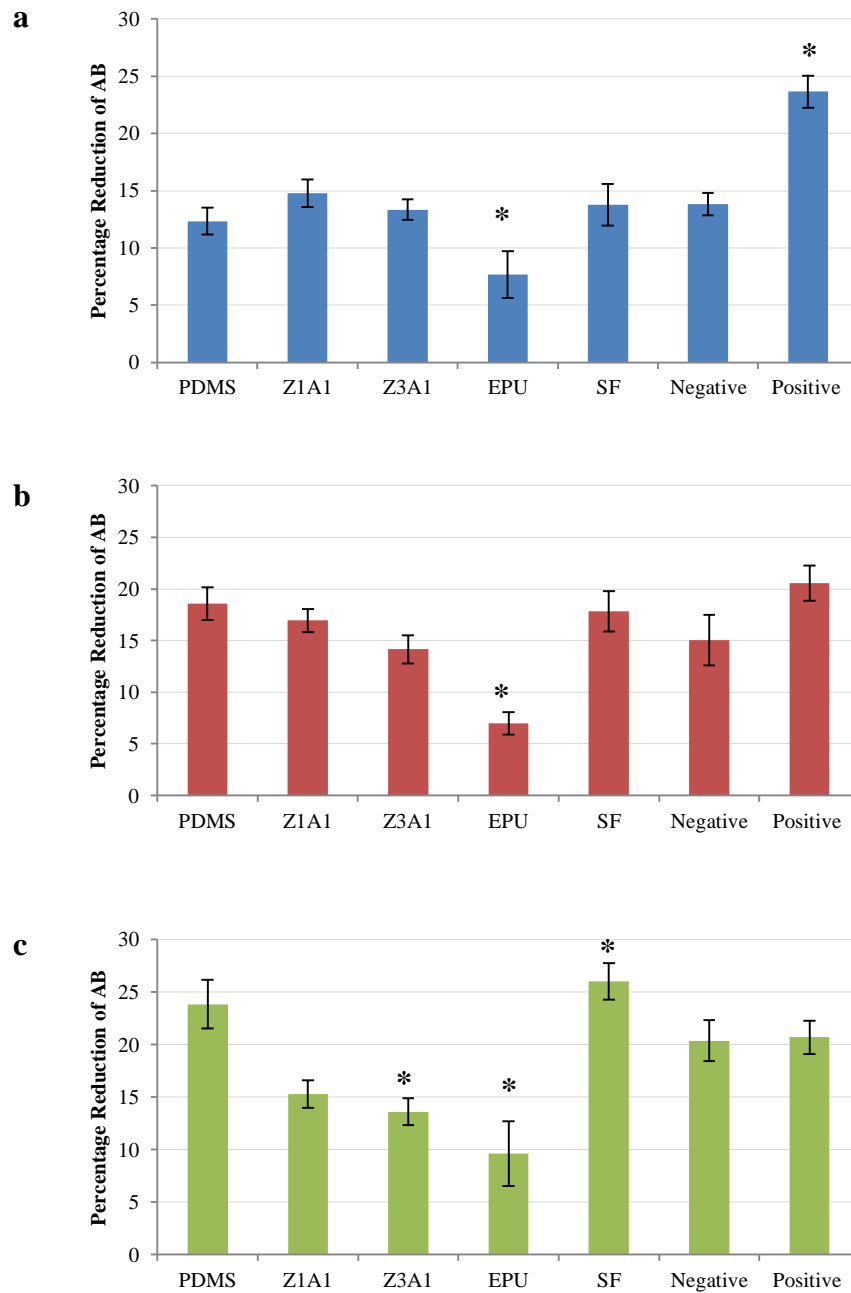


Figure 4.15: The mean reduction in AB expressed in percentage terms after 96 hours for astrocytes on PDMS, Z1A1, Z3A1, EPU, SF, Negative Control (Non-treated Plate P1) and Positive Control (Treated Plate P1) with BSA (a), non-treated (b) and Fn-BSA (c). Data points represent mean \pm standard error and $n = 18$. * denotes significant difference ($p < 0.05$) in cell viability compared to negative control for the corresponding treatment condition determined by one way ANOVA with a Dunnett's *post hoc*.

4.3.7 Form of material influences cell adhesion

PDMS samples achieved the highest levels of cell viability (as measured by AB assay) for both cell types (3T3 and astrocytes), for all treatments (BSA, Fn-BSA and non-treated) at different time points (48 and 96 hours). For the purpose of comparison, therefore, the data in Figures 4.16 and 4.17 were normalised with respect to the values for PDMS to establish the significance of any differences in terms of cell viability.

From Figure 4.16 (a) and (b) it is evident that, after 48 hours in culture, the numbers of cells present on all the materials (non-treated and Fn-BSA treated) were significantly ($p < 0.05$) lower in comparison to PDMS for both the cell types. On the other hand, after 96 hours in culture (Fig. 4.17 a and b), the number of viable cells present on polyurethanes (non-treated and Fn-BSA treated) was significantly ($p < 0.05$) lower for both cell types. EPU was the only material that performed significantly less well than PDMS in terms of supporting cell attachment and growth for all treatments and cell types.

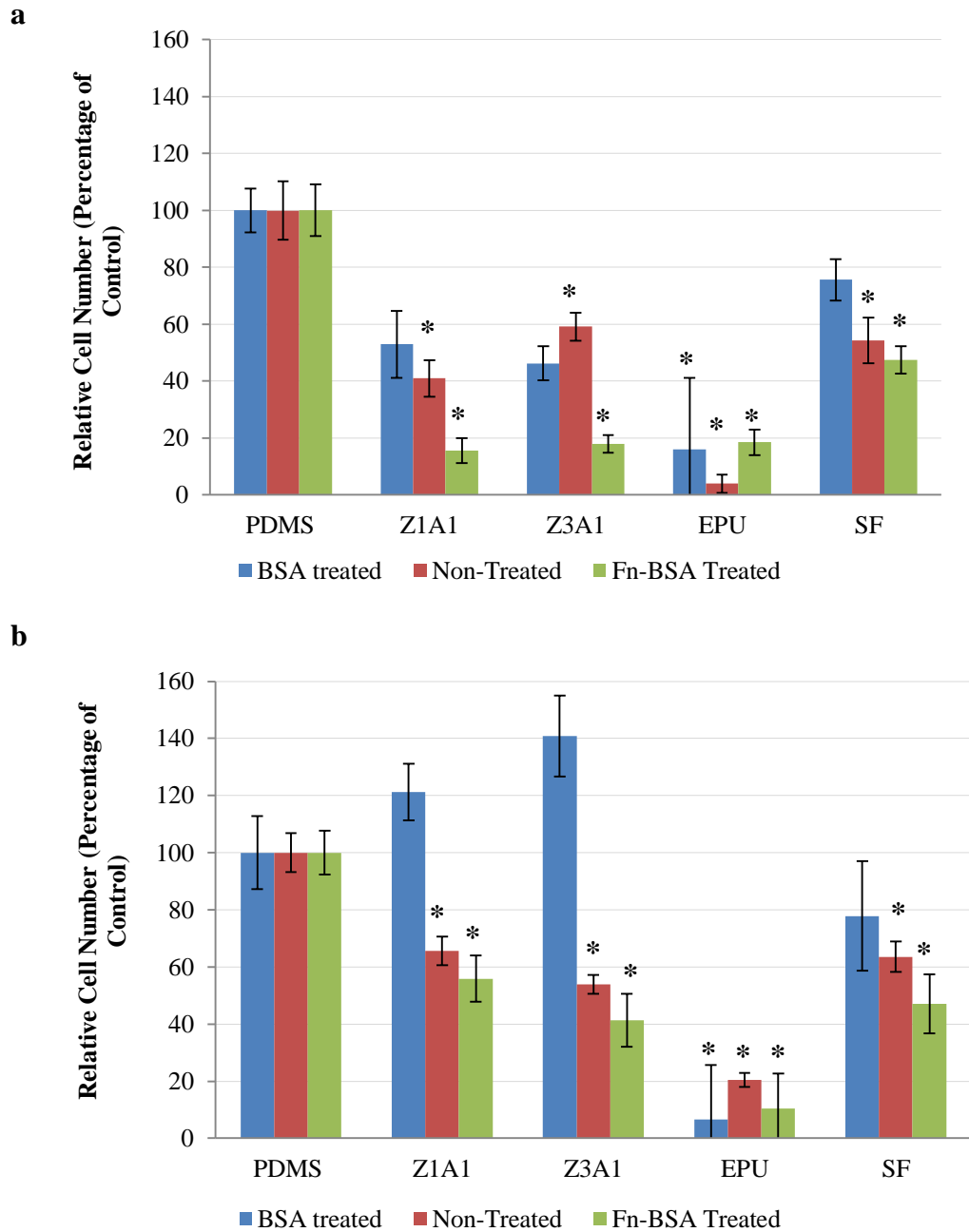


Figure 4.16: The relative cell number on Z1A1, Z3A1, EPU and SF in comparison to PDMS in percentage terms after 48 hours for 3T3 cells (a) and astrocytes (b) before and after treatment. Data points represent mean percentage relative to control \pm standard error ($n = 18$). * denotes the significant difference ($p < 0.05$) in cell viability compared to PDMS determined by one way ANOVA with a Dunnett's post hoc.

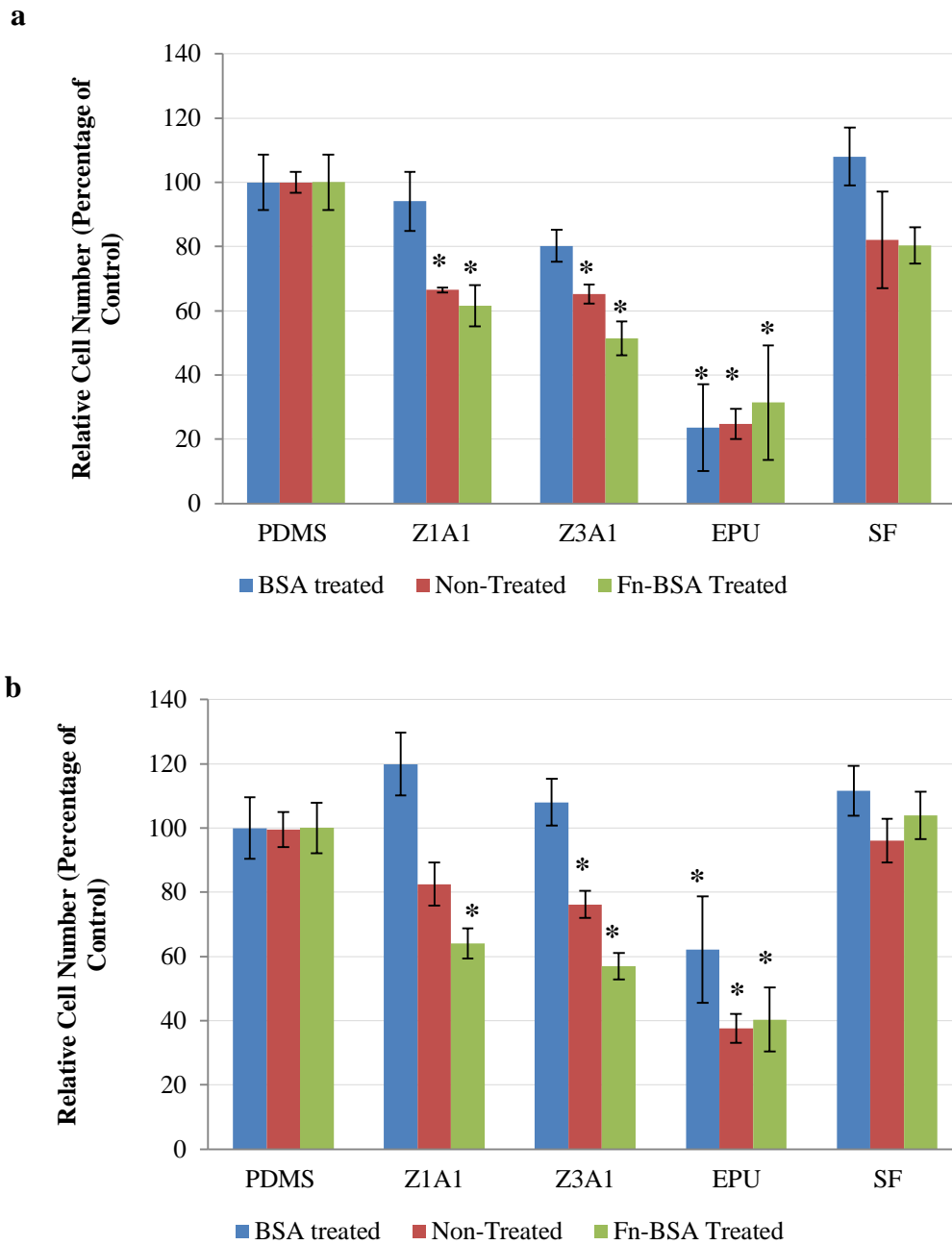


Figure 4.17: The relative cell number on Z1A1, Z3A1, EPU and SF in comparison to PDMS in percentage terms after 96 hours for 3T3 cells (a) and astrocytes (b) before and after treatment. Data points represent mean percentage relative to control \pm standard error ($n = 18$). * denotes the significant difference ($p < 0.05$) in cell viability compared to PDMS determined by one way ANOVA with a Dunnett's post hoc.

4.3. 8 Fluorescence microscopy control images

Fibroblasts were cultured on coverslips and exposed to 70% ethanol as negative control (Figure 4.18).

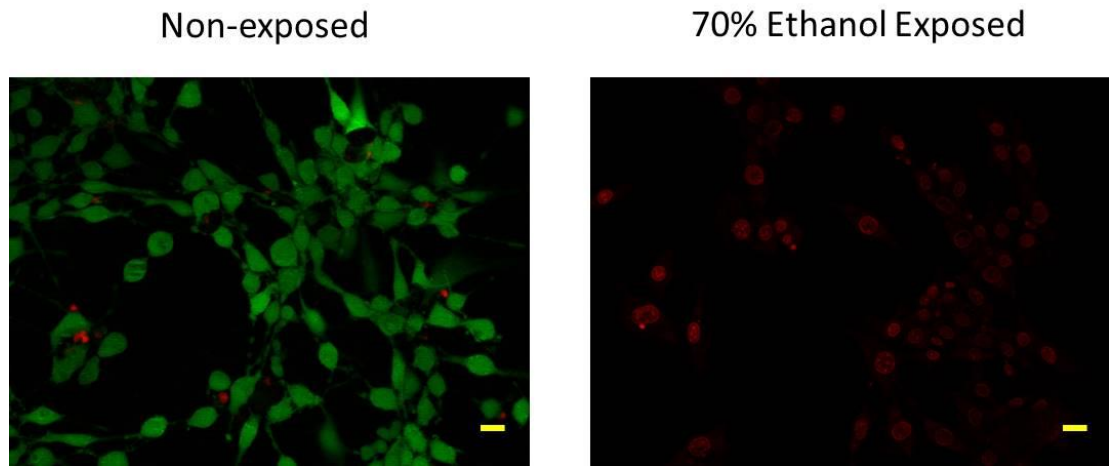


Figure 4.18: Fluorescence microscope images of 3T3 cells taken after 48 hours in culture on glass coverslips. Image on left shows viable fibroblasts (left) and fibroblast following exposure to ethanol by way of control (right). Live cells are stained green (Calcein AM) and dead cells are stained red (Ethidium homodimer – 1). Scale bars are 20 μ m.

4.3. 9 Fluorescence microscopy images of catheter material

Figures 4.19 and 4.20 show representative fluorescence images of 3T3 cells and astrocytes, respectively, after staining for viability (Live-Dead[®] assay) for each substrate, either non-treated or following Fn-BSA treatment. The Fn-BSA treated samples for all the substrates shows an increase in cell viability in comparison to non-treated but it is not significant.

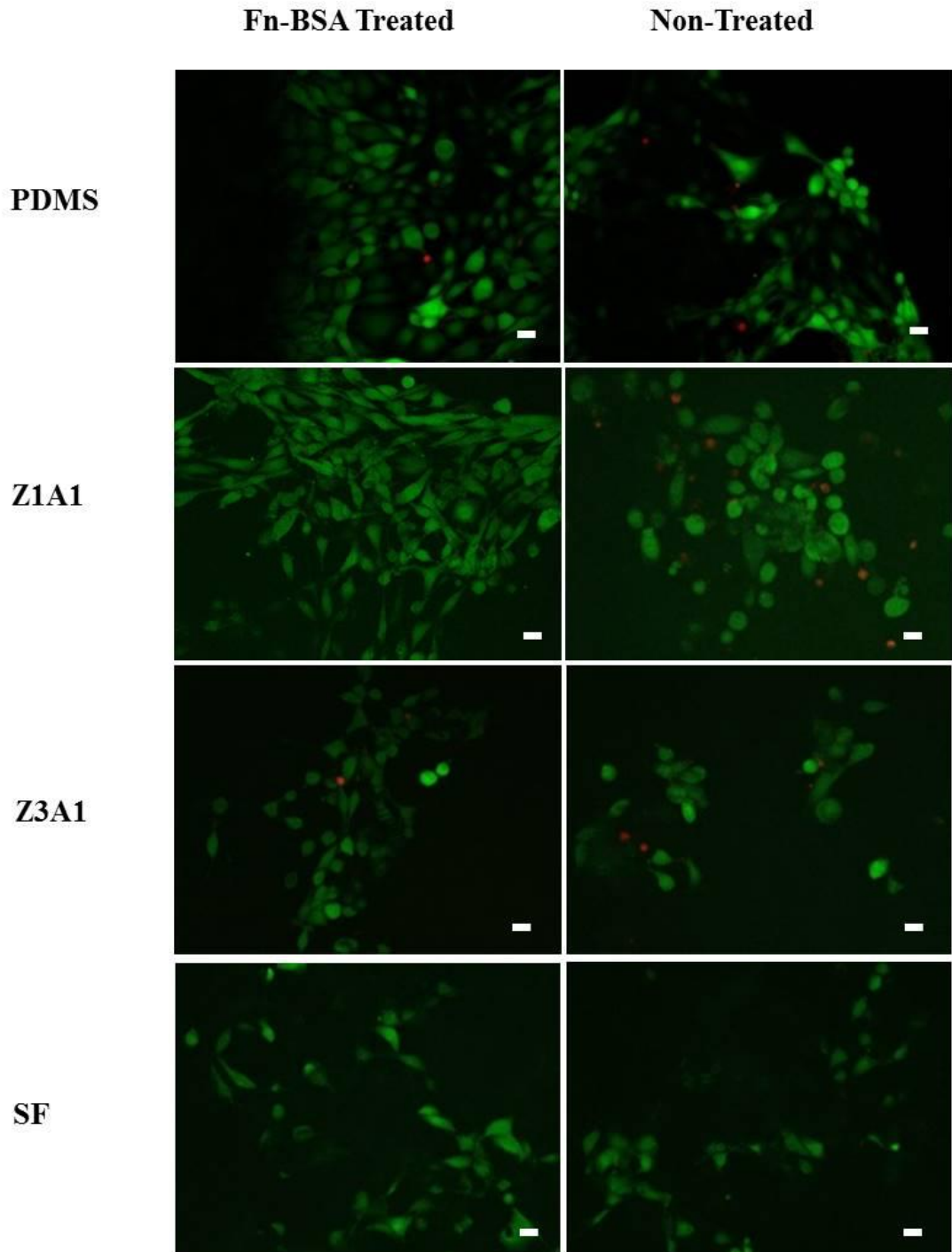


Figure 4.19: Fluorescence microscope images of 3T3 cells taken after 96 hours in culture on Fn-BSA treated and non-treated samples. Live cells are stained green (Calcein AM) and dead cells are stained red (Ethidium homodimer – 1). Scale bars are 20µm

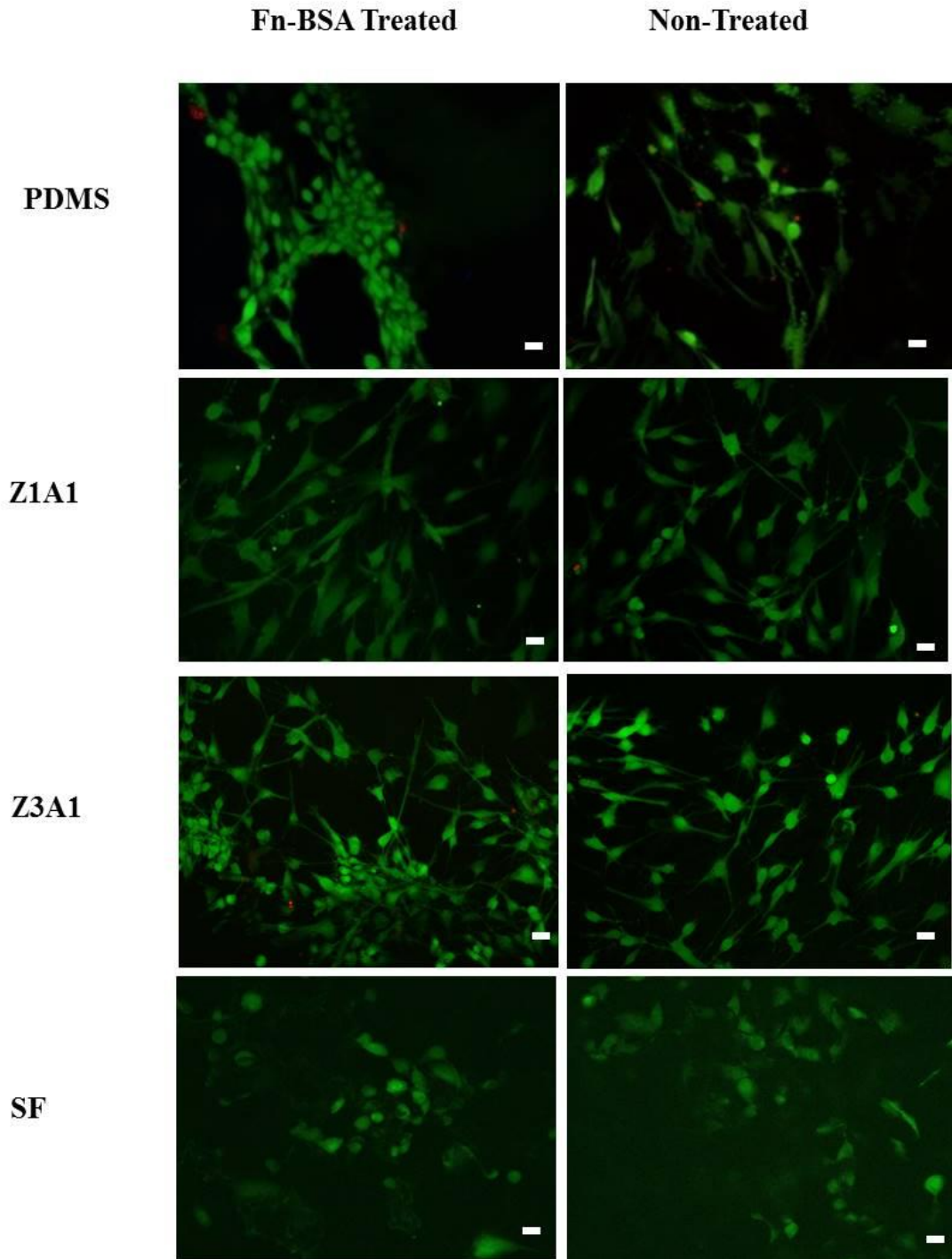


Figure 4.20: Fluorescence microscope images of Astrocytes taken after 96 hours in culture on Fn-BSA treated and non-treated samples. Live cells are stained green (Calcein AM) and dead cells are stained red (Ethidium homodimer – 1). Scale bars are 20 μ m

4.4 Discussion

Primary astrocytes were isolated from rat cortices according to an established protocol, and the phenotype of resulting cultures confirmed by immunostaining (Fig. 4.1). The isolation protocol is reported to achieve a pure primary astrocytes (Kim and Magrane 2011). Although astrocytes are the most abundant cells found in the explanted catheters, the presence of other cell types such as microglia and oligodendrocytes is likely. Hence, this level of purity is considered sufficient for the purposes of this study.

AB is an indicator dye based on the metabolic reactivity of the cells. The dye is non-toxic, and does not affect cell proliferation or viability (de la Puente *et al.*, 2011; Nakayama *et al.*, 1997). It has found wide application in cell culture studies, for example, cytotoxicity and biocompatibility testing, to determine the efficiency of cell seeding of scaffolds, and in cell proliferation studies (Gloeckner *et al.*, 2001). An important feature of this assay is that it allows repeated assaying without disturbing the cell activity. Hence, in the context of the experimental study described above, it facilitated the measurement of cell viability of the same samples at 48 and 96 hours.

From the standard growth curve it is evident that at lower seeding densities both the cell lines have a similar growth rate, although, at higher seeding densities, the immortalised cell line overtakes the primary cell culture (Fig. 4.2). It is evident from Figure 4.4 that astrocytes approach the stationary phase of growth after 48 hours in culture at higher seeding densities. Hence, in subsequent experiments the lower seeding density was selected to ensure that the cells were in the growth phase, and to facilitate comparison of the astrocyte and 3T3 behaviour on each substrate.

Preliminary control experiments were conducted by growing 3T3 cells on all the substrates, and comparing with the positive control (tissue culture treated plate) and negative control (silicone hydrogel). The results from this study support the conclusion that of all the substrates tested, EPU was the least likely to support cell growth compared to the negative controls, at both 48 and 96 hours (Fig. 4.5).

Following on from this observation, further experiments were carried out to test the hypothesis that the form of material may have a bearing on cell viability and growth.

The ability to grow the cells on the surface of the substrate without the cells escaping to the base of the well was achieved by securing a small PTFE tube which locks the substrate in position and allows the cells to proliferate on the desired substrate. This was validated by comparing the samples grown on treated and non-treated plates as no significant difference in cell growth on the substrate between the plates was observed (Figs. 4.6, 4.7, 4.8 and 4.9). The cell viability on different substrates was relatively the same regardless of the cell type.

The non-treated polystyrene plate used as the negative control in the experiment was found to show no significant increase in cell growth after 96 hours in culture when compared to 48 hours; whereas, the positive control (regular tissue culture plastic) shows a significant increase in cell growth after 96 hours in culture when compared to 48 hours (Figs. 4.10, 4.11, 4.12 and 4.13). The number of cells on the positive control surfaces was higher than all other substrates and treatments (BSA, Fn-BSA and non-treated) for both cell types. The presence of Fn-BSA on PDMS and SF has a positive effect on cell growth compared to non-treated and BSA treated surfaces of the same material. Although, a slight increase in cell number is evident between the treated and non-treated polyurethane samples, it is not significant. This finding is consistent with the microscopic images viable cells on each substrate obtained using the Live/Dead assay kit (Figs. 4.17 and 4.18).

The study confirms that PDMS supports the greatest numbers of cells than all of the other catheter materials and forms under static culture studies (Figs. 4.14 and 4.15). The results also shed some light on how the cells behave on each substrate. There was no significant difference between the cast film polyurethanes for both the time points. However when compared to PDMS, there was a significant difference after both time points in culture for BSA treated and Fn-BSA treated. The results suggest that polyurethanes do not encourage cell proliferation to the same level as PDMS even after longer time in culture. On the other hand, the macroporous sponge form of PDMS was significantly less at the initial time point but does not show a

significant difference with longer culture time. Therefore, it may be concluded that PDMS as a material is more suitable for cell proliferation than polyurethane.

The most interesting finding from this study concerns the microporous form of polyurethane, which supported the fewest numbers of cells compared to all other substrates at both the time points and treatments. The differences were significant after 48 and 96 hours in culture. The results suggest that the microfibrillar structure of the polymer presents a more challenging environment for the cells. Those cells that are unable to attach soon after seeding may eventually apoptose, with fewer cells remaining in contact with the surface to go on to proliferate. However, cell numbers do appear to recover after longer periods in the culture. The cell behaviour on a 3D scaffold or fibrous substrate was always different compared to a 2D substrate. In terms of surface available to proliferate and 3D structures represent ECM which should enhance cell growth. These findings were not reflected by the results of this study, one reason might be due to polyurethane as a material may not be enhancing the cell adhesion to the same extent as PDMS.

The choice of sterilisation method is known to influence the surface characteristics of polyurethane catheter materials. In a study by (Andrews *et al.*, 2007), exposure of EPU surfaces to UV-Ozone was found to increase surface roughness. Nevertheless, the intensity of UV radiation to which the samples were exposed in that study was much greater. Clearly, further investigation is required to determine the extent to which the samples used in this study were affected by UV. Alternative sterilisation methods such as microwave radiation are available, but equally may damage the surface through thermal effects. Whatever the method used (UV, gas, radiation) as an alternative to UV, the potential to damage the surface and bulk properties of polymer should be evaluated.

In contrast to reports elsewhere (Harris *et al.*, 2011a), the presence of fibronectin and albumin appeared to have no significant effect on the cell viability and growth in this study. Albumin is widely known for its role in blocking the binding of proteins, antibodies, etc., at surfaces, but the results did not show any decrease in cell viability. The explanation for this observation may lie in the protein concentrations

used in this study. Future studies should explore the effect of increasing the protein concentrations, along with measurement of protein adsorption onto each substrate.

The other limitations of this study shorter culture time and auto-fluorescence of EPU which made it impossible to view the cells presence. For future studies EPU should be imaged using SEM with a critical point dryer, in order to view both the material and cells presence. This would be an alternative to get around the auto-fluorescence of EPU.

Although the presence of fibronectin or albumin on EPU enhances cell growth only slightly, the difference is not significant; hence these treatments will be considered further in subsequent experiments carried out under perfusion conditions more representative of CSF flow. In the following chapter, the inter-relationship between hydraulic permeability, and the ability of the EPU samples, in particular, to support the growth of cells during perfusion culture, will be explored.

4.5 Conclusion

Primary astrocytes were successfully isolated and cultured from rat cortices. The alamarBlue assay was verified, and found to be effective and suitable for the purpose of this study. The results of these experiments reveal that, under static culture conditions, the growth of cells on a wide range of material substrates and forms is reproducible and reliable. The method of securing the substrates to the base of the 96-well plates, and the type of plate used in these experiments, do not appear to affect the ability of the assay to distinguish between the different test substrates. PDMS, either as cast film or macroporous form (SF), supports cell growth better than the corresponding polyurethane forms tested here. While the presence of proteins on the surface of both PDMS and SF increases cell growth when compared to non-treated samples, this was not the case for the polyurethane samples. The EPU form, of all the candidate materials tested supported the least numbers of cells compared to controls. The results of this study provide further evidence that cells on the microfibrinous form of EPU do not grow as effectively as they do in 2D culture on cast films, even in the presence of proteins.

CHAPTER 5

***IN VITRO* MODEL OF AN ALTERNATIVE CSF SHUNT CATHETER OBSTRUCTION**

5.1 Introduction

In Chapters 3 and 4, the fabrication and suitability of the electrospun material as proximal catheter was examined. The focus of this chapter is to further investigate the influence of flow on cells cultured on the microfibrinous form of polyurethane (EPU) and the potential of those cells for causing obstruction. As discussed in Chapter 2, there are few reports in the literature which have explored the obstruction of shunt catheter *in vitro*. Recently Harris *et al.* (2009) created a platform to study cell adhesion *in vitro* on a conventional catheter material. Later, this group used this same model to explore the cell adhesion characteristics on conventional PDMS catheters, catheters having larger perforations, and catheters that had been modified to render the surface more hydrophilic (Harris and McAllister 2011; Harris *et al.*, 2011a; b).

The work detailed in this chapter builds on the preliminary work presented in Chapters 3 and 4. The observation that EPU is the least conducive to cell growth will be further tested under perfusion conditions. The aim of this work is twofold: 1) to quantify the effect of perfusion on the growth of cells on the EPU catheter material in the presence of key CSF proteins; and 2) to quantify the impact of cell growth on the hydraulic permeability of the EPU samples under perfusion conditions representative of CSF flow *in vivo*.

5.2 Materials and Methods

5.2.1 EPU Preparation and Cell Culture

For this study both primary astrocytes and immortalised 3T3 cell line were used. The cell lines were cultured and maintained as described in Sections 4.2.2 and 4.2.3. DMEM with supplements as mentioned in Section 4.2.1, was used as growth medium for both cell lines. The EPU samples for this experiment were those that had been grouped as low, medium and high according to hydraulic permeability, as explained in Section 3.3.3. The EPU catheter was cut into two parts for the experiment, each of length 3 cm, one part being used for perfusion and the other for static culture. The samples were UV sterilised as described in Section 4.2.4 prior to protein coating and cell seeding. The ends of the EPU samples were fitted with microwave sterilised luer connectors to facilitate priming with medium and subsequent perfusion.

The Fn solution was prepared as detailed in Section 4.2.5. A bolus of 300 μ l of 4 μ g/ml of bovine plasma fibronectin (Invitrogen, Paisley, UK) was injected into the EPU sample with one end closed and after injection the other end was also closed. The sample was then placed on a rocker platform (Gyro-rocker, Stuart S170) at 30 rpm for 1 hour at 37 $^{\circ}$ C to achieve uniform adsorption of fibronectin on the substrate. Thereafter, the protein solution was discarded by opening the tap at one end and washed twice with PBS. The treated surface was then blocked by injecting 300 μ l of 1% w/v BSA (Sigma-Aldrich, UK) and placed on the rocker platform again for 1 hour at 37 $^{\circ}$ C. The protein solution was then removed and washed with PBS twice before seeding with cells.

A seeding density of 3.5×10^4 cells/cm² was chosen for this study. To achieve a uniform distribution of cell adhesion on the EPU substrate, the following seeding protocol was followed (Villalona *et al.*, 2010). A cell suspension of 300 μ l was injected into the protein treated and non-treated EPU using a 1 ml syringe; the ends of the EPU were closed after the introduction of cells. It was then transferred into a 20 ml centrifuge tube containing 3 ml of the growth medium, which immersed the

seeded EPU and provided enough nutrients until the seeding time period. The centrifuge tube was placed on a rocker platform at 30 rpm for 6 hours at 37 °C and 5% CO₂, that allowed the catheter inside the tube to roll at 180°. Before placing the seeded EPU catheters into the shunt obstruction model, the cell viability after seeding was measured using AB assay which is described in the following section.

5.2.2 *In vitro* Shunt Obstruction Model

In order to study the CSF flow due to shunt obstruction, the experimental condition requirements and assumptions need to be stated before proceeding. The model was designed to study the change of EPU properties due to cell growth. Therefore, the parameters to be recorded in this study were: cell viability after seeding and after a set period of perfusion (post-perfusion). A series of control experiments was conducted where the other half of each EPU catheter was seeded with cells and cultured under static conditions; all other experimental conditions (sample preparation, culture conditions, and assays performed) were identical. At the conclusion of each experiment, any change in hydraulic permeability was determined using the apparatus described in Chapter 3 and with reference to the hydraulic permeability results presented in Section 3.2.4.

A photograph of the shunt obstruction model is shown in Figure 5.1. It consists of essential elements to support cell growth and model the CSF flow. The flow of CSF was mimicked using the growth medium. A syringe pump (Cole Parmer, Vernon Hills, USA) was used to deliver the constant flow of CSF. The CSF flow through a conventional hydrocephalus shunt is 0.35 ml/min (Czosnyka Marek *et al.*, 2004). The corresponding rate of flow of the culture medium was calculated according to the surface area of the catheter to be modelled, that is, 0.07 ml/min (0.03 cm/min). The seeded EPU samples were placed inside a T-25 flask with one end blocked. The luer connector from the other end was fitted through the cap of the flask connecting the sample and tube (Tygon lab tubing, Cole Parmer, Vernon Hills, USA) delivering growth medium from the syringe pump. The flask was examined at the end of the study; it was found there was no contamination or cell growth at the bottom surface

of the flask. The entire setup was placed in an incubator and maintained at 37°C and 5% CO₂ atmosphere.

As a control group for this study, the EPU was seeded as described above and cultured under static conditions, which included placing the sample inside a 20 ml centrifuge tube with 3 ml of medium at 37⁰C and 5% CO₂ for the same time period (12 hours) as in the case of perfusion. The growth medium was changed after seeding and every 6 hours thereafter, which provided enough nourishment for the cells within the substrate. At the end of perfusion/static culture, the EPU sample was carefully removed from the flask and transferred to a 20 ml centrifuge tube containing 3 ml of growth medium, into which the AB dye was added to measure cell growth.

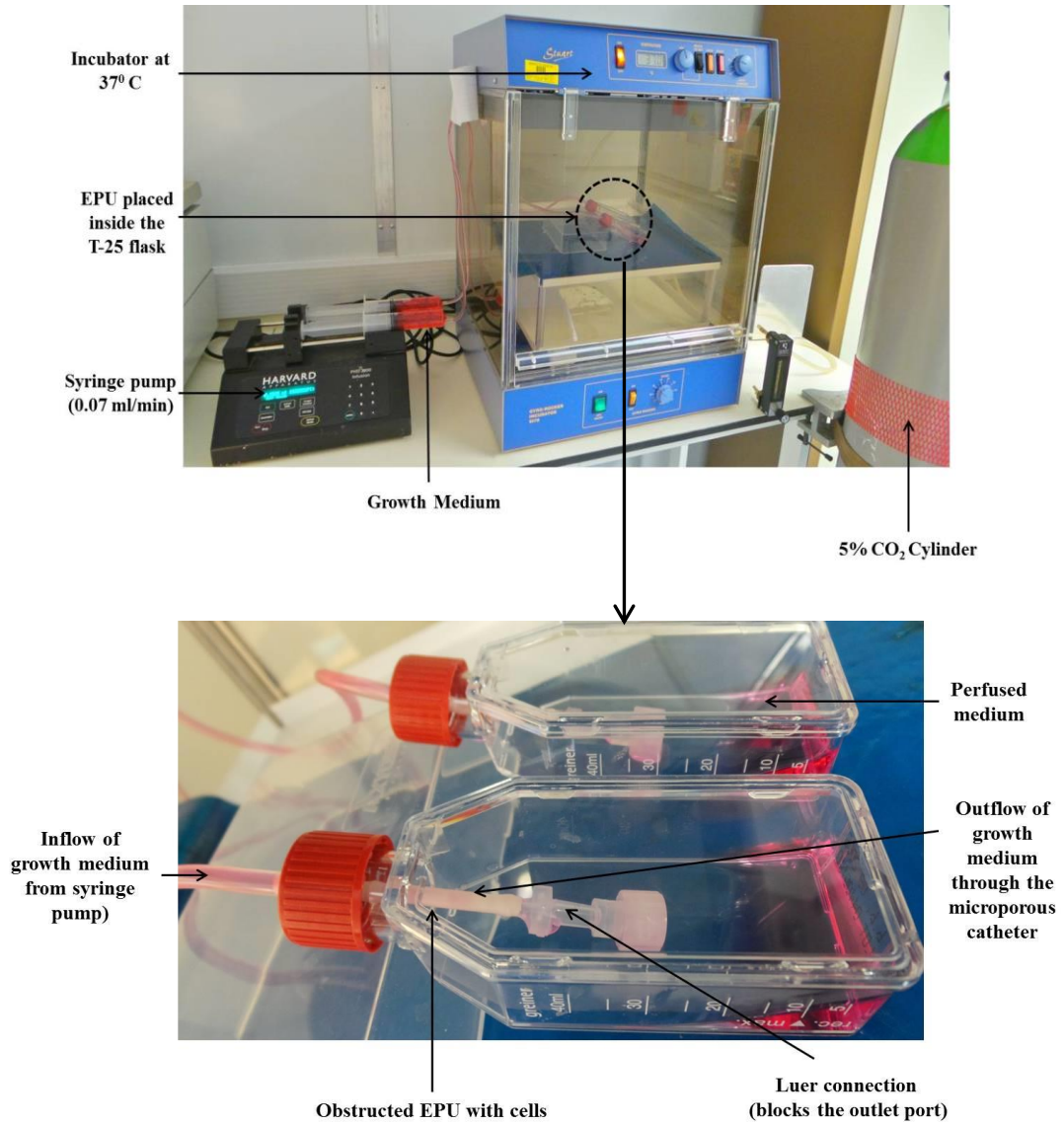


Figure 5.1: Schematic diagram of the shunt obstruction model. Syringe pump to deliver a constant flow rate of growth medium at 0.07 ml/min for 12 hours. T-25 flask contains the obstructed EPU samples. The EPU within the T-25 flask was placed inside an incubator maintained at 37° C and connected to a 5% CO₂ cylinder. The growth medium was not re-circulated but was retained inside the T-25 flask after passing through the walls of the EPU catheter.

5.2.3 Cell viability measurement

The cell viability was measured at two points: immediately after seeding (t=6 hours) and after 12 hours of perfusion (t=24 hours). The alamarBlue assay was used to quantify the numbers of cells present at each time point according to the protocol specified by the manufacturer. A bolus of 300 μ l of AB solution comprising 10% of growth medium was added to EPU samples present within the centrifuge tube containing 3 ml of growth medium after seeding/perfusion/static and left for 6 hours to allow the dye to reduce before measuring the absorbance. Then, 200 μ l of the reduced dye within the growth medium was transferred to each of the 15 wells of the 96-well plate and the absorbance measured at 540 and 620 nm in a plate reader (Multiskan Ascent). The absorbance for growth medium alone (blank) and with the addition of AB was measured at both the wavelengths in the same proportions and volumes as the test samples. The absorbance values were then converted to percentage reduction of AB using the formulae given in Section 4.2.6.

5.2.4 Hydraulic Permeability measurement

At the conclusion of each experiment (t=24 hours in culture), the pressure-flow relationships of each EPU samples was determined using a similar protocol to that detailed in Section 3.2.4. The ‘module’ in this case made use of the same luer connections that were used in the cell culture experiment. The catheter was inserted into an acrylic tube without coming in contact with the inner surface of the tube.

The hydraulic permeability was determined under flow control, as described in Section 3.2.4, de-aerated/distilled water was used to mimic CSF. The syringe pump was used to inject fluid at set flow rates (0.5, 1 and 1.5 ml/min) into the EPU inlet port and the displaced liquid was collected to measure the mass flow rate. The inlet pressure was monitored using the catheter pressure transducer that formed part of the Bose Electroforce System (Millar Mikro -Tip[®] Inc., Houston, TX, USA).

5.3 Results

5.3.1 Control Experiments for perfusion study

Astrocytes and 3T3 cells were seeded on the EPU catheters as mentioned in Section 5.2. AB was added after 6 hours of seeding and 12 hours of perfusion (Fig. 5.2). The cell viability was measured post seeding (after 6 hours of AB in contact with the cells) and post perfusion (after 12 hour perfusion and 6 hours of AB in contact with the cells). Figure 5.2 shows the percentage reduction of AB for EPU catheters grown on astrocytes and 3T3 cell line. There is a significant increase in number of cells after perfusion when compared to before perfusion ($p < 0.05$). The numbers of cells present on the catheter material remains the same for both cell types for the perfusion study.

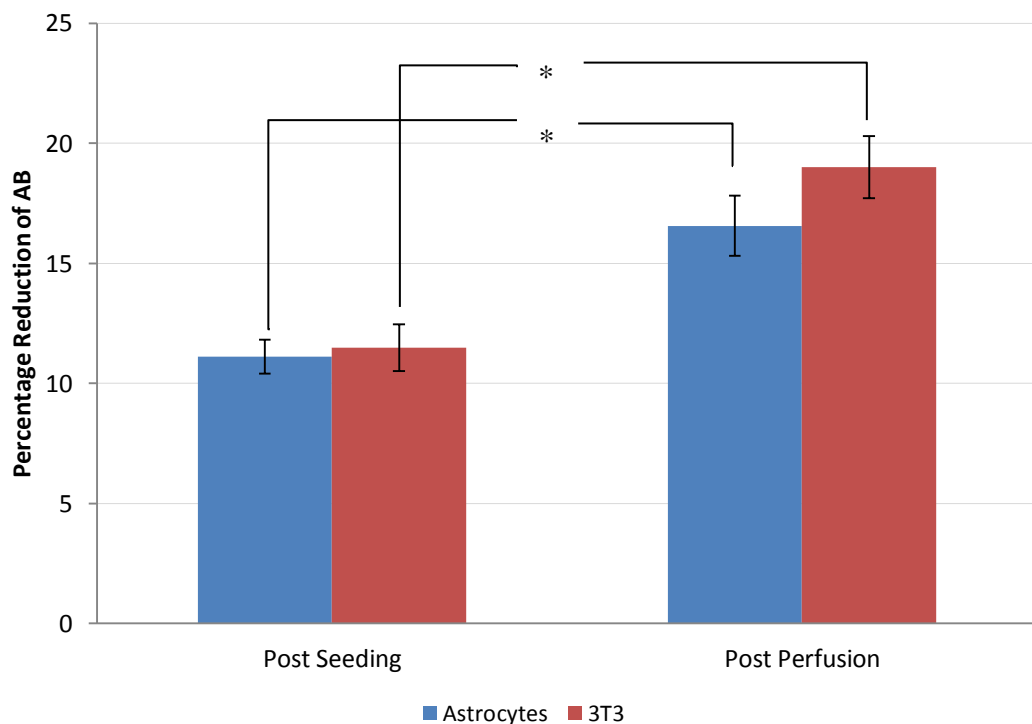


Figure 5.2: Mean percentage reduction of AB for astrocytes and 3T3 grown EPU catheters post seeding ($t=6h$) and post perfusion ($t=24h$). Data points represents mean \pm standard error and $n = 3$. * denotes the significant difference of cell viability after perfusion determined by Student *t*-test ($p < 0.05$).

At the end of perfusion experiment, the hydraulic permeability was measured. The hydraulic permeability measured before and after the perfusion culture experiments is plotted in Figure 5.3. There is a significant decrease in the permeability after perfusion ($p < 0.05$) irrespective of cell type. The hydraulic permeability of the EPU samples chosen for this study were the same (no significant difference $p = 0.53$).

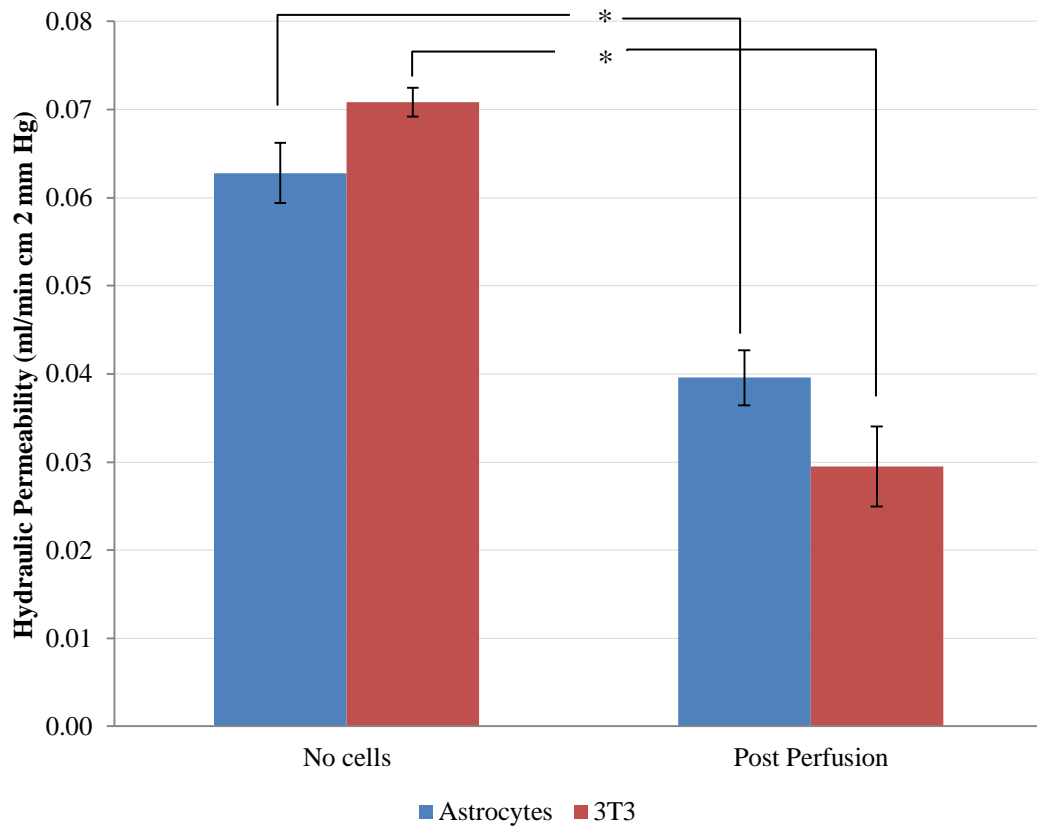


Figure 5.3: Hydraulic Permeability compared with no cell present and post perfusion ($t = 24h$) for astrocytes and 3T3 grown EPU catheters. Data points represent mean \pm standard error and $n = 3$. * denotes the significant difference of permeability after perfusion determined by Student t -test ($p < 0.05$).

5.3.2 Effect of sample permeability on cell adhesion and growth

In a further series of experiments, the EPU catheters were first treated with fibronectin and blocked with albumin and then seeded with 3T3 cells as described as above. As a control group, a number of EPU catheters were seeded with cells and maintained under static environment. The results of cell viability after seeding and at the end of perfusion/static for low, medium and high hydraulic permeability groups of EPU catheters are summarised in Figure 5.4. The numbers of cells on the Fn-BSA treated and non-treated samples from the low permeability group increased significantly ($p < 0.05$) for both static and post-perfusion samples compared to the numbers immediately after seeding. Likewise, the samples from the intermediate permeability group show a significant increase in cell numbers after perfusion whereas the corresponding static samples are no different to the controls for both treated and non-treated samples. The results for the high permeability group samples, on the other hand, were no different in case of Fn-BSA treated and non-treated EPU samples regardless of the culture conditions. There was no difference in cell viability for all the groups before and after perfusion. Fn-BSA treated and non-treated samples fail to show any significant change in cell numbers either during perfusion or after static culture.

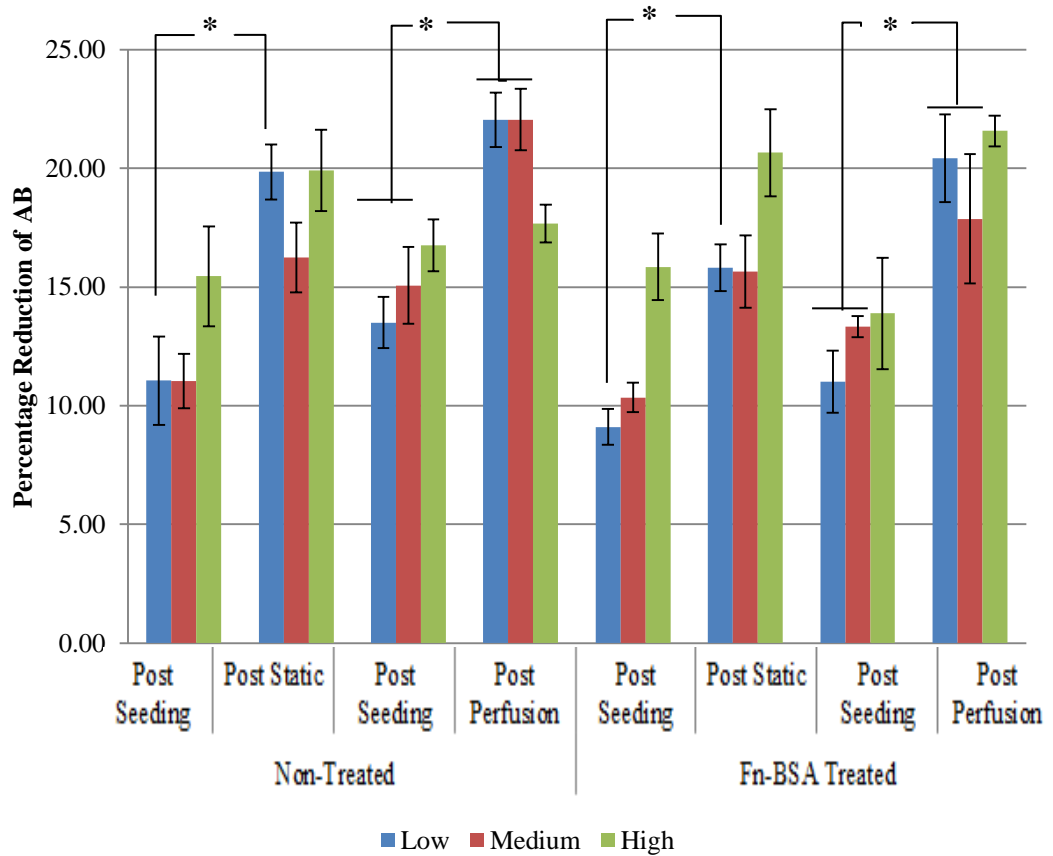


Figure 5.4: Mean percentage reduction of AB for post seeding ($t=6h$) and post perfusion/static ($t=18h$) compared with non-treated and Fn-BSA treated EPU catheter for Low, Medium and High groups. Data points represent mean \pm standard error and $n = 8$. * denotes the significant difference of cell viability after perfusion/static as determined by one way ANOVA with Tukey's posthoc analysis ($p < 0.05$).

5.3.3 Hydraulic permeability after obstruction

At the conclusion of the above cell culture experiments (Section 5.3.2) the hydraulic permeability of all EPU catheters was quantified for comparison with the values obtained for each sample beforehand. The results of this comparison are presented in Figure 5.5 in terms of hydraulic permeability for each group (low, medium and high) before seeding (no cells present) and at the conclusion of each experiment. While there is a significant reduction ($p < 0.05$) in hydraulic permeability due to cell obstruction for all groups, treatments and conditions (perfusion or static culture), there was no difference between the different groups obstructed by cells for any treatments or conditions. The level of reduction in the permeability before and after obstruction remains the same for all the groups. The obstructed EPU for all groups is still functional to clear CSF at 0.35 ml/min.

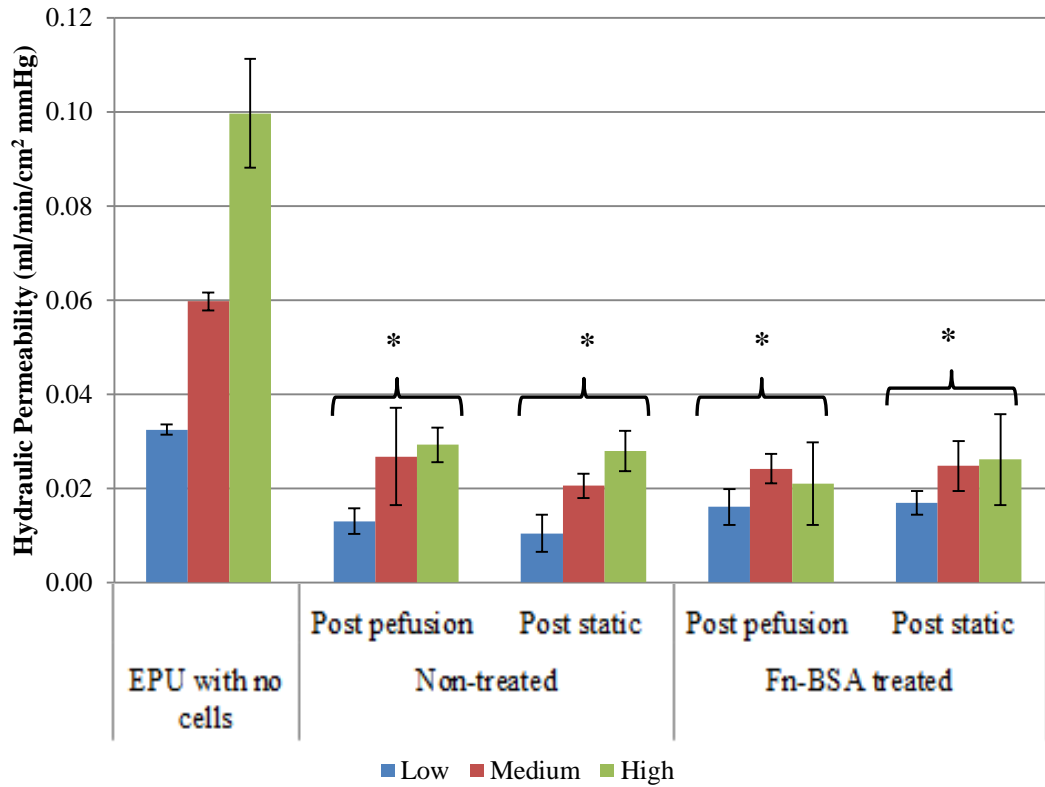


Figure 5.5: Hydraulic Permeability compared with no cells present (before seeding) and 12 hour after perfusion/static for non-treated and Fn-BSA treated EPU catheters. Data points represent mean \pm standard error and $n = 8$. * denotes the significant difference of permeability after perfusion/static relative to the control before seeding as determined by one way ANOVA with Tukey's posthoc analysis ($p < 0.05$).

5.4 Discussion

The aim of this study was to quantify cell adhesion, growth and subsequent obstruction by cells blocking the pores of an alternative form of shunt catheter. The cells were seeded inside the EPU walls, after which one end is connected to growth medium and the other end is blocked. Therefore, the only outlet for the growth medium is through the pores. The growth medium was perfused through the pores of the catheter for 12 hours. Due to this arrangement of perfusion set-up, shear force which occurs along the length of the catheter is assumed to be negligible.

A conventional catheter length is 15 cm but the length of the alternative catheter used in this study was ~4cm. Therefore, flowrate of 0.07 ml/min was chosen for the perfusion study calculated according to the length of the catheter exposed. The seeding density chosen for the shunt obstruction study was 3.5×10^4 cells/cm² which is three times that used for the 96-well plate static studies reported in Chapter 4. The higher seeding density was chosen because the duration of the experiment was shorter (30h as opposed to 96h in the case of previous study) and in order to evaluate the effect of those cells in terms of catheter obstruction under ‘worst case’ conditions. The chosen initial seeding density is comparable to values quoted in the literature. The study by Harris et al., for example, reported an initial seeding density of 1.8×10^4 cells/cm² (Harris *et al.*, 2010).

The immortalised 3T3 cell adhesion was compared with the astrocytes under flow conditions for a set of untreated EPU catheters and the resulting cell adhesion results were the same for both cell types (Section 4.5). The results of this preliminary study of shunt obstruction show no significant difference in terms of cell number or permeability. It follows that the flow of growth medium through the obstructed catheter does not influence cell growth of either cell type. In all subsequent experiments, therefore, 3T3 cell lines were used instead of primary astrocytes.

These cells adhered and proliferated on all the EPU catheters for the duration of each experiment. Treating the surface of each sample beforehand with fibronectin and albumin did not enhance cell adhesion or growth on any of the EPU catheter groups.

Likewise perfusion, although one cannot infer from this finding that flow does not have a bearing on cell proliferation. It may be that some cells proliferate more in some areas while others are inhibited or removed under perfusion, although this is unlikely as there was no evidence of viable cells either in the growth medium or on the surface of the T25 flask at the conclusion of the perfusion experiments. Due to the auto-fluorescence of the EPU material, a qualitative analysis is lacking. Hence the cell viability reference in this study is solely based on the AB assay.

The lack of any difference between each group may be due to the seeding density or perfusion time period chosen for the experiment. Even though the initial seeding density was higher, it remains a distinct possibility that a higher seeding density and perfusion over an extended period could give rise to quantifiable differences between static and perfusion cultures. Low and medium EPU groups post perfusion culture show greater numbers of cells compared to before perfusion but the high permeability group of EPU does not show any difference in cell viability. On the contrary, the high permeability group shows a slight increase in cell growth compared to other groups before perfusion for all treatments, but the difference was not significant. Nevertheless, due to no difference in cell growth compared to perfusion and static culture for high groups; it only means that the cell adhesion in larger pore sized catheter may not be improving as much as smaller pore size for longer time period. From these results it is implied that the porosity has an effect on cell growth on the catheter under flow conditions.

The only conclusion that we can draw is that the measure of hydraulic permeability reveals the contribution made by cells on the permeability of EPU catheters. Clearly, the physical presence of cells on the surfaces of the EPU material gives rise to a significant decrease in permeability, which would result in a reduction in CSF flow had the measurement been made under pressure control. The reduction in hydraulic permeability remains the same for all the EPU groups and treatments, which is due to there being more or less the same number of cells present on each sample at each time point.

The limitation of the study lies within the choice of controls, type of the cells, length of the catheter, perfusion time period and steady flow conditions instead of pulsatile flow. The permeability was measured at room temperature, though this is unlikely to have an impact on the measurement of permeability for these samples. The study included static and non-treated samples of EPU catheters as controls in the experiments. However, the ideal controls for this study would be PDMS and polyurethane with perforated holes. Due to time constraints these controls were not tested for perfusion study.

3T3 cells were chosen for these preliminary investigations on grounds of time and cost. In the comparison study of cell types, it was found that there was no significant difference in cell growth; the results from the 96-well plate study confirmed the same. While this compromise may be appropriate from a mechanistic point of view, the use of astrocyte cultures in mono- and co-cultures is desirable to gain a better understanding of cell-biomaterial interactions for this application. Harris *et al*, (2010) stated that cultured astrocytes and those found *in vivo* have the similarity limitations. One way of getting around this problem is to obtain cells from surgical revision specimens, but one might argue that the complete understanding of the cell-material interaction *in vitro* has its limitations under any circumstances. Hence, there is a restriction in understanding of the cell behaviour on these substrates for prolonged time points. The model constructed is adaptable for varying experimental condition; therefore moving on to the pulsatile flow condition is plausible. Therefore, related study with the electrospun polyurethane materials in a pulsatile environment can be carried out.

5.5 Conclusion

An *in vitro* model to study the catheter obstruction was constructed. The cell viability for EPU catheters with and without flow of growth medium remains the same. The protein coating has not shown any enhancement in cell growth for perfusion and static. The degree of obstruction of EPU catheter groups was determined using the hydraulic permeability measurements. The porosity may have an impact on how cells attach on to the micro porous catheters; larger pore sized catheters shows less cell promotion on the surface but not significant. The hydraulic permeability is greatly reduced due to cell presence and using the testing system the changes were measured. The degree of blockage on the EPU catheter groups remains the same which corroborates that the number of cells presents in all the groups' remains the same. Increased pore sized catheters might be the suitable option to decrease the cell attachment and retain the hydraulic permeability even after the obstruction of catheter.

CHAPTER 6

DISCUSSION

Despite the numerous advancements achieved since the introduction of shunt catheters for the treatment of hydrocephalus, the technology has a number of limitations, as is evident from the review of the literature presented in Chapter 2. The incidence of shunt failure is unacceptably high, with obstruction of the proximal catheter, in particular, being the most common cause of failure (Lutz *et al.*, 2013).

The present research has extended previous work by evaluating the hydraulic characteristics of an alternative form of catheter having permeable walls. The candidate catheter material took the form of a microfibrinous polyurethane conduit fabricated by an electrostatic spinning process. Each material was evaluated in both cast film and porous forms, and in comparison with standard tissue culture plastic polystyrene and a silicone hydrogel as positive and negative controls, respectively.

The work necessitated the development of two *in-vitro* models: one to quantify the hydraulic characteristic of the catheters; and a second for the purpose of conducting cell growth studies on each material, and to evaluate the role of the protein adsorption and perfusion in a dynamic cell-culture model of shunt obstruction.

In the discussion that follows, a number of research questions are posed, and the extent to which these are addressed is discussed with reference to the results obtained from the present study, and reports published in the scientific literature:

1. *Can the walls of a microporous catheter be made sufficiently permeable to sustain flows comparable to the physiological flow of CSF?* Specifically, can a microporous catheter be fabricated that has a hydraulic permeability equivalent to that of a conventional fenestrated catheter?

To address this question, an *in-vitro* hydraulic model was constructed, and the hydraulic resistances of both porous and conventional catheters, and the components of an existing shunt series, were compared

2. *To what extent do the materials, from which the catheter is made, and its form, influence cell adhesion and growth?*

A systematic investigation of cell growth and viability on both candidate and control materials, in various forms was carried out with a view to identifying the material/form least conducive to cell growth in the presence and absence of key CSF proteins.

3. *Do cells cultured on the surface of a microporous catheter cause obstruction, and to what extent is the hydraulic permeability affected? Does the flow of CSF enhance or adversely affect cell growth and viability?*

To answer these questions, a cell-culture model of shunt obstruction was established, and the hydraulic permeability of catheters that had been seeded with cells under static and dynamic perfusion determined.

Can the walls of a microporous catheter be made sufficiently permeable to sustain flows comparable to the physiological flow of CSF?

Having carried out a systematic review of the literature (Chapter 2), and reviewed the design and performance of a number of conventional shunt catheter designs, the inadequacies of the existing technology is self-evident.

The ideal shunt device should present a dynamically variable resistance to the flow of CSF, which, in the normal physiological range, should lie between 6 and 10 mmHg/ml/min. There is no hydrocephalus shunt available at present that satisfies this criterion for all types of hydrocephalus. The experimental study described in Chapter 3 was designed to test the hydrodynamic characteristics of a commercially available hydrocephalus shunt device. It is clear from the results (Section 3.3.2, Chapter 3) that the Codman Hakim shunt series as a whole did not meet the desired resistance. Of the various shunt components, the fenestrated proximal catheter offers

the least resistance to flow. In practice, the greatest resistance to flow of CSF is dependent on dimensions and length of the distal catheter (Czosnyka M. *et al.*, 1997; Czosnyka Z. *et al.*, 2002). The work of Ginsberga and colleagues reported that just one or two fenestrations are needed to transport the majority of CSF flow entering the shunt catheter.

Due to the location and confines of ventricular system of the brain, the design of the proximal catheter demands careful consideration. Consideration must be given also to the resistance it presents, and the distribution of CSF flow entering the catheter. The design should also take into account any adverse impact on the efficiency of the catheter brought about by the presence of cells, and how the flow dynamics change as a result. While a catheter with low resistance might increase the chances of overdrainage, a high resistance catheter might lead to under drainage and a gradual increase in ICP over time. In practice, the combined approach offered by the Miethke ProGAV[®] Shunt (Section 2.3.4; Fig. 2.11), for example, may be viewed as an acceptable compromise.

The concept of an alternative proximal catheter, one that has a distributed porosity so as to maintain the flow of CSF flow without an appreciable increase in resistance, is the subject of this thesis. An electrospinning technique was used to fabricate the micro porous polyurethane catheter, referred to in this study as EPU. The rationale for selecting polyurethane as the candidate material for this catheter was presented in Section 2.8.1. Electrospinning was identified as the most appropriate means to process this polymer as the technique is versatile, and allows the user to produce microfibrinous forms having the desired thickness, fibre diameter and pore size (Section 2.8.2, Chapter 2).

In terms of permeability, the EPU samples examined in this study exhibited greater hydraulic resistance for all the groups compared to a conventional fenestrated catheter. In practice, the resistance may be compensated by increasing the surface area exposed to flow, reducing the wall thickness, or by altering the microstructure of the material. Since the production of CSF is constant, any increase in resistance due to cell obstruction in a porous catheter will result in a corresponding increase in

ICP. The flux and resistance of a porous material are coupled: in another words, as the pores become progressively more blocked, the flux of CSF through the remaining surface exposed to flow increases, which is indirect contrast to a conventional fenestrated catheter, where much of the outer surface of the catheter can support cell growth, and only cells growing around the periphery of those holes are likely to be affected by the flow of CSF entering the catheter. Moreover, the uneven distribution of CSF flow that has been observed in conventional catheters means that cells growing around the periphery are more likely to overgrow those holes that do not participate in the flow of CSF.

In an effort to maintain a more uniform distribution of flow, researchers have taken a different approach by increasing the size of those holes. Lin *et al.* (2003), for example, suggested that by increasing the size of holes located closer to the tip of the catheter, the flow entering the catheter is distributed more uniformly along its length. Similarly, Thomale *et al.* (2010) demonstrated that the clinical performance of a catheter is improved if it has fewer, larger holes. Likewise Harris and McAllister (2011), who maintained that such a configuration gives rise to a better flow distribution. The results from their study show that larger holes generated less resistance and the lowest shear stress. Both studies (Harris and McAllister 2011; Thomale *et al.*, 2010) have increased the uniformity of flow by increasing the size of the perforations, while the overall area available to flow was maintained the same.

To what extent do the materials, from which the catheter is made, and its form, influence cell adhesion and viability?

Conventional proximal catheters are made of PDMS with perforated holes. There is no evidence that any other materials or forms have been considered for this application. The candidate materials examined in this study as an alternative proximal catheter were PDMS (form of cast film and macro porous) and polyurethane (form of cast film and micro porous). Cell viability of fibroblasts and astrocytes was established by means of a conventional metabolic assay (alamarBlue).

The results from the static cell-contact studies showed that cell viability on the cast film and microporous form of polyurethane (EPU) was significantly less than PDMS 48 and 96 hours after seeding on both BSA and Fn-BSA treated surfaces. The viability of cells cultured on macroporous forms of PDMS, on the other hand, was not significantly different (Section 4.3.7, Chapter 4). Likewise, cast film polyurethanes and EPU showed no significant difference in terms of cell viability; neither did the form the material took have a bearing on the adhesion and growth of cells at this time point. PDMS demonstrated the greatest capacity for cell growth, showing a statistically significant difference compared with polyurethane forms at 48 and 96h in culture. Contrast this observation with the data for SF at the later time point; the cells were equivalent to PDMS.

The topography, roughness and charge of the material surfaces each play an important part in cell attachment (Harris *et al.*, 2011b). This may explain why the cells adhered better on cast film and macro porous PDMS and treated plate, than on the cast film and micro porous polyurethane samples (Section 4.3.6, Chapter 4). Thus, according to results of this study, the PDMS remains in many respect the substrate of choice for cells to proliferate. On the other hand, reports in the literature suggest that the greater porosity and interconnectivity of microporous materials offer better nutrient and waste transport, and mimics more effectively the extra cellular matrix by providing structural and functional cues found in nature (Puschmann *et al.*, 2013; Sharifpoor *et al.*, 2010). In contrast, the results of the present study appear to indicate that cell-cell communications are impaired in comparison to the macroporous or cast film substrates. Certainly, it is clear from this study that the fibrous nature of the EPU does not support cell attachment and proliferation to the same degree. One explanation for this observation might be the use of the unmodified EPU as a substrate. It is known that modifying the fibres with poly-D-lysine or similar compounds initiates better adhesion and cell survival (Puschmann *et al.*, 2013); equally, the choice of polymer, which does not readily promote cell attachment without modification with extracellular matrix components (e.g. Jozwiak *et al.* 2008).

Cell attachment on substrates that had been treated with adsorbed proteins was also quantified. Surprisingly, the results indicate that the cell viability remains the same for all substrates and forms, regardless of surface treatment. Studies show that protein adsorption on a substrate depends on many factors, such as hydrogen bonding, ionic interaction, calcium bridges between carboxyl groups and time of exposure (Brydon *et al.*, 1998). This result may be due to the concentrations chosen for this study. Another alternative approach to that used in the present study would be to add protein supplements to the growth medium to study (Harris *et al.*, 2011b). Equally, the amount of protein on the material surface, which was not quantified in this study, warrants further investigation.

To what extent is the hydraulic performance of the microporous catheter affected after shunt obstruction?

An understanding of the behaviour of cells in the presence of flow is very critical in this context. Cell behaviour is mediated by many factors, both chemical and physical. The need to study obstruction of catheter materials under realistic flow conditions was clearly outlined by Harris and co-workers (2010). Hence, cell adhesion and growth under physiological flow conditions *in vitro* takes us one step closer to understanding how these materials might perform within the ventricular microenvironment.

Although the EPU samples in this study were grouped according to their hydraulic permeability before seeding with cells. The number of viable cells on each sample of catheter material was the same overall regardless of the treatments or culture conditions, or hydraulic permeability (Section 5.3.2, Chapter 5). This result is surprising insofar as other studies have reported that porosity and size of pores has a bearing on the ability of fibroblasts and astrocytes to bridge the pores (Sun *et al.*, 2011). When cell infiltration is limited by very small pore sizes, cell adhesion is unaffected. On the other hand large pores do not retain cells on the scaffold because cell-cell communication is impaired. Indeed it has been shown that cells become quiescent if the pore diameter is more than 20 μ m in electrospun polymers (Zander *et al.*, 2013). From the results, it is noticed that the low group permeability may be

enhancing cell adhesion better than high group with prolonged time period in culture. However, no significant difference in cell viability was noted between the sample groups due to restriction in sample size. Therefore, more importance should be given to the fact that porosity affects cell adhesion.

The model of shunt catheter obstruction showed a significant decrease in hydraulic permeability for all samples (Section 5.3.3, Chapter 5). The obvious inference is that the cells and cell debris have blocked the pores resulting in a reduction in flow through the catheter when subjected to a fixed pressure gradient. Remarkably, there was no difference noted in the blockage between perfusion or static and Fn-BSA treated and non-treated samples. After blockage, the order of hydraulic permeability compared to before seeding followed the same trend, but there was no significant difference between the groupings so no firm conclusions may be drawn. Although flow through the obstructed EPU was reduced almost three fold for all the groups, catheter material remains permeable to flow. As the pressure gradient across the walls of the catheter rises, however, there would likely be a corresponding increase in flow entering the catheter. The extent to which cell obstruction affects the catheter permeability over longer periods remains to be shown.

Is EPU a viable alternative ventricular catheter material?

From the review of the literature electrospun polyurethane has not been considered as a candidate for CSF catheters. In the context of neural Tissue Engineering, electrospun polyurethane has been studied, but only after surface modification since the untreated material has been shown to exhibit poor astrocyte viability and adhesion when compared to the samples coated with substance which promotes cell growth (Puschmann *et al.*, 2013).

The results of this study are consistent with those of Puschmann *et al.*, (2013) although the conclusions of the latter study was that without surface modification the potential of EPU as a scaffold for cells was limited. Under static conditions, this study verifies that cell growth on EPU was significantly less than on PDMS, and

lowest among all the substrates and forms considered here, which, for the present application at least, is considered advantageous.

Clearly, the specifications of an actual EPU catheter would be different from those tested here in that its surface area and permeability would require optimisation to ensure that there is sufficient CSF transfer. Kaufman and Park (1999) suggested that a shorter inlet length (1 cm) on the proximal catheter would prevent occlusion especially in smaller ventricles. An EPU proximal catheter that is less susceptible to occlusion would not be subject to this restriction: the exposed portion of the catheter would transport the excess CSF from the choroid plexus and non-porous transfers the CSF to the valve.

To cope with increased cell adhesion at extended time points, it is likely that the untreated EPU would benefit from surface modification designed to inhibit cell adhesion. There are research groups which are focusing on surface modification of PDMS in order to minimise undesired protein adsorption and cell adhesion. It is known that hydrophilic surfaces exhibit poor cell adhesion (Harris *et al.*, 2011a; b; Patel *et al.*, 2006). PDMS is relatively hydrophobic. Consequently CSF proteins will readily adsorb onto its surface and subsequent cell adhesion increases the risk of obstruction (DeFife *et al.*, 1998). Recently, Harris *et al.* (2011a,b) employed surface modification using PEG and NAC (Harris *et al.*, 2011a) and plasma oxidation (Harris *et al.*, 2011b). Achyuta *et al.* (2010) determined that immobilised trypsin in PDMS was able to reduce cell adhesion. Similar techniques have been employed to incorporate chemicals, polymers, peptides, etc., with EPU, albeit to promote cell adhesion (e.g. Jozwiak *et al.*, 2008), but modification with hydrophilic substances is equally possible by these means.

Is EPU an effective alternative ventricular catheter, which is functional even with the presence of glial cells? Although challenging to accomplish, this research is the first of its kind to propose the use of polyurethane as a substrate and implementing electrospinning fabrication technology to produce a micro porous form of the catheter. The results obtained from this research support the argument that alternative materials and forms influence cell adhesion. The findings from shunt

obstruction model show that obstructed EPU retains a level of permeability that is reduced by about a third. Clearly, more studies need to be carried out to explore the full potential of EPU for this application. The following chapter regarding future work outlines those aspects of research to be continued with author's recommendations.

Limitations of the study

All experimental models have their limitations. The cell culture techniques employed in this study are a poor representation of the microenvironment present within the ventricular system of the brain. The choice of materials, cell types, seeding densities, time points and duration of study cannot be expected to replicate the complex interactions between an implanted device and host in a manner that can predict long-term performance or replicate failure modes. The present study made use of two cell types, astrocytes and immortalised 3T3, but explant studies confirm that other cell types are involved, for example macrophages (Thomale *et al.*, 2010). The 3T3 cell line was chosen for practical and cost considerations. Nevertheless, having established that the behaviour of 3T3 on the substrates used in this study was similar to astrocytes, these cells were considered a suitable model for shunt obstruction. In further studies, however, it is recommended that such experiments are conducted using co-cultures of macrophages and astrocytes to replicate better the conditions present *in vivo*, and to elucidate the role of inflammatory cells and signalling involved in mediating the host response to the implanted materials. For longer-term studies, consideration should be given to the use of animal models, where local and systemic responses and device performance can be studied along with adverse events.

CHAPTER 7

CONCLUSIONS AND FUTURE WORK

7.1 Overall Conclusions

The ventricular catheter of the hydrocephalus shunt series has been identified as the most likely component to fail, and decrease the life expectancy of the shunt as a whole. The consequences of failure of these devices lead to substantial discomfort for patients, and the prospect of expensive revision surgery, and poor outcomes.

One of the major reasons for failure of the catheter is through obstruction. This mode of failure is largely due in large part to the materials and design of the catheters in use at present. Therefore, the rationale of the research was to demonstrate the feasibility of an alternative form of ventricular catheter that can overcome some of these drawbacks. The material chosen for this study is medical grade polyurethane. The material was electrospun to produce fibrous structures with varied pore size to promote distributed porosity, instead of the perforated holes as seen in the conventional catheters which remains as the major source of blockage. The hydrodynamic properties of the conventional and alternative catheters were studied using the model built in-house. The hydraulic permeability of EPU was determined using a purpose built test rig. Although the hydraulic resistance of the candidate catheter material was higher than that of an existing proximal catheter, it is likely that a comparable resistance could be achieved by optimising the processing parameters.

Of all the substrates and forms examined in this study, the microporous polyurethane (EPU) was found to be least conducive to cell growth. There were significantly fewer cells ($p < 0.05$) than on the conventional catheter material (PDMS) and tissue culture plastic, comparable to the numbers present on the negative control (silicone hydrogel), whereas the results for PDMS were comparable to the positive control (tissue culture plastic).

The viability and growth of cells cultured this material under perfusion conditions representative of CSF flow were comparable to static cultures. The presence of cells had a significant impact on the hydraulic permeability of the EPU, the resistance to flow being some three-fold higher after only 24 hours in culture. Nevertheless, CSF was still able to flow through the obstructed EPU catheter, albeit at a higher pressure.

In developing and implementing the *in-vitro* model of shunt obstruction presented in this thesis, it has become possible to model the flow of CSF through a partially obstructed, porous catheter material, and thereby to study the interplay between flow, cell viability and hydraulic permeability of those materials. To our knowledge, the work presented in this thesis is the first of its kind to adopt this approach for this specific application.

7.2 Future Work

Further research using electrospun polyurethane as an alternative hydrocephalus shunt catheter needs to be carried out, to improve performance and develop a shunt which has longer life span, and thereby improve the quality of life of patients with this condition. There follows a brief outline of those areas where further work is needed.

The experiments and results reported in this thesis were obtained under steady flow conditions, whereas the flow of CSF is pulsatile. The results could well be affected by the pulsatile nature of CSF, both in terms of the measurement of hydraulic performance of the catheter components, and their obstruction by cells. Hence, efforts to improve and extend the methods described in this thesis to model pulsatile pressure and flow waveforms representative of the arterial/intracranial pulse pressure. Since cells are known to be sensitive to fluid mechanical cues, future studies should explore the effects of pulsatile flow conditions on cell morphology, growth and retention on catheter materials.

The electrospinning technique is versatile which provides the user to fabricate a desirable catheter at ease. Further work should include varying porosity along the length of the porous catheter which provides a variable resistance to CSF flow. This allows CSF to pass through the catheter without being blocked by the cells at the site of entry.

By implementing surface modifications for the electrospun material to reduce cell adhesion can be investigated. The selection of silicone hydrogel as negative control was made because such materials do not promote cell growth. Coating the electrospun material with a hydrogel-like substance should help to minimise cell growth still further. At present there are researchers who are implementing PEG hydrogel based surface modification on PU materials to avoid inflammatory response (Zachman *et al.*, 2013). Similar techniques of surface treatment along with electrospun materials may lead to further improvements in performance.

In the longer term, the concept of creating a proximal catheter which is efficient even in the presence of glial cells could be developed further into an artificial parenchymal based scaffold like structure that participates in CSF absorption. The cell adhesion on proximal catheters is manifest but taking a tissue engineering approach in fabricating a scaffold which can function like a fluid compartment participating in CSF circulation is worth considering. The investigation of suitable porosity of electrospun catheter which is able to function in the presence of glial and inflammatory cells in long term should be done.

Polyurethanes are demonstrated to be slow degrading polymer which was one of the main reasons for choosing this polymer. Alternatives such as polycaprolactone (PCL) which has been used as scaffolds in tissue engineering (Baiguera *et al.*, 2010) should also be considered. Explorations of tissue engineering approaches, alternative to polyurethane, surface modification to increase hydrophilic property and, peptide immobilisation to reduce cell adhesion will broaden the options available to produce a successful electrospun ventricular catheter.

REFERENCES

- Achyuta AK, Stephens KD, Lewis HG, Murthy SK. 2010. Mitigation of reactive human cell adhesion on poly(dimethylsiloxane) by immobilized trypsin. *Langmuir* 26: 4160-4167.
- Allin DM, Czosnyka ZH, Czosnyka M, Richards HK, Pickard JD. 2006. In vitro hydrodynamic properties of the Miethke ProGAV hydrocephalus shunt. *Cerebrospinal Fluid Research* 3: 9.
- Allin DM, Czosnyka M, Richards HK, Pickard JD, Czosnyka ZH. 2008. Investigation of the hydrodynamic properties of a new MRI-resistant programmable hydrocephalus shunt. *Cerebrospinal Fluid Res* 5: 8.
- Andrews KD, Hunt JA, Black RA. 2007. Effects of sterilisation method on surface topography and in-vitro cell behaviour of electrostatically spun scaffolds. *Biomaterials* 28: 1014-1026.
- Angarita-Jaimes N, Kouchakpour H, Liu J, Panerai RB, Simpson DM. 2014. Optimising the assessment of cerebral autoregulation from black box models. *Med Eng Phys*.
- Arnell K, Koskinen LO, Malm J, Eklund A. 2009. Evaluation of Strata NSC and Codman Hakim adjustable cerebrospinal fluid shunts and their corresponding antisiphon devices. *J Neurosurg Pediatr* 3: 166-172.
- Aschoff A, Kremer P, Benesch C, Fruh K, Klank A, Kunze S. 1995. Overdrainage and shunt technology - A critical comparison of programmable, hydrostatic and variable resistance valves and flow-reducing devices. *Child' Nerve Syst* 11: 193-202.
- Baiguera S, Del Gaudio C, Fioravanzo L, Bianco A, Grigioni M, Folin M. 2010. In vitro astrocyte and cerebral endothelial cell response to electrospun poly(epsilon-caprolactone) mats of different architecture. *J Mater Sci Mater Med* 21: 1353-1362.

- Bayston R. 1994. Hydrocephalus shunt infection. *Journal of Antimicrobial Chemotherapy* 34: 75-84.
- Boretos JW. 1980. Past, present and future role of polyurethanes for surgical implants. *Pure & Appl. Chem* 52: 1851-1855.
- Borgbjerg BM, Gjerris F, Albeck MJ, Hauerberg J, Borgesen SE. 1995. Frequency and cases of shunt revisions in different cerebrospinal fluid shunt types. *Acta Neurochir (Wien)* 136: 189-194.
- Bork T, et al. 2010. Development and in-vitro characterization of an implantable flow sensing transducer for hydrocephalus. *Biomed Microdevices* 12: 607-618.
- Bromby A, Czosnyka Z, Allin D, Richards HK, Pickard JD, Czosnyka M. 2007. Laboratory study on "intracranial hypotension" created by pumping the chamber of a hydrocephalus shunt. *Cerebrospinal Fluid Res* 4: 2.
- Browd SR, Gottfried ON, Ragel BT, Kestle JR. 2006a. Failure of cerebrospinal fluid shunts: part II: overdrainage, loculation, and abdominal complications. *Pediatr Neurol* 34: 171-176.
- Browd SR, Ragel BT, Gottfried ON, Kestle JR. 2006b. Failure of cerebrospinal fluid shunts: part I: Obstruction and mechanical failure. *Pediatr Neurol* 34: 83-92.
- Brydon HL, Keir G, Thompson EJ, Bayston R, Hayward r, Harkness W. 1998. Protein adsorption to hydrocephalus shunt catheters: CSF protein adsorption. *J Neurol Neurosurg Psychiatry* 64: 643-647.
- Carlberg B, Axell MZ, Nannmark U, Liu J, Kuhn HG. 2009. Electrospun polyurethane scaffolds for proliferation and neuronal differentiation of human embryonic stem cells. *Biomed Mater* 4: 045004.
- Chabrerie A, Black PM. 2002. Ventricular Shunts. *Journal of Intensive Care Medicine* 17: 218-229.

- Cheatle JT, Bowder AN, Agrawal SK, Sather MD, Hellbusch LC. 2012. Flow characteristics of cerebrospinal fluid shunt tubing. *J Neurosurg Pediatr* 9: 191-197.
- Chumas P, Tyagi A, Livingston J. 2001. Hydrocephalus - what's new? *Arch Dis Child Fetal Neonatal Ed* 85: F149-F154.
- Clatz O, Litrico A, Delingette H, Paquis P, Ayache N. 2007. Dynamic Model of Communicating Hydrocephalus for Surgery Simulation. *IEEE Transactions on Biomedical Engineering* 54: 755-758.
- Cohen B, Voorhees A, Vedel S, Wei T. 2009. Development of a theoretical framework for analyzing cerebrospinal fluid dynamics. *Cerebrospinal Fluid Res* 6: 12.
- Czosnyka M, Pickard JD. 2004. Monitoring and interpretation of intracranial pressure. *Journal of Neurology, Neurosurgery & Psychiatry* 75: 813-821.
- Czosnyka M, Czosnyka Z, Whitehouse H, Pickard JD. 1997. Hydrodynamic properties of hydrocephalus shunts: United Kingdom Shunt Evaluation Laboratory. *Journal of Neurology, Neurosurgery & Psychiatry* 62: 43-50.
- Czosnyka M, Czosnyka Z, Momjian S, Pickard JD. 2004. Cerebrospinal fluid dynamics. *Physiological Measurement* 25: R51-R76.
- Czosnyka Z, Czosnyka M, Richards HK, Pickard JD. 2002. Laboratory testing of hydrocephalus shunts -- conclusion of the U.K. Shunt evaluation programme. *Acta Neurochir (Wien)* 144: 525-538; discussion 538.
- Czosnyka ZH, Czosnyka M, Richards HK, Pickard JD. 2005. Evaluation of three new models of hydrocephalus shunts. *Acta Neurochir* 95: 223-227.
- de Jong DA, Delwel EJ, Avezaat CJJ. 2000. Hydrostatic and hydrodynamic considerations in shunted normal pressure hydrocephalus *Acta Neurochir (Wien)* 142: 241-247.

- de la Puente P, Ludena D, Fernandez A, Aranda JL, Varela G, Iglesias J. 2011. Autologous fibrin scaffolds cultured dermal fibroblasts and enriched with encapsulated bFGF for tissue engineering. *J Biomed Mater Res A* 99: 648-654.
- DeFife KM, Shive MS, Hagen KM, Clapper DL, Anderson JM. 1998. Effects of photochemically immobilized polymer coatings on protein adsorption, cell adhesion, and the foreign body reaction to silicone rubber. *Journal of Biomedical Materials Research* 44: 298-307.
- Demir MM, Yilgor I, Yilgor E, Erman B. 2002. Electrospinning of polyurethane fibers. *Polymer* 43: 3303-3309.
- Doi K, Matsuda T. 1997. Significance of porosity and compliance of microporous, polyurethane-based microarterial vessel on neoarterial wall regeneration. *Journal of Biomedical Materials Research* 34: 573-584.
- Doi K, Nakayama Y, Matsuda T. 1996. Novel compliant and tissue-permeable microporous polyurethane vascular prosthesis fabricated using an excimer laser ablation technique. *Journal of Biomedical Materials Research* 31: 27-33.
- Doshi J, Reneker DH. 1995. Electrospinning process and applications of electrospun fibers. *Journal of Electrostatics* 35: 151-160.
- Drake JM, Kestle JRW, Tuli S. 2000. CSF shunt 50 yrs on - past, present and future. *Child' Nerve Syst* 16: 800-804.
- Eide PK, Park EH, Madsen JR. 2010. Arterial blood pressure vs intracranial pressure in normal pressure hydrocephalus. *Acta Neurol Scand* 122: 262-269.
- Eklund A, Koskinen LO, Malm J. 2004a. Features of the Sinushunt and its influence on the cerebrospinal fluid system. *J Neurol Neurosurg Psychiatry* 75: 1156-1159.

Eklund A, Lundkvist B, Koskinen LO, Malm J. 2004b. Infusion technique can be used to distinguish between dysfunction of a hydrocephalus shunt system and a progressive dementia. *Med Biol Eng Comput* 42

644-649.

Eklund A, Smielewski P, Chambers I, Alperin N, Malm J, Czosnyka M, Marmarou A. 2007. Assessment of cerebrospinal fluid outflow resistance. *Med Biol Eng Comput* 45: 719-735.

Eymann R, Kim YJ, Bohle RM, Antes S, Schmitt M, Menger MD, Kiefer M. 2012. Microstructural alterations of silicone catheters in an animal experiment: histopathology and SEM findings. *Acta Neurochir Suppl* 113: 87-90.

Faghih Jouibari M, Baradaran N, Shams Amiri R, Nejat F, El Khashab M. 2011. Huge hydrocephalus: definition, management, and complications. *Childs Nerv Syst* 27: 95-100.

Francel PC, Honeycutt J, Tompkins P. 2001. The effect of alignment on the pressure/flow characteristics of flow control shunt valves. *Child's Nervous System* 17: 471-471.

Friden H, Ekstedt J. 1982. Instrumentation for cerebrospinal fluid hydrodynamic studies in man. *Med Biol Eng Comput* 20: 167-180.

Ginsberga HJ, Sum A, Drake JM, Cobbold RSC. 2000. Ventriculoperitoneal shunt flow dependency on the number of patent holes in a ventricular catheter. *Pediatr Neurosurg* 33: 7-11.

Gloekner H, Jonuleit T, Lemke H. 2001. Monitoring of cell viability and cell growth in a hollow-fiber bioreactor by use of the dye Alamar Blue. *Journal of Immunological Methods* 252: 131-138.

- Grasl C, Bergmeister H, Stoiber M, Schima H, Weigel G. 2010. Electrospun polyurethane vascular grafts: in vitro mechanical behavior and endothelial adhesion molecule expression. *J Biomed Mater Res A* 93: 716-723.
- Greitz D, Greitz T, Hindmarh T. 1997. A new view on the CSF-circulation with the potential for pharmacological treatments of childhood hydrocephalus. *Acta Paediatr* 86: 125-132.
- Guan J, Fujimoto KL, Sacks MS, Wagner WR. 2005. Preparation and characterization of highly porous, biodegradable polyurethane scaffolds for soft tissue applications. *Biomaterials* 26: 3961-3971.
- Harris CA, McAllister JP, 2nd. 2011. Does drainage hole size influence adhesion on ventricular catheters? *Childs Nerv Syst* 27: 1221-1232.
- Harris CA, Resau JH, Hudson EA, West RA, Moon C, McAllister JP, 2nd. 2010. Mechanical contributions to astrocyte adhesion using a novel in vitro model of catheter obstruction. *Exp Neurol* 222: 204-210.
- Harris CA, Resau JH, Hudson EA, West RA, Moon C, Black AD, McAllister JP, 2nd. 2011a. Reduction of protein adsorption and macrophage and astrocyte adhesion on ventricular catheters by polyethylene glycol and N-acetyl-L-cysteine. *J Biomed Mater Res A* 98: 425-433.
- . 2011b. Effects of surface wettability, flow, and protein concentration on macrophage and astrocyte adhesion in an in vitro model of central nervous system catheter obstruction. *J Biomed Mater Res A* 97: 433-440.
- Józwiak AB, Kielty CM, Black RA. 2008. Surface functionalization of polyurethane for the immobilization of bioactive moieties on tissue scaffolds. *Journal of Materials Chemistry* 18: 2240.
- Kaufman BA, Park TS. 1999. Ventricular anatomy and shunt catheters. *Pediatr Neurosurg* 31: 1-6.

- Khan S, Newaz G. 2010. A comprehensive review of surface modification for neural cell adhesion and patterning. *J Biomed Mater Res A* 93: 1209-1224.
- Khorasani MT, Shorgashti S. 2006. Fabrication of microporous thermoplastic polyurethane for use as small-diameter vascular graft material. I. Phase-inversion method. *J Biomed Mater Res B Appl Biomater* 76: 41-48.
- Kiefer M, Eymann R, Meier U. 2002. Five years experience with gravitational shunts in chronic hydrocephalus of adults. *Acta Neurochir (Wien)* 144: 755-767; discussion 767.
- Kim HJ, Magrane J. 2011. Isolation and culture of neurons and astrocytes from the mouse brain cortex. *Methods Mol Biol* 793: 63-75.
- Kulkarni AV, Hui S, Shams I, Donnelly R. 2010. Quality of life in obstructive hydrocephalus: endoscopic third ventriculostomy compared to cerebrospinal fluid shunt. *Childs Nerv Syst* 26: 75-79.
- Kurosaki K, Hamada H, Hayashi N, Kurimoto M, Hirashima Y, Endo S. 2002. A rare case of shunt malfunction attributable to blockage of a Codman-Hakim programmable shunt valve. *Childs Nerv Syst* 18: 183-185.
- Kurtom KH, Magram G. 2007. Siphon regulatory devices: their role in the treatment of hydrocephalus. *Neurosurg Focus* 22: E5-.
- Lee SA, Lee H, Pinney JR, Khialeeva E, Bergsneider M, Judy JW. 2011. Development of microfabricated magnetic actuators for removing cellular occlusion. *Journal of Micromechanics and Microengineering* 21: 054006.
- Lefranc M, Ko JY, Peltier J, Fichten A, Desenclos C, Macron JM, Toussaint P, Le Gars D, Petitjean M. 2010. Effect of transcranial magnetic stimulation on four types of pressure-programmable valves. *Acta Neurochir (Wien)* 152: 689-697.
- Lin J, Morris M, Olivero W, Boop F, Sanford RA. 2003. Computational and experimental study of proximal flow in ventricular catheter *J Neurosurg* 99: 426-431.

- Linninger AA, Sweetman B, Penn R. 2009a. Normal and hydrocephalic brain dynamics: the role of reduced cerebrospinal fluid reabsorption in ventricular enlargement. *Ann Biomed Eng* 37: 1434-1447.
- Linninger AA, Xenos M, Zhu DC, Somayaji MR, Kondapalli S, Penn RD. 2007. Cerebrospinal fluid flow in the normal and hydrocephalic human brain. *IEEE Transactions on Biomedical Engineering* 54: 291-302.
- Linninger AA, Xenos M, Sweetman B, Pongshe S, Guo X, Penn R. 2009b. A mathematical model of blood, cerebrospinal fluid and brain dynamics. *J. Math. Biol* 59: 729-759.
- Liu SQ, Kodama M. 1992. Porous polyurethane vascular prostheses with variable compliance. *Journal of Biomedical Materials Research* 26: 1489-1502.
- Lundkvist B, Eklund A, Koskinen LO, Malm J. 2003. An adjustable CSF shunt: advices for clinical use. *Acta Neurol Scand* 108: 38-42.
- Lutz BR, Venkataraman P, Browd SR. 2013. New and improved ways to treat hydrocephalus: Pursuit of a smart shunt. *Surg Neurol Int* 4: S38-50.
- Madsen JR, Egnor M, Zou R. 2006. Cerebrospinal Fluid Pulsatility and Hydrocephalus: The Fourth Circulation. *Clinical Neurosurgery* 53: 48-52.
- Magram G. 1995. A cerebrospinal fluid shunt: a theoretical concept. *Child' Nerve Syst* 11: 604-606.
- Martins A, Reis RL, Neves NM. 2008. Electrospinning: processing technique for tissue engineering scaffolding. *International Materials Reviews* 53: 257-274.
- Maurer MH. 2010. Proteomics of brain extracellular fluid (ECF) and cerebrospinal fluid (CSF). *Mass Spectrom Rev* 29: 17-28.
- McAllister JP. 2011. Getting into the root of hydrocephalus. *Sci Transl Med* 3: 1-2.

- McGirt MJ, Buck DW, 2nd, Sciubba D, Woodworth GF, Carson B, Weingart J, Jallo G. 2007. Adjustable vs set-pressure valves decrease the risk of proximal shunt obstruction in the treatment of pediatric hydrocephalus. *Childs Nerv Syst* 23: 289-295.
- McMilln CR. 2006. Biomedical applications of rubbers and elastomers. *Rubber Chemistry and Technology* 79: 500-519.
- Meier U, Mutze S. 2004. Correlation between decreased ventricular size and positive clinical outcome following shunt placement in patients with normal-pressure hydrocephalus. *J Neurosurg* 100: 1036-1040.
- Miwa K, Kondo H, Sakai N. 2001. Pressure changes observed in Codman-Medos programmable valves following magnetic exposure and flipping. *Child' Nerve Syst* 17: 150-153.
- Momani L, Al-Nuaimy W, Al-Jumaily M, Mallucci C. 2011. A mechatronic valve in the management of hydrocephalus: methods and performance. *Med Biol Eng Comput* 49: 121-132.
- Nakayama GR, Caton MC, Nova MP, Parandoosh Z. 1997. Assessment of the Alamar Blue assay for cellular growth and viability in vitro. *Journal of Immunological Methods* 204: 205-208.
- Naradzay JFX, Browne BJ, Rolnick MA, Doherty RJ. 1999. Cerebral ventricular shunts. *The Journal of Emergency Medicine* 17: 311-322.
- Oreskovic D, Klarica M. 2010. The formation of cerebrospinal fluid: nearly a hundred years of interpretations and misinterpretations. *Brain Res Rev* 64: 241-262.
- Paes N. 1996. A new self-adjusting flow-regulating device for shunting of csf. *Child' Nerve Syst* 12: 619-625.
- Panerai RB. 2003. The critical closing pressure of the cerebral circulation. *Medical Engineering & Physics* 25: 621-632.

—. 2013. Nonstationarity of dynamic cerebral autoregulation. *Med Eng Phys*.

Patel KR, Tang H, Grever WE, Simon Ng KY, Xiang J, Keep RF, Cao T, McAllister JP, 2nd. 2006. Evaluation of polymer and self-assembled monolayer-coated silicone surfaces to reduce neural cell growth. *Biomaterials* 27: 1519-1526.

Pena A, Harris NG, Bolton MD, Czosnyka M, Pickard JD. 2002. Communicating Hydrocephalus: The Biomechanics of Progressive Ventricular Enlargement Revisited. *Acta Neurochir* 81: 59-63.

Puschmann TB, Zanden C, De Pablo Y, Kirchhoff F, Pekna M, Liu J, Pekny M. 2013. Bioactive 3D cell culture system minimizes cellular stress and maintains the in vivo-like morphological complexity of astroglial cells. *Glia* 61: 432-440.

Reed AM, Potter J, Szycher M. 1994. A solution grade biostable polyurethane elastomer: ChronoFlex AR. *Journal of Biomaterials Applications* 8: 210-236.

Reiber H. 2003. Proteins in cerebrospinal fluid and blood: Barriers, CSF flow rate and source related dynamics. *Restorative Neurology and Neuroscience* 21: 79-96.

Rekate HL. 2008. The definition and classification of hydrocephalus: a personal recommendation to stimulate debate. *Cerebrospinal Fluid Res* 5: 2.

Rivera AM, Strauss KW, van Zundert A, Mortier E. 2005. The history of peripheral intravenous catheters : How little plastic tubes revolutionized medicine. *Acta Anaesth. Belg* 56: 271-282.

Romero L, Ros B, Ibáñez G, Ríus F, González L, Arráez MA. 2013. Endoscopic third ventriculostomy: can we predict success during surgery? *Neurosurgical Review* 37: 89-97.

Ross N, Eynon CA. 2005. Intracranial pressure monitoring. *Current Anaesthesia & Critical Care* 16: 255-261.

- Schley D, Billingham J, Marchbanks RJ. 2004. A model of in-vivo hydrocephalus shunt dynamics for blockage and performance diagnostics *Mathematical Medicine and Biology* 21: 347-368.
- Schuhmann MU, Engel M, Runge L, Samii M, Brinker T. 2000. Application of clinically recorded ICP patterns - an extension of conventional shunt testing *Child' Nerve Syst* 16: 856-861.
- Segal MB. 1993. Extracellular and Cerebrospinal Fluids. *J. Inher. Metab. Dis* 16: 617-638.
- Sharifpoor S, Simmons CA, Labow RS, Santerre JP. 2010. A study of vascular smooth muscle cell function under cyclic mechanical loading in a polyurethane scaffold with optimized porosity. *Acta Biomater* 6: 4218-4228.
- Sin D, Miao X, Liu G, Wei F, Chadwick G, Yan C, Friis T. 2010. Polyurethane (PU) scaffolds prepared by solvent casting/particulate leaching (SCPL) combined with centrifugation. *Materials Science and Engineering: C* 30: 78-85.
- Sivaloganathan S, Stastna M, Tenti G, Drake JM. 2005. A viscoelastic approach to the modelling of hydrocephalus. *Applied Mathematics and Computation* 163: 1097-1107.
- Smillie A, Sobey IAN, Molnar Z. 2005. A hydroelastic model of hydrocephalus. *Journal of Fluid Mechanics* 539: 417.
- Sotelo J. 2012. The hydrokinetic parameters of shunts for hydrocephalus might be inadequate. *Surg Neurol Int* 3: 40.
- Stein SC, Guo W. 2008. Have we made progress in preventing shunt failure? A critical analysis. *J Neurosurg Pediatr* 1: 40-47.
- . 2009. The prevalence of shunt-treated hydrocephalus: a mathematical model. *Surg Neurol* 72: 131-137.

- Stivaros SM, Jackson A. 2007. Changing concepts of cerebrospinal fluid hydrodynamics: role of phase-contrast magnetic resonance imaging and implications for cerebral microvascular disease. *Neurotherapeutics* 4: 511-522.
- Stokes K, McVenes R, Anderson JM. 1995. Polyurethane elastomer biostability. *Journal of Biomaterials Applications* 9: 321-354.
- Sun T, Donoghue PS, Higginson JR, Gadegaard N, Barnett SC, Riehle MO. 2011. The interactions of astrocytes and fibroblasts with defined pore structures in static and perfusion cultures. *Biomaterials* 32: 2021-2031.
- Thomale UW, Hosch H, Koch A, Schulz M, Stoltenburg G, Haberl EJ, Sprung C. 2010. Perforation holes in ventricular catheters--is less more? *Childs Nerv Syst* 26: 781-789.
- Thomale UW, Knitter T, Schaumann A, Ahmadi SA, Ziegler P, Schulz M, Miethke C. 2013. Smartphone-assisted guide for the placement of ventricular catheters. *Childs Nerv Syst* 29: 131-139.
- Trost HA. 1995. Is there a reasonable differential indication for different hydrocephalus shunt systems? *Child' Nerve Syst* 11: 189-192.
- Tsui YK, Gogolewski S. 2009. Microporous biodegradable polyurethane membranes for tissue engineering. *J Mater Sci Mater Med* 20: 1729-1741.
- Tuli S, Drake JM, Lawless J, Wigg M, Lamberti-Pasculli M. 2000. Risk factors for repeated cerebrospinal shunt failures in pediatric patients with hydrocephalus *J Neurosurg* 92: 31-38.
- Turner SG, Hall WA. 2006. Programmable shunt-related suicide attempt. *Acta Neurochir (Wien)* 148: 1307-1310.
- Villalona GA, et al. 2010. Cell-Seeding Techniques in Vascular Tissue Engineering. *Tissue Eng Part B* 16: 341-350.

von Koch CS, Gupta N, Sutton LN, Sun PP. 2003. In utero surgery for hydrocephalus. *Childs Nerv Syst* 19: 574-586.

Whitehouse HE, Czosnyka M, Pickard JD. 1994. Shunt audit: a computerized method for testing the performance characteristics of CSF shunts in vitro. *Child's Nerve Syst* 10: 158-161.

Williams MA, et al. 2007. Priorities for hydrocephalus research: report from a National Institutes of Health-sponsored workshop. *J Neurosurg* 107: 345-357.

Zachman AL, Page JM, Prabhakar G, Guelcher SA, Sung HJ. 2013. Elucidation of adhesion-dependent spontaneous apoptosis in macrophages using phase separated PEG/polyurethane films. *Acta Biomater* 9: 4964-4975.

Zander NE, Orlicki JA, Rawlett AM, Beebe TP, Jr. 2013. Electrospun polycaprolactone scaffolds with tailored porosity using two approaches for enhanced cellular infiltration. *J Mater Sci Mater Med* 24: 179-187.

Zdrachala RJ, Zdrachala IJ. 1999. Biomedical applications of polyurethanes: A review of past promises, present realities and a vibrant future *Journal of Biomaterials Applications* 14: 67-90.

Zhang J, Williams MA, Rigamonti D. 2006. Genetics of human hydrocephalus. *J Neurol* 253: 1255-1266.

Book:

Batu V, CRC Press. 2005. *Applied Flow and Solute Transport Modeling in Aquifers: Fundamental Principles and Analytical and Numerical Methods*.

APPENDIX A

Dimensional analysis of conventional shunt components

The shunt components which include proximal catheter, distal catheter, fixed pressure valve (70 mm H₂O) and programmable valve from Codman Shunt System were generously donated by Dr. Paul Chumas, Leeds Hospital. The proximal and distal catheters were studied for its dimension and surface characterisation. In order to measure the ID, OD, thickness of the catheter, perforation holes dimensions (ID and OD of small and large holes) and distance between each perforated holes, a small piece of the catheter was imaged using Axio Imager Z1 (Carl Zeiss, Hertfordshire, UK) at 40x magnification lens. Each measurement of the diameter (OD and ID) and thickness of both the catheters were taken five times at different position of the catheters. To measure the distance between perforated holes, the most linear side with holes present were measured.

The surface properties and elements they are made of were measured using imaging and energy-dispersive X-Ray spectroscopy (EDS) of Hitachi TM 1000 SEM (Krefeld, Germany). A small piece of the respective catheter was cut along the length, the cut portion was then sliced diametrically so as to expose inner and outer surface of the catheters for imaging and elemental analysis. SEM does not require sample preparation.

Figure A.1 illustrates the microscopic images of the proximal and distal catheter used for analysis of the catheter dimensions. Three microscopic images were taken at different position of the catheters to measure the OD and ID of the catheters and perforations hole (OD and ID). The collected images were then used for dimensional analysis using the software provided within the microscope. The red coloured marking in the image represent the location of measurement and the value. The summary of all the dimensional values including the mean and standard deviations are detailed in Table A.1.

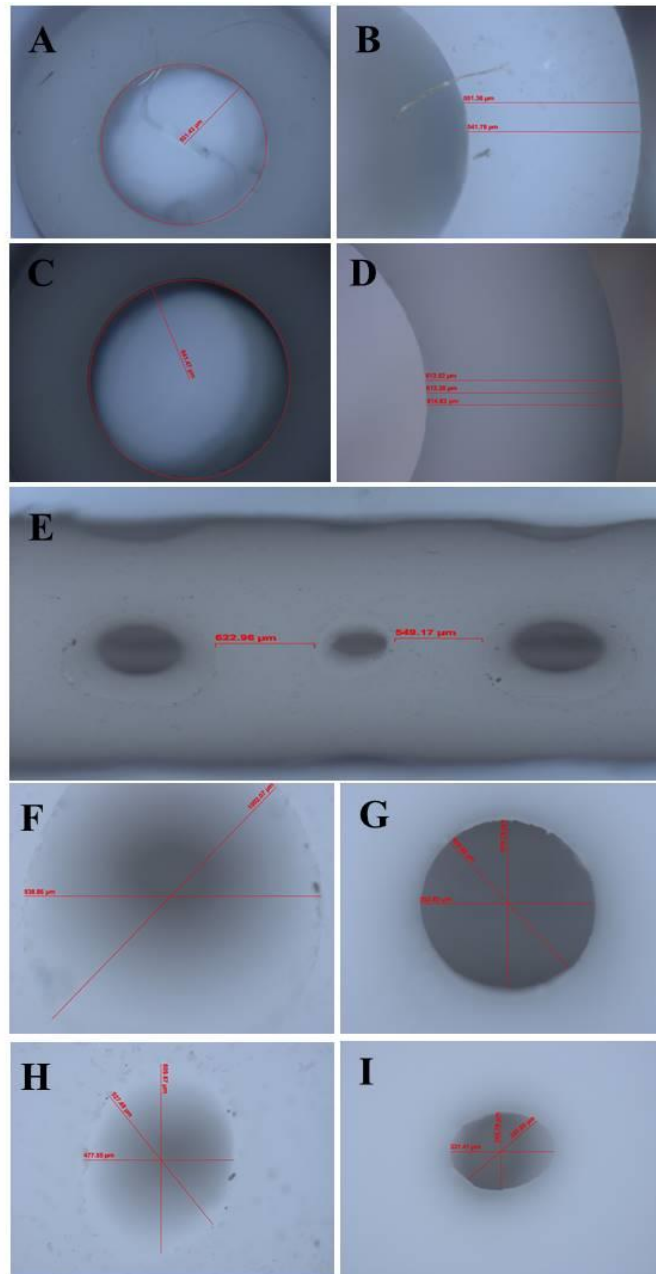


Figure A.1: Cross-section of the small piece of distal catheter (A-B) and proximal catheter (C-D). Perforated holes present in the proximal catheter (E-I). A - ID of distal catheter, B- thickness of distal catheter, C - ID of proximal catheter, D - thickness of proximal catheter, E – distance between the holes of the perforation, F - OD of large perforation hole, G – ID of large perforation hole, H - OD of small perforation hole, I – ID of small perforation hole. The red lines in the images indicate the measurements in μm .

Dimension	Proximal Catheter (Mean \pm SD)	Distal Catheter (Mean \pm SD)
OD (μm) (1/10")	2525 \pm 9	2142 \pm 24
ID (μm) (1/20")	1292 \pm 10	1083 \pm 27
Thickness (μm)	616 \pm 1	530 \pm 5
Perforation length (cm)	1.22	0
Total length (cm)	15	75
No of large perforation	20	0
No of small perforation	20	0
Large perforation OD (μm)	929 \pm 35	0
Small perforation OD (μm)	556 \pm 20	0
Large perforation ID (μm)	540 \pm 19	0
Small perforation ID (μm)	278 \pm 11	0
Distance between each perforation (μm)	558 \pm 29	0
Depth of Large perforation (μm)	649	0
Depth of small perforation (μm)	627	0
Area of 20 Large Perforation (m^2)	1.35457 $\times 10^{-5}$	0
Area of 20 Small Perforation (m^2)	4.85493 $\times 10^{-6}$	0

Table A.1: Dimensions of proximal and distal catheter

The total contact area of the perforated sections of the proximal catheter is 0.184 cm^2 . The cross sectional area of the proximal catheter is 0.0131 cm^2 . Due to the presence of the perforated holes, the contact surface area of the flow of CSF is increased by 14 times.

APPENDIX B

Characterisation of the shunt components

The scanning electron microscopy elemental analysis verifies that the given shunt catheters are made of majority of Silicone, Barium and minor contribution from other elements.

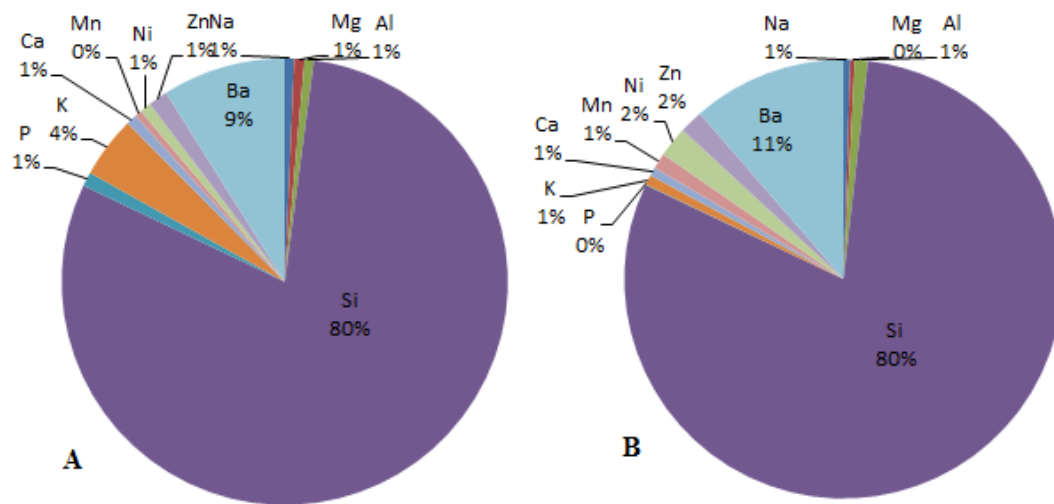


Figure B.1: Elemental distribution of proximal catheter (A) and distal catheter (B).

In both the catheters Silicone contributes 80% of the catheter and ~10% with Barium.

The proximal and distal catheter surface properties were studied using scanning electron microscopy. The outer and inner surface was imaged separately for each catheter to understand any difference between them. Figure B.2 and B.3 shows that the outer surface is smoother when compared to inner surface for both the catheter types. In both outer and inner surface the crystal like structures confirms from elemental analysis that they are Barium sulphide and the remaining portion is majority Silicone and other elements.

Inner Surface

Outer Surface

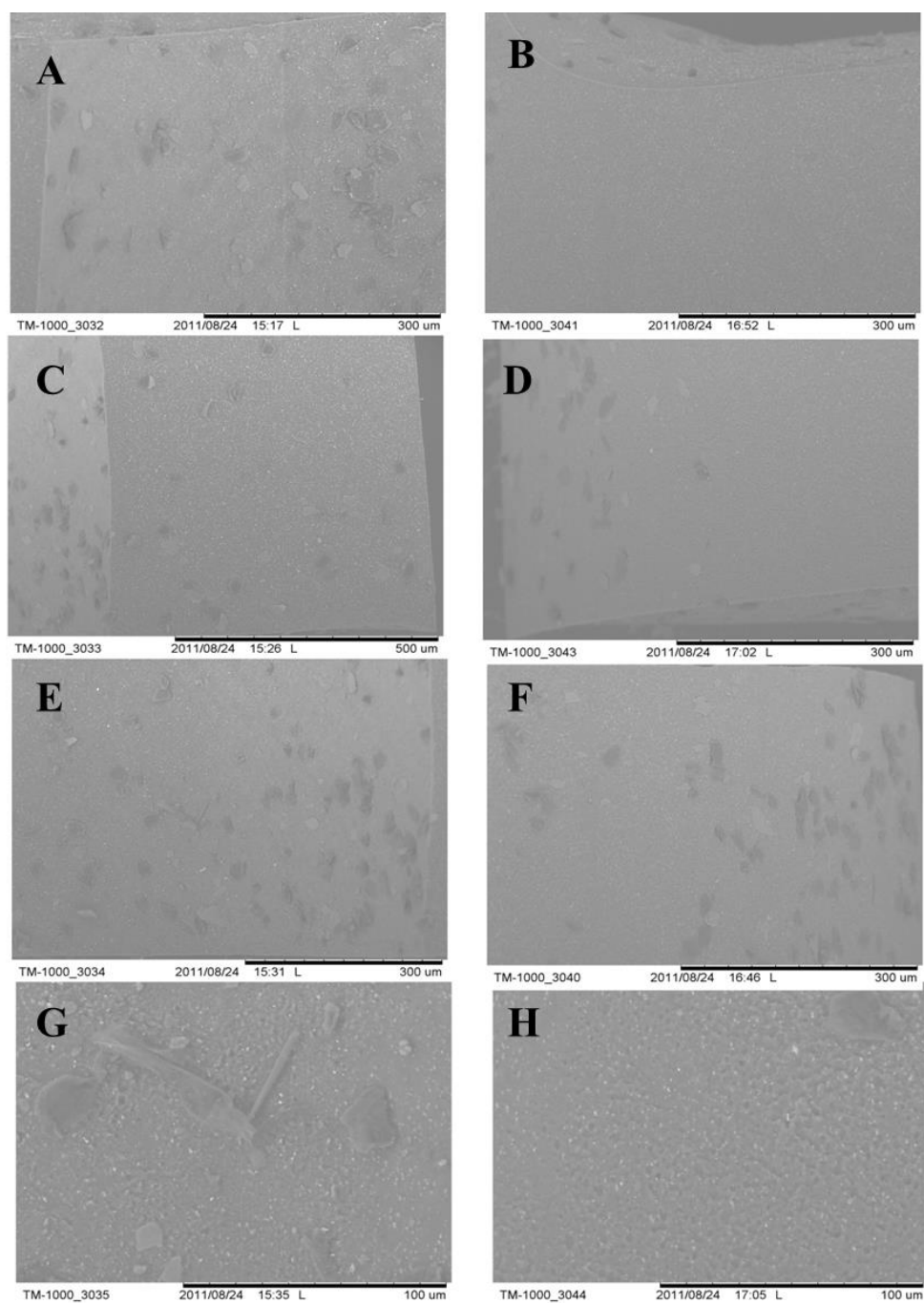


Figure B.2: Scanning electron microscopy images of distal catheter. A and C - Cut phase of the proximal catheter inner surface, B and D - Cut phase of the proximal catheter outer surface, E and F – inner and outer surface respectively and G and H – Higher magnification of inner and outer surface respectively

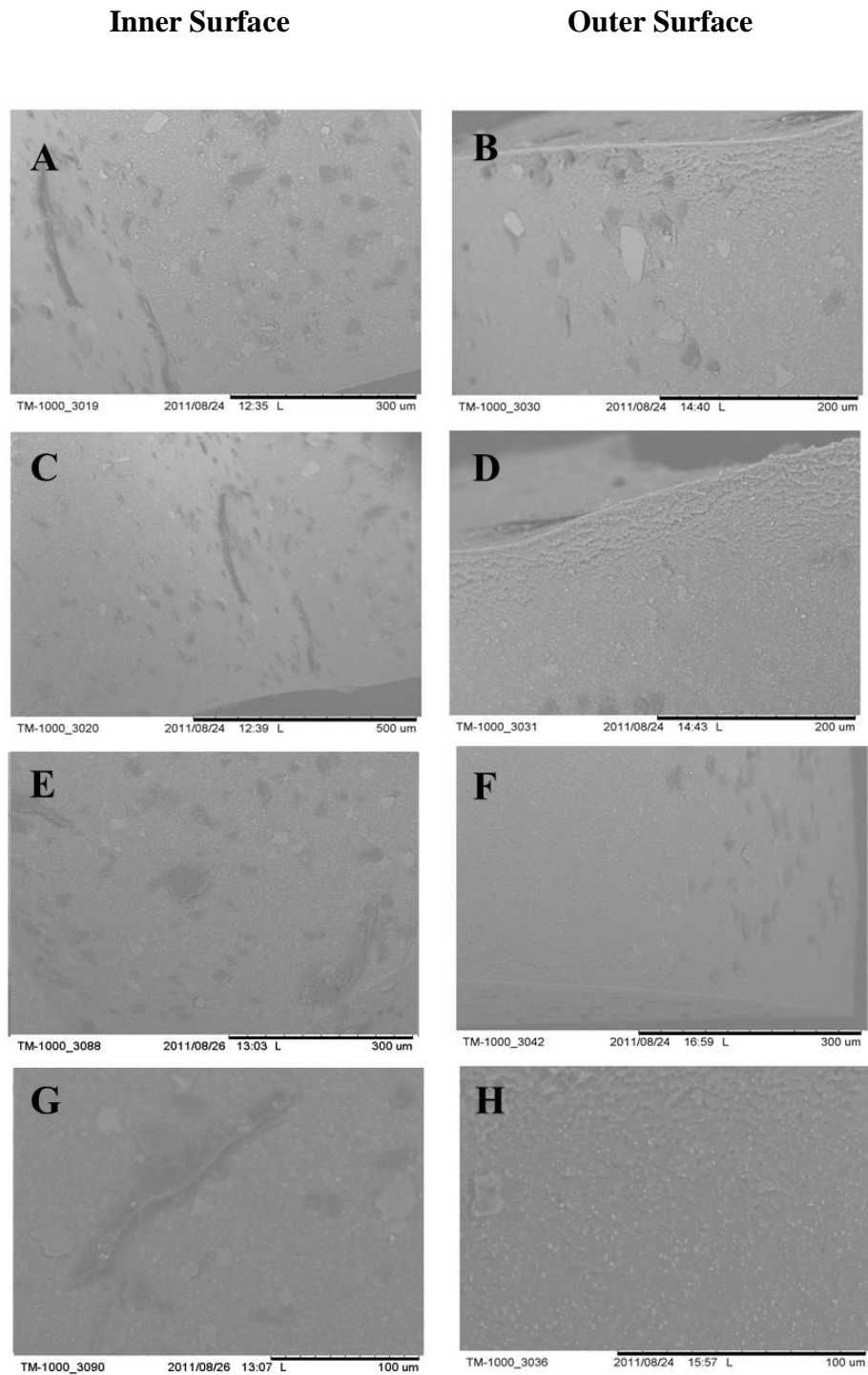


Figure B.3: Scanning electron microscopy images of distal catheter. A and C -Cut phase of the distal catheter inner surface, B and D - Cut phase of the distal catheter outer surface, E and F – inner and outer surface respectively and G and H – Higher magnification of inner and outer surface respectively

APPENDIX C

Pressure and flow properties of shunt components

The flowrate of CSF through the proximal and distal catheter and fixed and programmable valve was measured respectively for a constant head of pressure using the in-built physical model as explained in Section 3.2.3. All the pressure-flow plotted using the *in vitro* model is an average of three values and standard error was very low hence was not plotted. Figure C.1, C.2 and C.3 summarise the finding there is a linear relationship found between pressure and flow for both the catheters and valves. The opening pressure is the x-intercept from the graph; hence for fixed pressure valve it is 6.41 mmHg and programmable valve is 4.97 mmHg without distal catheter (Fig. C.3). The given valve's pressure setting and types are distinguished through physical examination. From the manufacturer guidelines the valve that has 3 diagonal dots present on its surface is categorised as a fixed pressure valve with an opening pressure of 70 mm H₂O (5.1 mm Hg) and programmable valve has no dots on its surface and identified by viewing its inbuilt mechanism (Fig. 2.9). Its opening pressure is indicated by the step where the tip of the spring rests (5th step which indicates 70 mm H₂O). The operating condition or the duration of usage of these valves at the time of testing was unknown. The opening pressure of the fixed pressure valve is measured as 6.8 mmHg; whereas, the opening pressure of the programmable valve is measured as 5.0 mm Hg. The shunt system provided may not be new, prolonged usage affects the hydrodynamic properties of the system (Lundkvist *et al.*, 2003). Hence, unable to explain why there is an increase in opening pressure for the fixed pressure valve.

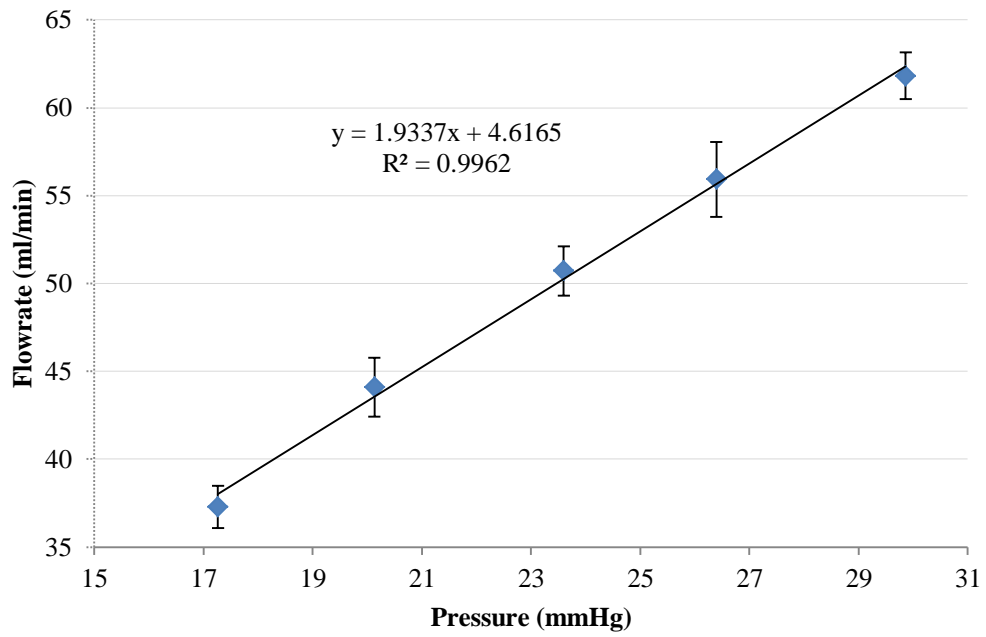


Figure C.1: Conventional proximal catheter flow dynamics. All points represents mean \pm standard error and $n = 3$

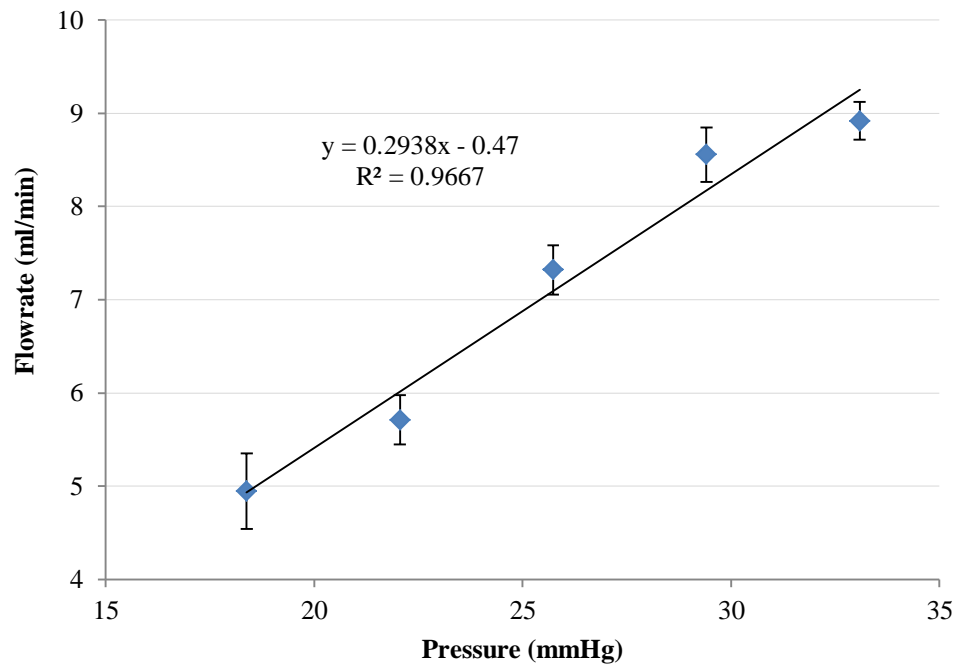


Figure C.2: Distal catheter flow dynamics. All points represents mean \pm standard error and $n = 3$

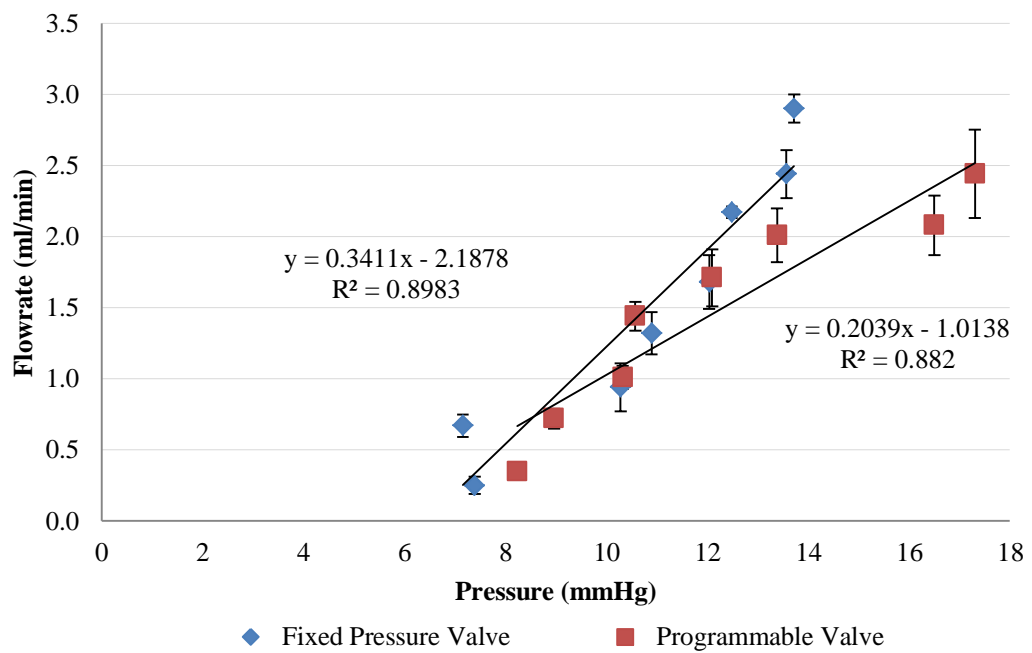


Figure C.3: Fixed pressure and programmable valve flow dynamics. All points represents mean \pm standard error and $n = 3$

APPENDIX D

Optical microscopy of EPU

Images of EPU and a glass slide acquired by optical microscopy (Zeiss Apotome, Zeiss, UK) are shown in Figure D.1. The results illustrate the difficulty in acquiring images of cells on the EPU material. Therefore, the images of Live/Dead assay on EPU were not included because auto-fluorescence of EPU made it impossible to view the cells.

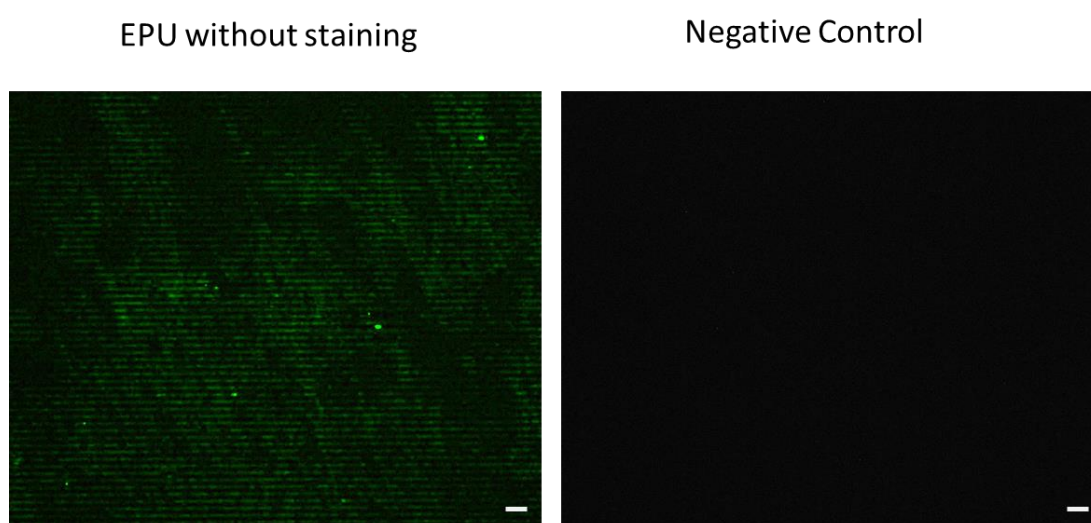


Figure D.1: Fluorescence microscope images without the presence of cells on EPU and glass slide. Image on left shows EPU and right shows glass slide. Scale bars are $20\mu\text{m}$